/
Article / Book Information

( )	
Title(English)	Fundamental Diagrams and Traffic State Estimation Methods: Analysis and Modeling using Zen Traffic Data
( )	Dahiya Garima
Author(English)	Garima Dahiya
( )	: , : , : 12220 , :2022 9 22 , : , : , , , , ,
Citation(English)	Degree:Doctor (Engineering), Conferring organization: Tokyo Institute of Technology, Report number: 12220 , Conferred date:2022/9/22, Degree Type:Course doctor, Examiner:,,,,,
( )	
Type(English)	Doctoral Thesis

Fundamental Diagrams and Traffic State Estimation Methods: Analysis and Modeling using Zen Traffic Data

by

Garima Dahiya

A dissertation submitted to the
Department of Civil and Environmental Engineering
School of Environment and Society
in partial fulfilment of the requirements for the degree of

DOCTOR OF ENGINEERING

at the

TOKYO INSTITUTE OF TECHNOLOGY

September 2022

東京工業大学
Tokyo Institute of Technology

Tokyo Institute of Technology
Transport Studies Unit

FUNDAMENTAL DIAGRAMS AND TRAFFIC STATE ESTIMATION METHODS: ANALYSIS AND MODELING USING ZEN TRAFFIC DATA

GARIMA DAHIYA
Tokyo Institute of Technology

DOCTORAL DISSERTATION

Supervisor:

Associate Professor Toru SEO
Seo Lab. (*Transportation Research with Data Science*)
Department of Civil and Environmental Engineering
School of Environment and Society
Tokyo Institute of Technology
Email: seo.t.aa@m.titech.ac.jp

Ex-Supervisor:

Professor Emeritus Yasuo ASAKURA
(*Tokyo Institute of Technology*)

Doctoral Committee Members:

Professor Shinjiro KANAE

Professor Shinya HANAOKA

Professor Tetsuo YAI

Professor Yasuo ASAKURA

Associate Professor Toru SEO

Associate Professor Yasunori MUROMACHI

Garima Dahiya
dahiya.g.aa@m.titech.ac.jp

To my parents.

ACKNOWLEDGEMENTS

ABSTRACT

FUNDAMENTAL DIAGRAMS AND TRAFFIC STATE ESTIMATION METHODS: ANALYSIS AND MODELING USING ZEN TRAFFIC DATA

SEPTEMBER 2022

GARIMA DAHIYA

B.Sc., UNIVERSITY OF DELHI

M.Sc., INDIAN INSTITUTE OF TECHNOLOGY MANDI

Doctorate, TOKYO INSTITUTE OF TECHNOLOGY

Traffic congestions is causing poor road traffic performance that has negative impacts on economic productivity, environmental quality, and safety. Earlier these kinds of problems were usually addressed through development of new infrastructure however, building new transportation networks is neither an advantage in terms of cost nor it is a sustainable solution. Therefore, it is required to use the existing road network in an optimized manner, together with a shift towards sustainability. For doing so, one of the several challenges is to provide accurate information about current traffic state (flow q, density k, speed v). Understanding the current traffic flow characteristics provides essential input for design, planning, operations, traffic management and control, and information provision for route choice guidance.

Traffic state variables are vital for traffic control and operations however, obtaining these parameters simultaneously is difficult as they are not measured everywhere due to the associated financial and technological limitations. On this account, the process of inferencing these variables on a road segment at certain spatiotemporal resolution using partially observed traffic data is referred to as traffic state estimation (TSE).

The Fundamental diagram (FD) describes the empirical relationship between traffic states and contains remarkable information about traffic characteristics. Hence, sound mathematical models that better represent the FD prepare a solid foundation for traffic flow analysis and efficient traffic control. Researchers have been examining simple and low computational FDs that can sufficiently describe the traffic dynamics. Once it is known, all that is needed for TSE is to locate where the

system is on the FD at any desired moment. These allow in describing the evolution of traffic dynamics and lead to smart solutions to optimize the existing traffic system.

The aim of this dissertation is to systematically analyze various existing FDs and develop a physical model-based TSE method by utilizing data assimilation (DA) framework. This dissertation consists of seven chapters. In chapter 1, the background, objectives, and outline of the thesis are introduced. Chapter 2 summarizes the literature review on fundamentals and traffic state variables, FD and TSE and discusses the scope of the doctoral research. Chapter 3 discusses about the traffic data collection methodologies, the complete trajectory data utilized for this research namely, Zen Traffic Data (ZTD) and advantages associated with utilizing ZTD over other high-tech trajectory datasets. Moving on, in this research towards analysis and modeling of FDs and TSE methods, three main objectives are introduced.

Chapter 4 describes the first objective of this dissertation which contributes to the empirical analysis of various existing speed-density ($v - k$) FDs by estimating and studying their parameters at varying spatiotemporal resolutions using ZTD, followed by a theoretical investigation with respect to the stationarity and continuity of traffic flow. The objective is twofold: first, to identify a model a.) with less complex form; b.) based on '*weaker*' assumptions; c.) reasonably achieves mathematical elegance and empirical accuracy, which are all desirable to have; and second, to make the validation more reliable by conducting it over various space-time resolutions which provides theoretical and practical support to practitioners in decisively choosing most workable FD at a particular resolution.

Over past decades, researchers have also contributed to development of several TSE methods using probe vehicle data including ones that don't rely on any '*strong*' assumptions, such as explicit priori knowledge of traffic dynamics like FD, or historic data, which renders the method robust against uncertain traffic phenomena. However, their estimation capabilities have not been validated using high-resolution, complete trajectory data with wide coverage. Chapter 5 elaborates the second objective of this dissertation that contributes to the analysis of a '*weaker*' assumption-based TSE method (proposed by Seo *et al.*, (2015b)) at different spatiotemporal resolutions and probe penetration rates using ZTD.

The third objective of this dissertation contributes to the development and implementation of a physical model-based TSE method and is described in chapter 6. To improve the estimation capability at fine space-time resolution, using fewer probe vehicles, in both the regimes, free-flow

and congested, and in complete space-time domain, it extends the '*weaker*' assumption-based approach to estimate the traffic state more accurately by utilizing a DA framework. In it, the state variable, density k, is estimated by first, simulating the k obtained from a physical model (Cell Transmission Model) which are then integrated with the observed traffic states (k and v from probe data) using Ensemble Kalman Filtering technique. In addition, the parameters of physical model are obtained by automatic calibration of a triangular FD. The results from this adaptive calibration and estimation show that the accuracy of estimating the traffic state using this approach increases and the estimated k corresponds well with the k computed using Edie's generalized definitions (Edie, 1963) and 100% trajectory data (ground truth).

In chapter 7, conclusions, achievements, and future research directions are summarized.

TABLE OF CONTENTS

LIST OF NOTATIONS

Following notations are used throughout in the dissertation unless specified otherwise.

a, θ_1:	Scalar parameter
A:	Space-time region or cell
$A_{T,X}$:	Rectangular spatiotemporal area of a cell A in a space-time mesh
Ave:	Mean of vehicles' speed (m/s)
$a_n(A)$:	Spatiotemporal area between a vehicle n and its leading vehicle within A
$a_n(A_{T,X})$:	Spatiotemporal area between a probe n and its leading vehicle in $A_{T,X}$
$|A|$:	Area of space-time region A
C_j:	Kinematic wave speed at jam density (m/s)
c%:	Covering percentage
$d(A)$:	Distance travelled by all the vehicles in space-time region A
$d_n(A)$:	Distance travelled by vehicle n in space-time region A
det:	Matrix determinant
F:	Function representing triangular FD
f_i:	Total flow leaving cell i to off-ramp
f_t:	System model
g:	Cost based objective function
g^1:	Objective function calculated using initial feasible solution
h:	Time headway (s)
h_{av}:	Average time headway (s)
h_m:	Average headway of vehicle m in a cell
$h_{m,\tau}$:	Headway of vehicle m at time τ in a cell
h_t:	Observation model
H_t:	Matrix constructed based on locations where measurements are acquired
i, j:	Non-negative indices
k:	Density (veh/m)

$k(A)$:	Density in a space-time region A (veh/m)
k_c:	Critical density (veh/m)
$k_d(t)$:	Measured downstream boundary density at time index t (veh/m)
$k_i(t)$:	Density for cell i at time index t (veh/m)
k_J or k_j:	Jam density (veh/m)
k_m:	Optimum density (veh/m)
k_t:	Inflection point where the $q - k$ curve turns from free-flow to congested
$k_u(t)$:	Measured upstream boundary density at time index t (veh/m)
$k.p.$:	Kilopost
$k(x,t)$:	Density at a location x and time t
$\hat{k}_i(t)$:	Measured density of cell i at time index t (veh/m)
l:	Ensemble index
l_i:	Length of cell i (m)
M:	Total number of ensembles for EnKF
m, n:	Shape parameters representing environment and type of facility
n_t:	Number of vehicles passing a particular point in a defined time t
n_x:	Number of vehicles on a roadway of length x at a given instance of time
η_t:	Observation noise
$\eta^{density}$:	Error model for density
$\eta^{velocity}$:	Error model for velocity
$N(A)$:	Set of all vehicles in space-time region (cell) A
$\mathcal{N}$:	Normal distribution
O_i:	Empirically observed data
P_i or E_i:	Value estimated by the model
$P(A)$:	Set of all probe vehicles in space-time region (cell) A
p%:	Probe penetration rate
$p(x_t \vert z_1,..,z_t)$:	Most probable state
q:	Flow (veh/s)
$q(A)$:	Flow (veh/s) in a space-time region A (s)
$q_d(t)$:	Measured downstream boundary flow at time index t (veh/s)

$q_i(t)$:	Total flow entering cell i during time interval $[t\Delta t, (t+1)\Delta t)$ (veh/s)
$q_i(t+1)$:	Total flow leaving cell i during time interval $[t\Delta t, (t+1)\Delta t)$ (veh/s)
$q_u(t)$:	Measured upstream boundary flow at time index t (veh/s)
Q_M:	Maximum allowable flow (veh/s)
R_i:	Space-time region
r_i:	Total flow entering cell i from on-ramp
s:	Space headway (m)
s_{av}:	Average space headway (m)
s_m:	Average spacing of vehicle m in a cell
$s_{m,\tau}$:	Spacing of vehicle m at time τ in a cell
t:	Time
$t(A)$:	Time spent by all vehicles in a space-time region A (s)
$t_n(A)$:	Time spent by vehicle n in space-time region A
(t_0, x_0):	Coordinates of the predetermined origin
(t_i, x_i):	Coordinate of vehicle's position (on its trajectory) in a space-time domain
(t_i, x_j):	Co-ordinates of the upper-left corner of region A_i^j
$t-1\|t$:	Subindex denoting the prior of a variable
$t\|t$:	Subindex denoting the posterior of a variable
v:	Velocity (m/s)
$v(A)$:	Velocity (veh/s) in a space-time region A (s)
v_b:	Average travel speed at saturation region (m/s)
v_f:	Free-flow speed (m/s)
v_i:	Spot speed (m/s)
v_m:	Optimum speed (m/s)
v_s:	Space mean speed (m/s)
v_t:	Time mean speed (m/s)
ϑ:	Coefficient of variation
w_c:	Backward congestion wave speed (m/s)
ω_t:	System noise
x:	Space

x: Vector of all decision variables

x^1: Initial feasible solution (FD parameters)

x^*: Optimal solution

x_i: Decision variable

x_t: State vector

z_t: Observation vector

λ: Proportionality factor

θ, E: Shape parameters

θ_2: Lopsidedness of the curve

σ: Standard deviation

δ: Percent error

ε_1: Tolerance for optimization problem

$Iter_m$: Maximum iteration number

Δx or dx: Spatial resolution

Δt or dt: Temporal resolution

$\Delta \tau$: Small time duration

LIST OF ABBREVIATIONS

Following abbreviations are used throughout in the dissertation.

AC:	Automatic calibration
ADAS:	Advanced driving assistance systems
ARE:	Average relative error
ATIS:	Advanced traveler information system
ATM:	Active traffic management
AVI:	Automatic vehicle identification
AVL:	Automatic vehicle location
BVP:	Boundary value problem
CDR:	Call-details record
CFL:	Courant–Friedrichs–Lewy
CL:	Conservation law
CTM:	Cell transmission model
DA:	Data assimilation
DLS:	Damped least-squares
DRG:	Dynamic route guidance
EKF:	Extended Kalman filter
EnKF:	Ensemble Kalman filter
FCD:	Floating car data
FCM:	Fuzzy c-means
FD:	Fundamental diagram
FIFO:	First-in first-out
GNA:	Gauss–Newton algorithm
GPS:	Global positioning system
ICT:	Information and communication technology
IDL:	Inductive detector loops
IT:	Information technology

ITS:	Intelligent transport systems
KF:	Kalman filter
KFT:	Kalman filtering technique
kNN:	k-Nearest neighbors
KR:	Kernel regression
LM or LMA:	Levenberg–Marquardt optimization algorithm
LS:	Least-square
LWR:	Lighthill–Whitham–Richards
MAE:	Mean absolute error
MAPE:	Mean absolute percentage error
MB:	Mean bias
MFD:	Macroscopic fundamental diagram
ML:	Machine learning
NLP:	Nonlinear programming
OBD–II:	Second generation n–board diagnostics systems
PDE:	Partial differential equation
PF:	Particle filter
RFID:	Radio-frequency identification
RMSE:	Root mean square error
SQP:	Sequential quadratic programming
TS:	Traffic state
TSE:	Traffic state estimation
TTM:	Travel time transition
UKF:	Unscented Kalman filter
VID:	Video image detection
V2X:	Vehicle-to-everything
WIM:	Weigh-in-motion
$xFCD$:	Extended-floating car data
ZTD:	Zen traffic data
πNEUMA:	New era of urban traffic monitoring with aerial footage

LIST OF TABLES

LIST OF FIGURES

xviii

1 INTRODUCTION

1.1 Background

Traffic engineering pertains to the analysis of traffic behavior and to design transportations networks and infrastructures for a safe, smooth, and economical operations of traffic (NPTEL, 2012). Traffic engineers conduct studies related to traffic volume to keep the efficiency of a transportation system high. However, with a continuous increase in population, the demand for mobility is constantly increasing and traffic problems are emerging in all large cities. The vehicular traffic is tremendously increasing resulting in increased congestion. Traffic congestion is causing poor traffic performance that has negative impacts on economic productivity, environmental quality and safety through higher fuel consumption, increased costs of goods and services, delays, increased air pollution, and worsened safety conditions (Sutandi, 2007). Earlier these kinds of problems were usually addressed through increased capacity by developing new infrastructure to increase the number of existing transportation systems however, building new transportation networks is not a feasible solution (Hills, 1996; Goodwin, 1996; Litman, 2004). It is neither an advantage in terms of cost nor it is a sustainable solution. Therefore, it is required to use the existing road network in an optimized manner, together with a shift towards sustainability.

It requires development of alternatives that increase the capacity through improved efficiency of existing systems that focuses on building fewer lane-miles, while investigating Intelligent Transport Systems (ITS). To reduce congestion and optimize the existing traffic systems, it is vital to study and explore smart solutions and one of the several challenges is to provide accurate information about current and future traffic state. Understanding the current traffic flow characteristics provides essential input for design, strategic transportation planning such as infrastructure improvements, operations, traffic management and control such as ramp metering, variable speed limit, pricing, and information provision for route choice guidance that can be used to influence the choices made by travelers. Nevertheless, accurate information about the traffic

1

state is crucial to establish a successful traffic control strategy and will help traffic managers in taking actions before the system reaches the state of congestion.

1.2   Research objectives and contribution

On a roadway link, at a macroscopic level, traffic can be represented by the three fundamental parameters of traffic flow namely, Flow (q), which is the number of vehicles that pass a given point per unit time; Density (k), which is the number of vehicles per unit length of a roadway at a given instance of time; and Speed (v), which is the mean of the instantaneous speeds among vehicles. Flow and speed are also known as volume and velocity, respectively. A subset of (q, k, v) is known as *traffic state*. By combining all possible steady traffic states (*equilibrium or stationary traffic*) in an equilibrium function, the *Fundamental diagram* (FD) is obtained which describes the empirical relationship between traffic states and can be graphically described using three two-dimensional diagrams namely, speed-density $(v - k)$ relation, flow-density $(q - k)$ relation, and speed-flow $(v - q)$ relation. The FD has been the foundation of traffic flow theory and transportation engineering for many years as it contains remarkable information about traffic flow characteristics. Based on prevailing traffic conditions, that information can assist active traffic management (ATM) in alleviating congestion by accessing network dynamics accurately such as when and where congestion builds and how it dispatches. It plays a crucial role for traffic control and assignment, predicting the capability of road system, or predict its behavior when applying inflow regulations and speed limits. Hence, sound mathematical models that better represent the FD prepare a solid foundation for traffic flow analysis and efficient traffic control. Researchers have been examining simple and fast, in terms of computational cost, FDs that can sufficiently describe the dynamics of a roadway. Once it is known, all that is needed to have a traffic state estimate is to locate where the system is on the FD at any desired moment. These allow in describing the evolution of traffic dynamics and lead to smart solutions to optimize the existing traffic system.

Traffic state variables are vital for traffic control and operations however, obtaining these parameters simultaneously is difficult as they are not measured everywhere due to the associated financial and technological limitations. Traditionally, traffic conditions were monitored by conventional fixed-location sensors such as inductive loop detectors and ultrasonic detectors, but

due to the recent advancements in information and communication technologies (ICTs), the collection of traffic data is gradually shifting to more mobile sensor-based data collection. Vehicles with sensors such as on-vehicle Global Positioning System (GPS) devices and call-details records (CDRs) are often referred to as probe vehicles or floating cars. Unlike fixed-point data which have multiple demerits associated to them such as unreliability of accuracy and precision, frequent misses or double counting, high operational costs and insufficiency of data, the probe vehicles can cover wide spatiotemporal domain and collect vast amount of trajectory data with much more detailed and rich information. On this account, the process of inferencing the traffic state variables on a road segment with high spatiotemporal resolution using partially observed traffic data is referred to as *Traffic State Estimation* (TSE). In this research towards analysis and modeling of FDs and TSE methods, *three* objectives are introduced.

Objective 1: *First objective of this dissertation is to contribute to the empirical analysis of various existing speed-density ($v - k$) fundamental diagrams by estimating and studying their parameters at varying spatiotemporal resolutions using complete vehicles' trajectory data followed by a theoretical investigation with respect to the stationarity and continuity of traffic flow.*

The objective is twofold: first, to identify a model a.) with less complex form; b.) based on 'weaker' assumptions; c.) reasonably achieves mathematical elegance and empirical accuracy, which are all desirable to have; and second, to make the validation more reliable by conducting it over various space-time resolutions which provides theoretical and practical support to practitioners in decisively choosing most workable FD at a particular resolution. In the past, several studies have contributed to similar analysis however, in some of them the investigation was carried out either only with sampled or aggregated datasets or complete data with limited coverage, and a few of them included only the empirical analysis and the mathematical discussion on the stationarity and continuity was not included. Moreover, none of the previous studies have analyzed the model performance and application conditions with respect to the space-time resolution, in addition with a focus on simple (less complex and compact natured), less parameterized, 'weaker' assumption-based $v - k$ model. As an effort of such a pursuit, the objective is to identify such a $v - k$ relation which are empirically accurate and mathematically elegant and, are easy to handle for practitioners working with extensive traffic data. This study

will assist in understanding the fundamentals of traffic dynamics in detail and with more accuracy, at different space-time resolutions. Using such detailed empirical evidence, it is feasible to predict congestion and its propagation, and mutual relationship between change in level of services and traffic volume.

Objective 2: The second objective of this dissertation contributes to the analysis of a 'weaker' assumption and extended floating car data ($xFCD$)-based TSE method (proposed by Seo et al., (2015b)).

Over past decades, researchers have contributed to development of several TSE methods using probe vehicle data including ones that do not reply on '*strong*' assumptions, such as explicit a priori knowledge of traffic dynamics or historic data, which renders the method robust against uncertain traffic phenomena. However, their estimation capabilities have not been validated using vehicles' high-resolution, complete, and detailed trajectory data with high space-time coverage. The analysis of the estimation capability of the method using real world complete trajectory data is vital and essential because the method does not rely on '*strong*' assumptions, rather is based on '*weaker*' assumptions, which are preferable for practical applications. Moreover, at an age of near ubiquitous sensor (e.g., cell phone) penetration, and with the massive emergence of connected vehicles, the TSE methods based on '*weaker*' assumptions might become prevalent in the near future for transportation planning purposes. Like the pursuit of the first objective to identify a model based on '*weaker*' assumptions, which are preferable for practical applications, the motivation, here, is to analyze the validity of this TSE method at different settings: temporal resolution, spatial resolution, and probe penetration rate, using high-resolution complete trajectory data.

Objective 3: The third objective of this doctoral research is to contribute to the development and implementation of a physical model-based method for traffic state estimation and to facilitate an adaptation of the model to the conditions of highways and roadway links.

Continuing to the above discussion, to be able to retrieve much accurate traffic state estimates in complete spatiotemporal domain (including unobserved cells i.e., cells via which no probe

vehicle traversed) at high space-time resolution by utilizing fewer probe vehicles in both the regimes, congested and non-congested, is always desirable. Hence, with a focus on such requirements, the third objective of this doctoral research is to contribute to the development and implementation of a physical model-based method for traffic state estimation and to facilitate an adaptation of the model to the conditions of highways and roadway links. To improve the estimation capability at fine space-time resolution, using fewer probe vehicles, in both the regimes, free-flow and congested, and in complete space-time domain, it extended the '*weaker*' assumption-based approach to estimate the traffic state more accurately by utilizing a data assimilation (DA) framework and probe vehicles' data. The hypothesis is that utilization of DA techniques in formulating a model-based TSE method shall provide more accurate estimates under the discussed requirements. In it, the state variable, density (k), is estimated by simulating the k obtained from a physical model (Cell Transmission Model: CTM) (Daganzo, 1994) which are then integrated (fused) with the observed traffic states (k and v) using Ensemble Kalman Filtering (EnKF) technique. As per literature review, several other studies have utilized the KFTs for estimating the traffic states. However, it is clear that numerous proposed TSE methodologies have either been mostly validated through microscopic or macroscopic simulations and not complete (100% vehicles') real traffic data, experimental data or rarely utilized real traffic data with small spatiotemporal coverage. The nature of the past studies differs from the study related to third objective in terms of calibration methods of the FD, the choice of traffic flow model, the kind of data assimilation technique used to estimate the state variable, and as mentioned before, whether the estimation capability of the method was validated with real traffic data. In addition, the parameters of physical model are obtained by automatic calibration (AC) of a triangular FD which involves solving the SQP to minimize the discrepancy between the simulated traffic density and observed traffic density by probe vehicles at every time step. It renders the TSE method to be more robust by adapting to the dynamics of traffic data. The results from the calibration and estimation show that the accuracy of estimating the traffic state using this approach increases and the estimated k corresponds well with the k computed using Edie's generalized definitions (Edie, 1963) and 100% trajectory data (ground truth).

Utilization of Zen Traffic Data: The underlying advantage of contributions made through this research to the vast literature of transportation engineering lies in the utilization of a high-tech,

high-resolution, detailed, and complete trajectory data namely, Zen Traffic Data (ZTD), provided by Hanshin Expressway Co. Ltd. The massive ZTD sets can be considered appropriate for traffic studies that involve TSE and can also give meaning to validation of physical models that are not solely data driven (Dahiya *et al.*, 2022). A major part of the motivation for this doctoral research also comes from the fact that ZTD has extreme potential in the evaluation of classical concepts in the fundamental theory of traffic flow, traffic flow models, functional forms of FDs, traffic state estimation methods, several of which have been developed and proposed by researchers over past decades, some based on theoretical assumptions and others driven by data, and have not been evaluated or validated with complete trajectory data (ground truth) to verify their capabilities. In addition, ZTD can be utilized in formulation and evaluation of new traffic state estimation methods which can possibly estimate TS at high spatiotemporal resolutions and complete space-time domain. One of the practical outcomes of utilizing ZTD is the retrieval of detailed information for making better informed decisions.

In fact, these are the principal postulates that motivates the studies carried out as per the research plan of this thesis. It is within the context that information technology (IT) and traffic blend together to create ITS. In summary, this thesis studies analysis and modeling of FDs and TSE methods using complete trajectory data: ZTD. We expect the analyses and the devised TSE method to be utilized and implemented in real-world traffic design, management, and control to mitigate traffic issues, congestion being the major one.

1.3   Outline of the dissertation

The aim of this dissertation is to systematically analyze various existing FDs and develop a physical model-based TSE method by utilizing data assimilation (DA) framework. This dissertation consists of seven chapters and the structure of the thesis can be visualized in Figure 1.1. In this chapter, the background, objectives, and outline of the thesis are introduced. Chapter 2 summarizes the literature review on fundamentals and traffic state variables, FD and TSE and discusses the scope of the doctoral research. Chapter 3 discusses about the traffic data collection methodologies, the complete trajectory data utilized for this research namely, Zen Traffic Data (ZTD) and advantages associated with utilizing ZTD over other high-tech trajectory datasets.

Chapter 4 describes the first objective of this dissertation which contributes to the empirical analysis of various existing speed-density $(v - k)$ FDs by estimating and studying their parameters at varying spatiotemporal resolutions using ZTD followed by a theoretical investigation with respect to the stationarity and continuity of traffic flow. Chapter 5 elaborates the second objective of this dissertation that contributes to the analysis of a '*weaker*' assumption and extended floating car data $(xFCD)$-based TSE method at different spatiotemporal resolutions and probe penetration rates using ZTD. The third objective of this dissertation contributes to the development and implementation of a physical model-based TSE method using DA framework and complete trajectory dataset. It is described in chapter 6. In chapter 7, conclusions, achievements, and future research directions are summarized.

Chapter 1: Background, objectives and outlines of the dissertation

Chapter 2: Literature review

Chapter 3: Traffic data collection methodologies and Zen Traffic Data (ZTD)

Chapter 4: Analysis of the single-regime speed-density fundamental relationships for varying spatiotemporal resolutions using ZTD

Chapter 5: Exploring the performace of xFCD-based traffic state estimation (TSE) method using complete trajectory data

Chapter 6: Adaptive approach to automatically calibrate the FD and TSE using model-based method with data assimilation (DA) framework

Chapter 7: Conclusions, achievements and future research directions

Figure 1.1 Structure of thesis

1.4   Conferences and publications

Dahiya, G., Asakura, Y., & Nakanishi, W. (2020). A study of speed-density functional relations for varying spatiotemporal resolution using Zen Traffic Data. *2020 IEEE 23rd International Conference on Intelligent Transportation Systems (ITSC)*. (pp. 1–8). Rhodes, Greece.

Dahiya, G., & Asakura, Y. (2020). Evaluation of probe vehicle-based traffic states estimation method using Zen Traffic Data. *18th International Transport System (ITS) Symposium*. Matsuyama, Japan.

Dahiya, G., & Asakura, Y. (2021). Exploring the performance of streaming-data-driven traffic state estimation method using complete trajectory data. *International Journal of Intelligent Transportation Systems Research , 19*, 572–586.

Dahiya, G., Asakura, Y., & Nakanishi, W. (2021). Analysis of single-regime speed-density fundamental relationships for varying spatiotemporal resolution using Zen Traffic Data. *The 14th International Conference of Eastern Asia Society for Transportation Studies (EASTS)*. Hiroshima, Japan.

Dahiya, G., Asakura, Y., & Nakanishi, W. (2022). Analysis of the single-regime speed-density fundamental relationships for varying spatiotemporal resolution using Zen Traffic Data. *Asian Transport Studies, 8*, 2185–5560.

Dahiya, G., Seo, T., & Asakura, Y. An adaptive approach to automatically calibrate fundamental diagram and estimate traffic state through a data assimilation framework. *Transportation Research Part B: Methodological*. (To be submitted)

2 LITERATURE REVIEW

2.1 Traffic state

This section summarizes basic concepts and traffic state variables which are a fundamental part of the Traffic Flow Theory.

2.1.1 Introduction

The stream of traffic consists of a combination of driver behavior and vehicle behavior which are both non-uniform in nature. Traffic is influenced by the individual characteristics of the vehicle, the human beings, and their interactions with each other. Therefore, the flow of traffic changes with location and time corresponding to the variation in human behavior. However, for the purpose of design and planning, traffic engineers assume that these changes are within certain range and traffic stream involves some parameters based on which its characteristics can be predictable.
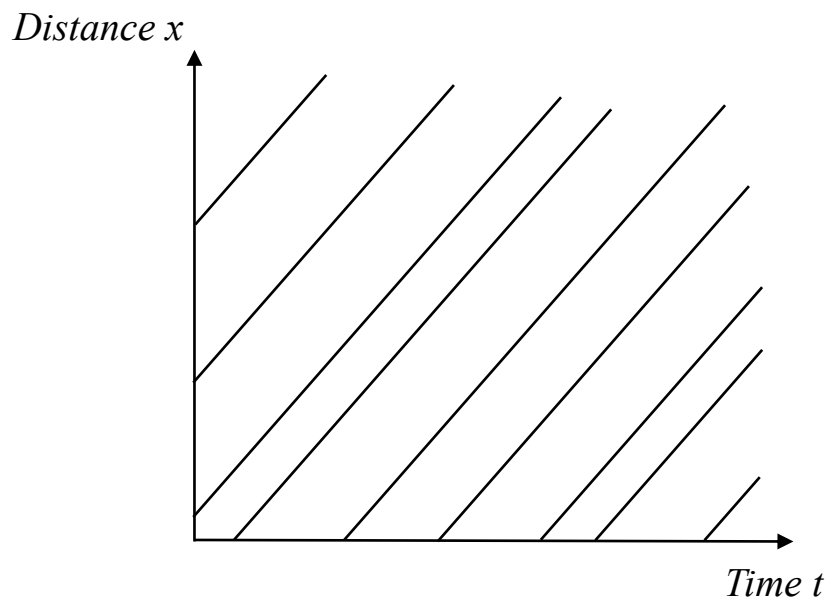
Figure 2.1 Space-time diagram

These parameters can be macroscopic which characterize the traffic as a whole, or microscopic that studies the behavior of individual vehicles with respect to each other in a traffic stream. While the microscopic parameters include the measurement of separation between the vehicles i.e., the headway which can be either time headway or spacing headway, the macroscopic parameters are also the fundamental parameters of traffic flow which are density, flow, and speed.

The position of a moving vehicle on a distance of x and in time interval t can be represented by a coordinate in space-time (t, x) plane where x will be a function of t along the road stretch. These coordinates generate a graph that gives the relation of the vehicle's position on the road stretch relative to time and this graphical representation of $x(t)$ is known as a *trajectory*. It provides an intuitive, clear, and complete summary of vehicular motion in one dimension. Space-time diagram, as shown in Figure 2.1, is a 2D plot and is a convenient tool in understanding the motion of a vehicle or multiple vehicles. Its analysis can assist in determining the fundamental parameters of traffic flow like $q, k \; and \; v$ and other derived characteristics such as headway and spacing.

2.1.2   Traffic state variables

Traffic flow has several parameters associated with it that provide information regarding the nature of traffic flow and help analysts in determining any variation in the traffic flow characteristics. A thorough knowledge of traffic stream parameters and their mutual relationships is required to understand the traffic behavior. Density, flow, and average speed (or simply speed, also known as velocity) are the three fundamental parameters of traffic flow. They provide information regarding the nature of traffic on a link at a macroscopic level and aid analysts in detecting any variation in the flow characteristics, which in turn aids in traffic operations and planning. The flow (q), also known as the flow rate or volume by practitioners, is the number of vehicles that pass a given point per unit time. The density (k) is the number of vehicles per unit space at a given instance of time. The average speed (v) is the mean of the instantaneous speeds of the vehicles. Edie (1963) proposed a generalized definition of traffic states in a space-time region A, defined as follows:

$$q(\boldsymbol{A}) = \frac{d(\boldsymbol{A})}{|\boldsymbol{A}|} \qquad\qquad (2.1)$$

$$k(A) = \frac{t(A)}{|A|} \qquad\qquad (2.2)$$

$$v(A) = \frac{d(A)}{t(A)} \qquad\qquad (2.3)$$

In these equations, $d(A)$ represents total distance traveled by all the vehicles in region A $(veh\ m)$, $t(A)$ is total time all the vehicles spent in region A $(veh\ s)$, and $|A|$ depicts the space-time area of region A $(m\ s)$. These definitions can be applied to either a single lane or multiple lanes in a link.

2.1.2.1   Flow

The flow (or volume q) is the number of vehicles that pass a given point on roadway during a specific time interval. The measurement is carried out by counting the number of vehicles, n_t, passing a particular point in a defined time t.

$$q = \frac{n_t}{t} \qquad\qquad (2.4)$$

Conventionally, flow is measured by manual counting, detector/sensor, moving-car observer method etc. Flow is treated as an important parameters of traffic flow as it assists in determining the design of a highway and the related facilities by establishing the importance of a particular route with respect to other routes, distribution of traffic on road, and the fluctuations in flow. Figure 2.2 illustrates the flow q on a space-time domain computed using real traffic trajectory data and Edie's generalized definition.

2.1.2.2   Density

The density (k) is defined as the number of vehicles occupying a given length of a roadway at a given instance of time and can be expressed as follows:

$$k = \frac{n_x}{x}$$

(2.5)

where, k represents the density and n_x is the number of vehicles on a roadway of length x at a given instance of time. Density (k) is the measure most directly related to the traffic demand, and it measures the proximity of vehicles in the traffic stream. Figure 2.3 illustrates the density k on a space-time domain computed using real traffic trajectory data and Edie's generalized definition.
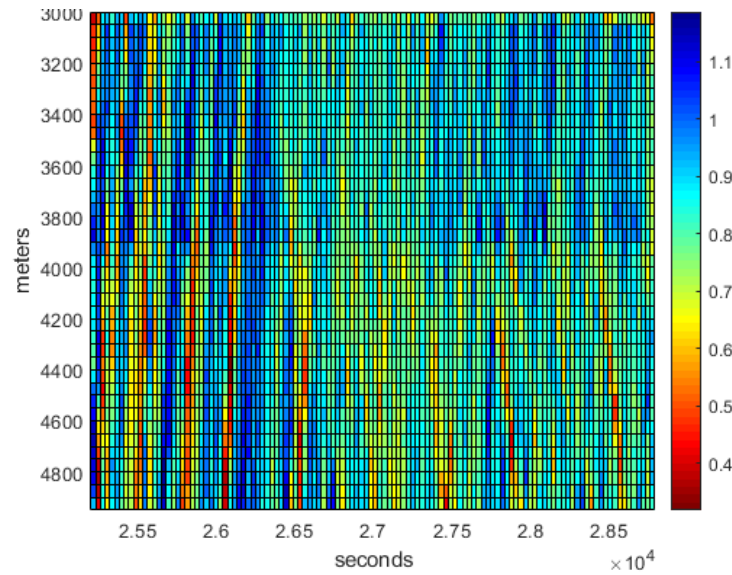
Figure 2.2 Flow q (veh/s) in a spatiotemporal mesh
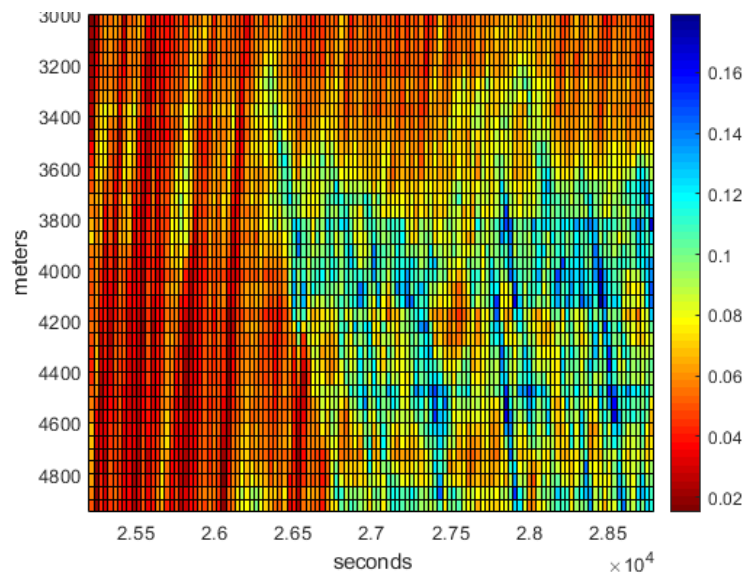
Figure 2.3 Density k (veh/m) in a spatiotemporal mesh

2.1.2.3   Speed

Speed (or velocity v) is defined as the rate of motion in distance per unit of time and can be considered as a quality measurement of travel because drivers and passengers are usually concerned about the speed of the journey than the design aspect of the transportation network. It can be mathematically represented as:

$$v = \frac{d}{t}$$

(2.6)

where, v (in m/s) is the speed of vehicle, d (in m) is the distance travelled in time t (in s). Figure 2.4 illustrates the speed v on a space-time domain computed using real traffic trajectory data and Edie's generalized definition.
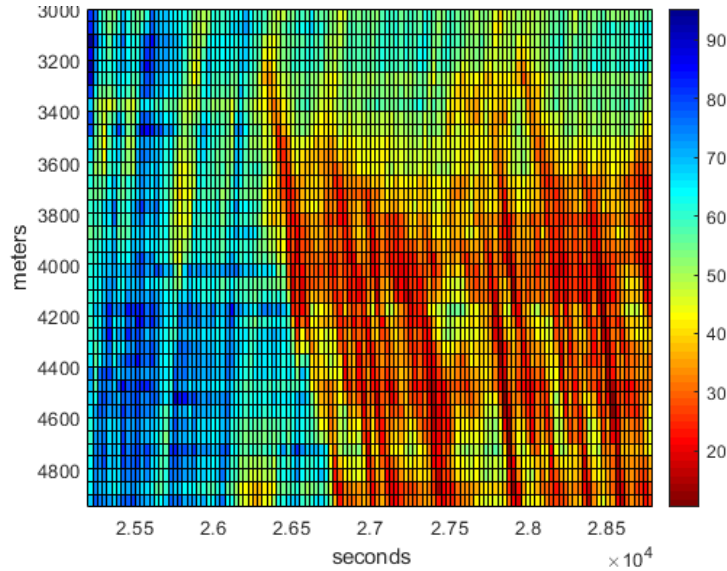
Figure 2.4 Velocity v (m/s) (or speed) in a spatiotemporal mesh

In practice, several types of speed are utilized such as spot speed, running speed, journey speed, time mean speed and space mean speed.

1. **Spot speed**: It is the instantaneous speed of a vehicle at a specific location and is utilized for designing the geometry of road, location, design and size of traffic signs, safe speed and speed zone, accident analysis, and road maintenance.

13

2. **Running speed**: It is the average speed of a vehicle maintained over a particular course of time while the vehicle is in motion i.e., it does not consider the time while the vehicle was not in motion.

3. **Journey speed**: It is the effective speed of a vehicle between two points including the time when the vehicle was not in motion. The journey speed is always less or equal to the running speed and in case it is less, it indicates that the journey included stop–go motions with enforced acceleration and deceleration.

4. **Time mean speed (v_t)**: It is the average of the speeds of all vehicles passing a particular point on a roadway and is a simple average of spot speeds denoted by:

$$v_t = \frac{1}{n} \sum_{i=1}^{n} v_i \qquad (2.7)$$

where, v_i is the spot speed of ith vehicle, and n is the number of observations.

5. **Space mean speed**: It is the average speed of all the vehicles occupying a given section of a roadway at a given instance of time. Let v_i be the spot speed of ith vehicle and t_i be the time the vehicle takes to travel unit distance and is thus, given by $\frac{1}{v_i}$. If there are n such vehicles, then the average travel time t_s is given by:

$$t_s = \frac{\sum t_i}{n} = \frac{1}{n} \sum \frac{1}{v_i} \qquad (2.8)$$

and the average speed v_s is given by:

$$v_s = \frac{n}{\sum_{i=1}^{n} \frac{1}{v_i}} \qquad (2.9)$$

14

2.1.3   Derived characteristics

A few other significant parameters of traffic flow viz., time headway and distance headway, can be derived from the fundamental parameters of traffic flow and can be visualized in Figure 2.5.

1. **Time headway**: It is a microscopic characteristic related to the traffic flow and time headway or simply headway is the time difference between the passage of two successive vehicles (two consecutive rear bumpers) as they cross a given point. On a space-time diagram, the horizontal gap between any two trajectories, representing the motion of vehicles, is basically the time headway. Flow (q) is the number of vehicles n_t measured in a time interval t and if all headways h during this time are added then,

$$\sum_{1}^{n_t} h_i = t \qquad\qquad (2.10)$$

$$q = \frac{n_t}{t} = \frac{n_t}{\sum_1^{n_t} h_i} = \frac{1}{h_{av}} \qquad\qquad (2.11)$$

   where, h_{av} is the average headway and is the inverse of the flow.

2. **Distance headway**: It is the distance between corresponding points of two successive vehicles at any given instance of time, for example the distance from the rear bumper of a leading vehicle to rear bumper of the following vehicle at a given point of time. On a space-time diagram, the vertical gap between any two trajectories, representing the motion of vehicles, is basically the distance headway. Density (k) is the number of vehicles n_x present on a roadway of length x at a given instance of time and if then all the space headways s are added then,

$$\sum_{1}^{n_x} s_i = x \qquad\qquad (2.12)$$

15

$$k = \frac{n_x}{x} = \frac{n_x}{\sum_1^{n_x} s_i} = \frac{1}{s_{av}}$$
(2.13)

where, s_{av} is the average distance headway and is the inverse of the density k and is sometimes also referred to a spacing.
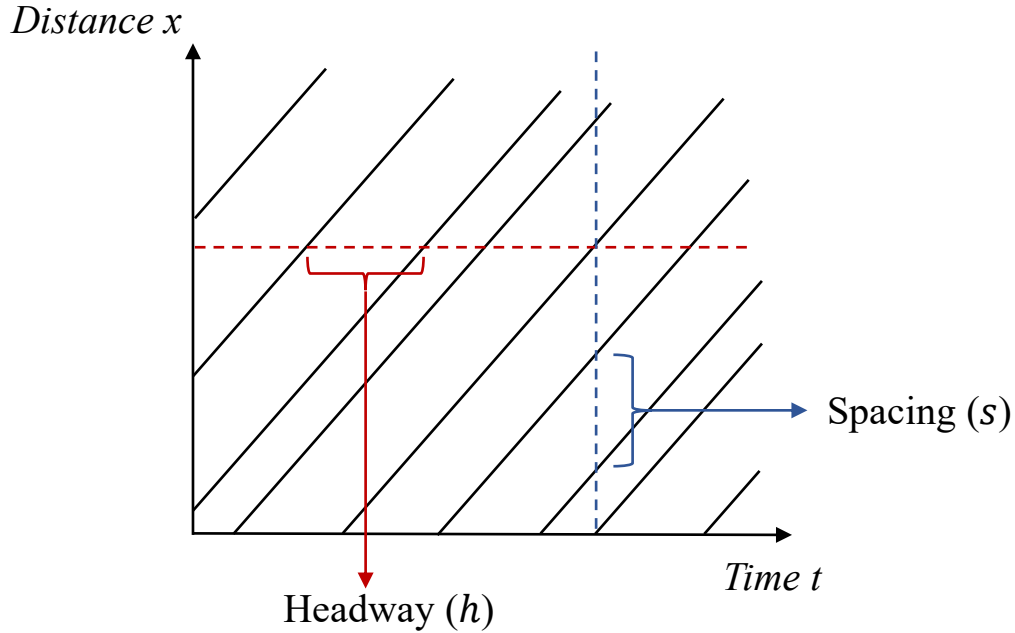
Figure 2.5 Representation of headway and spacing in a space-time diagram

2.2 Fundamental Diagram (FD)

2.2.1 Introduction and applications of FD

The relationship between the fundamental parameters of traffic flow (or traffic state variables) namely, flow q, density k and speed v, is referred to as the fundamental relation of traffic flow and the fundamental equation of traffic flow is given by:

$$q = k \times v$$
(2.14)

where, q is the flow, k is the density and v is the speed. The fundamental diagram (FD) is obtained by combining all possible steady traffic states (sometimes referred to as *equilibrium* or *stationary traffic*) in an equilibrium function that can be graphically described using three two-dimensional diagrams which are speed-density $(v - k)$ relation, flow-density $(q - k)$ relation, and the speed-flow $(v - q)$ relation. A traffic state with a density greater than critical density (k_c) is considered as congested regime and the state with density lower than or equal to k_c is referred to as free-flow regime.

1. **Flow-Density $(q - k)$ curve**: The flow q and density k vary with time and location and the relationship between flow and density is normally represented by a parabolic curve as shown in Figure 2.6. When the density is zero, the flow will also be zero since there are no vehicles on the road. As the number of vehicles gradually increases, both the density and the flow, increases. It reaches a situation where the flow becomes maximum (Q_M) and density at that point is referred to as critical density (k_c). Beyond that, when more and more vehicles add on, the flow starts to decrease and at the maximum density (also called jam density, k_J) the vehicles can't move anymore. Hence, the flow is zero because there's no motion.
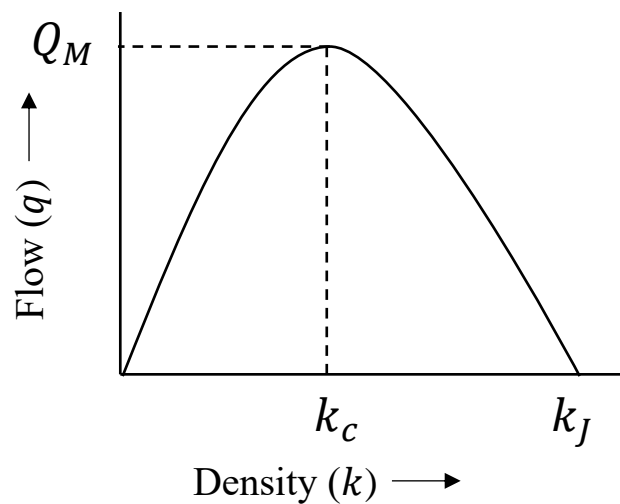
Figure 2.6 Flow-Density $(q - k)$ FD

2. **Speed-Density ($v - k$) curve**: As illustrated in Figure 2.7, the relationship between speed and density can be a weakly monotonic non-linear relation however, the simplest assumption made in literature with respect to this relationship is that speed varies linearly with density. Corresponding to the zero density, vehicles will flow at their desired speed or maximum speed which is referred to as the free-flow speed (v_f). When the density reaches to the point of jam density, the speed becomes zero.

3. **Speed-Flow ($v - q$) curve**: In the $v - q$ relation, the flow is zero either because there are no vehicles on the roadway or there are too many vehicles that they cannot move and the speed at this point is zero due to zero motion. At the maximum flow (Q_M), the speed is between zero and the free-flow speed (v_f). The same can be visualized in Figure 2.8.
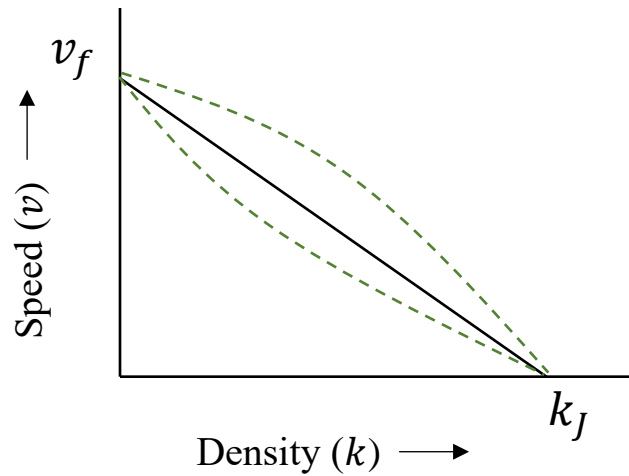
Figure 2.7 Speed-Density ($v - k$) FD
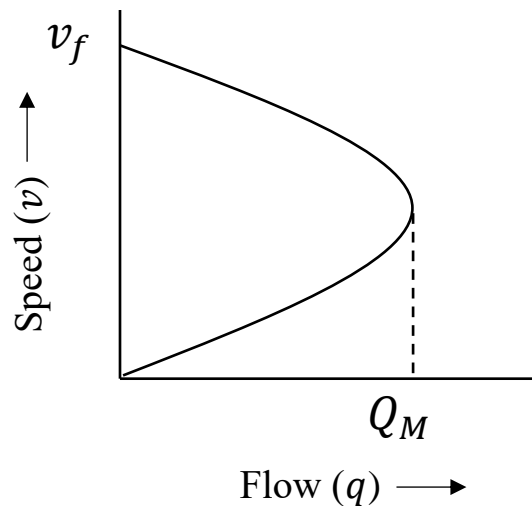
Figure 2.8 Speed-Flow ($v - q$) FD

The relationship between these fundamental relations can visualized by combing the three diagrams as shown in Figure 2.9. One of the most widely used functional form of a FD is the triangular FD (Newell, 1993) which simplifies a FD as a piecewise linear function which two lines in $q - k$ relation. The FD describes the empirical relationship between the traffic states and is a vital tool which enables analysis of fundamental relationships. The traffic states follow the fundamental diagram if the region is steady and conversely, non-steady region's traffic states will not be reflected on the FD. The necessary condition for the steadiness of a region is that the speeds of two probe vehicles of the region are time invariant and equal. Under such situation, $v = V(k)$, where V represents the speed-density $(v - k)$ FD. Based on prevailing traffic conditions, the information on the FD can assist active traffic management to alleviate congestion by accessing network traffic dynamics accurately. FD is useful for traffic assignment and developing new models for traffic operations. Now, traffic flow simulations by accurate traffic models are extremely valuable for design and evaluation of traffic surveillance and management strategies. Compared with microscopic models, macroscopic models simulate aggregated traffic behavior meanwhile, offer reliable, fast simulations, which make them suitable for integration into a real-time traffic management system. They are categorized as 1st order and 2nd order models and 1st order models are widely used in ATM systems as they're capable of capturing many important traffic phenomena in an efficient and stable manner. The FD, which represents the relation between q and k, plays a vital role in 1st order traffic models and must be calibrated before deploying the model.

Calibration of FD is to estimate its parameters accurately to maximize the model's descriptive power to reproduce traffic flow characteristics. It is, therefore, a vital research problem. In addition, the FD contains remarkable information about traffic characteristics and helps in understanding fundamentals, such as free-flow speed, maximum flow rate, critical density, and capacity (Greenshields et al., 1935), which are used for traffic control and assignment, predicting the capability of road system, or predict its behavior when applying inflow regulations and speed limits. Hence, sound mathematical models, that better represent the FD, prepare a solid foundation for traffic flow analysis and efficient traffic control. Furthermore, FD also plays a significant role in Traffic States Estimation (TSE) methods whose estimation approach is essentially model driven. On this account, it becomes important to identify sound mathematical models that better represent the FD by calibrating them with detailed traffic state information.
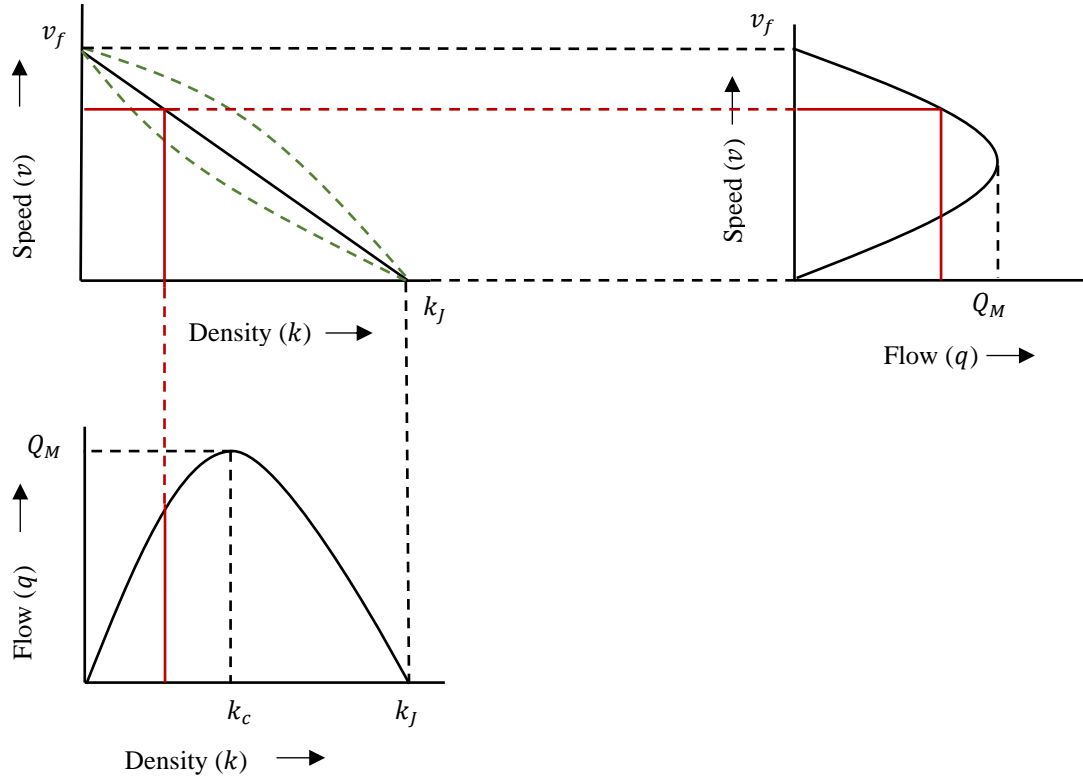
Figure 2.9 Combined FD

2.2.2 Background and literature review on FD

Among the three FDs, the speed-density $(v - k)$ relationship, first documented in Greenshields' seminal work (Greenshields *et al.*, 1935), is straightforward and easy to explain because it is a one-to-one relation between the driver behavior and the number of vehicles which are present on the road. Since then, a variety of equilibrium models have been developed with two competing goals: *mathematical elegance* and *empirical accuracy*. Some researchers have relied almost completely on the statistical analysis of data for developing functions (with no theoretical background, being based primarily on the researcher's observations), while others have begun with a purely theoretical concept, from which relationships were derived and later tested (Drake *et al.*, 1966). In the former approach, an analytical expression containing several parameters is proposed. The expressions are then calibrated based on traffic data and lastly, an interpretation of the parameters in terms of properties of traffic flow is sought. The latter approach is more phenomenological or

behavioral as it is based on assumptions about the driver behavior with respect to some traffic variables.

Although none of these two approaches should give superior results, a relation is suitable, realistic, and is considered to be accurate if it is statistically able to reproduce the empirical traffic data of the traffic stream and follows the static and dynamic properties related to the stationarity and continuity of the traffic flow which are attractive to mathematical modeling of traffic dynamics. In addition, the assumptions on the formulation of relationship can be *'weak'* or *'strong'*. An assumption is '*stronger*' if it requires validation of extensive empirical data for its justification. Relations with such kind of assumptions are developed based on the empirical observations, including shape of the curve of empirical data, and the values of model parameters which are subject of empirical observations. If the assumptions are valid, it can be extensively used, however, excessive errors can be caused if the assumptions become invalid (for example, under unpredictable or uncertain traffic conditions). Therefore, in general, it is practically preferable if the relationship is developed with '*weaker*' assumptions, i.e., requiring little prior knowledge such as assumption of linearity between traffic flow variables of density (k) and speed (v). For example, Greenshields' model is frequently used for illustrative and pedagogical purposes because it contains a simple linear equation (Wang *et al.*, 2010). Therefore, a model can be easily utilized by practitioners working with big data if it (1) reasonably achieves the two goals of mathematical elegance and empirical accuracy; (2) is primarily less complex in terms of number of parameters, which would make it easy to handle, i.e., it is a simple functional form with parameters of physical significance; (3) works over the entire density range (i.e., single-regime in one equation); and (4) is based on '*weaker*' assumptions.

Decades of extensive work of modelers since 1935, has significantly contributed to developing single-regime stream models with varying degrees of success in terms of empirical accuracy and by preserving mathematical elegance of being a single-equation form. Single-regime relationships are ones that involves a single mathematical function which is differentiable over the complete regime including free-flow regime and congested regime. In other words, a single mathematical function describes the relationship between the traffic state variables for complete regime and these relationships are continuous throughout without any break in the continuity at or around critical density. However, these models vary in their parameters, structure, and calibrating data sources, all of which impact model utility (Xu *et al.*, 2014). Eighty-five years after the seminal Greenshields

model, a variety of further improvements are also made by decomposing single-regime equations to multi-regime for better fitting leading to better empirical accuracy but reduced mathematical elegance and analytical tractability. For instance, after Edie (1961) several authors, such as Koshi *et al.* (1983) and Payne (1984), have suggested that discontinuous functions are required to properly describe the speed-density ($v - k$) dependence. However, Del Castillo and Benítez (1995) and Hall *et al.* (1986) have argued against the findings of Edie (1961) and Koshi *et al.* (1983) by stating that the data used do not necessarily correspond to equilibrium conditions and the results and the ($v - k$) curves obtained were influenced by the nature of traffic operations at the particular location of the study. Del Castillo and Benítez (1995) pointed out that the method of finding equilibrium points by Payne (1984) might be the cause of discontinuity. Also, this dissertation shares the opinion of Del Castillo and Benítez on the matter that if one assumes a discontinuous or a non-differentiable speed-density ($v - k$) curve, one rules out, beforehand, the possibility of a smooth transition regime. This also serves as an argument to support the assumption of continuity and differentiability of a mathematically elegant $v - k$ curve.

2.2.3   Literature review on analysis of $v - k$ fundamental relations and research gap

One of the first study to conduct a statistical analysis of speed-density ($v - k$) hypotheses was by Drake *et al.* (1966). However, the investigation was carried out only with sampled traffic flow characteristics captured by motion and presence detectors. Wang *et al.* (2010) and Wang *et al.* (2013) analyzed various existing multi- and single-regime $v - k$ models with varying number of parameters, including Greenshields' (Greenshields *et al.*, 1935), Greenberg's (Greenberg (1959)), Underwood's (Underwood (1961)), Northwestern's, Drew's (Drew (1968)), and Pipes–Munjal's models, and proposed the logistic model that outperformed other considered $v - k$ relationships. However, the study included only the empirical analysis of $v - k$ models, and the mathematical discussion on stationarity and continuity was not included. Moreover, the used GA 400 ITS data (containing only speed data with a temporal sampling rate of $20\ s$) was aggregated every $5\ mins$ to generate the FD. Gaddam and Rao (2019) performed a very similar analysis by considering only some of those single-regime models and including 4 more models of May and Keller (1967), Papageorgiou *et al.* (1989), Lee *et al.* (1998), and Wang *et al.* (2010). In addition to that, several

static and dynamic properties were evaluated followed by proposal of two new models, one being a modified version of Lee *et al.*'s model by introducing two more shape parameters in the functional form. Xu *et al.* (2014) summarized and analyzed ten typical $v - k$ relation models by parameter calibrations and fitting errors using field data collected by a detector. They concluded that the fitting errors were not sensitive to using different sets of field data, whereas some physically meaningful parameters, such as free-flow speed and jam density, varied widely under different sets of field data. In addition, the model fit relative errors cannot be the sole basis for judging the validity of model. Lu *et al.* (2019) investigated variable structure models with two limbs of the inverse λ-shape and compared with a few models over time at fixed location using properly aggregated next-generation simulation (US Department of Transportation, 2006) data with only a focus on saturated traffic as the data for the free-flow regime were not available. In addition, the spatial-temporal coverage of NGSIM dataset is still limited to $600\ m$ and $15\ min$.

However, none of the previous studies have analyzed the model performance and application conditions with respect to the space-time resolutions, in addition with a focus on simple, less parameterized, '*weaker*' assumption-based $v - k$ model which makes it easy for practitioners working with extensive data. As an effort of such a pursuit, one of the objectives of this doctoral research is to evaluate and study the important single-regime $v - k$ relations, and the sensitivity of the fitting errors and calibrated parameters of the considered $v - k$ forms to different space-time resolutions. The identification of the most suitable functional form at a particular space-time resolution will help in understanding the fundamentals such as maximum flow rate, critical density, free-flow speed more accurately at different space-time resolutions, which are very important to evaluate the quality of the road and road networks. It will help practitioners in decisively choosing the most workable FD at desired spatiotemporal resolution (based on the available traffic data). Using such detailed empirical evidence, it becomes feasible to predict the congestion and its propagation, and mutual relationship between change in level of services and traffic volume. Since it is meaningful to highlight the importance of the models that have high empirical accuracy, are based on simple assumptions, and are easy to handle with their noncomplex and compact nature, for practitioners with extensive traffic data in actual scenario, the goal is also to identify *such* a $v - k$ relation that pursues both, mathematical elegance, and empirical accuracy. This is done by performing a statistical analysis of different forms and their parameters at varying resolutions and highlight their mathematical properties. Most importantly, to demonstrate the models' applicable

conditions and capabilities to track empirical data using spatiotemporally detailed and complete traffic data at temporal sampling rate as fine as $0.1\ s$ (no aggregation).

2.3   Traffic State Estimation (TSE)

2.3.1   Introduction: definition, importance, and challenges

The process of the inference of traffic state variables at observed and unobserved areas on a road segment with high spatiotemporal resolution using partially observed traffic data at observed areas is referred to as *Traffic State Estimation* (TSE). It is a key component of traffic control and operations as traffic states are not measured everywhere due to technological and financial limitations. For instance, traffic control, such as ramp metering, variable speed limit, pricing, and information provision for root choice guidance, require precise traffic state information in order to mitigate congestion effectively.
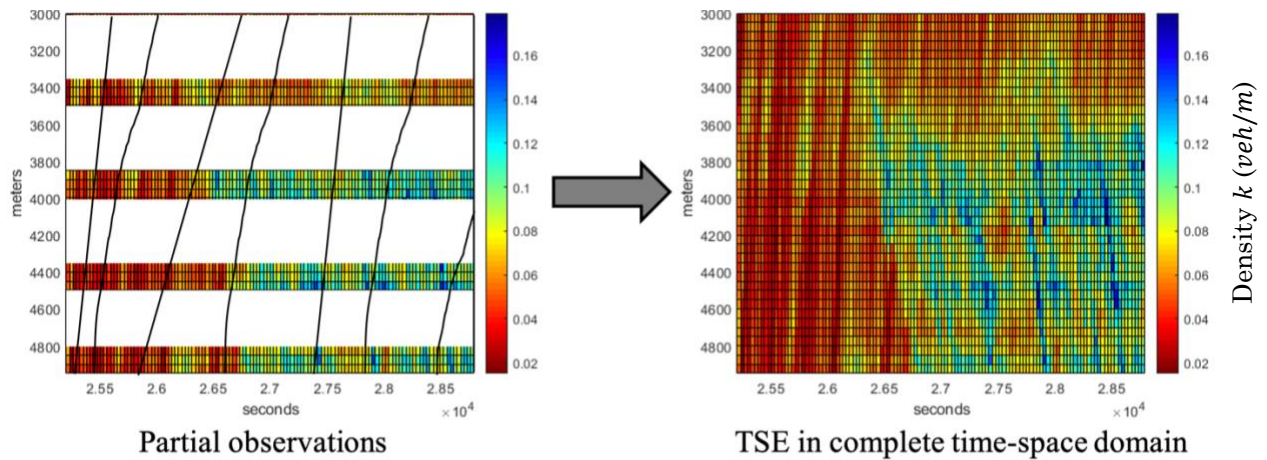
Figure 2.10 Traffic state estimation (TSE) process

Strategic transportation planning such as infrastructure improvements, road construction etc. also requires traffic state estimates because these operations and planning tasks can be greatly improved by efficient and accurate traffic estimates. Since actual traffic observations are not available everywhere and the available ones are associated with noises thus, it is required to

estimate the traffic states in the unobserved areas and the available observations also need to be denoised and estimated accurately. Obtaining TS in a complete space-time domain is associated with great technological and financial cost, especially at fine spatiotemporal resolutions.

2.3.2   Estimation approaches

Traffic state estimation depends on the estimation approach, traffic flow model, and input data (Seo *et al.*, 2017). The estimation approach can be model-driven, data-driven or streaming-data-driven based on the input data and the assumptions made by the method on traffic dynamics.

2.3.2.1   Model-based approaches

The physics-based mathematical models of traffic flow, utilized by the model-driven estimation approach, describe the physical and theoretical aspects of traffic dynamics. They are representative of physics of traffic and add value to the observations. TSE methods based on models developed using empirical observations are considered to have '*strong*' assumptions because these methods rely on an explicit a priori knowledge of traffic dynamics and can be vulnerable under uncertain phenomena. Although they have high explanatory power and can be integrated with traffic control operations directly, a poor physical model or poor calibration of the model may lead to poor TSE. Moreover, they are not always consistent with the detailed disaggregated mobile datasets that are recently garnering significant attention owing to recent advancements in ICT. Solving boundary value problems (BVPs) can be regarded as model-driven TSE, where the boundary conditions and models are assumed to be correct. Several methods have been developed to combine mobile data with stationary data using first or second order models and filtering techniques such as Kalman filtering techniques (KFTs) (such as Kalman filter (Kalman and Bucy, 1961), Ensemble Kalman filter, Extended Kalman filter, Particle filter etc.) for TSE.

2.3.2.2   Data-driven approaches

To deal with the limitations of model-based approaches, it is required to either improve these theoretical models or to utilize of data-driven or streaming-data-driven estimation approaches (Seo

et al., 2017). Now, even though the data-driven approaches do not rely on physical traffic flow models, they rely extensively on historical data to find dependence using statistical methods or machine learning (ML). Although ML is capable of efficiently predicting non-linear phenomena often found in the transportation field, the computation costs for training and learning can be high. Moreover, the methods can be considered black boxes, and it is difficult to obtain deductive insights. Additionally, they may fail if irregular events or long-term trends occur. Imputation methods have been developed to complement missing data and techniques such as kernel regression (KR), fuzzy c-means (FCM), k-nearest neighbors (kNN) etc., and have been used to incorporate more spatial-temporal information. Traffic flow models and the use of (statistical) dependency on historical data are considered '*strong*' assumptions.

2.3.2.3   Streaming-data-driven approaches

The streaming-data-driven approaches rely on streaming data and use '*weaker*' assumptions such as Conservation Law (CL). They require less a priori knowledge and no historical data. They can be robust against uncertain phenomena and unpredictable incidents. For instance, the moving observer method and its variants have been used for TSE with only a random sampling assumption. In a few studies, extended floating car data ($xFCD$) were used with and without the conservation law. In general, it is preferable for practical applications if accurate TSE is achievable based on '*weaker*' assumptions (Seo *et al.*, 2017).

2.3.3   Literature review on TSE

Extensive research has been done in formulating traffic state estimation methods. In context of data-driven TSE approaches, Ni and Leonard (2005) utilized Bayesian estimation by incorporating time series-based model to Bayesian network for improving the robustness of method. Tan *et al.* (2014) proposed a TSE method based on robust principal component analysis. van Erp *et al.* (2017) evaluated traffic sensing data-based estimation error characteristics in macroscopic TSE. Sunderrajan *et al.* (2016) presents an analysis of using probe vehicle for reconstructing traffic state and estimate the state from floating car data and describes the probe penetration rate for accurate TSE.

With reference to the streaming-data-driven TSE approaches, several studies have contributed to the development of TSE method that rely on streaming data and '*weaker*' assumptions such as random sampling condition or Conservation Law. For instance, a TSE method using connected vehicles and stationary detectors was proposed by Grumert and Tapani (2018) where the only required information were the speed and the position of the connected vehicles and made use of the sparsely located stationary detectors to limit the dependence on the infrastructure equipment. Seo *et al.*, (2015b) proposed a $xFCD$-based TSE method that provides estimates of flow and density using headway and spacing measurements recorded by the probe vehicles.

Solving the traffic flow models, based on deterministic theories, with given initial and boundary conditions using data from sources such as probe vehicles is also regarded is model-based TSE. For instance, Bladin *et al.* (2013) and Fan *et al.* (2014) used physics-based models to estimate non-stationary traffic state. Coifman (2002) proposed a method for utilizing disaggregated stationary data for vehicle trajectories based on the application of Lighthill–Whitman–Richards (LWR) model (Lighthill and Whitham, 1995; Richards, 1956). Certain model-based TSE methods have been proposed that utilize first and second order traffic flow models as part of data assimilation frameworks to produce traffic state estimates by combing mobile data with stationary data.

2.3.3.1   Data assimilation (DA) and TSE using DA techniques

Data assimilation (DA), also referred to as inverse modeling, are a class of techniques that aim at fusing information from both sides, computational sciences, and real measurements, to provide better estimates of the system's state and therefore, they lie at the interface between the two sides. It is used to refer to the problems of estimation (or inference) or modelcalibration (or system identification) respectively. In particular, such techniques yield optimized state of a system that describe the system's dynamics and evolution by combining prior information about initial system's state and parameterization, possibly incomplete dynamical models, and sparse and corrupted measurement data. The mechanism of DA from a higher level is shown in Figure 2.11.

In context of traffic state estimation (TSE), DA approaches are widely employed by TSE studies, and they fall under the model-based traffic states estimation approach where neither the traffic flow models, nor the data are considered as perfect. The most popular DA techniques

employ the Kalman Filter (KF) (Kalman and Bucy, 1961) and its extensions and variations (KFTs: KF–like techniques). The goal is to estimates 'the most probable state' which may not be identical to both model prediction and observation. This approach corrects the model's prediction based on the observations and it has the benefit of integrating the modeling and measurement errors.
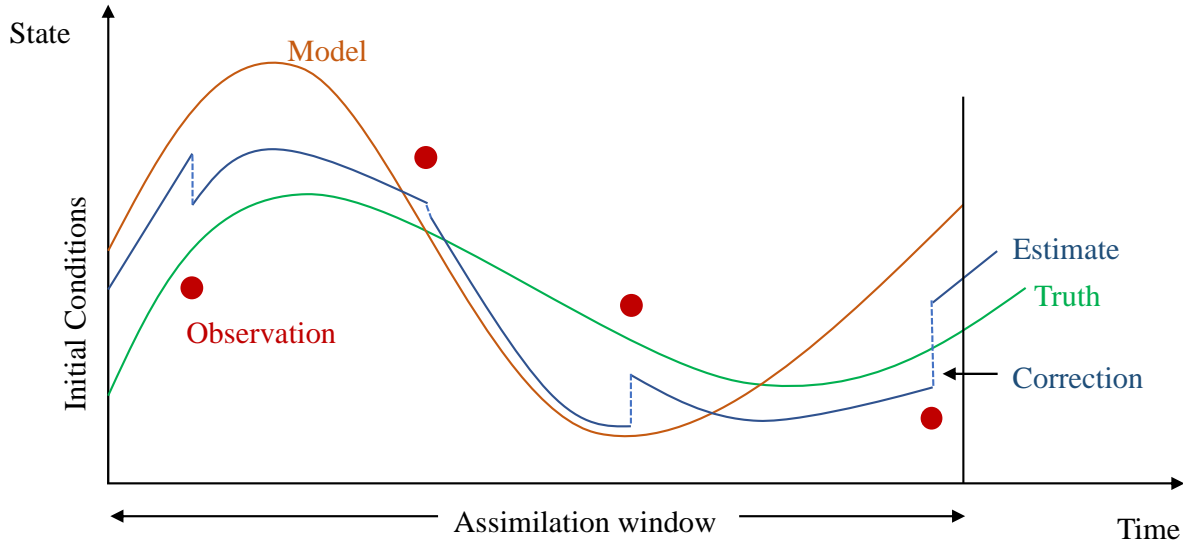
Figure 2.11 Mechanism of data assimilation

In general, the KFTs are based on state-space model consisting of a system or process equation (2.15) and an observation or measurement equation (2.16). The system equation represents the dynamics of the system, and the observation equation represents observations of the system.

$$x_t = f_t(x_{t-1}, \omega_{t-1})$$
(2.15)

$$z_t = h_t(x_t, \eta_t)$$
(2.16)

where at time t,

x_t:	state vector	z_t:	observation vector
f_t:	system model	h_t:	observation model
ω_t:	system noise	η_t:	observation noise

Mathematically, the main objective of KFTs is to obtain the x_t (system's state vector) that maximizes $p(x_t|z_1, z_2, .., z_t)$ (most probably state) with respect to an available observation vector, assumed system model, and noises of the system and the observations. In the context of TSE, x_t often corresponds to a discretized traffic state (such as density) or cummulative flow that is the subject of TSE. Then, f_t represents the numeric scheme used for the continuous PDE of the traffic flow model, to which the model noise ω_t is added. Now, ω_t can either be explicitly modeled from its source or assumed as simple white noise with a given deviation and it encompasses the modeling error or uncertainty. The model parameters, such as FD parameters, are either endogenously estimated together with the traffic state or exogenously assumed. The observation vector z_t corresponds to the observed traffic data. The observation model h_t corresponds to a mapping from traffic state to observed traffic data. A linear observation model, which means that the state variables are directly observed, is often employed. It is easy to construct an observation model when working with stationary data and a conventional traffic flow model however, when working with mobile data certain challenges associated with the low probe penetration rates or low temporal sampling rate arise, which require special techniques to handle those issues (Seo *et al.*, 2017). Measurement errors are represented by the observation noise η_t.

In context of the model noise and observation noise, two kinds of noises that are majorly assumed are additive noise and multiplicative noise. Multiplicative noise is due to random scattering in the state under test and it is coherent with the driving state to a varying degree whereas additive noise is noncoherent. Additive noise, such as Gaussian noise, is less impactful and complex than multiplicative noise, such as Gamma distribution, in which the noise is multiplied to the system state. For instance, the spread of ensembles is very vast, dynamic, and much more turbulent in phenomena such as weather. However, the flow in phenomena like river and traffic is different from anomalous climate dynamics. Even though, the multiplicative noise can be handled by converting them into additive noise by converting multiplicative nature into additive using logarithmic transformation followed by applying any filtering technique and late inverse log is used to get the correct result. However, utilizing additive noise for traffic phenomenon reduces the complexity and the computational cost of KFT implementation for estimation. In fact, it is meaningful to utilize multiplicative noise if we assume that the random term (or noise) depends on (is coherent with) the state of the system.

Extensive literature has studied have utilized the KFTs for estimating the traffic states through various combinations of observations and system models[1]. Some of the KFTs are listed below along with their key features.

Kalman Filter (KF): It is the most basic KFT that assumes both, the system model and observation equation to be linear. It is efficient in terms of computational cost; however, standard traffic flow models are nonlinear and for that reason simple KF are not widely used. Sun *et al.* (2003) and Thai and Bayen (2015) employed Kalman Filtering technique where the system model behaves linearly.

Extended Kalman Filter (EKF): It can use non-linear model to some extent however, it can't be used with models that are non-differentiable (such as Eulerian CTM). Tampere and Immers (2007) applied Extended Kalman Filter for TSE using CTM with implicit mode switching and dynamic parameters. Wong and Wong (2002) and Göttlich *et al.* (2013) are some of the other applications of Extended Kalman Filter where Lax–Friedrichs scheme was used.

Unscented Kalman Filter (UKF): UKF overcomes the shortcoming of EKF as it can use nonlinear system model and it doesn't require an analytical differential. Mihaylova *et al.* (2006) and Yuan *et al.* (2012) utilized the Godunov discretization scheme (Godunov, 1959) and employed Unscented Kalman Filter and Extended Kalman Filter, respectively.

Particle Filter (PF): PF extensively uses Monte–Carlo simulation to represent non-linear phenomena and unlike other KFTs it doesn't require matrix inversions. It has a high computation cost, and it is difficult to apply to large scale estimations. Mihaylova and Boel (2004) and Wright and Horowitz (2016) are a couple of applications of Particle Filter in the context of traffic state estimation.

---

[1] For additional reviews on KFT-based TSE methods refer to Seo *et al.*, (2017); El Faouzi *et al.* (2011); van Lint and Hoogendoorn (2010).

Ensemble Kalman Filter (EnKF): EnKF overcomes the shortcomings of Extended Kalman Filter, employs Monte–Carlo simulation and can use nonlinear and/or non-differentiable system models. Work *et al.* (2008) and Seo *et al.* (2015a) employed Ensemble Kalman Filter.

In continuation to above discussion, Ouessai and Keche (2019) proposed a real-time traffic state estimation method based on second-order divided difference Kalman Filter. Yang *et al.* (2018) proposed a Lagrangian space Kalman filter approach for freeway TSE. Zheng *et al.* (2018) utilized Ensemble filtering techniques for DA and proposed a method for traffic state estimation using stochastic Lagrangian dynamics. Bekiaris-Liberis *et al.* (2016) addressed the problem of estimating traffic states in highway segments in the presence of mixed connected and conventional vehicles. Wang *et al.* (2009) devised a real-time nonlinear freeway traffic state estimator using detector data and second order traffic flow model with a particular focus on its adaptive features. Nanthawichit *et al.* (2003) utilized probe vehicle data and integrated into the observation equation of Kalman Filter to provide real-time TSE and short-term travel time prediction on a freeway. Wang and Papageorgiou (2005) used freeway detector data and second order traffic model for estimating traffic state. van Lint *et al.* (2008) estimated state and parameters using detector data and first-order traffic flow model. Herrera and Bayen (2010) utilized aggregated speed data of probe vehicles, boundary detector data and speed-based traffic flow model for estimating traffic state. Disaggregated prove vehicle data and boundary flow data were used by Yuan *et al.* (2012) to estimate traffic state by using Lagrangian-coordinate first order traffic flow model.

2.3.4   TSE: research gap and contribution

From the literature, it is also clear that numerous proposed TSE methodologies, be it *'weaker'* assumptions-based or model-based, have either been mostly validated through microscopic or macroscopic simulations, experimental data or rarely utilized real traffic data with small spatiotemporal coverage and/or aggregated type datasets; and not complete (100% vehicles') and detailed real traffic data.

In context with model-based estimation approaches for TSE, for instance, Tampere and Immers (2007) utilized the Extended Kalman Filter. Since Extended Kalman Filter can handle nonlinear model to some extent, this study linearized the CTM model around its current state based

on certain assumptions and illustrated the application of approach in a short time real and a simulated case study. On the other hand, Ouessai and Keche (2019) increased the complexity of the TSE method by utilizing a higher-order traffic flow model with Divided Difference Kalman Filter. In addition, the real-world dataset of highway traffic collected included mean traffic speed and mean traffic flow, using which the density was derived based on fundamental relation of traffic flow. Yang *et al.* (2018) proposed a less complex TSE method by utilizing the simple Linear Kalman Filter with a first order model: travel time transition model (TTM). However, the calibration of FD was based on fixed or least-square fitting and, the method was not validated with real traffic data rather it was based on VISSIM simulated data. Nanthawichit *et al.* (2003) proposed a method for dealing with probe data along with conventional detector data to estimate traffic state using Kalman Filter. However, this method employed a second order model and was then tested under several traffic conditions by using hypothetical data only.

Now, in context with *'weaker'* assumptions-based approach for TSE, at an age of near ubiquitous sensor (e.g., cell phone) penetration, and with massive emergence of connected vehicles, these *'weaker'* assumptions-based TSE methods might become prevalent in near future. As an effort of such a pursuit, this doctoral research, first, analyzes a '*weaker*' assumption and extended floating car data ($xFCD$)-based TSE method (proposed by Seo *et al.*, (2015b)), under current low penetration environment, that do not reply on '*strong*' assumptions and whose estimation capabilities have not been validated using vehicles' high-resolution, complete, and detailed trajectory data with high space-time coverage. Then following that, to improve the estimation capability at fine space-time resolution, using fewer probe vehicles, in both the regimes, free-flow and congested, and in complete space-time domain, it extended the '*weaker*' assumption-based approach to estimate the traffic state more accurately through an adaptive approach by utilizing a data assimilation (DA) framework and probe vehicle data. The hypothesis is that utilization of DA techniques in formulating a model-based TSE method shall provide more accurate estimates under the discussed requirements. The nature of this study of proposition, development, and implementation of a model-based TSE method (referred to as 'This study' in Figure 2.12) differs from the past similar studies (as illustrated in Figure 2.12) in terms of calibration methods of the FD, the choice of traffic flow model, the kind of data assimilation technique used to estimate the state variable, and as mentioned before, whether the estimation capability of the method was validated with real traffic data. For instance, a very similar study to the current study is Seo *et al.*

(2015a), that utilized an Ensemble Kalman Filtering technique with a first-order traffic flow model: CTM.

The following discussion compares the study with the current study, explains the need of improving the methodology through current study, and highlights the theoretical merits of the current study over it. Firstly, the FD calibration method in Seo *et al.* (2015a) is based on a LS fit which is done by performing a regression analysis to find minimum distance from points calculated from headway-spacing measures from the probe vehicle data and a triangular FD. LS fit does not consider the dynamics of traffic and without an accurately performed steady state analysis it is difficult to obtain a FD with reasonably accurate FD parameters. Moreover, in absence of (q, k) points from the congested regime the LS fit may not be able to infer the backward wave speed and jam density correctly. To remedy this, the FD Calibration method in the current study involves an iterative process to automatically calibrate the FD by solving the SQP to minimize the discrepancy between the simulated traffic density and observed traffic density by probe vehicles at every time step. It renders the TSE method to be more robust by adapting to the dynamics of traffic data. Secondly, in terms of EnKF specifications, Seo *et al.* (2015a) utilizes only density measures from the probe vehicles as part of the observation equation. However, it is possible to obtain additional observed information from the same probe vehicle data which can help in improving the quality of TSE. In such a pursuit, this study uses the observed density and velocity measures, making the observation equation as nonlinear, to calculate the covariance in the Kalman Gain calculation step. This additional information on velocity observation from probe vehicles contributes to the increased prospects of better estimation results. Finally, the validation of the proposed TSE method involves analyzing numerical characteristics through statistical metric scores by using the ZTD provided by Hanshin Expressway Co. Ltd. The validation with real traffic data enhances the reliability and applicability of a proposed model or estimation method. In contrast, Seo *et al.* (2015a) investigated the numerical characteristics of the TSE method through a simulation experiment.
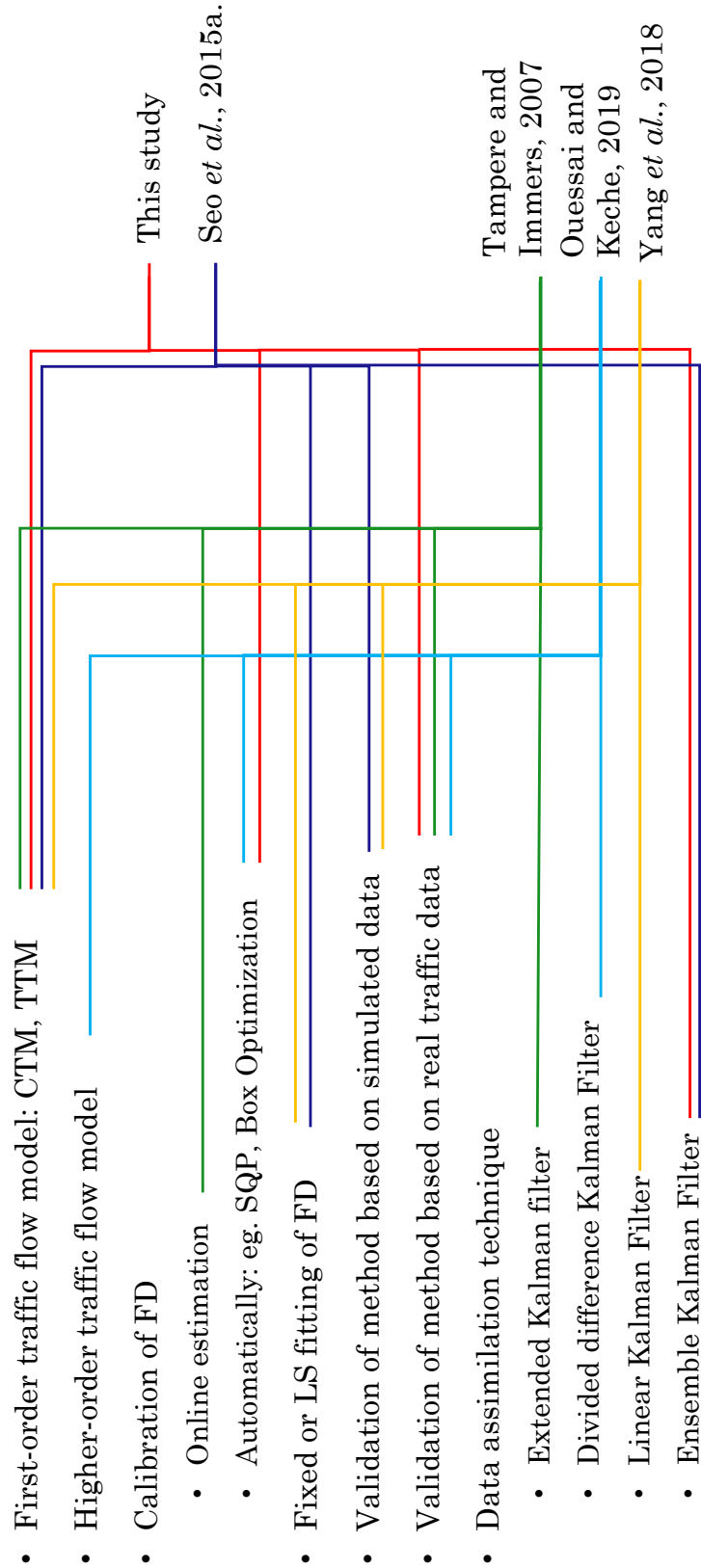
Figure 2.12 Literature review of similar studies on model-based TSE using DA

2.4   Research scope of the dissertation

This dissertation "*Fundamental Diagram and Traffic State Estimation Methods: Analysis and Modeling using Zen Traffic Data*" systematically studies the traffic states (TS) and fundamental diagrams (FD), which are the most fundamental concepts of the theory of traffic flow, and then shifts the focus to the traffic state estimation (TSE). As discussed in section 1.1, for traffic modeling, management, and safe, smooth, and economical traffic operations, it is very critical to understand the current state of traffic through estimating the traffic states using partially observed traffic data and also to understand the inter-relationship between the traffic state variables through FD of road traffic. This dissertation answers three major research questions which were left unanswered by the extensive literature or, except for a meagre prospect, were left unproved without reasonable assurance in accuracy and applicability. They are:

1. *While working with extensive data, which FD is most potential for traffic engineers in terms of accuracy, mathematical alignments to the continuity and stationarity of traffic flow, less computation cost, dependence on no strong assumptions? Moreover, which is the most workable form of FD at a specific resolution subject to traffic flow analysis?*

2. *Can the information on current state of traffic obtained from a probe data based-TSE method (Seo et al., (2015b)), that does not rely on strong assumptions, be relied upon and how much accuracy can be expected in estimates at a resolution for which the estimates are desired? Also, what are the factors that affect the accuracy of such methods? Is it spatial resolution at which the estimates are required, or temporal resolution or is it the number of probe vehicles that are present on the freeway?*

3. *How can a DA framework-based TSE method be best designed as to deliver highly reliable estimates of traffic states at high spatiotemporal resolution and using few percentages of probe vehicles, which can be implemented on a wide space-time domain that even undergoes the state of congestion?*

Amidst the growing traffic problems, this study contributes to the practices for keeping the efficiency of traffic system high without building new transportation infrastructures. By taking advantage of the advancements in ITS technologies, the studies conducted as part of this dissertation provides a deeper and much reliable comprehension of traffic flow analysis through studying FDs, TSE methods and devising advanced TSE methodology, which produces quite accurate estimates of traffic states using data from only a few numbers of probe vehicle and roadside detectors, that can help traffic engineers in alleviating congestion.

Besides the methodological contributions, this thesis also makes practical contributions. The results from a.) the analysis of FDs, and b.) the analysis of *'weaker'* assumption based-TSE method, are suitable for *direct appliance* in understanding the dynamics of traffic. In addition, the proposed model-based TSE method is developed with the aim of real-world implementation and is suitable for the current low-penetration-rate vehicle environment. It can provide essential input for improving the efficiency of short-term traffic performance through operations, traffic management and control before the freeway reaches the state of congestion. For instance, the control measures that are typically employed in freeway networks include ramp metering, link control that comprise of lane control, variables speed limit, congested warning, keep-lane instructions etc., and driver information and guidance system.

Speaking specifically of link control measures, the information on estimated current state of density can help in managing the changeable message signs with indications for 'keep lane' or congestion warning to drivers which may help drivers in deciding the choice of route. This information can be used in controlling traffic by prohibiting the usage of a link or a lane which are heavily used or around incident locations. These measures are believed to homogenize the traffic flow (i.e., more homogeneous speeds of cars within a lane and of average speeds on different lanes) which helps to reduce the risk of falling into congestion at high traffic densities and to increase the freeway's capacity.

Also, route guidance traffic control strategies can utilize sufficiently interpreted current traffic state measurements on different links on the network to recommend the route to the road users through reactive strategies (which react to estimated current traffic states without the real-time use of mathematical models or predictive tools) and predictive strategies (which can predict future traffic conditions in order to improve the quality of provided recommendations).

Therefore, we expect the proposed method in this thesis to be implemented on an even larger scale and help traffic engineers and transportation agencies in solving more real-world issues related to traffic, congestion being a major one.

3 **TRAFFIC DATA**

3.1 Introduction

ITS aims to enhance public safety, reduce congestion, improve access to travel and transit information, generate cost savings to motor carriers, transit operators, toll authorities and government agencies, and reduce detrimental environmental impacts. Intelligence requires information, and information requires data, which is generated by experiments and surveillance. Traffic engineering studies differ from other studies in that they require extensive data from the field, which cannot be accurately generated in a laboratory (Dahiya and Asakura, 2021). In order to mitigate the congestion, traffic data collection is one of the most essential elements required for traffic flow analysis. However, collecting information from the entire transportation system is not always possible due to the associated technological limitations and financial costs.

Several methodologies for collecting traffic data without any significant assumptions, including a variety of information such as cumulative flow, vehicles' speeds, positioning, travel time etc., have been developed since the genesis of traffic engineering (Greenshields *et al.*, 1935). At present, there exist numerous automated ways of obtaining traffic data. Because of recent advancement in ICT, a wide variety of empirical data is available at present time that includes volume count, vehicle classification, vehicle occupancy, travel time, delay, vehicular speed, and position etc. Stationary data (or Eulerian data) obtained from in-situ technologies and mobile data (or Lagrangian data) obtained from in-vehicle technologies are two major categories of empirical traffic data available based on the measurement methodology. Another independent categorization of traffic data introduced by Seo *et al.* (2017) is of aggregated (information from multiple vehicles is aggregated and stored) and disaggregated data (data is not aggregated but stored as collected). Disaggregated data contains more information than the aggregated one. Analysis, calibration and modeling of fundamental relations and TSE methods have mostly utilized stationary sensors' data, mobile data, such as the GPS probe vehicles that only contain average speed or sampled trajectories

data. This means that other traffic state variables cannot be obtained from it without some additional assumptions.

The remainder of this chapter discusses about the traffic data collection methodologies in section 3.2 and 3.3, including fixed-point data and mobile data, respectively. Then it introduces the complete trajectory data utilized for this research namely, Zen Traffic Data (ZTD) and several advantages associated with utilizing ZTD over other high-tech trajectory datasets in section 3.4.

3.2 Fixed-point data

Fixed sensors, such as inductive detector loops (IDL), pneumatic tube detectors, embedded magnetometers, ultrasonic detectors, passive or active infrared detectors, laser detectors, weigh-in-motion (WIM) and closed-circuit television cameras, can be considered as conventional that collect stationary or fixed-point data. The in-situ technology utilizes the detectors located on or along the roadside and are split into two categories of intrusive and non-intrusive methods based on method of data collection. The intrusive methods consist of a data recorder and a sensor placed on or inside the roadway, installation of which causes a potential disruption of traffic, whereas non-intrusive methods are based on remote observations and are mounted at or above the road surface and their installation causes less or no disruption of traffic. Passive magnetic or magneto-meter sensors, an intrusive technology with a circular or elliptical offset zone of detection, are either permanently mounted within holes in the roads or affixed to the road in some fashion and communicates information, such as short-term traffic counting, vehicle classification by axle counts and spacing, to a nearby base station through wired or wireless communication. It reads the fluctuations in the relative strength of the Earth's magnetic field with the presence of a moving metal object i.e., a vehicle. Generally, in order to receive speed or vehicle classification assessment at least two sensors are required because a single sensor can only provide flow and occupancy information. IDL, an intrusive technology, consist of coated wire coils buried in grooves cut on the surface of road and are sealed over with bituminous fillers and communicates to the processing unit via cables buried with the loops. A single loop can collect data related to flow q and density k and with two detectors other parameters like speed and vehicle length can also be obtained. Another intrusive technology, WIM consist of a piezoelectric sensor system laid across the road and are usually coupled with other intrusive or non-intrusive technologies to provide additional

data. It detects the variation in voltage caused by pressure exerted on the sensor by an axle and thereby obtain the axle's weight and spacing based on the time the vehicle takes to cross. The non-intrusive technologies, such as video image detection (VID), infrared sensors, microwave-Doppler and Radar, ultrasonic sensors, and passive acoustic array sensors, are expanding rapidly with continuing advancements in the field of signal processing and are providing supplemental traffic information for specific locations or applications such as queue detection. The roadside mast-mounted sensors cover an oblique upstream or downstream area a field of regard. VIDs collect variety of data by performing frame-by-frame analysis of images processed from the videos obtained from roadside cameras and makes it possible to capture all desired traffic information. Detectors mounted under gantries or the underside of bridges, a non-intrusive technology, have the field of regard directly below them. Open path monitors are mounted on the roadside at ground level that fire beams across the road for side-by-side masking. Other overhead mounted sensor technology–infrared sensors, are used for signal control and view approaching or departing traffic, sometimes from a side-looking configuration. Another non-intrusive technology–passive acoustic arrays sensors use an array of microphones to detect the sound of an approaching vehicle which is above an ambient threshold using which aid in estimating vehicle location and speed information, occupancy etc. through signal processing.

Technologies for collecting fixed-point data vary as to their ability to provide accurate additional information and their reliability. However, their accuracy and precision may not be reliable, for instance, because of frequent misses and/or double counting by loop detectors, sensitivity towards weather conditions or environmental effects affecting sensor performance like sound propagation degradation in pulse and active ultrasonic sensors and passive acoustic array sensors. The problem of missing data arises mainly because of the sparse sensor installation owing to the impracticality of installing detectors everywhere and the generally high operational costs of roadside sensors. For instance, the tube installation in magnetic sensors is not durable with a life span of less than a month and are not suitable for high flow or high-speed roads. Similarly, the piezoelectric sensors for WIM systems must be replaced at least once every three years. Likewise, the loops of the IDL are damaged easily. Moreover, they have a very low sample rate for data collection. Therefore, the limitation to the fixed-point sensors is that the amount of data they provide is not always sufficient for traffic control.

3.3 Mobile data

Over the past three decades, the in-vehicle technologies generically termed as Automatic Vehicle Location (AVL) systems, that have a direct impact on the policy instruments available to authorities for the operation of ITS and are believed to play a vital role in improving efficiency of transportation networks, have really come into realization through the advantage of satellite-based technologies. They provide either positioning information whenever a vehicle equipped with transponders, that receive and transmit information from roadside units, passes a specific point in the transportation network, or continuous information as the vehicle, equipped with Global Positioning System (GPS) technology, travel through the network. One such mobile data collection technology is radio-frequency identification (RFID) or transponder systems. It is an automatic identification method which utilizes RFID tags or transponders for the purpose of collecting data using radio waves. These tags are comprised of a microchip and an antenna to collect information and transmit data to readers, respectively. However, there are certain drawbacks associated to the RFID such as reader collision when signals from two or more readers overlap, and sometimes the tags are unable to respond to simultaneous queries.

Owing to recent advancements in information and communication technologies (ICTs), mobile sensors, such as on-vehicle GPS devices, signpost-based transponders, automatic vehicle identification (AVI) transponders, call detail records (CDRs), dynamic route guidance (DRG), and second generation on-board diagnostics systems (OBD–II), collect the mobile data with broader coverage of road network and are relatively new as compared to fixed-point sensors. As a result of emerging connected and automated vehicles, the mobile sensors are increasingly used as sources of data. Vehicles with such sensors, often referred to as probe vehicles or floating cars, are a cost-effective way to collect data termed as Floating Car Data (FCD). Probe vehicles use on-board electronics to determine its position and register experienced traffic conditions to a traffic center where the received traffic data is combined and processed with other data from other monitoring sources to provide relevant traffic information which is vital for Advanced Traveler Information System (ATIS). The principle of FCD is to collect real-time traffic data such as car location, speed, and direction of travel, by locating the vehicle over the network via mobile phones or GPS that act as sensors for the road network. This data is sent anonymously to a central processing center where traffic engineers use this information for extracting useful insights such as status of traffic and

alternative routes and redistribute to the drivers on road. GPS has recently gained a much popularity due to their ability to provide real-time location data with high precision. However, only a limited number of vehicles are equipped with GPS, and it deals with high equipment costs as compared to floating cellular data. FCD is an alternative or rather complement source of high-quality data to existing technologies which are becoming crucial in developing new Intelligent Transport Systems (ITS) as they are potentially able to improve reliability of the transportation system, its efficiency and safety. Two important characteristics of probe vehicle data are penetration rate (ratio of probe vehicles to all the traffic) and temporal sampling rate (time interval between consecutive reporting of data). In general, it is preferable if both the characteristics are high when collecting the data. Probe vehicles are capable of collecting mobile data from a wider spatiotemporal domain and are relatively cheaper traffic data collection tool as compared to stationary sensors (Herrera *et al.*, 2010; Zito *et al.*, 1995). The new type of mobile data, collected by probes that are equipped with advanced on-vehicle sensors, consists of more than just the positioning and speed of the vehicle trajectory; thus, it has been named extended floating car data ($xFCD$) (Huber *et al.*, 1999). However, the probe vehicle data may contain biases based on sampling and differences in the driving behavior of the probes. For instance, if the probe vehicles belong to a logistic fleet, they may travel at slower than average speeds. In addition, vehicles with recent advanced driving technologies (e.g., ADAS and connected vehicles), which may be used as probe vehicles, may exhibit different driving characteristics compared to completely manually operated vehicles and progressively change driving and traffic patterns.

3.4 Zen Traffic Data (ZTD)

For this doctoral research, complete and high-tech data, with a high temporal sampling rate of 0.1 s, have been utilized, namely the Zen Traffic Data (ZTD). The data consists of wide range and long period of all vehicle trajectory data and any other data affecting traffic events and as a result, the real complicated traffic phenomenon itself, that no one has been able to grasp so far with in depth details of each vehicle, has been digitalized (source: https://zen-traffic-data.net/). It has been developed using image sensing technology by targeting congestion bottlenecks. Image processing involves frame-by-frame analysis of video images captured by roadside cameras and depending on the processing methodology, complex systems allow extraction of all desired traffic information,

including parameters that are not readily obtainable using other types of detectors. A video image processor system typically consists of multiple cameras, microprocessor-based computers for digitalizing and processing the imagery of traffic scene to determine changes between successive frames, and software for interpreting the images and converting them into traffic flow data. Generally, the algorithms are designed to remove the gray level variation in the image background caused due to weather conditions, shadows, daytime or nighttime artifacts and color imagery can also be exploited to obtain the data. As described in Figure 3.1, the system design consists of four major stages namely, vehicle image collection, vehicle detection via detection of frame features, vehicle searches that matches the detected features of frames, and database creation by refining matched vehicle features.

For ZTD, the cameras, for recoding the videos and observe all vehicles at an interval of 0.1 second, are installed on light poles of height close to $10\ m$ and they are installed on the full length of the target section of the Hanshin Expressway at an interval of $40\ m$ distance. The image sensing devices collect the image data of moving vehicles from the rear side of the vehicle from a distance so that the personal information of the driver or vehicle, such as passenger's face or driving license plate numbers, cannot be identified. Now, creating these images is a difficult task due to the inability of computers, unlike humans, in distinguishing the background and vehicles by considering a single image. So, a greater number of frames improve the quality of image data which are analyzed frame-by-frame to detect features corresponding to moving vehicles in the scene. This is done by removing the static background resulting in images consisting of blobs (collection of pixels with non-zero values) corresponding to the identified vehicle which are further enhanced by processing. At times, presence of false blobs, due to excessive noise in the image, requires further processing for extracting traffic data. Then, vehicle tracking or vehicle searches are done by matching the detected features from previous frames with those of the current frame to generate sequential vehicle trajectory. These matched vehicle features can be redefined to correct features in the frame. At last, the final database consisting of demographic information about the roadway such as longitude, cross slopes, road curvature etc., vehicle trajectory, vehicle specific information such as car length etc., location at $0.1\ s$ interval, and information of nearby vehicles is created. This vehicle trajectory database contains roughly 100% of each vehicle's continuous trajectory in the target sections and is intended to realize a safer, more secure, and comfortable driving for all highway users (source: https://zen-traffic-data.net/).
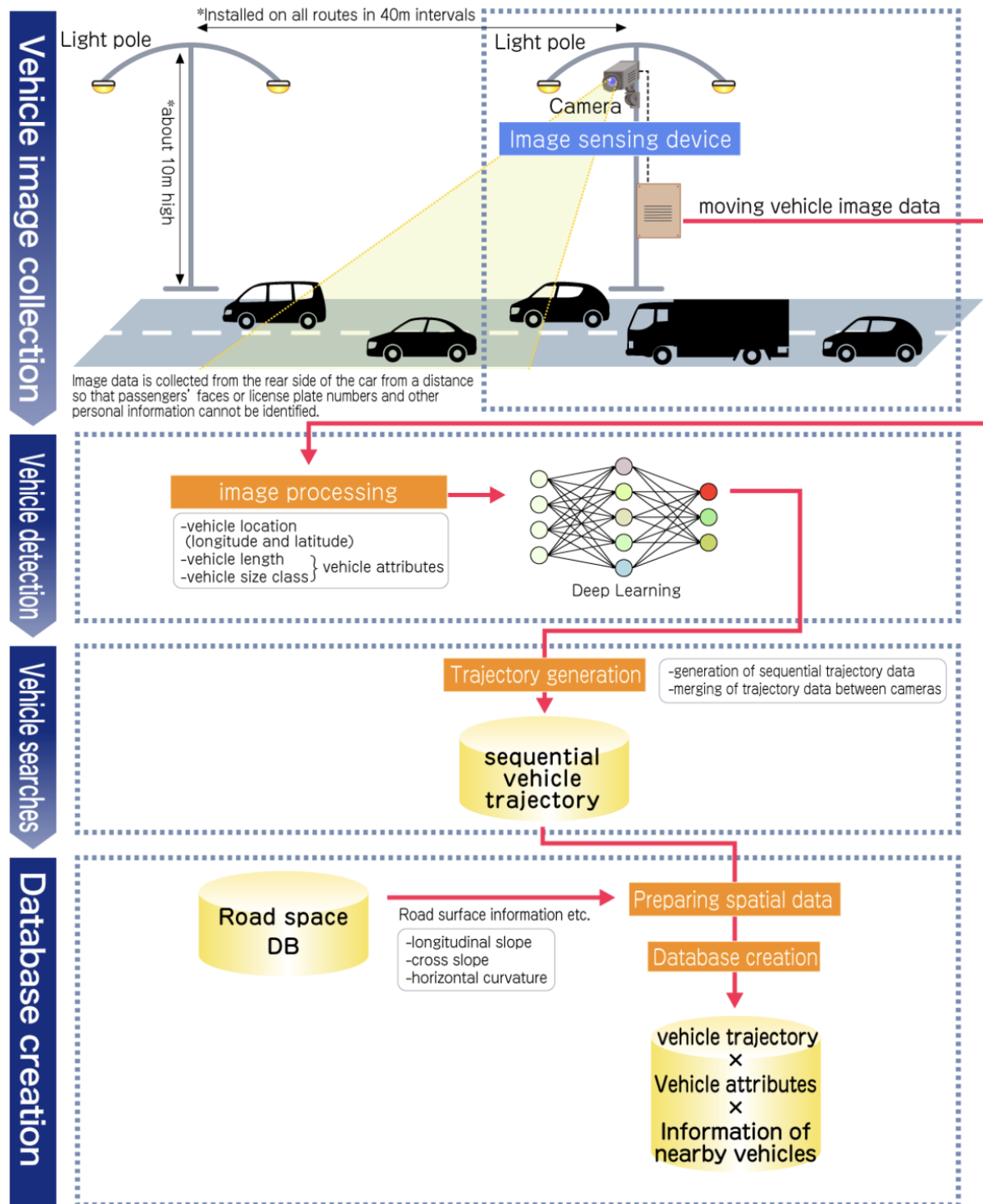
Generating processes of the vehicle trajectory database

Figure 3.1 Data generation process for ZTD

(Source: https://zen-traffic-data.net/english/generate/)

3.4.1 Sections observed and data characteristics

ZTD is a large-scale trajectory dataset developed by Hanshin Expressway Co. Ltd. for sections on two routes as depicted in Figure 3.2, 3.3 and 3.4:

- Hanshin Expressway Route 11 (Ikeda route Osaka bound) nearby the Tsukamoto Junction
- Hanshin Expressway Route 4 (Wangan route Osaka bound) at the Ohama-Sambo Junction

The section on the Ikeda Route 11, around Tsukamoto Junction ($5.0 - 3.0 \ k.p.$, in the inbound direction) is initially an 'S'-shaped curve, which subsequently becomes a simple straight line, as shown in Figure 3.3. It consists of two lanes, a merging section with a major on-ramp, two slightly curved sections, and a sag section.

Figure 3.2 Sections observed on Hanshin Expressway for obtaining ZTD
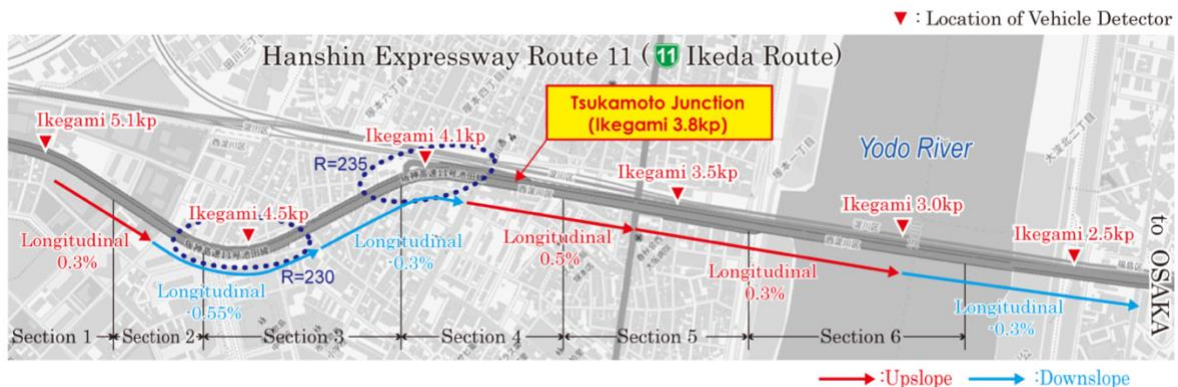
Figure 3.3 Target section Hanshin Expressway Route 11 (Ikeda route)
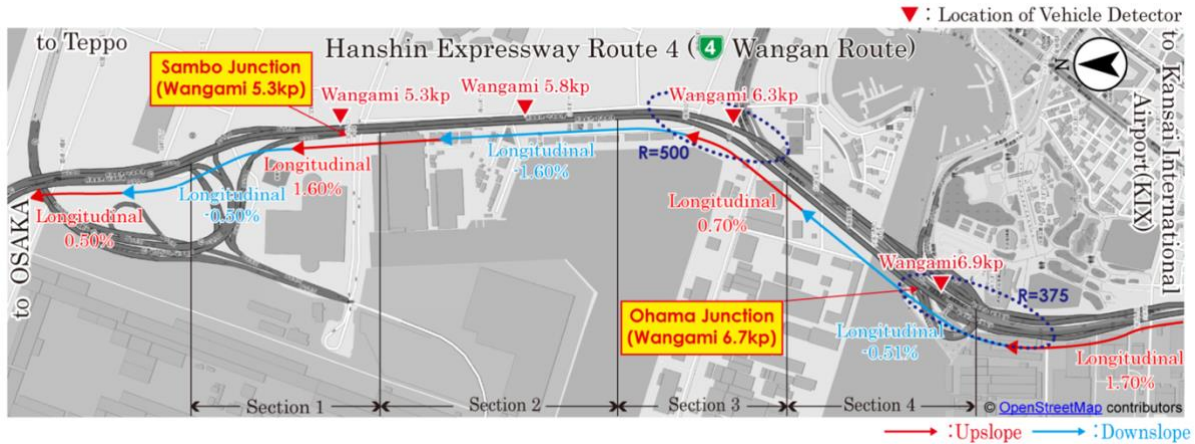
Figure 3.4 Target section on Hanshin Expressway Route 4 (Wangan route)

(Source of Figures 3.2, 3.3 & 3.4: https://zen-traffic-data.net/english/outline/dataprovision.html?area=tsukamoto)

Table 3.1 Vehicle specific data obtained through ZTD

■L00_F000_trajectory.csv

No.	COLUMN	TYPE	FRACTIONAL DIGITS	UNIT	DESCRIPTION	SAMPLE	UNIQUE
1	vehicle_id	int			Vehicle ID	4316	*
2	datetime	string			Datetime HHMMSSFFF	070216100	*
3	vehicle_type	int			1: normal vehicle 2: large vehicle(bus, truck, etc.)	1	
4	velocity	decimal	1	km/h	Velocity	63.1	
5	traffic_lane	int			Traffic lane ID 1: driving lane 2: passing lane 3: entrance lane	1	
6	longitude	decimal	7	degree	Longitude measured as WGS84 system	135.4598866	
7	latitude	decimal	7	degree	Latitude measured as WGS84 system	34.7209920	
8	kilopost	decimal	1	meter	Distance from starting point of the expressway route	5070.7	
9	vehicle_length	decimal	1	meter	Estimated vehicle length from image recognition. Value is rounded to 0.5 [m].	5.5	
10	detected_flag	int			1: detected record by image recognition 0: interpolated record	1	

For this section there are 5 data products available: L001_F001, L001_F002, L001_F003, L001_F004, L001_F005 containing continuous trajectory details of 100% vehicles driving for a distance of $2\ km$ (5.0 – 3.0 $k.p.$) for 1 $hour$ (different times of day, 2 for 7 – 8 a.m., 2 for 3 – 4 p.m. and 1 for 10 – 11 a.m.).

These 5 datasets have a wide spatiotemporal coverage and are specifically used for this research datasets to perform empirical spatiotemporal analysis. As tabulated in Table 3.1 and 3.2, the ZTD includes continuous trajectory information (and any other data affecting traffic events) of all the vehicles (almost 100%) as described by parameters, namely vehicle_id (vehicle ID), datetime (time with a 0.1 s precision), vehicle_type (Type 1: normal or Type 2: large vehicles,

such as bus, truck etc.), velocity, traffic_lane (driving, passing or entrance), kilopost (distance from the starting point of the expressway route), vehicle_length (estimated vehicle length obtained from image recognition), latitude, longitude etc. for each vehicle. For instance, the traffic data L001_F001, contains the details of 3,375 vehicles with vehicle IDs ranging from 0 to 3,734 from 7:00 a.m. to 8:00 a.m. for $2\ km$ ($5\ k.p.$ to $3\ k.p.$). For the purpose of clear visualization of *this* particular dataset of ZTD, Figure 3.5 shows the velocity heat plot observed in each lane of Hanshin Expressway Route 11.

Table 3.2 Demographic specific data obtained by each vehicle using ZTD

■L00_F000_alignment.csv

No.	COLUMN	TYPE	UNIT	DESCRIPTION	SAMPLE	UNIQUE
1	vehicle_id	int		Vehicle ID	4316	*
2	datetime	string		Datetime HHMMSSFFF	070216100	*
3	curvature_radius	decimal	meter	The radius of the circular arc at that point.	1870.82842	
4	longitudinal_slope	decimal	%	The rate of change of roadway elevation with respect to distance in the direction of vehicle	0.3	
5	transverse_slope	decimal	%	The rate of change of roadway elevation with respect to distance perpendicular to the direction of vehicle. +:Right, -:Left	-1.5	

(Source of Table 3.1 & 3.2: https://zen-traffic-data.net/)
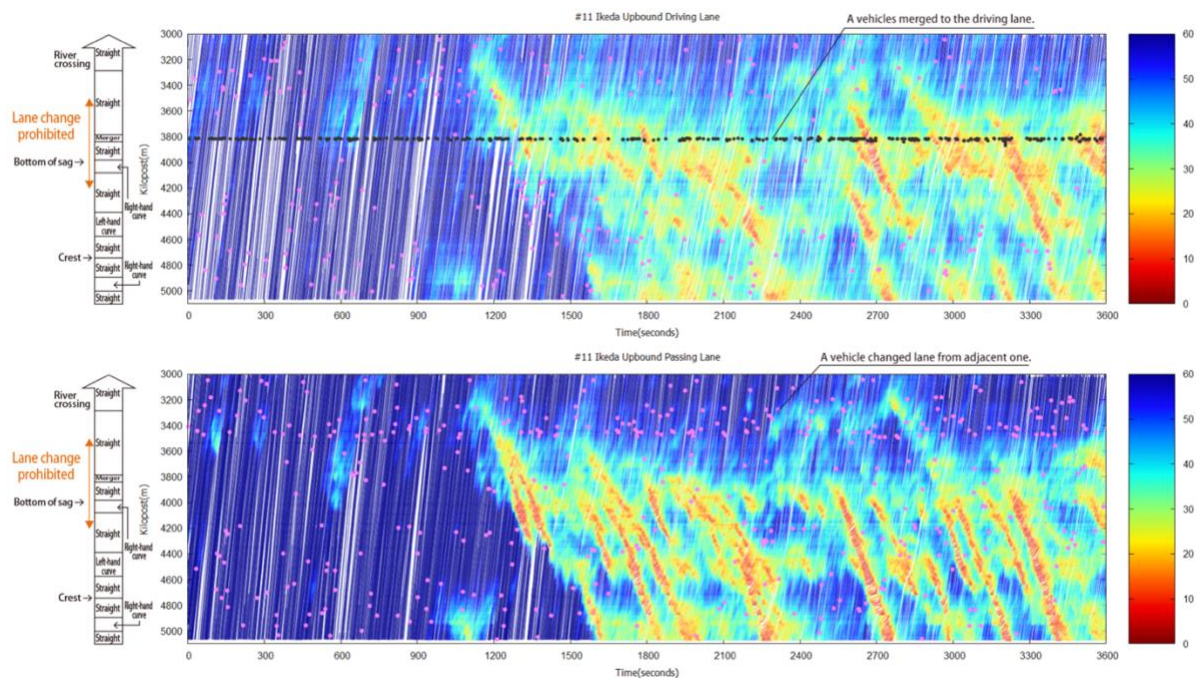
Figure 3.5 Observed velocity in the space-time diagram per lane (nearby Tsukamoto Junction of Hanshin Expressway Route 11 Ikeda Line (Osaka bound)

(Source: https://zen-traffic-data.net/english/outline/)

It can be seen that within a morning peak hour the vehicles were driving at their desired velocity of around $50 - 60\ km/hr$. In the latter half of the time domain there are several instances where the velocities of vehicles even dropped less than $15\ km/hr$.

For the ZTD L001_F001, Edie's generalized definitions of were used to calculate the traffic state variables at spatiotemporal resolutions of $\{50\ m$ x $10\ s\}$ and $\{400\ m$ x $60\ s\}$. Figures 3.6, 3.7 and 3.8 shows the flow q, density k, and the velocity v at the resolution of $\{50\ m$ x $10\ s\}$ and Figures 3.9, 3.10 and 3.11 show the heat plot of traffic state variables at the resolution of $\{400\ m$ x $60\ s\}$. It can be inferred that the flow q on the section from 07:00 a.m. to 08:00 a.m. ranges from 0 to 1.5 veh/s, density k ranges from 0 to 0.18 veh/m, and velocity ranges from 0 to 30 m/s.
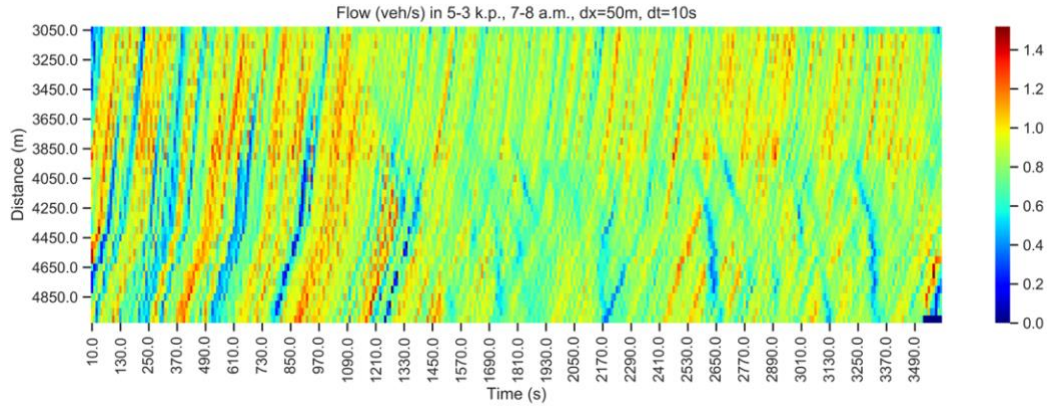
Figure 3.6 Flow q (veh/s) calculated using Edie's definitions for ZTD: L001_F001 at a space-time resolution {50 m x 10 s}
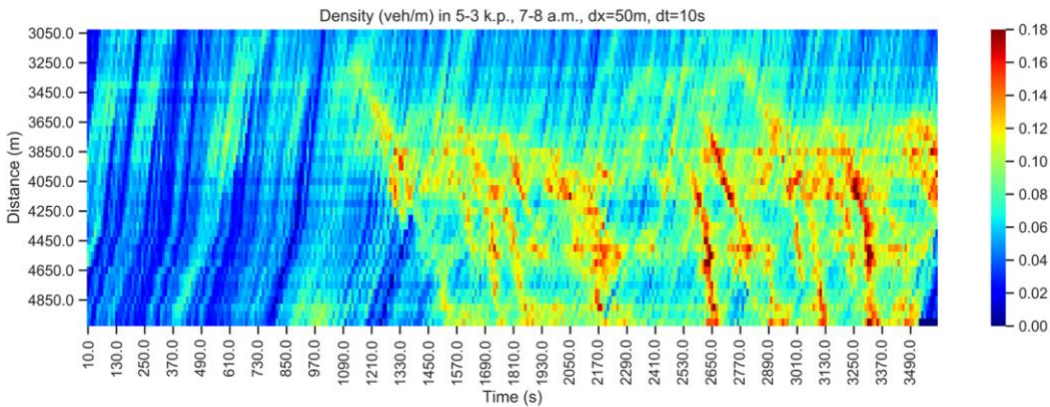
Figure 3.7 Density k (veh/m) calculated using Edie's definitions for ZTD: L001_F001 at a space-time resolution {50 m x 10 s}
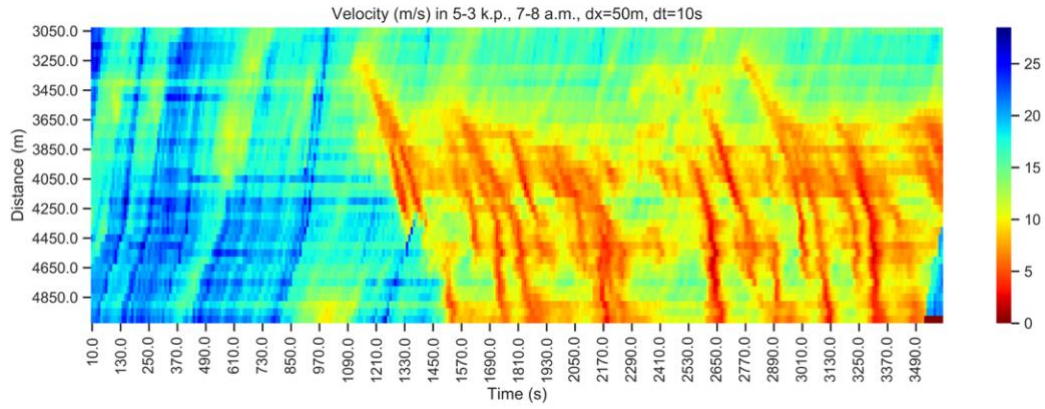
Figure 3.8 Velocity v (m/s) calculated using Edie's definitions for ZTD: L001_F001 at a space-time resolution {50 m x 10 s}
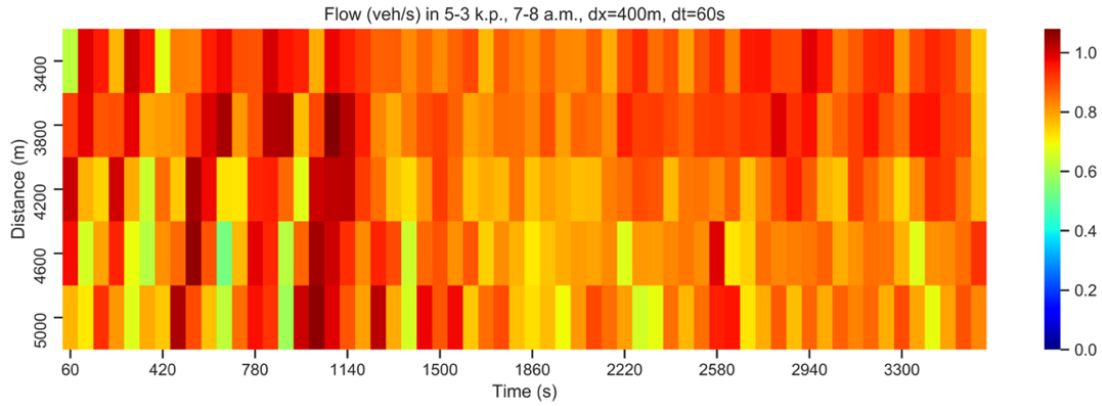
Figure 3.9 Flow q (veh/s) calculated using Edie's definitions for ZTD: L001_F001 at a space-time resolution {400 m x 60 s}
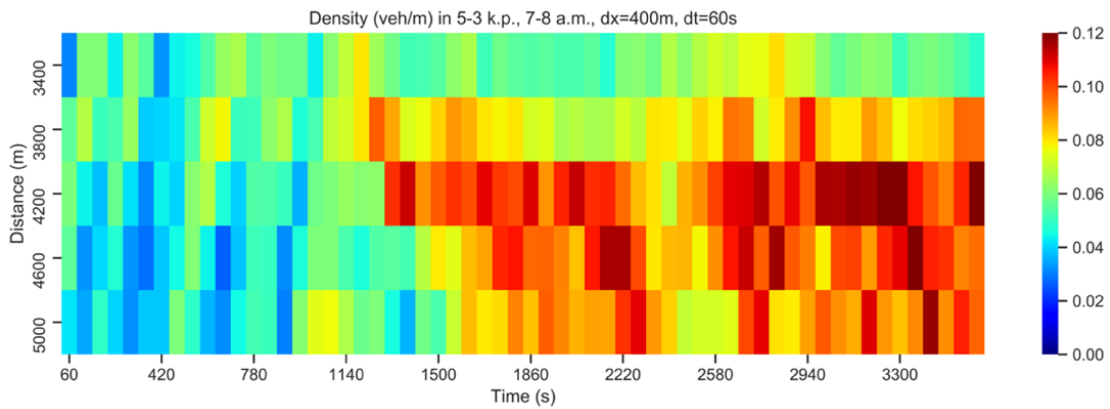
Figure 3.10 Density k (veh/m) calculated using Edie's definitions for ZTD: L001_F001 at space-time resolution {400 m x 60 s}

Velocity (m/s) in 5-3 k.p., 7-8 a.m., dx=400m, dt=60s
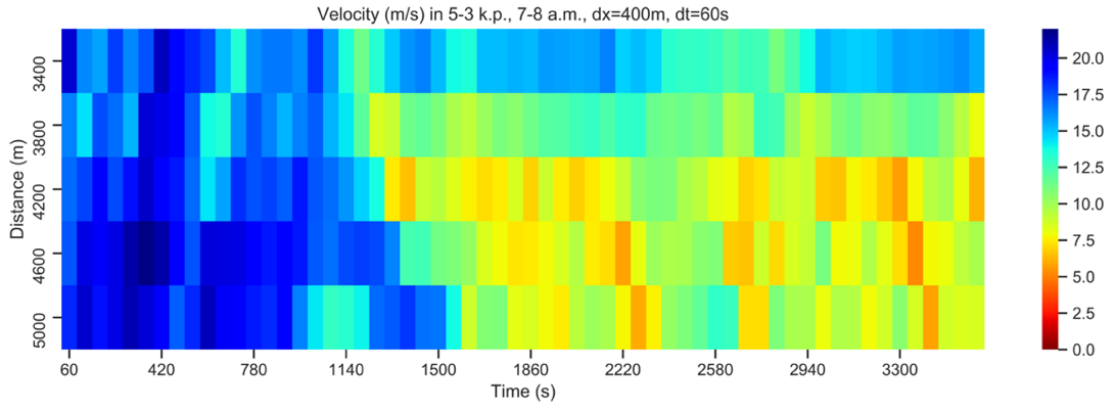
Figure 3.11 Velocity v (m/s) calculated using Edie's definitions for ZTD: L001_F001 at a space-time resolution {400 m x 60 s}

Since highly detailed and technical data like ZTD is not possible to be obtained and utilized for real application over all transportation networks, the objectives of this doctoral research utilize the ZTD by creating probe vehicles-like situation (datasets). The objectives related to the analysis and modeling are all aimed to be conducted in the limelight of real-world situation where probe penetration rates of $2 - 5\%$ can be expected. Keeping such conditions under consideration, $p\%$ of probe vehicles can be randomly extracted from ZTD (along with their corresponding ZTD) and can be utilized as probe vehicles with $p\%$ probe penetration rate into the actual traffic flow. Figure 3.12 illustrates trajectories of such randomly extracted probe vehicles from complete ZTD. It shows traffic trajectories of 5% vehicles randomly selected from 100% vehicles driving on Lane 1 of a subsection (300 m length out of 2 km section) for 1 $hour$ (07:00 $-$ 08:00 a.m.: morning peak hour).

Probe Trajectories on Lane 1, 300m section, 7:00-8:00 a.m. (p%=5%)
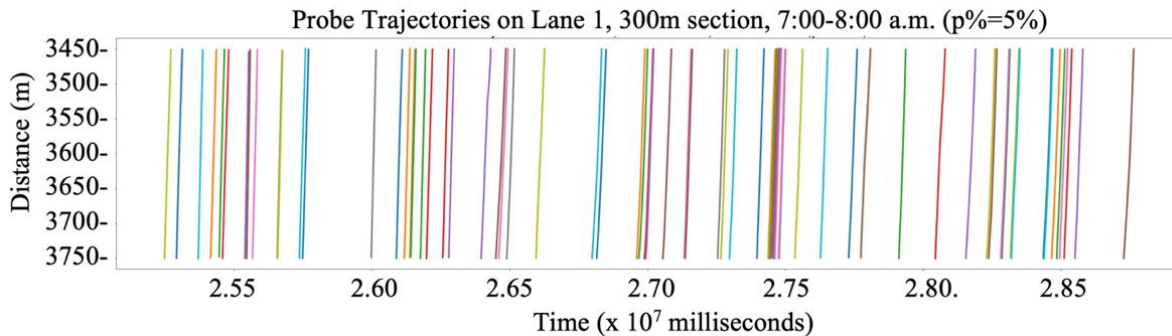
Figure 3.12 Space-time diagram of 5% vehicles driving on lane 1 of a 300 m section (3.75 k. p. to 3.45 k. p.) for ZTD:

L001_F001

The accuracy of the ZTD has been evaluated by Seo *et al.* (2021) concluding the recall rate to be 96.8% and the precision rate to be 97.1%. The evaluation also concluded that the detection performance was almost insensitive to traffic conditions, weather conditions, and the time of the day. The ZTD can be considered equivalent to data obtained from all vehicles equipped with advanced driving assistance systems (ADAS), which can be utilized as a source of data for volume-related information and to verify classical concepts in the fundamental theory of traffic flow, traffic flow models, functional forms of FDs, traffic state estimation methods, several of which have been developed and proposed by researchers over past decades, some based on theoretical assumptions and others driven by data, but have not been evaluated with complete high-resolution trajectory data.

3.4.2   Merits of utilizing ZTD over other high-tech trajectory datasets

The accuracy evaluation of the ZTD by Seo *et al.* (2021) concluded the recall rate and the precision rate to be very high and the detection performance was almost insensitive to exogenous conditions. The problems of data delay, data loss, inaccurate data, and inconsistent data, which are usually present even in data obtained from recently developed conventional vehicle-to-everything (V2X) technologies, as stated by Sun *et al.* (2017), are non-existent in ZTD to a great extent. In practice, it is very difficult to collect complete trajectory datasets because of the wide ranging spatiotemporally phenomenon nature of traffic flow. Probe vehicles can collect sampled vehicle trajectory data from a wide-ranging domain (Herrera *et al.*, 2010), but they are not complete due to their small penetration rate. In 2005, NGSIM (US Department of Transportation, 2006) datasets were collected by deploying seven or eight synchronized cameras with image recognition systems. However, the spatiotemporal coverage was limited to $600\ m$ and $15\ min$ (Seo *et al.*, 2021). Moreover, as shown in previous works (Coifman and Li, 2017; Montanino and Punzo, 2015), raw NGSIM trajectories cannot be used for further analysis as false-positive trajectory collisions and physically illogical vehicle speeds and accelerations happen to occur in the datasets (Krajewski *et al.*, 2018). In October 2018, πNEUMA (New Era of Urban traffic Monitoring with Aerial footage) datasets recorded traffic streams in multi-modal congested environment using a swarm of ten drones hovering over the central business district of Athens, Greece (Barmpounakis and Geroliminis, 2020). However, there were "blind gaps" of about $10\ mins$ after regular time

intervals where no trajectory data were recorded. This allows the setup to monitor traffic continuously for $15-20$ $mins$ only. Those gaps are used for technical tasks, which are to change the batteries of the drones and then send them back in their previous hovering position. In addition, there are some time periods when no data is available for certain zones within the coverage area due to technical issues where one or more drones may have stopped working. Like πNEUMA datasets, highD datasets include post-processed trajectory data extracted from drone video recordings at German highways around Cologne during 2017 and 2018 (Krajewski *et al.*, 2018). However, the spatiotemporal coverage of each recording is limited to 420 m and 17 min where each vehicle is visible for a median duration of 13.6 s.

Thus, compared to other high-tech vehicle trajectory datasets, it is quite advantageous to utilize ZTD for traffic studies as discussed. The spatiotemporal coverage of 2 km and 1 $hour$ is high and the detailed continuous trajectory information for all the vehicles is available at a minuscule temporal sampling rate of 0.1 s without any data loss. A unique vehicle ID is allocated to each vehicle which is maintained throughout the section. All these aspects make ZTD a potential traffic trajectory data of supreme quality which can aid in understanding traffic phenomenon and dynamics much more precisely and accurately.

4 ANALYSIS OF $v - k$ RELATIONS

This chapter discusses the empirical analysis of various existing speed-density $(v - k)$ FDs by estimating and studying their parameters at varying spatiotemporal resolutions using ZTD followed by a theoretical investigation with respect to the stationarity and continuity of traffic flow.

4.1 Objective

This study[2] aims to empirically analyze various existing single-regime $v - k$ relationships of different forms by estimating and studying their parameters at varying spatiotemporal resolutions using complete vehicles' trajectory data. The empirical validation using statistical procedures is followed by a theoretical analysis of the considered $v - k$ relations which was not discussed at all in some studies or not completely concluded for all $v - k$ relations in few research works. The objective is twofold: *first*, to identify a model a.) with less complex form; b.) based on '*weaker*' assumptions; c.) reasonably achieves mathematical elegance and empirical accuracy, which are all desirable to have; and *second*, to make the validation more reliable by conducting it over various space-time resolutions which also provides theoretical and practical support to practitioners in decisively choosing most workable $v - k$ functional relation at a particular resolution setting. One of the main contributions of this study is the calibration of FDs using *detailed spatiotemporally information*. This study utilizes complete trajectory data to compute more accurate values of fundamental parameters at fine resolutions which is not possible with other conventional datasets. The approach of this research is not to propose a new $v - k$ functional form but to validate several existing forms using detailed traffic states obtained from complete trajectory data and to study their sensitivity to varying time and space resolutions.

---

[2] This section is majorly based on the research conducted with Prof. Yasuo Asakura and Assoc. Prof. Wataru Nakanishi published in *Asian Transport Studies* (Dahiya *et al.*, 2022).

The remainder of the chapter is structured as follows: section 4.2 elaborates the considered $v - k$ relations where subsections 4.2.1 and 4.2.2, discusses the parameters involved in those considered $v - k$ relations and describes the static and dynamic properties of $q - k - v$ relations, respectively. Section 4.3 describes the data preparation methodology for utilizing ZTD and is followed by section 4.4 on parameter estimation. Sections 4.5 and 4.6 details the empirical validation conducted through statistical analysis using ZTD and theoretical investigation, respectively. Finally, the chapter concludes the findings in section 4.7. The gist of the analysis is covered in section 4.8 that reviews the analysis.

4.2   Functional forms of the $v - k$ relations

Because no consensus has been reached so far on the continuity of the speed-density ($v - k$) functions, this study considers only the single-regime $v - k$ relations. They can be categorized into classes based on their nature namely, linear, logarithmic and exponential, and complex functional forms of $v - k$ equations. Drake *et al.* (1966) is among the initial works that presented and analyzed $v - k$ relations based on such classification of mathematical nature. Table 4.1 lists all the single-regime $v - k$ relations considered in this study. Structure of a similar table was initially described by Wang *et al.* (2010) and has been further modified and reused by Xu *et al.* (2014) and Gaddam and Rao (2019). The contents of Table 4.1 are alike to one by Gaddam and Rao (2019). Based on the assumption that the velocity decreases linearly with density, the linear models are developed and are the simplest in nature. Greenshields *et al.* (1935) was devoted to the investigation of a continuous linear curve with an attractive mathematical simplicity. Even though, in past studies, it has proved to be insufficient to match empirical observations, the model was of groundbreaking significance and has been widely used, including in the *Highway Capacity Manual* 1965 edition and 1985 edition. Model by May and Keller (1967), containing shape parameters m and n (both > 0), is the generalized form of all the linear equations. By changing the values of these parameters (both or one) to 1, the other equations of Greenshields *et al.* (1935), Drew (1968) and Pipes (1967) can be generated. Based on the hydrodynamic analogy, Greenberg (1959) introduced the logarithmic form of $v - k$ equation which involves the parameters optimum speed (v_m) and jam density (k_j). They combined the equations of motion and continuity for one-dimensional compressible flow by treating the traffic as a perfect stream. It bridges the gap

between macroscopic models and the third General Motors car-following model, but it produces infinite speed at free-flow conditions (May, 1990). Gazis *et al.* (1959) showed that this relationship can be independently derived from their microscopic car-following theory for the case in which the sensitivity of the following vehicle is inversely proportional to the spacing between vehicles.

Upon failure of curve by Greenberg (1959) to remain finite at zero density, Underwood (1961) suggested that perhaps the infinity asymptote should be along the density scale. This relation can be traced to the car-following rule, where sensitivity is directly proportional to the speed of the following vehicle and inversely proportional to the square of the spacing (Drake *et al.*, 1966). The exponential model of Papageorgiou *et al.* (1989) is a generalized form of Drake's model (Drake *et al.*, 1966) and Underwood's model, where parameter a takes values 2 and 1, respectively.

The complex form of Newell (1961) $v - k$ model is derived from nonlinear car-following theories and comprises of a proportionality factor (λ) which is a function of C_j and k_j at macro level (Gaddam and Rao, 2019). It is computed by comparing the model of Del Castillo and Benítez (1995) and Newell (1961) such that $-\dfrac{\lambda}{k_j} = C_j$. The traffic flow behavior is strongly characterized by the kinematic wave speed of the vehicles at jam density (C_j), as believed and utilized by Del Castillo and Benítez's $v - k$ models of single and double exponential forms also known as exponential curve and generalized sensitive curve, respectively. Model by Lee *et al.* (1998) consisting of 4 parameters is a rational model and model by Wang *et al.* (2010) consisting of 5 parameters is a logistic model, developed to capture the dynamic behavior of traffic flow occurring at the highway ramps. The latter has been developed using 100 stations data on GA 400 expressway in Atlanta. A rational function is a simple math model that works on the theory of correlation. It can be more accurate than polynomials or thin plate spline as it considers elevation and has less physical significance to the underlying phenomenon of traffic theory. Similarly, the logistic model is stochastic in nature and finds application in a range of fields, including biomathematics, economics, statistics etc.

Table 4.1 Speed-Density $(v - k)$ functional relationship

Author	Functional Form	Parameters
Linear		
Greenshields *et al.* (1935)	$v = v_f \left(1 - \dfrac{k}{k_j}\right)$	v_f, k_j
Drew (1968)	$v = v_f \left[1 - \left(\dfrac{k}{k_j}\right)^m\right]$	v_f, k_j, m
Pipes (1967)	$v = v_f \left(1 - \dfrac{k}{k_j}\right)^n$	v_f, k_j, n
May and Keller (1967)	$v = v_f \left[1 - \left(\dfrac{k}{k_j}\right)^m\right]^n$	v_f, k_j, m, n
Logarithmic		
Greenberg (1959)	$v = v_m \ln\dfrac{k_j}{k}$	v_m, k_j
Exponential		
Underwood (1961)	$v = v_f \exp\left(\dfrac{-k}{k_m}\right)$	v_f, k_m
Drake *et al.* (1966)	$v = v_f \exp\left[-\dfrac{1}{2}\left(\dfrac{k}{k_m}\right)^2\right]$	v_f, k_m
Papageorgiou *et al.* (1989)	$v = v_f \exp\left[-\dfrac{1}{a}\left(\dfrac{k}{k_m}\right)^a\right]$	v_f, k_m, a
Complex		
Newell (1961)	$v = v_f \left\{1 - \exp\left[\dfrac{-\lambda}{v_f}\left(\dfrac{1}{k} - \dfrac{1}{k_j}\right)\right]\right\}$	v_f, k_j, λ
Del Castillo and Benítez (1995)	*Exponential curve* $v = v_f \left\{1 - \exp\left[\dfrac{\|C_j\|}{v_f}\left(1 - \dfrac{k_j}{k}\right)\right]\right\}$ *Maximum sensitivity curve* $v = v_f \left\{1 - \exp\left[1 - \exp\left(\dfrac{\|C_j\|}{v_f}\left(\dfrac{k_j}{k} - 1\right)\right)\right]\right\}$	v_f, k_j, C_j
Lee *et al.* (1998)	$v = \dfrac{v_f\left(1 - \dfrac{k}{k_j}\right)}{1 - E\left(\dfrac{k}{k_j}\right)^\theta}$	v_f, k_j, E, θ
Wang *et al.* (2010)	$v(k, \theta) = v_b + \dfrac{v_f - v_b}{\left[1 + \exp\left(\dfrac{k - k_t}{\theta_1}\right)\right]^{\theta_2}}$	$v_f, k_t, v_b, \theta_1, \theta_2$
Modified Lee *et al.* model by Gaddam and Rao (2019)	$v = \dfrac{v_f\left[1 - \left(\dfrac{k}{k_j}\right)^a\right]}{1 + E\left(\dfrac{k}{k_j}\right)^\theta}$	v_f, k_j, E, θ, a

4.2.1   Parameters involved in the $v - k$ relations

For the discussed $v - k$ models, the list of parameters that have physical significance includes the free-flow speed (v_f), jam density (k_j), m and n (representing the environment and type of facility, respectively), optimum density (k_m), optimum velocity (v_m), proportionality factor (λ) (a function of the relative speed and the inter-vehicles distance), kinematic wave speed of vehicles at jam density (C_j), inflection point where the $q - k$ curve turns from free-flow to congested flow (k_t), and average travel speed of vehicles at saturation region (stop-and-go) (v_b). Kinematic wave speed at jam density (C_j), is claimed to strongly characterize the traffic flow relationships by Del Castillo and Benítez (1995). For Wang *et al.*'s model v_f and v_b are the upper and lower asymptotes of the $v - k$ curve, respectively. θ_1 (a scalar parameter) describes the stretch of curve over the whole density range, θ_2 controls the lopsidedness of the curve and k_t is the point of transition of curve from free-flow to congested flow. Usually, v_f mostly lies between speed limit and highway design speed and is relatively easy to estimate from empirical data. As per the literature review, the value of k_j is observed in the range $115-155\ veh/km$ and that of C_j lies between $-6.94\ m/s$ to -4.16 m/s (Duckstein *et al.*, 1970; Lam and Rothery, 1970; Ozaki, 1993). Since the first proposed equation by Gaddam and Rao (2019) yielded complex values of parameters and could not be estimated using the ZTD therefore, it was not considered in this analysis.

4.2.2   Static and dynamic properties of the functional relations

The first group of mathematical properties of the flow-speed-density ($v - k$) curves, which a precise model should satisfy, are the following static properties (based on stationarity of traffic flow), that may be regarded as trivial or obvious:

1) Free-flow property: $v(k)_{k \to 0} = v_f$.
2) Independent property: $v'(0) = 0$; i.e., the vehicle moves at the free-flow speed when the interaction between vehicles is negligible.
3) Jam density property: $v(k)_{k \to k_j} = 0$; i.e., vehicles stop at the jam density.
4) Density range: $0 < k \leq k_j$; i.e., density varies from zero to maximum density.

5) Speed range: $0 < v \leq v_f$; i.e., speed varies between zero and free-flow speed.

6) Slope property: speed decreases with density, i.e., $v'(k) < 0$.

The abovementioned properties can be deduced by considering the traffic flow as a stationary phenomenon and were already stated by Greenshields (1935). Hence, as "static", they have been referred to again by Del Castillo and Benítez (1995). The representation of a stable shock wave propagation in saturated congested flow region is very essential and to study the continuity of traffic flow two dynamic properties are introduced. The first one was introduced by Del Castillo and Benítez, and it implies that the kinematic wave speed (C_j) of the traffic at a jam condition must be a negative constant (i.e., $q'(k)_{k \to k_j}$ is a negative constant). It represents shock wave propagation in a saturation flow region. A shockwave in real traffic would correspond to a sudden change of speed and to produce stable shock waves at congested conditions, it is required for flow-density relation to be convex (i.e., $q''(k)_{k \to k_j} > 0$, second property). Otherwise, stable shock waves can only occur as transitions from low to high density. However, if there exists a subdomain where the relation has a convex curvature then stable start waves can arise when traffic accelerated from this subdomain to a region of lower density.

4.3 Utilization of ZTD

For this study, the ZTD L001_F001, covering space-time profile of distance of 2 km (5 $k.p.$ to 3 $k.p.$ i.e., 5000 m to 3000 m) and 1 $hour$ (7:00 a.m. to 8:00 a.m.), is utilized. The whole 2 km section of expressway is considered as one link, where traffic can be represented as a set of vehicle trajectories. The ZTD contains data of vehicle trajectories, and it can be a reasonable assumption if the lanes (driving and passing) are considered as sufficiently wide area where effects of lane-changing can be ignored. For the analysis of the $v - k$ relations at different space-time resolutions, the entire space-time area was divided into mesh of varying spatial (hereafter, dx) and temporal resolutions (hereafter, dt). The value of dx varied as $\{25\ m, 50\ m, 100\ m, 200\ m, 400\ m, 500\ m\}$ and the dt varied as $\{1\ s, 5\ s, 10\ s, 30\ s, 60\ s\}$ (forming total 30 datasets). At a macroscopic level, the traffic state, which is a set of the following variables: flow (q), density (k), and average speed (v), for each cell of mesh, was computed using the Edie's definition (Edie, 1963) for every

combination of dx and dt. In order to visualize the traffic states on the $q - k$ FD, the set of all the near-steady traffic states of near-steady areas were extracted. According to the definition of steadiness, for each dataset, the coefficient of variation (ϑ), i.e., the ratio of standard deviation (σ) and the mean of vehicles' speed (Ave) of all the vehicles in each cell, was calculated from empirical data and the cell was considered a steady cell if the ratio is less than or equal to 0.15, i.e., $\vartheta \left(= \frac{\sigma}{Ave} \right) \leq 0.15$. The $q - k$ plots of steady and non-steady traffic states for varying spatiotemporal resolution were visualized, and since there is not enough room and no need to include all of the processed figures here, Figure 4.1 represents one of the plots for $dx = 50\ m$ and $dt = 10\ s$. The x-axis of the plot represents the density (veh/m), and the y-axis represents the flow (veh/s); the blue colored points represent the steady traffic states, and the red colored points are for the non-steady traffic states. After extracting the steady traffic states for each dataset, separate flow-density ($q - k$) and velocity-density ($v - k$) plots were visualized. Figure 4.2 and Figure 4.3 represents one of the $q - k$ plots and $v - k$ plots each, respectively for $dx = 50\ m$ and $dt = 10\ s$. In the $q - k$ plot in Figure 4.2, the x-axis represents the density (veh/m), and the y-axis represents the flow (veh/s). In the $v - k$ plot shown in Figure 4.3, the x-axis represents the density (veh/m), and the y-axis represents the velocity (m/s).
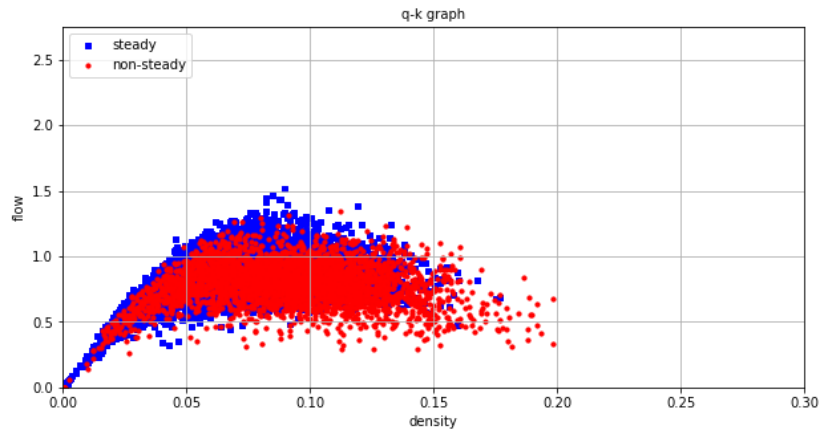
Figure 4.1 q-k plot (steady & non-steady) computed using Edie's definitions for ZTD L001_F001 (7:00 – 8:00 a.m.) for space-time resolution {50 m x 10 s}
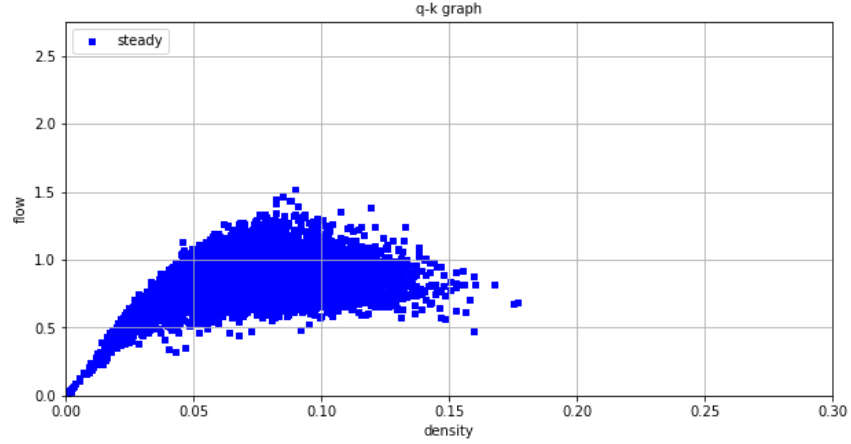
Figure 4.2 q-k plot (steady) computed using Edie's definitions for ZTD L001_F001 (7:00 – 8:00 a.m.) for space-time resolution {50 m x 10 s}
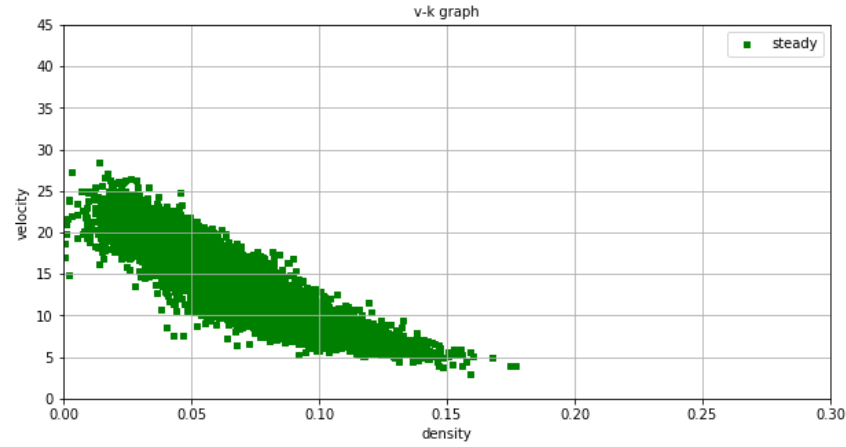
Figure 4.3 $v - k$ plot (steady) computed using Edie's definitions for ZTD L001_F001 (7:00 – 8:00 a.m.) for space-time resolution {50 m x 10 s}

4.4   Parameter estimation

4.4.1   Parameters obtained from the empirical observations

This section discusses the estimation of parameters of the $v - k$ relations considered in the study and their sensitivity to the spatiotemporal resolutions. Some of the parameters involved in the mathematical formulation of the $v - k$ relationships are directly computed from the empirical data and then in turn used to estimate other parameters with the use of an optimization algorithm. For

each dataset, varying as per the spatiotemporal resolution, the maximum velocity (or maximum speed) observed in any cell is considered as the free-flow speed for that dataset. The jam density and the kinematic wave speed are the parameters which are very difficult and challenging to be directly observed and estimated from the empirical data. For 1 $hour$ (7:00–8:00 a.m.), ~89% of the vehicles were of Type 1 with an average vehicle size of 3.93 m, while ~11% of the vehicles were of Type 2 with an average vehicle size of 9.17 m. Correspondingly, the jam density (k_j) (veh/m) was approximated, keeping in mind the critical distance to be around 1.5 m to 0.346 veh/m which was close to the range of 115–155 veh/km mentioned in the literature. Using the coordinates of the optimum point (k_m, q_m), at which the flow was observed to be maximum for each stationary dataset extracted from the whole data, and $(k_j, 0)$, the value of C_j is approximated for each dataset which lies within the range of –25 to –15 km/hr mentioned in literature (except for few outliers). The optimum velocity was calculated using the fundamental equation of traffic flow. At macroscopic level, the proportionality factor (λ) is a function of the kinematic wave speed and jam density of the vehicular flow and can be derived by comparing the Newell's and Del Castillo's exponential equations where $-\frac{\lambda}{k_j}$ represents C_j therefore, $\lambda = C_j k_j$ (Gaddam and Rao, 2019).

Using the original data containing the trajectory details of 3,735 vehicles, certain areas with saturated flow was visualized and the average speeds maintained by all the vehicles in those areas were calculated. The mean of average speed maintained by all the vehicles in different saturated areas accounted to be 6.753 m/s, and hence considered for analysis. Certain parameters (average value over varying dx, dt), such as optimum density (0.083 veh/km), proportionality factor (1.807) and kinematic wave speed of vehicles at jam density (–5.314 m/s) seem promising, well estimated from empirical data and they remained stable throughout the varying spatiotemporal resolution, with their standard deviations standing at 0.019, 0.665, and 1.957, respectively.

4.4.2   Parameters estimated using Levenberg–Marquardt algorithm

The shape parameters of different $v - k$ models namely, m of Drew's, n of Pipes', m and n of May and Keller's, a of Papageorgiou $et\ al.$'s, E and θ of Lee $et\ al.$'s, k_t, θ_1 (a scalar parameter, which describes how the $v - k$ curve is stretched out over the whole density curve) and θ_2 (which

controls the lopsidedness of the curve) of Wang *et al.*'s and a, E, and θ of modified Lee *et al.*'s, were estimated for each dataset using the Levenberg–Marquardt (LMA or just LM) optimization algorithm, also known as damped least-squares (DLS) method, implemented in MATLAB. The LM algorithm interpolates between the method of gradient descent and Gauss–Newton algorithm (GNA) and is more robust, which means that in many cases even if it starts very far off the final minimum, it still finds a solution. It is the most commonly used non-linear least square algorithm. It has been widely used for calibration; Wang *et al.* (2010), Xu *et al.* (2014), and Gaddam and Rao (2019) have used it. Table 4.2 shows the parameter values estimated for all combinations of dx and dt.

The mean and standard deviation of each of the parameters estimated directly from empirical datasets, and using LM algorithm, were calculated over all spatiotemporal resolutions. Most of the parameters estimated using the LM algorithm namely (average value over varying dx, dt), m (0.493), n (3.006), a (1.402), θ (1.912), k_t (0.093), θ_1 (0.036), θ_2 (2.649), θ (2.915) (modified Lee *et al.*), are estimated for each dataset with standard deviation less than 1. It implies that these parameters are not very sensitive to the variations in temporal resolution or spatial resolution. However, for certain parameters such as v_f, a trend could be visualized. The free-flow speed (v_f) was observed to be highest (43 m/s) at the finest resolution {25 m x 1 s} and lowest (21.721 m/s) at the coarsest resolution {500 m x 60 s}. The value of parameter decreased with increase in spatial resolution (maintaining dt at a constant value) and also decreased with increase in temporal resolution (maintaining dx at a constant value). The highest variation occurred in the parameter E in both, Lee *et al.*'s and modified Lee *et al.*'s models, with a standard deviation of 25.188 and 18.956, respectively.

4.5   Curve fitting and statistical evaluation

Geometric fitting of each kind of linear, exponential and logarithmic, and complex (including rational and logistic) forms of $v - k$ models is performed for each dataset. Figure 4.4 shows the geometric fitting of the linear $v - k$ models of Greenshields *et al.*, Drew, Pipes, and May and Keller for several spatiotemporal resolutions (for $dx = 25\ m$, $100\ m$, and $500\ m$ and for all values of dt) and Figure 4.5 shows the fitting of the exponential and logarithmic $v - k$ models of Greenberg, Underwood, Drake *et al.*, and Papageorgiou *et al.*

Table 4.2 Values of estimated parameters using LM algorithm for ZTD: L001_F001

dx, dt	v_r (m/s)	m (Drew)	n (Pipes)	m (May & Keller)	n (May & Keller)	v_m (m/s)	k_m (veh/m/ 2 lanes)	a (Papageorgiou et. al.)	λ	C_j (m/s)	E	θ	k_t	$θ_1$	$θ_2$	a (modified Lee et.al.)	E (modified Lee et.al.)	θ (modified Lee et.al.)
25m1s	43.00	0.022	6.047	0.106	0.626	16.526	0.152	0.523	4.402	-12.948	-2.017	0.174	0.099	0.099	3.000	0.019	-0.942	0.025
25m5s	32.60	0.334	4.187	0.540	1.664	16.233	0.103	0.789	2.344	-6.893	-3.145	0.724	0.095	0.049	3.000	0.374	7.383	2.662
25m10s	31.51	0.352	4.008	0.725	2.354	17.177	0.088	0.904	1.992	-5.860	-4.765	1.009	0.092	0.041	3.000	0.432	9.850	2.438
25m30s	28.91	0.402	3.569	1.008	3.620	16.598	0.067	1.266	1.408	-4.140	-7.854	1.426	0.089	0.033	2.903	0.554	14.900	2.420
25m60s	26.55	0.462	3.134	1.261	5.073	14.214	0.075	1.273	1.341	-3.945	-12.110	1.817	0.088	0.029	2.799	0.748	15.620	2.226
50m1s	42.00	0.241	5.598	0.205	0.886	16.154	0.130	0.582	3.304	-9.718	-2.373	0.310	0.095	0.077	3.000	0.244	62.970	5.849
50m5s	29.41	0.394	3.523	0.725	2.090	17.228	0.098	0.918	2.324	-6.835	-3.500	0.952	0.100	0.043	2.994	0.459	10.800	2.781
50m10s	28.44	0.414	3.375	0.928	2.955	16.837	0.089	1.024	2.000	-5.883	-5.711	1.293	0.095	0.037	2.979	0.538	11.660	2.474
50m30s	26.45	0.465	3.034	1.249	4.737	15.637	0.076	1.299	1.495	-4.396	-11.140	1.819	0.091	0.030	2.841	0.704	17.160	2.439
50m60s	24.04	0.547	2.564	1.610	7.503	13.958	0.077	1.484	1.366	-4.019	-23.240	2.457	0.094	0.026	3.000	1.481	20.820	2.153
100m1s	32.50	0.356	3.969	0.514	1.480	17.959	0.099	0.839	2.447	-7.198	-2.382	0.628	0.102	0.052	2.995	0.381	38.350	4.038
100m5s	28.00	0.436	3.208	0.902	2.677	17.233	0.094	1.020	2.190	-6.440	-4.498	1.208	0.101	0.039	3.000	0.527	16.950	2.932
100m10s	26.37	0.472	2.949	1.152	3.871	17.487	0.085	1.188	1.936	-5.693	-7.881	1.644	0.097	0.033	2.907	0.656	14.570	2.519
100m30s	25.29	0.499	2.790	1.396	5.570	15.892	0.075	1.431	1.500	-4.413	-14.620	2.094	0.096	0.029	3.000	0.806	19.370	2.485
100m60s	22.65	0.604	2.265	1.867	10.020	14.371	0.076	1.701	1.378	-4.052	-41.480	2.995	0.095	0.024	3.000	7.639	39.760	2.509
200m1s	28.00	0.463	3.101	0.913	2.627	8.169	0.082	1.164	1.930	-5.678	-3.863	1.165	0.102	0.039	2.969	0.535	44.110	3.604
200m5s	28.00	0.447	3.167	1.007	3.208	17.835	0.081	1.165	1.842	-5.419	-5.639	1.361	0.095	0.037	2.706	0.547	31.280	3.237
200m10s	25.14	0.522	2.666	1.372	5.146	16.710	0.082	1.338	1.763	-5.186	-12.260	2.034	0.078	0.028	1.780	0.756	22.070	2.725
200m30s	23.91	0.544	2.526	1.620	7.269	17.182	0.068	1.824	1.436	-4.223	-23.460	2.526	0.092	0.026	2.668	1.035	22.470	2.468
200m60s	22.42	0.599	2.263	1.903	10.230	14.063	0.078	1.682	1.391	-4.090	-44.190	3.084	0.092	0.023	2.643	7.522	40.250	2.551
400m1s	25.60	0.579	2.455	1.208	3.664	18.118	0.070	1.616	1.562	-4.594	-5.786	1.643	0.084	0.031	1.844	0.662	16.670	4.359
400m5s	24.73	0.586	2.384	1.492	5.866	16.960	0.072	1.653	1.511	-4.445	-14.980	2.249	0.083	0.028	1.883	0.757	63.720	3.521
400m10s	24.17	0.598	2.315	1.633	7.224	17.069	0.070	1.785	1.471	-4.326	-23.570	2.569	0.094	0.028	2.570	0.828	55.490	3.341
400m30s	23.23	0.607	2.255	1.849	9.774	16.915	0.068	1.996	1.414	-4.158	-42.250	3.006	0.099	0.026	3.000	1.107	33.850	2.768
400m60s	21.88	0.645	2.088	2.151	14.380	15.356	0.070	2.132	1.323	-3.891	-91.860	3.640	0.089	0.021	2.427	6.617	53.370	2.788
500m1s	24.72	0.629	2.208	1.234	3.479	17.300	0.070	1.733	1.492	-4.388	-5.149	1.690	0.093	0.033	2.049	0.728	52.770	3.613
500m5s	24.14	0.635	2.164	1.518	5.683	17.138	0.069	1.847	1.462	-4.300	-14.730	2.332	0.087	0.030	1.824	0.798	55.060	3.470
500m10s	23.81	0.637	2.150	1.634	6.856	15.609	0.075	1.696	1.469	-4.321	-22.400	2.604	0.083	0.031	1.624	0.846	51.070	3.342
500m30s	22.99	0.634	2.150	1.902	10.350	7.132	0.066	2.160	1.383	-4.068	-50.110	3.153	0.102	0.028	2.994	1.114	37.980	2.870
500m60s	21.72	0.654	2.054	2.190	15.020	14.696	0.073	2.022	1.328	-3.905	-104.300	3.748	0.086	0.021	2.071	7.010	58.760	2.851
Mean	27.073	0.493	3.006	1.260	5.530	15.792	0.083	1.402	1.807	-5.314	-20.375	1.912	0.093	0.036	2.649	1.547	31.271	2.915
Std. Dev.	5.139	0.141	0.984	0.541	3.742	2.508	0.019	0.454	0.665	1.957	25.188	0.949	0.006	0.016	0.468	2.276	18.956	0.935

Figure 4.6 shows the fitting of the complex forms of the Newell, Del Castillo and Benítez, Lee *et al.*, Wang *et al.*, and modified Lee *et al.* models for similar spatiotemporal resolutions. Figure 4.4 graphically depicts the trend which is common for all the datasets, that amongst the linear forms, May and Keller's $v - k$ model proves to be outperforming in capturing the nature of the empirical data as compared to other linear forms. Greenshields *et al.*'s model seems to overestimate the velocity, irrespective of the spatial or temporal resolution, and is unable to capture the curvature of the actual data most primarily because of the absence of the shape parameters m and n, which are present in rest three linear forms (one or both). The reason could be that the seminal $v - k$ model by Greenshields was formulated by utilizing only seven data points collected from one lane in a two-way rural road (7th data point was taken from a different road) which are surely not enough to generate a whole picture of a speed-density ($v - k$) model. Similarly, the functional form of the Pipes model commences to overestimate the velocities beyond the critical density as the spatial or temporal resolution becomes coarser.

From Figure 4.5, the trend of logarithmic and exponential $v - k$ relation, common to all the datasets, can be graphically visualized. It was observed that the model proposed by Papageorgiou *et al.* is a better estimator of velocity as compared to overestimating models of Greenberg and Drake *et al.* (for finer spatiotemporal resolutions) and the underestimating model of Underwood (at coarser temporal resolutions). Even though Greenberg's model gained popularity after Greenshields' model as it bridged the gap analytically however, its main criticism is its inability to predict speed at lower densities which can very well be visualized from the plots. Similarly, it can be graphically concluded from Figure 4.6 that among the complex forms, modified Lee *et al.*'s and Wang *et al.*'s models are better candidates to be considered for fitting the empirical velocity-density data. Whereas the form by Lee *et al.* overestimates velocity as finer temporal resolutions.

$\{dx = 25\ m,\ dt = 1\ s\}$ $\{dx = 100\ m,\ dt = 1\ s\}$ $\{dx = 500\ m,\ dt = 1\ s\}$

$\{dx = 25\ m, dt = 5\ s\}$ $\{dx = 100\ m, dt = 5\ s\}$ $\{dx = 500\ m, dt = 5\ s\}$

$\{dx = 25\ m, dt = 10\ s\}$ $\{dx = 100\ m, dt = 10\ s\}$ $\{dx = 500\ m, dt = 10\ s\}$

$\{dx = 25\ m, dt = 30\ s\}$ $\{dx = 100\ m, dt = 30\ s\}$ $\{dx = 500\ m, dt = 30\ s\}$

$\{dx = 25\ m, dt = 60\ s\}$ $\{dx = 100\ m, dt = 60\ s\}$ $\{dx = 500\ m, dt = 60\ s\}$
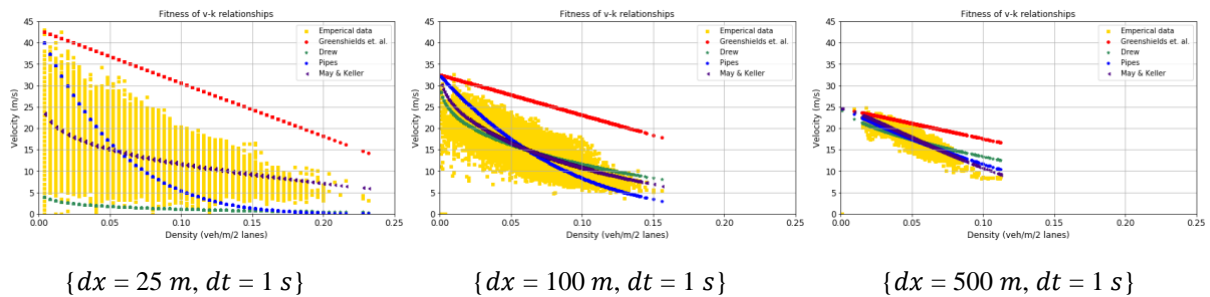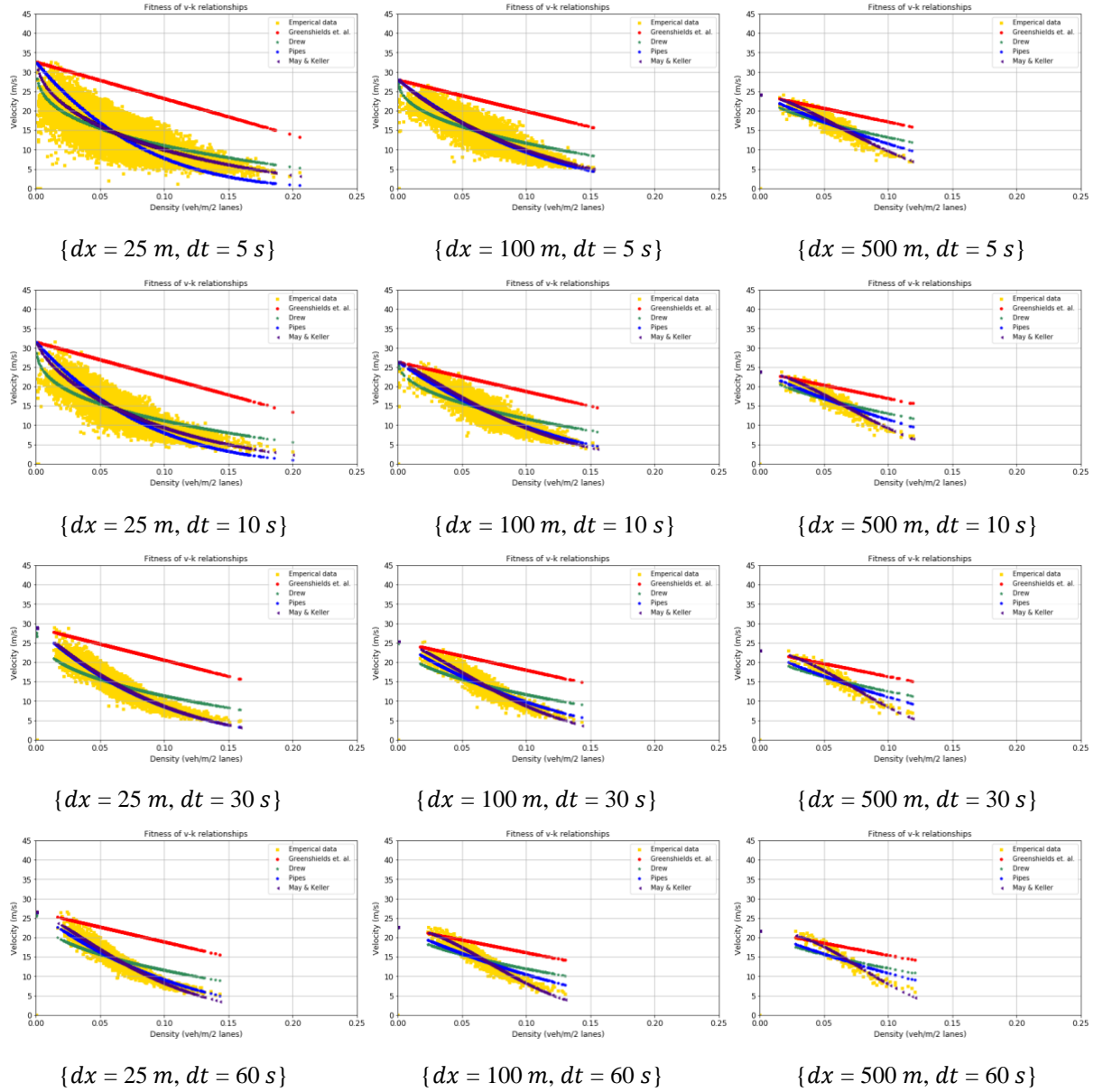
Figure 4.4 Geometric fitness of the linear traffic stream models for (steady) ZTD (7:00 – 8:00 a.m.) for varying spatiotemporal resolutions

$\{dx = 25\ m, dt = 1\ s\}$ $\{dx = 100\ m, dt = 1\ s\}$ $\{dx = 500\ m, dt = 1\ s\}$

$\{dx = 25\ m, dt = 5\ s\}$ $\{dx = 100\ m, dt = 5\ s\}$ $\{dx = 500\ m, dt = 5\ s\}$

$\{dx = 25\ m, dt = 10\ s\}$ $\{dx = 100\ m, dt = 10\ s\}$ $\{dx = 500\ m, dt = 10\ s\}$

$\{dx = 25\ m, dt = 30\ s\}$ $\{dx = 100\ m, dt = 30\ s\}$ $\{dx = 500\ m, dt = 30\ s\}$

$\{dx = 25\ m, dt = 60\ s\}$ $\{dx = 100\ m, dt = 60\ s\}$ $\{dx = 500\ m, dt = 60\ s\}$
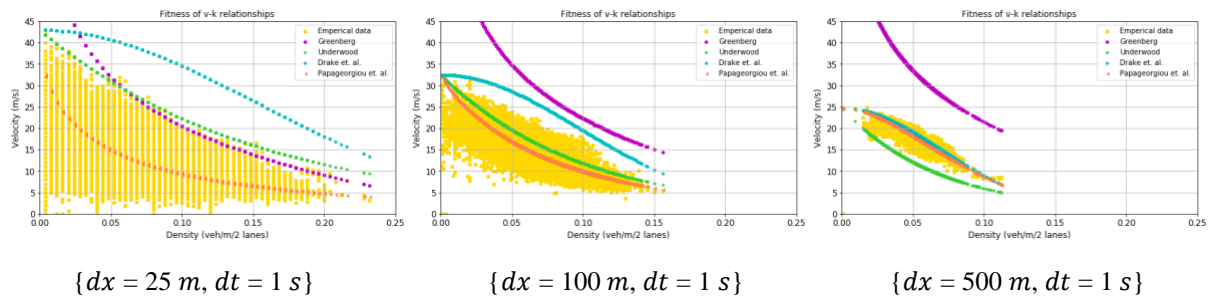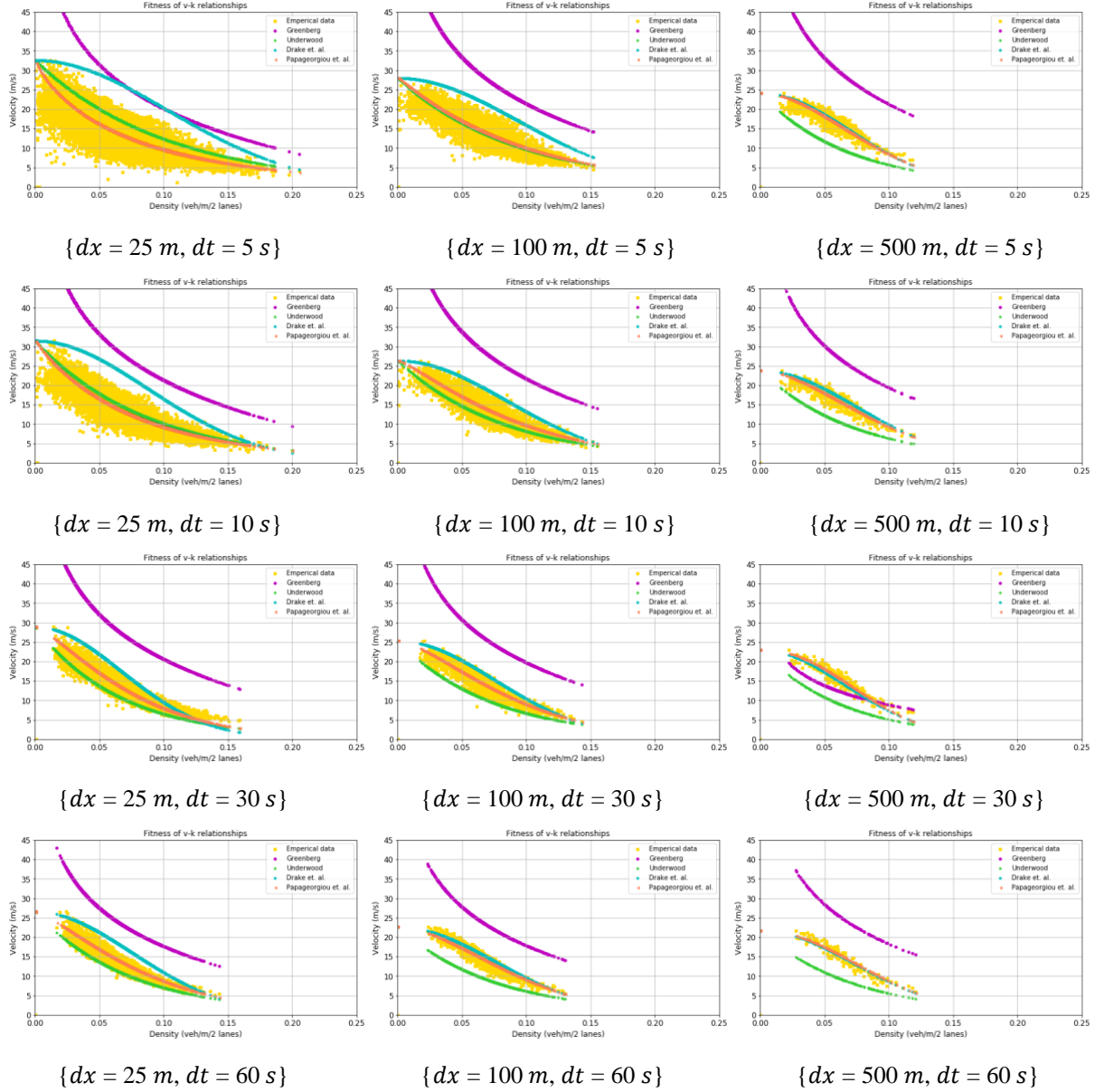
Figure 4.5 Geometric fitness of the exponential and logarithmic traffic stream models for (steady) ZTD (7:00 – 8:00 a.m.) for varying spatiotemporal resolutions

$\{dx = 25\ m, dt = 1\ s\}$ $\{dx = 100\ m, dt = 1\ s\}$ $\{dx = 500\ m, dt = 1\ s\}$

$\{dx = 25\ m,\ dt = 5\ s\}$ $\{dx = 100\ m,\ dt = 5\ s\}$ $\{dx = 500\ m,\ dt = 5\ s\}$

$\{dx = 25\ m,\ dt = 10\ s\}$ $\{dx = 100\ m,\ dt = 10\ s\}$ $\{dx = 500\ m,\ dt = 10\ s\}$

$\{dx = 25\ m,\ dt = 30\ s\}$ $\{dx = 100\ m,\ dt = 30\ s\}$ $\{dx = 500\ m,\ dt = 30\ s\}$

$\{dx = 25\ m,\ dt = 60\ s\}$ $\{dx = 100\ m,\ dt = 60\ s\}$ $\{dx = 500\ m,\ dt = 60\ s\}$
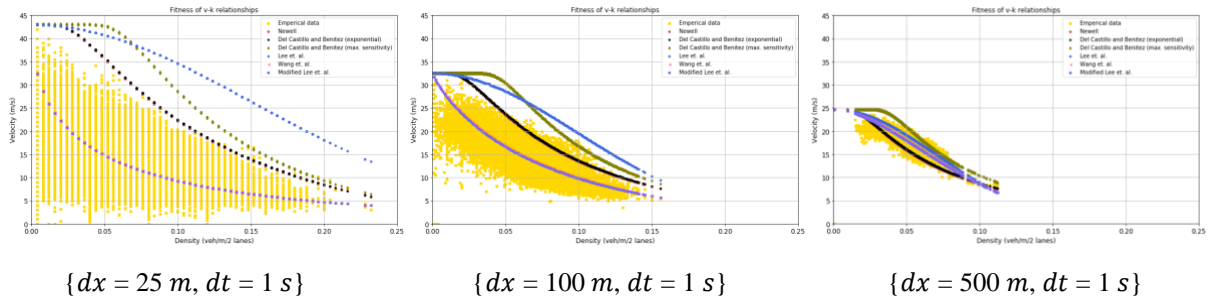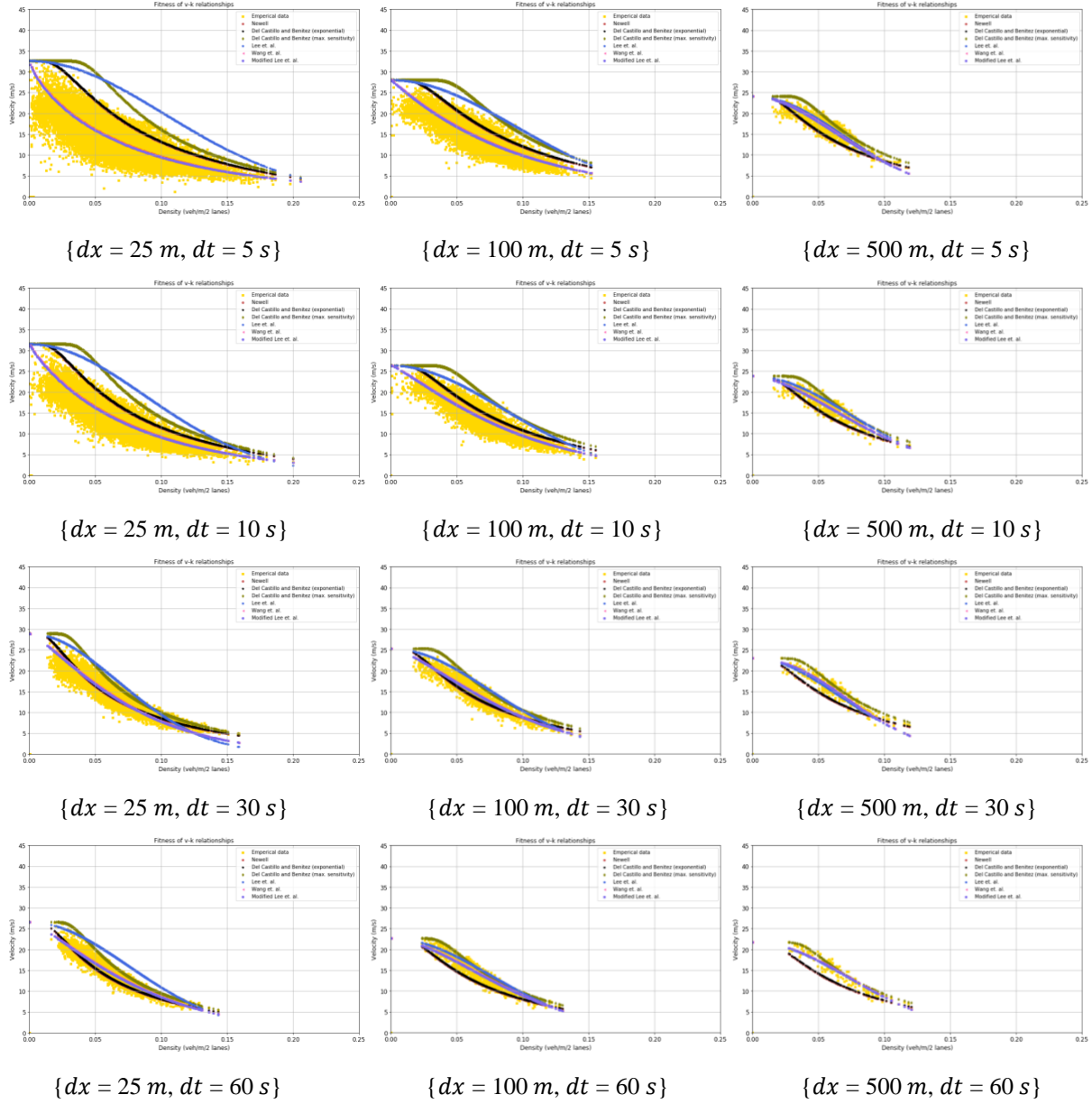
Figure 4.6 Geometric fitness of the complex traffic stream models for (steady) ZTD (7:00 – 8:00 a.m.) for varying spatiotemporal resolutions

The wide scatter often found in $q - k$ plots is mainly because it may include non-equilibrium states and if such non-equilibrium states are removed, an actual data-based bivariate $q - k$ plots will be well-defined (Cassidy, 1998; Coifman, 2014). However, the $q - k$ and $v - k$ data, as per Figure 4.2 and Figure 4.3, plotted using stationary traffic states (with assumed condition on stationary) displays a great deal of scatter. The scatter in the congested regime is known as hysteresis phenomenon in which trajectories of heterogenous vehicles with their respective driving

styles of acceleration and deceleration forms different curves when transitioning from lower density to higher or that from higher to lower (Newell, 1962; Treiterer and Myers, 1974; Laval, 2011). Figure 4.7 and Figure 4.8 depicts the $q - k$ and $v - k$ plots for the spatiotemporal resolutions of $\{dx = 400\ m,\ dt = 60\ s\}$ and it can be seen that the relationship can be said to exist only between data averaged over fairly long periods of time and space. Certain models do not fit to the actual traffic data accurately because they either depend on parameters estimated from empirical observations (such as Greenberg's model) or have a fixed form (such as Greenshields *et al.* model with "linear" form) (Dahiya *et al.*, 2020).
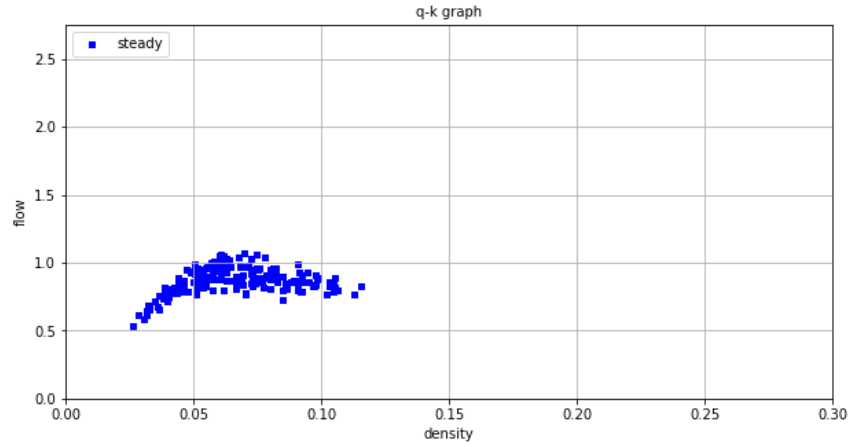
Figure 4.7 $q - k$ plot of (steady) ZTD L001_F001 (7:00 – 8:00 a.m.) for space-time resolution {400 m x 60 s}
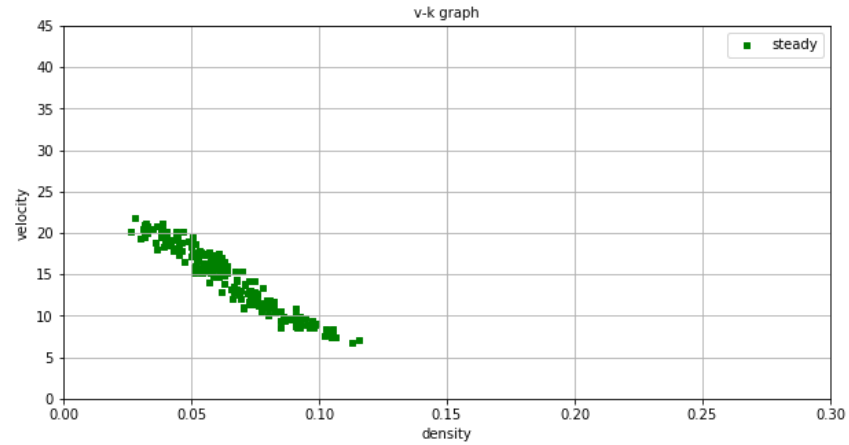
Figure 4.8 $v - k$ plot of (steady) ZTD L001_F001 (7:00 – 8:00 a.m.) for space-time resolution {400 m x 60 s}

To analyze the models' fitness deeply and evaluate the well fitted models of $v - k$ relationships numerically, statistical analysis is done. To do so, statistical scores such as the root

mean square error (RMSE) and the average relative error (ARE), are calculated as per definitions in equations (4.1) and (4.2). RMSE is a measure of the spread of prediction errors (also known as residuals), i.e., the standard deviation. Residuals are a measure of how far from the regression line the data points are. Likewise, ARE is another tool for computing model accuracy in predicting the data. The lower the values of ARE and RMSE are, the greater is the model accuracy.

$$Root\ mean\ square\ error\ (RMSE) = \sqrt{\frac{\sum_{i=1}^{n}(P_i - O_i)^2}{n}} \tag{4.1}$$

$$Average\ relative\ error\ (ARE) = \frac{1}{n}\sum_{i=1}^{n}\frac{|P_i - O_i|}{|O_i|} \tag{4.2}$$

where at a specific value of density at i^{th} point, O_i represents empirically observed data, P_i is the value estimated by the model and n is the number of data points in the dataset.

Each $v - k$ model is ranked based on the values of RMSE and ARE separately, using which an overall rank is computed by taking the arithmetic mean of RMSE ranking and ARE ranking, for each model in each dataset as can be visualized in Table 4.3 (for case $dx = 25\ m$, $dt =$ varying). Moreover, Table 4.4 represents the variation of overall rankings of all the models for different spatiotemporal resolutions and gives insights about the model performance which can be utilized or applied at a particular resolution. From the analysis, it can be concluded that Wang *et al.*'s and modified Lee *et al.*'s model are the best performing models in the category of complex models and that they outperform all other $v - k$ models overall as well. The spatiotemporally detailed information aids in determining the sensitivity of the $v - k$ models to spatiotemporal resolutions. For example, Wang *et al.*'s model outperforms all the other models considered in capturing the nature of the empirical data when the spatial resolution is finer than $400\ m$.

Likewise, at coarser spatial resolutions, RMSE and ARE in modified Lee *et al.*'s model starts to decrease when traffic state values are aggregated for longer distances and performs better than Wang *et al.*'s model. Following them are the models of May and Keller and Papageorgiou *et al.* which are also the best-performing models in their categories of Linear and Exponential & Logarithmic models, respectively. Greenshields *et al.*'s and Greenberg's model have throughout performed poorly in representing the data, with large values of RMSE and ARE for almost all spatiotemporal resolutions. The accuracy of Underwood's model deteriorates as the spatial

resolution becomes coarser, irrespective of time resolution. From the statistical analysis and graphical representation, it can be concluded that some models are sensitive to resolution, and some are not. Even being a simple linear model, May and Keller's model has been amongst the top 3 models in terms of the statistical error, for almost all the datasets.

Digging deep, statistical metric, mean bias (MB) amongst predicted and empirical data, has been calculated for the models of Wang *et al.*, modified Lee *et al.*, and May and Keller, for each dataset. The MB captures the average bias in the prediction and in the observed as defined by equation (4.3), which uses the same variables as equations (4.1) and (4.2).

$$Mean\ bias\ (MB) = \frac{1}{n}\sum_{i=1}^{n}(P_i - O_i)$$ (4.3)

It was found that the May and Keller's model had the least value of MB when averaged for all datasets (for varying spatiotemporal resolutions). The values were 0.011, 0.191, and 0.041 for the models of May and Keller, Wang *et al.*, and modified Lee *et al.*, respectively. The models which are more stochastic in nature with a large number of parameters, such as Wang *et al.*'s model (five parameters), and modified Lee *et al.*'s model (five parameters), are sound descriptors of empirical data. By incorporating the parameter "a" in Lee *et al.*'s model (four parameters), to formulate modified Lee *et al.*'s model, the accuracy has been considerably improved. However, the noncomplex and linear form of $v - k$ relation of the May and Keller's model can be considered of high potential in practical applications. Thus, by identifying May and Keller's model as a model of less complexity that was developed based on '*weaker*' assumptions and which reasonably achieves empirical accuracy (which are all desirable to have); and by empirically analyzing various existing $v - k$ relations of different forms and estimating their parameters at varying spatiotemporal resolutions using the trajectory data of 100% vehicles (which also makes their identification and validation more reliable), the two objectives of the study have been achieved. The empirical validation using statistical procedures is followed by a theoretical analysis of the considered $v - k$ relations which was not discussed at all in some related previous studies or not completely concluded for all $v - k$ relations in few research works. To ascertain whether the models follow the static and dynamic properties of traffic flow, the following section presents a theoretical analysis. Collectively with empirical analysis it will provide theoretical and practical support to practitioners in decisively choosing most workable $v - k$ functional relation.

Table 4.3 Ranking the $v - k$ relations based on statistical metric scores for spatial resolution dx = 25m

dx, dt	Errors	Greenshields et al.	Drew	Pipes	May & Keller	Greenberg	Underwood	Drake et al.	Papageorgiou et al.	Newell	Del Castillo & Benitez (Exponential curve)	Del Castillo & Benitez (Max. Sensitivity curve)	Lee et al.	Wang et al.	Modified Lee et al.'s model
		Linear				**Logarithmic & Exponential**					**Complex**				
25m1s	RMSE	21.029	13.225	7.127	3.703	18.134	15.117	24.657	4.425	18.196	18.381	23.756	3.671	3.628	3.693
	RMSE Ranking	12	7	6	4	9	8	14	5	10	11	13	2	1	3
	ARE	0.597	7.726	0.604	0.210	0.510	0.503	0.636	0.244	0.540	0.544	0.619	0.208	0.204	0.204
	ARE Ranking	10	14	11	4	7	6	13	5	8	9	12	3	2	1
	Overall Rank	**11**	**10.5**	**8.5**	**4**	**8**	**7**	**13.5**	**5**	**9**	**10**	**12.5**	**2.5**	**1.5**	**2**
25m5s	RMSE	12.523	2.680	3.031	2.523	15.485	4.504	12.285	2.591	6.756	6.910	11.453	2.566	2.455	2.482
	RMSE Ranking	13	6	7	3	14	8	12	5	9	10	11	4	1	2
	ARE	0.470	0.156	0.183	0.141	0.505	0.216	0.465	0.142	0.292	0.299	0.431	0.144	0.138	0.140
	ARE Ranking	13	6	7	3	14	8	12	4	9	10	11	5	1	2
	Overall Rank	**13**	**6**	**7**	**3**	**14**	**8**	**12**	**4.5**	**9**	**10**	**11**	**4.5**	**1**	**2**
25m10s	RMSE	11.655	2.450	2.209	2.025	16.598	2.502	9.699	2.054	4.603	4.754	9.052	2.284	1.962	1.987
	RMSE Ranking	13	7	5	3	14	8	12	4	9	10	11	6	1	2
	ARE	0.454	0.147	0.130	0.114	0.533	0.129	0.405	0.114	0.216	0.224	0.373	0.122	0.111	0.115
	ARE Ranking	13	8	7	2	14	6	12	3	9	10	11	5	1	4
	Overall Rank	**13**	**7.5**	**6**	**2.5**	**14**	**7**	**12**	**3.5**	**9**	**10**	**11**	**5.5**	**1**	**3**
25m30s	RMSE	9.517	2.273	1.454	1.454	15.128	3.010	4.509	1.530	1.668	1.663	4.273	1.484	1.411	1.431
	RMSE Ranking	13	9	4	3	14	10	12	6	8	7	11	5	1	2
	ARE	0.399	0.138	0.082	0.082	0.514	0.241	0.220	0.090	0.087	0.085	0.192	0.082	0.079	0.083
	ARE Ranking	13	9	3	4	14	12	11	8	7	6	10	2	1	5
	Overall Rank	**13**	**9**	**3.5**	**3.5**	**14**	**11**	**11.5**	**7**	**7.5**	**6.5**	**10.5**	**3.5**	**1**	**3.5**
25m60s	RMSE	7.534	2.217	1.335	1.200	10.798	2.930	4.329	1.209	1.634	1.540	3.196	1.193	1.168	1.187
	RMSE Ranking	13	9	6	4	14	10	12	5	8	7	11	3	1	2
	ARE	0.335	0.131	0.076	0.069	0.427	0.215	0.223	0.068	0.095	0.087	0.151	0.066	0.064	0.067
	ARE Ranking	13	9	6	5	14	11	12	4	8	7	10	2	1	3
	Overall Rank	**13**	**9**	**6**	**4.5**	**14**	**10.5**	**12**	**4.5**	**8**	**7**	**10.5**	**2.5**	**1**	**2.5**

Speed-Density Functional Relationships

Table 4.4 Overall ranking of $v - k$ relations using ZTD L001_F001 for varying spatiotemporal resolutions

dx, dt	Linear				Logarithmic & Exponential						Complex			
	Greenshields et al.	Drew	Pipes	May & Keller	Greenberg	Underwood	Drake et al.	Papageorgiou et al.	Newell	Del Castillo & Benitez (Exponential curve)	Del Castillo & Benitez (Max. Sensitivity curve)	Lee et al.	Wang et al.	Modified Lee et al.'s model
25m1s	11	10.5	8.5	4	8	7	13.5	5	9	10	12.5	2.5	1.5	2
25m5s	13	6	7	3	14	8	12	4.5	9	10	11	4.5	1	2
25m10s	13	7.5	6	2.5	14	7	12	3.5	9	10	11	5.5	1	3
25m30s	13	9	3.5	3.5	14	11	11.5	7	7.5	6.5	10.5	3.5	1	3.5
25m60s	13	9	6	4.5	14	10.5	12	4.5	8	7	10.5	2.5	1	2.5
50m1s	12.5	3.5	6	3.5	10.5	7	14	5	8	9	12.5	10.5	1	2
50m5s	13	7.5	6.5	3	14	7	11	4	9	10	12	5	1	2
50m10s	13	8	5	2.5	14	7	11	4	9	10	12	5.5	1	3
50m30s	13	8	5.5	2.5	14	10	10.5	5.5	6	5	9.5	2	12	1.5
50m60s	12.5	9.5	6	4	14	12.5	11	5	8.5	7	9	3	1.5	1.5
100m1s	13	5.5	7	3	14	8	11.5	5	9	10	11.5	4.5	1	2
100m5s	13	8	3.5	3.5	14	6.5	11	5	9	10	12	6.5	1	2
100m10s	13	8	6	3.5	14	9.5	11	5	7.5	9	12	3	1	2.5
100m30s	12.5	9	7.5	4.5	14	12.5	10	4	7.5	6	11	2.5	1	3
100m60s	12	10.5	7.5	4.5	13.5	13.5	6	4	10.5	9	7.5	3.5	1	1
200m1s	14	7	3.5	4	8	10	12	5	9.5	10.5	13	5.5	2	2
200m5s	13	8	4.5	3.5	14	9.5	11	4	7.5	9.5	12	6	1	2
200m10s	13	9	7.5	3.5	14	11	10.5	5	6	7.5	11.5	3	1	2.5
200m30s	12.5	10.5	7	4	13.5	13	6	5	9	8	10.5	3	1.5	1.5
200m60s	12.5	11	8	3.5	13.5	13	6	5	10	9	7	3.5	1.5	1.5
400m1s	12	6	4	2	14	13	9.5	5	9	7.5	11	3	1	8
400m5s	12	8	6	3.5	14	13	8	5	10	8	11	3.5	2	1
400m10s	12	8	7	3.5	13.5	13.5	6	4.5	10.5	9	10.5	1.5	4	1.5
400m30s	12	9.5	7.5	3.5	13.5	13.5	5.5	5.5	11	9.5	7.5	2.5	2.5	1.5
400m60s	11.5	9	8	4	13.5	13.5	6	3	11.5	10	7	5	2	1
500m1s	12	7	5	3	14	13	8	6	10.5	9	10.5	4	2	1
500m5s	12	8	6.5	3	13.5	13.5	6.5	5	10.5	9.5	10	2	2	1
500m10s	12	8	6	3.5	13.5	13.5	7	3.5	10.5	9.5	10	1.5	4	1
500m30s	12.5	9	7.5	3	12.5	14	6	4.5	11	10	7.5	2	5	1.5
500m60s	11.5	9	8	4	13.5	13.5	4	4	11.5	10	7	6	1.5	1.5

1st Best Performing   2nd Best Performing   3rd Best Performing   4th Best Performing

4.6   Theoretical analysis

Following the empirical analysis of the considered $v - k$ relations, the static and dynamic properties of the models are validated in this section. Even though the data considered in the statistical evaluation of the $v - k$ relations were extracted using the definition of stationarity but for a model to accurately represent the traffic behavior, it is required for it to satisfy the static properties that are derived from the fact that traffic flow is stationary and is always at equilibrium. Dynamic properties that are obtained from the continuum theory of traffic flow relates to the stable propagation of shock wave in the saturation flow region and kinematic wave speed, which is an important characteristic of traffic flow behavior. Table 4.5 presents information about which all properties are satisfied by the different $v - k$ models.

4.6.1   Evaluation of the static properties of the models

As discussed earlier, static properties consist of six major properties related to the mathematical nature of the $v - k$ curve and boundary value conditions of velocity and density. These properties are evaluated mathematically through first-order derivative and/or limit calculations of the $v - k$ relations based on the definition of properties. The value of vehicular speed must range between the free-flow speed $(v(k)_{k \to 0} = v_f$ and 0 $(v(k)_{k \to k_j} = 0)$. $v'(k)_{k \to 0} = 0$ is a local property and implies that as the traffic density approaches zero, the variation of velocity with respect to density would be zero, i.e., the dependence of velocity on density disappears. The value of density ranges between zero and jam density (k_j) and the speed of vehicles tends to 0 as the traffic approaches a jam situation. It can also be graphically visualized that the speed decreases with density, i.e., $v'(k) < 0$. Table 4.5 shows that the models of Drew, May and Keller, Newell, Del Castillo and Benítez, and modified Lee *et al.* satisfy all the six static properties. Greenberg's model fails to predict speed at lower densities, because as the density approaches zero, the speed tends to increase to infinity. Even though Underwood's model was developed as an attempt to overcome the limitations of Greenberg's model, however, it fails to satisfy the speed range properties because the speed becomes zero only when the density reaches infinity. So, it cannot be utilized for predicting speeds at higher densities. A similar theoretical investigation was conducted by Gaddam

and Rao (2019) and concluded the inability of models of Underwood, Drake *et al.*, and Papageorgiou *et al.* in satisfying both, the jam density property and speed range property. Even though the analytical conclusion of this study is like theirs but not completely. It depends on the ratio of the jam density (k_j) and optimum density (k_m). This is empirically supported by parameter estimation results, which revealed that for all the datasets considered in this study, with varying spatiotemporal resolution, the velocity actually stood very close to zero when the density reached jam density. For each dataset, the value of estimated velocity is less than or around 1 m/s when $k \rightarrow k_j$. Moreover, almost any jam always has some finite movement (Drake *et al.*, 1966). However, the statistically dominating logistic model of Wang *et al.* is unable to satisfy the jam density property, density range property and speed range property. Among the three $v - k$ models that perform best statistically, only two, namely, the *simple linear form* of May and Keller and highly parameterized form of modified Lee *et al.* model, satisfy all six static properties. This adds mathematical elegance as another property to May and Keller's model, which has been identified as having high potential in previous section.

4.6.2   Evaluation of the dynamic properties of the models

The validation of the two dynamic properties for the models that are neither sound estimators of empirical data nor satisfies all the static properties holds not much meaning to itself. Models such as Greenshields *et al.* and Greenberg are poor representors of the actual traffic data with large values of RMSE as compared to other models as well as do not satisfy some of the static properties. The last two columns of Table 4.5 show the evaluation of the $v - k$ relation towards dynamic properties: kinematic wave speed property and stable shock wave property.

Kinematic wave speed property is checked by finding the value of first-order derivative of the flow equation with respect to density, as $k \rightarrow k_j$. For a model to satisfy this property, the value of this gradient at jam density has to be a negative constant. From the analysis, it is observed that the property holds good for Greenberg's model, amongst the Logarithmic and Exponential models; Newell's, Del Castillo and Benítez's, Lee *et al.*'s, and modified Lee *et al.*'s models from the complex forms of models, where the value of $q'(k)$ as $k \rightarrow k_j$ becomes a negative constant. For all linear forms and remaining logarithmic and exponential forms (models of Underwood, Drake

et al., and Papageorgiou *et al.*), the values of $q'(k)$ as $k \to k_j$ are either tending to 0 or close to the negative of free-flow velocity (v_f). The only complex form that does not satisfy this property is Wang *et al.*'s model, the only model producing $-\infty$ value of $q'(k)$ as $k \to k_j$. The stable shock wave property is analyzed by obtaining the second–order derivative of the flow equation with respect to density, as $k \to k_j$. Amongst the linear models, the model of Pipes, and May and Keller show a positive curvature based on some mathematical conditions of inequalities. Among the logarithmic and exponential models, only exponential forms of Underwood, Drake *et al.*, and Papageorgiou *et al.* models show convex nature in their subdomain and thus can produce stable shock waves. Only Lee *et al.* and modified Lee *et al.* models of complex forms satisfy the stable shock wave property. The analysis of the dynamic properties reveals that none of the existing models, except modified Lee *et al.* model, satisfies both the properties. Also, except Modified Lee *et al.*'s model, none of the considered speed-density ($v-k$) models entirely fulfills the abovementioned restrictions, including both static and dynamic properties. Some of them extend over an infinite range of densities or speeds, which is obviously not realistic, and the property more often violated is that of stable shock wave property.

Table 4.5 Validation of mathematical (static & dynamic) properties of $v-k$ relations

	v-k Relations	Static Properties						Dynamic Properties	
		Free flow property (i)	Independent property (ii)	Jam density property (iii)	Density range property (iv)	Speed range property (v)	Slope property (vi)	Kinematic wave speed property	Stable shock wave property
Linear	Greenshields et. al.	✓	✗	✓	✓	✓	✓	✗	✗
	Drew	✓	✓	✓	✓	✓	✓	✗	✗
	Pipes	✓	✗	✓	✓	✓	✓	✗	O
	May & Keller	✓	✓	✓	✓	✓	✓	✗	O
Logarithmic & Exponential	Greenberg	✗	✗	✓	✓	✗	✓	✓	✗
	Underwood	✓	✗	✗	✗	✗	✓	✗	✓
	Drake et. al.	✓	✓	✗	✗	✗	✓	✗	✓
	Papageorgiou et. al.	✓	✓	✗	✗	✗	✓	✗	O
Complex	Newell	✓	✓	✓	✓	✓	✓	✓	✗
	Del Castillo & Benitez (Exponential curve)	✓	✓	✓	✓	✓	✓	✓	✗
	Del Castillo & Benitez (Max. Sensitivity curve)	✓	✓	✓	✓	✓	✓	✓	✗
	Lee et. al.	✓	✗	✓	✓	✓	✓	✓	O
	Wang et. al.	✓	✓	✗	✗	✗	✓	✗	✗
	Modified Lee et. al.'s model	✓	✓	✓	✓	✓	✓	✓	✓

✓	satisfies	✗	does not satisfy	O	satisfy based on certain condition of inequalities

4.7   Conclusions and discussions

This study aimed to analyze statistically and theoretically the performance of single-regime speed-density $(v - k)$ functional relationships at varying spatiotemporal resolutions in simulating the real traffic using the high resolution and complete trajectory data, namely, the ZTD. One of the key foci of this study was on identifying a model with less complex form, based on '*weaker*' assumptions, reasonably achieves mathematical elegance, and empirical accuracy, which are all desirable to have; and second, to make the validation more reliable by conducting it over various space-time resolutions. The study assumed the existence of the stationary traffic state and considered the $v - k$ relations to be fundamental diagrams.

Conclusions: The statistical analysis initiated by estimating the parameters of the considered $v - k$ relations from empirical data and using the LM Optimization Algorithm and studying their sensitivity to variation in spatial and temporal resolutions. Upon analysis it was concluded that modified Lee *et al.* model, Wang *et al.* model and May and Keller's model empirically outperformed the rest of the $v - k$ forms in that order for all the considered spatiotemporal resolutions. Modified Lee *et al.*'s and Wang *et al.*'s models are complex and highly parameterized, whereas the model of May and Keller is based on a simple assumption of linearity. The analysis revealed the models' performances and their sensitivity to the variation of spatial and temporal resolutions. The reason for the poor performances of certain models, irrespective of resolutions, could be attributed to the assumptions taken into consideration while formulating the models in theoretical sense. Leading the discussion towards the theoretical analysis, the advantages of a theoretically strong functional form are as follows: firstly, it adds value to the relationship among the traffic states if it is representative of the physics of traffic. Therefore, utilizing a theoretically strong fundamental relationship, for instance in traffic states estimation where the approach is based on physical traffic flow models, will eventually help in estimating an accurate traffic state even with less dependency on large input data. In addition, it has high explanatory power, i.e., even if there are errors present in the estimation, it would be possible to identify the reasons as well as confidence intervals. The theoretical analysis of the considered $v - k$ relations reveals that only the modified Lee *et al.*'s model by Gaddam and Rao (2019) is capable of satisfying all the static and dynamic properties, which also has an empirically strong functional form. Following to

it are the models of Newell and Del Castillo and Benítez (both satisfy 7 properties (static: 6, dynamic: 1); but performed poorly in statistical analysis); May and Keller (static: 6, dynamic: 1 (conditionally)), and Lee *et al.* (static: 5, dynamic: 1+1 (conditionally)). It is unavoidable to mention that in spite of the fact that Newell's complex $v - k$ relation theoretically performs very well by satisfying all 6 static properties and the kinematic wave speed dynamic property, it statistically showed poor performance. Nonetheless, the graphical fits of Newell's form along with modified Lee *et al.*'s form give an indication of existence of some uniform bias in the estimation, which can either be bias corrected or reconsidered in regard to theoretical assumptions made while it was formulated, in order to revamp the Newell's functional $v - k$ relationship.

Discussions: Simple and easy-to-handle compact equation with low computational cost that reasonably achieves empirical and mathematical elegance can prove to be more efficient in terms of quality and quantity when using with emerging extensive data. Conclusively, the linear model of May and Keller can be considered as a potential fundamental relationship for practitioners, analysts and traffic engineers working on extensive voluminous data for the following reasons:

1) Its compact and less complex linear form with only two shape parameters and two parameters of physical significance makes it easy-to-handle for computational work.
2) The formulation approach is not data driven, rather is based on a simple mathematical argument. The rationale for this argument arises from the assumption that the speed decreases linearly with density.
3) The empirical accuracy of the model is very close to the outperforming complex forms of modified Lee *et al.* (rational model) and Wang *et al.* (logistic model) models.
4) In terms of mathematical elegance, it satisfies all the static properties and one dynamic property (conditionally). Other $v - k$ relations with similar performance are those developed by Drew, Newell, Del Castillo and Benítez, and modified Lee *et al.* However, the first three are empirically poor estimators and also, the models of Newell and Del Castillo and Benítez have more complex mathematical equations as compared to that of May and Keller. The modified Lee *et al.*'s model, with three shape parameters, is a rational and comparatively more complex form of function.

The importance of the research also lies in the utilization of the spatiotemporally detailed and complete ZTD to compute more accurate values of the fundamental parameters at fine resolutions, which was not possible with other conventional datasets. ZTD is more reliable for deducing inferences from the performance or accuracy evaluation done on fundamental relations or TSE methods because of its spatiotemporally detailed information (at a temporal sampling rate of 0.1 s). Wide-ranging and detailed data is difficult to be acquired simultaneously (using loop detectors or fixed-point observation methods) because the observable area of the methods is limited to the vicinity of the devices' installed points. In ZTD, a unique vehicle ID is allocated to each vehicle that traveled on the expressway, which is observed and maintained throughout the target section of road and target time duration. There is a continuity of data at 0.1 s time step with no loss. Such detailed information was rarely available in the past.

4.8   Gist: input, assumptions, output

This chapter included analysis of the single-regime speed-density ($v - k$) relationships for urban expressways using high resolution ZTD containing all vehicles' trajectory data. The steady-state (*an assumption*) traffic data were extracted for varying spatiotemporal resolutions (*input*). It is followed by estimation of traffic flow parameters (*output*), namely, jam density, kinematic-wave-speed, and proportionality factor (a behavioral parameter) using empirical data. Functional and shape parameters (*output*) were estimated using the Levenberg–Marquardt algorithm.

Statistical metrics were used to assess the performance and model fitness in all categories of linear, exponential and logarithmic, and complex forms of $v - k$ relationships for different resolutions. It concluded complex forms of Wang's model, modified Lee *et al.*'s model, and linear form of May and Keller's model are top 3 best performing models. The theoretical analysis reveals that certain relationships satisfy all the static properties and that only one satisfies both the dynamic properties of traffic behavior. Highly parameterized forms had the lowest errors. However, the linear form of model developed by May and Keller (1967) has high application potential. The limitation and future research directions are discussed in section 7.2.1.

5 ANALYSIS OF $xFCD$-BASED TSE METHOD

This chapter elaborates the analysis of a '*weaker*' assumption and extended floating car data ($xFCD$)-based TSE method and explores its estimation capability at different spatiotemporal resolutions and probe penetration rates using ZTD.

5.1 Objective

This study[3] aims to evaluate the performance of an extended floating car data ($xFCD$)-based traffic state estimation method proposed by Seo *et al.*, (2015b), which does not rely on any strong assumptions such as Fundamental Diagram, using high-resolution complete trajectory data: ZTD. The method is *'weaker'* assumption-based traffic state estimation method which utilizes only mobile data: $xFCD$, where each probe vehicle could measure the spacing between it and its leading vehicle. With continuous advancements in autonomous technologies and the massive emergence of connected vehicles, this approach may become prevalent in the near future, provided it can estimate nearly accurate traffic state. However, currently, only a few percentages of probes are expected on the highways of Japan, where the maximum size of the spatiotemporal cell can be 200 m x 300 s. Additionally, ramp metering and signal control require spatiotemporally detailed information for the target road sections. This study aims to analyze the performance of the estimation method at different *settings*, namely, probe penetration rate, spatial resolution, and temporal resolution. In other words, the objective is to explore that using this TSE method how much accuracy can be expected under finer spatiotemporal resolution and fewer probe penetration rates. Traffic state estimated by this method, considering randomly sampled trajectories of ZTD as those of probe vehicles with known penetration rates, are compared with ones obtained by complete ZTD by applying Edie's generalized definitions (Edie, 1963). The variation in estimation

---

[3] This section is majorly based on the research conducted with Prof. Yasuo Asakura published in *International Journal of Intelligent Transportation Systems Research* (Dahiya and Asakura, 2021).

errors and covering percentages are analyzed for varying *settings*: spatiotemporal resolution and probe penetration rates.

The remainder of the chapter is structured as follows: section 5.2 describes the TSE method, section 5.3 explains the methodology and the utilization of ZTD for the analysis, and section 5.4 showcases the details of the estimation results. Following to that, section 5.5 elaborated the empirical analysis of the TSE method conducted through statistical analysis using ZTD and concludes with discussions in section 5.6. The gist of the analysis is covered in section 5.7 that reviews the analysis.

5.2   The estimation method (Seo *et al.*, 2015b) and the need for study

The estimation of high-resolution traffic states is mainly beneficial for traffic control to mitigate congestion. Over the past decade, researchers have contributed to the methodologies for estimating traffic state, i.e., the density, flow, and velocity, from traffic data without any exogenous assumptions on traffic flow characteristics, such as Fundamental Diagram (FD), which renders the estimation methods robust against unpredictable or uncertain traffic phenomena. The considered '*weaker*' assumption-based traffic state estimation method obtains volume-related variables in predetermined space-time regions by employing vehicles that could measure their positions and the distances to their leading vehicle (space headway between the probe vehicle and its leading vehicle in the same lane). The estimators for the flow, density, and velocity, are formulated (using Edie's definitions) (Edie, 1963) as follows:

$$q(\boldsymbol{A}) = \frac{d(\boldsymbol{A})}{|\boldsymbol{A}|} \Rightarrow q(A) = \frac{\sum_{n\in N(A)} d_n(A)}{\sum_{n\in N(A)} |a_n(A)|} \Rightarrow \hat{q}(A) = \frac{\sum_{n\in P(A)} d_n(A)}{\sum_{n\in P(A)} |a_n(A)|} \tag{5.1}$$

$$k(\boldsymbol{A}) = \frac{t(\boldsymbol{A})}{|\boldsymbol{A}|} \Rightarrow k(A) = \frac{\sum_{n\in N(A)} t_n(A)}{\sum_{n\in N(A)} |a_n(A)|} \Rightarrow \hat{k}(A) = \frac{\sum_{n\in P(A)} t_n(A)}{\sum_{n\in P(A)} |a_n(A)|} \tag{5.2}$$

$$v(\boldsymbol{A}) = \frac{d(\boldsymbol{A})}{t(\boldsymbol{A})} \Rightarrow v(A) = \frac{\sum_{n\in N(A)} d_n(A)}{\sum_{n\in N(A)} t_n(A)} \Rightarrow \hat{v}(A) = \frac{\sum_{n\in P(A)} d_n(A)}{\sum_{n\in P(A)} t_n(A)} \tag{5.3}$$

In $\sum_{n \in N(A)} |a_n(A)|$, $a_n(A)$ represents the space-time region between vehicle *n* and its leading vehicle in a spatiotemporal cell, *A*, of a meshed spatiotemporal region, *R*, *N(A)* represents the set of all vehicles in the cell *A*. $d_n(A)$ is the total distance traveled by vehicle *n* in cell *A* and $t_n(A)$ is the total time spent by vehicle *n* in cell *A*. When estimating traffic states using probe vehicles, *N(A)* is replaced by *P(A)*, which depicts the set of all probe vehicles in region *A*, as illustrated in Figure 5.1.

This method was previously verified by comparing traffic states estimated by the method, using the data obtained from the employed 20 probes equipped with mono-eye cameras and GPS loggers that drove multiple laps, and those observed by detectors at certain settings that involved two probe vehicle penetration rates and two spatiotemporal resolutions. The spatiotemporal area between a probe vehicle and its leading vehicle was computed by using approximations based on the spacing measured by the probe vehicle. The TSE method under consideration relies on '*weaker*' assumptions of '*error free assumption*' (measurements by probes have no error and the driving route is identified without error) and '*random sampling assumption*' (probes are randomly distributed in traffic with unknown penetration rates during estimation and the driving behavior of probes and non-probes are similar). However, the study stated that the data acquired from the probe vehicle that was used for its validation contained biases (i.e., the random sampling assumption was not satisfied) such as differences between the driving behavior of probes and differences between the spacing measurements. It suggests that without such biases, the estimation accuracy may be improved. The spacing measurement method involved the identification of leading vehicles in the images (captured by probes), from which their apparent sizes were measured. The spacing was calculated based on the apparent size, assumed actual size, angle of view of the camera, etc. The actual body length was assumed to be the same as that of the probe vehicles ($5 \, m$). Other variables were manually measured using the images. If the assumed or measured variables contained errors, the estimated spacing contained errors, which in turn affected the calculation of $a_n(A)$. Although the assumed variables were based on common knowledge of statistics and regulations and detector data, the amount of the errors could not be determined because there is no ground truth data for the vehicle size during the experiment.

The proposed method relied on assumptions that may not always be satisfied in the real world, namely the error free and random sampling assumptions (Seo *et al.*, 2015b). With the advancement in data acquisition technologies and the advent of connected vehicles in the near future, it is

expected that probe vehicles with advanced driver assistance system (ADAS), potentially capable of recording the exact spatiotemporal coordinates of the leading vehicle too, will be used to obtain data similar to ZTD. The spatiotemporal resolution considered in this analysis was not coarse; therefore, for the sake of analyzing the accuracy of the method, the objective of this study is to analyze the validity of the discussed probe vehicle-based traffic states estimation method using the high-resolution ZTD for different *settings*: spatial resolution (hereafter, Δx), temporal resolution (hereafter, Δt), and probe vehicle penetration rate (hereafter, $p\%$). In this study, $p\%$ vehicles are randomly selected from 100% vehicles driving on a lane for a fixed distance and time, instead of employing probe drivers, to evaluate the true estimation capability of the TSE method. In addition, the ZTD contains comprehensive trajectory details of 100% vehicles, which aids in identifying the leading vehicle to each vehicle in every lane. Therefore, exact spatiotemporal coordinates of a vehicle and its leading vehicle were used to calculate a nearly accurate value of the spatiotemporal area between a vehicle and its leading vehicle ($a_n(A)$) without any approximation. This satisfied the random sampling assumption of the estimation method, where the possibility of bias in the driving characteristics of the selected probes to the rest is absent.

5.3   Methodology and utilization of ZTD

For this study, the ZTD L001_F001, covering space-time profile of distance of 2 km (5 $k.p.$ to 3 $k.p.$ i.e., 5000 m to 3000 m) and 1 $hour$ (7:00 a.m. to 8:00 a.m.), is utilized. In it the lane changing is prohibited for the distance between 4200 m and 3400 m, and a merging to the driving lane from outside the entrance lane occurs at 3.8 $k.p.$ (Tsukamoto junction) as depicted in Figure 5.2. The color bar in the figure aids in understanding the speed profiles of all the vehicles at all space-time locations for both, the driving and the passing lanes for 1 $hour$ on the said 2 km distance.

Assumption 5.1: In this lane change prohibited distance, for simplification of analysis two sections: 4250 m to 3850 m (400 m long section) and 3750 m to 3450 m (300 m long section) are specifically considered that have minimum lane-changing behavior and maintain the conservation of vehicles throughout each section. In each lane of these sections there is no vehicle's overtaking nor merging/diverging sections (i.e., a first-in first-out (FIFO) condition and a conservation law (CL) is satisfied).
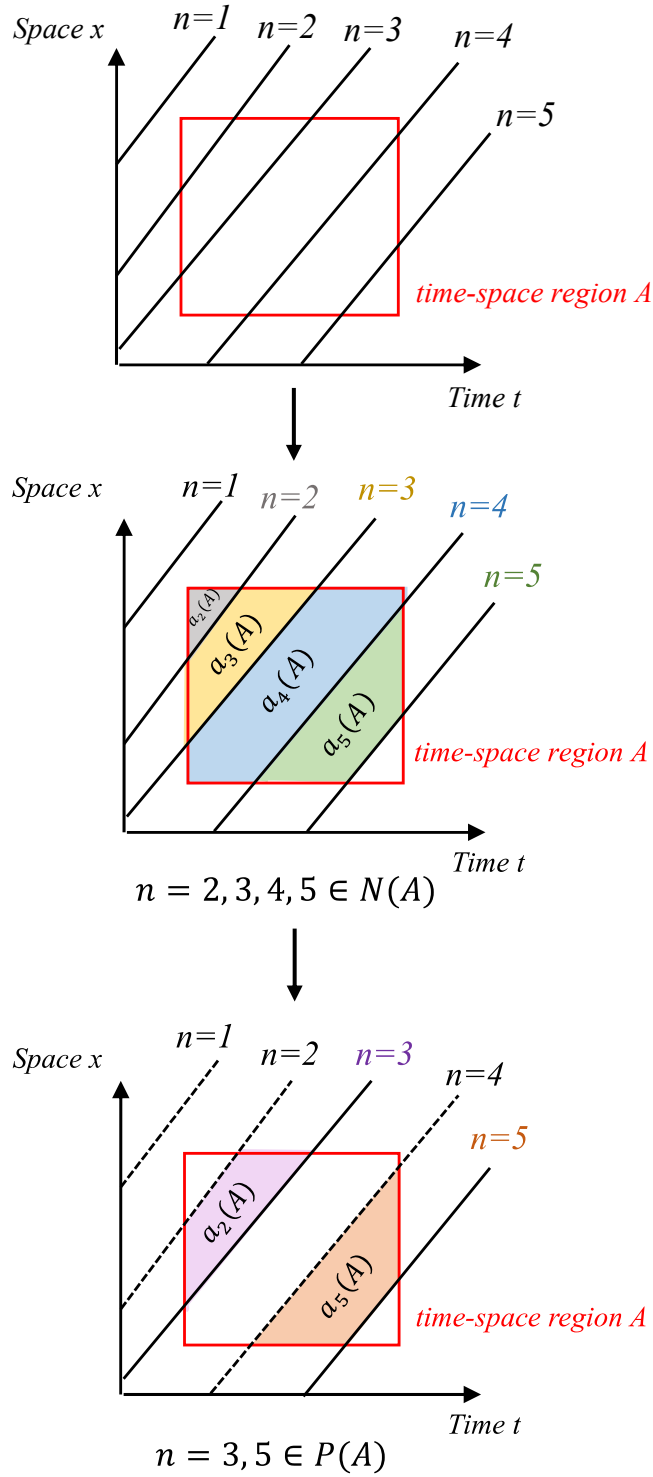
Figure 5.1 Illustration of formulation of $xFCD$-based TSE method (Seo et al., 2015b)
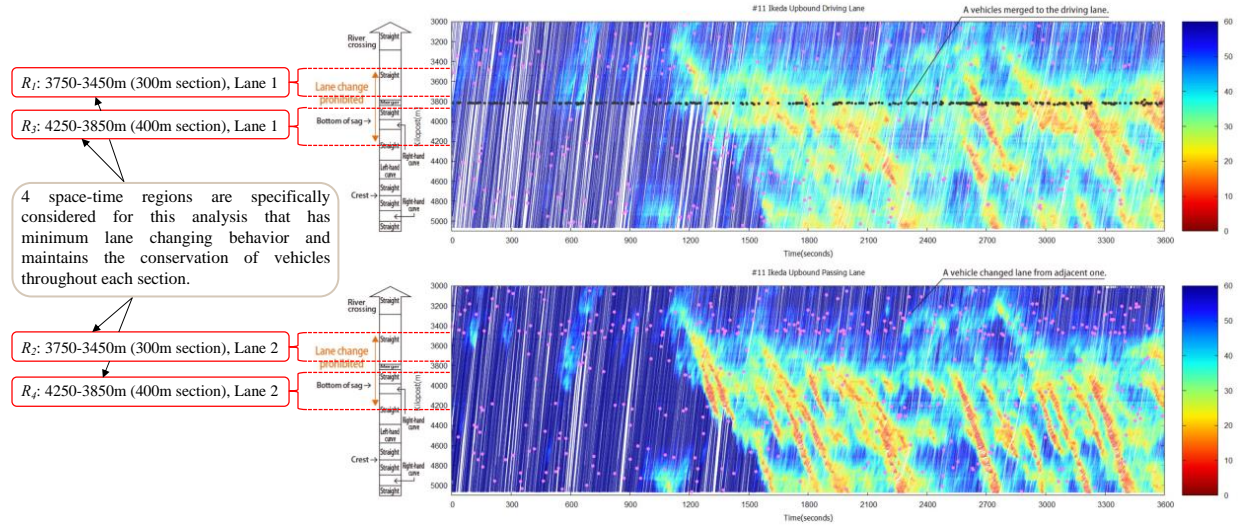
Figure 5.2 Four space-time sub-sections considered due to prohibition of lane changing behavior
(Source: https://zen-traffic-data.net/english/outline/)

However, from 7:00 a.m. to 8:00 a.m., some lane changing behavior was still observed in both these sections: 106 out of 3405 vehicles (3.1%) changed lanes on the 300 m section and 389 out of 3391 vehicles (11.5%) changed lanes on the 400 m section, as also tabulated in Table 5.1. The percentage of vehicles showing differences in driving behavior was not high; therefore, these were excluded from the analysis to assume homogenous driving behavior among drivers. Resultingly, the number of considered vehicles that drove on 300 m section (lane 1) (R_1), 300 m section (lane 2) (R_2), 400 m section (lane 1) (R_3) and 400 m section (lane 2) (R_4) for one $hour$ (7:00 a.m. to 8:00 a.m.) without changing lanes were 1400, 1735, 1182 and 1715 respectively. Using voluminous ZTD, it was possible to identify the sequential order of vehicles driving in each lane of each section for one morning peak $hour$ for 2 km and which was maintained throughout the section. Hence, the leading vehicle to each vehicle was identified along with their trajectories in their respective space-time regions (R_i). This serves as an essential ingredient in estimating traffic states by the estimation method using ZTD.

Table 5.1 Percentage of vehicles observed changing lanes in the lane change prohibited area for 300 m section and 400 m section of ZTD: L001_F001

	300 m section	400 m section
Number of vehicles changing lanes	106 out of 3405 (3.1%)	389 out of 3391 (11.5%)
Number of vehicles considered	1400 (Lane 1), 1735 (Lane 2)	1182 (Lane 1), 1715 (Lane 2)

Each space-time area is divided into meshes of varying spatiotemporal resolutions i.e., each space-time region (R_i) subject to the traffic state estimation is divided into multiple discrete, identical, and rectangular space-time regions that can be horizontal or vertical depending on the combination of spatial and temporal resolutions as per Figure 5.3. Any rule can be used to divide the space-time region of the traffic flow. The simplest rules are employed in this study, where the traffic flow is divided into Eulerian rectangles of identical sizes. These are familiar coordinates in current traffic flow data, where fixed-point detectors are installed at a certain time and space resolution or interval. The coordinates can be represented as follows:

$$A_i^j = \{(t,x) | t_i \leq t \leq t_{i+1}, x_j \leq x \leq x_{j+1}\}\, i \geq 0, j \geq 0 \tag{5.4}$$

$$t_{i+1} = t_i + \Delta t \tag{5.5}$$

$$x_{j+1} = x_j + \Delta x \tag{5.6}$$

where,

i, j: non-negative indices for time and space,

(t_0, x_0): coordinates of the predetermined origin,

(t_i, x_j): coordinates of the upper-left corner of region A_i^j,

Δt: predetermined time resolution i.e., $\Delta t = \{15\ s,\ 30\ s,\ 60\ s,\ 120\ s,\ 300\ s\}$,

Δx: predetermined space resolution i.e., $\Delta x = \{25\ m,\ 50\ m,\ 100\ m,\ 150\ m,\ 300\ m\}$ for R_1 and R_2, and $\Delta x = \{25\ m,\ 50\ m,\ 100\ m,\ 200\ m,\ 400\ m\}$ for R_3 and R_4.

The value of x varies as $3450 \leq x \leq 3750$ for R_1 and R_2 and $3850 \leq x \leq 4250$ for R_3 and R_4, and t varies as $25200000\ ms \leq t \leq 28800000\ ms$ (7:00 a.m. to 8:00 a.m.). Corresponding to each R_i, there are 25 combinations of Δt and Δx (25 meshes), where each cell of each mesh is identified by cell A_i^j (hereafter, A).
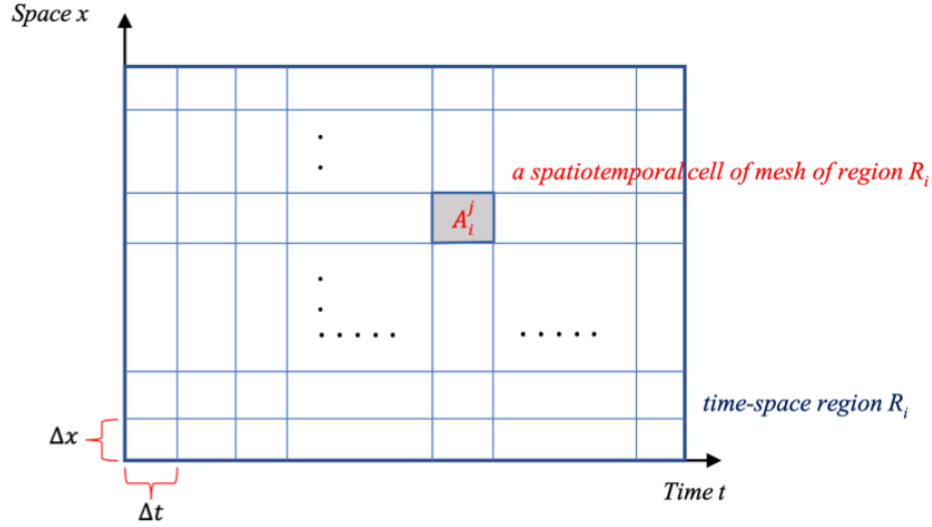
Figure 5.3 Space-time area divided into mesh of Eulerian rectangles

5.4   Estimation results over varying settings

First, the traffic state, which at a macroscopic level is a set of the following variables: flow q, density k, and average speed v, is computed using Edie's definitions for each cell (A) of each mesh (for every combination of Δx and Δt) corresponding to every R_i. Under every *setting*, the trajectory information from the ZTD of all vehicles driving through a cell is used to compute q (veh/s), k (veh/m), and v (m/s). Assuming the ZTD as a source of ground truth, these values are used to make comparison with the traffic state computed using the estimation method. Figure 5.5 illustrates the trajectories of 100 % vehicles driving on the Lane 1 of 300 m section (R_1) of L001_F001. Using the described methodology, Figure 5.6 shows the actual traffic flow computed for $\Delta x = 25\ m$ and $\Delta t = 30\ s$ on R_1 (for instance). For all space-time regions R_i, the traffic flow ranges from 0.3 to 0.5 veh/s (18–30 veh/min) in a majority of the meshed cells (A), and at a few positions and times on the sections the traffic flow is over 0.6 veh/s (36 veh/min) (reaching values of flow at critical density), which mostly occurs on lane 2 and before 7:20 a.m.

Estimating the traffic state using the estimation method requires random sampling of $p\%$ vehicles (hereafter referred to as probe vehicles) from the total number of vehicles driving through each space-time region R_i. Each vehicle (with its trajectory data) is chosen entirely by chance by utilizing the pseudo–random decimal numbers (real numbers between 0 and 1) generated by the *RAND* function in *MS Excel* and has an equal probability of being selected as an element of the

random sample, in alignment to the probability theory and statistics. The selection isn't based on any uniform pattern, such as the selection of a vehicle after every fixed number of vehicles or in every fixed unit of time. These $p\%$ selected vehicles are a part of the actual traffic and not deployed for analysis. For instance, Figure 5.7 a.), b.), c.) and d.) depicts the traffic trajectories of $5\%, 3\%, 1\%$ and 0.5% randomly selected vehicles from 100% of vehicles driving (total 1400) in region Lane 1 of $300\,m$ section (R_l), respectively. For varying $p\%$ values, the traffic states are estimated using the equations $(5.1) - (5.3)$ (right) for each cell (A) of each mesh (for every combination of Δx and Δt) corresponding to every R_i, through which at least one probe vehicles pass. For computing the spatiotemporal area ($a_n(A)$) between a probe vehicle (n) and its leading vehicle in the same lane (as illustrated in Figure 5.4), identified using the ZTD, the exact spatiotemporal coordinates of their trajectories at a 0.1s pitch are used. For doing so, Gauss's area formula, described by Meister (1769) and by Carl Friedrich Gauss in 1795 was implemented in Python. It is also known as the Surveyor's formula (Braden, 1986) and is considered as a special case of Green's theorem (first presented by (Cauchy, 1846)). Let the set of spatiotemporal coordinates of vehicle n and its leading vehicle enclosed within the space-time region of cell A, which form a polygon in the clockwise or anticlockwise direction in the spatiotemporal plane, be represented as $\{(t_1, x_1), (t_2, x_2), \dots, (t_N, x_N)\}$. The area $a_n(A)$ is derived as follows:

$$a_n(A) = \frac{1}{2}\left|\sum_{i=1}^{N-1} t_i x_{i+1} + t_N x_1 - \sum_{i=1}^{N-1} t_{i+1} x_i + t_1 x_N\right| \tag{5.7}$$

Alternatively,

$$a_n(A) = \frac{1}{2}\left|\sum_{i=1}^{N} t_i (x_{i+1} - x_{i-1})\right| = \frac{1}{2}\left|\sum_{i=1}^{N} x_i (t_{i+1} - t_{i-1})\right| \tag{5.8}$$

$$a_n(A) = \frac{1}{2}\left|\sum_{i=1}^{N}(t_i x_{i+1} - t_{i+1} x_i)\right| \tag{5.9}$$

$$a_n(A) = \frac{1}{2}\left|\sum_{i=1}^{N}(t_{i+1} + t_i)(x_{i+1} - x_i)\right| = \frac{1}{2}\left|\sum_{i=1}^{N} det\begin{pmatrix} t_i & t_{i+1} \\ x_i & x_{i+1} \end{pmatrix}\right| \tag{5.10}$$
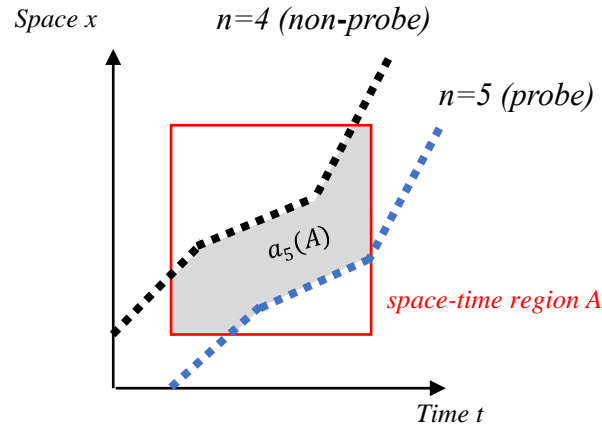
Figure 5.4 Representation of spatiotemporal area between a probe vehicle and its leading vehicle in a space-time cell
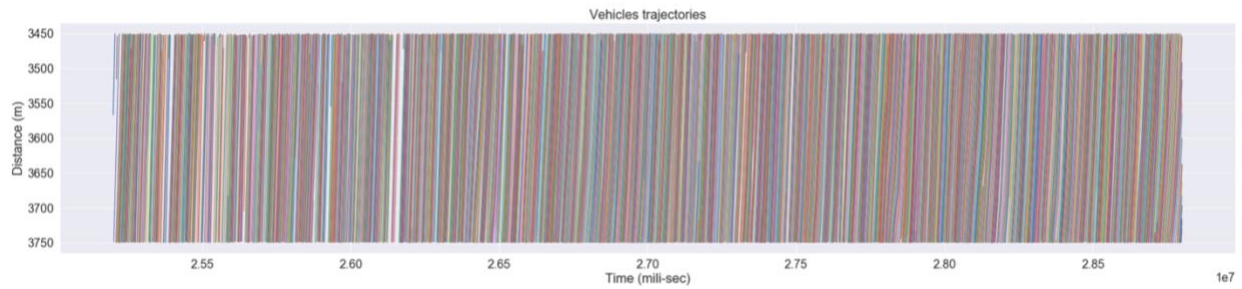
Figure 5.5 Trajectories of 100% vehicles driving on the Lane 1 of 300 m section of ZTD: L001_F001
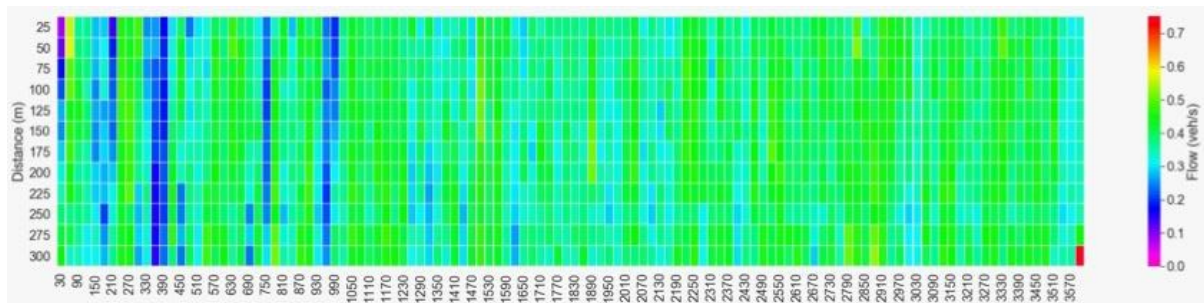
Figure 5.6 Actual flow on Lane 1 of 300 m section of ZTD: L001_F001 computed using 100% vehicles' trajectory information and Edie's generalized definitions
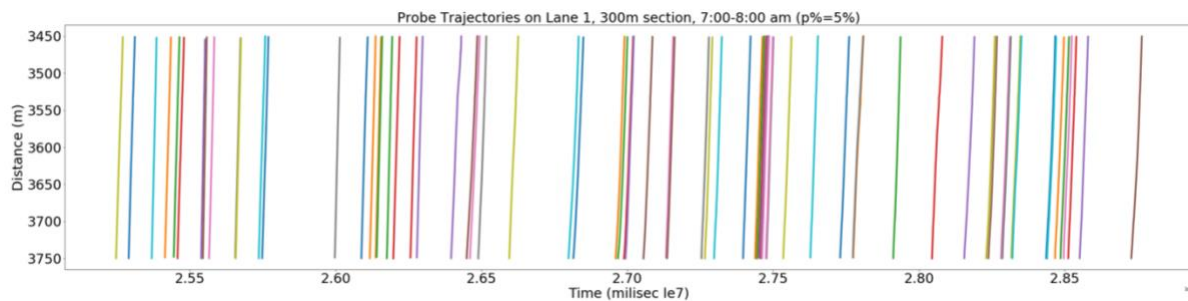
a.)
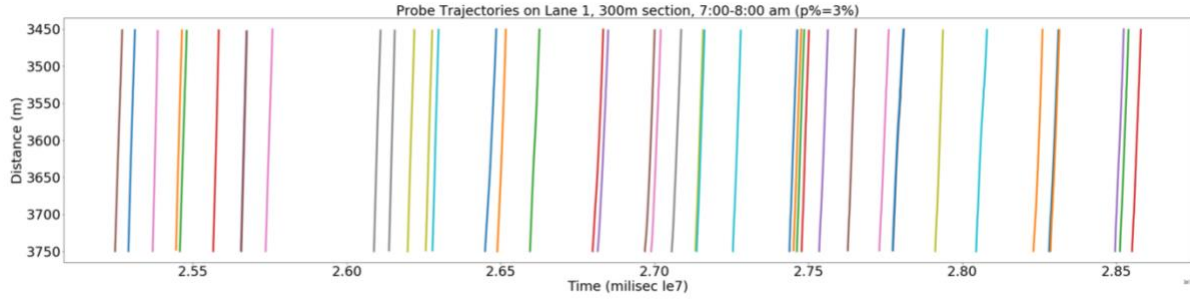
b.)
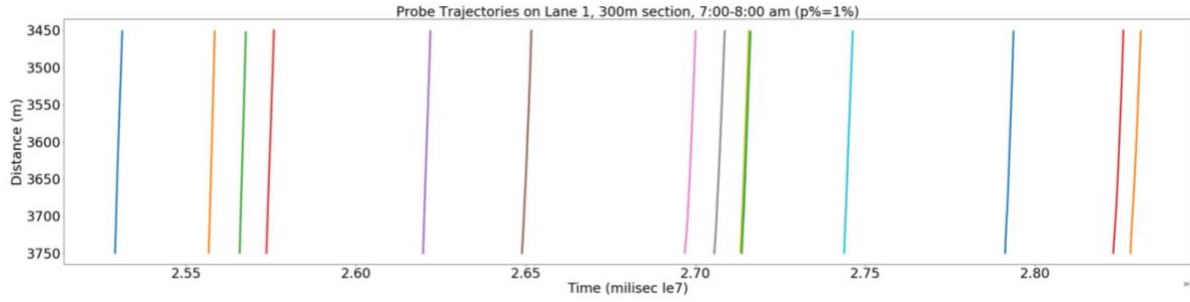
c.)
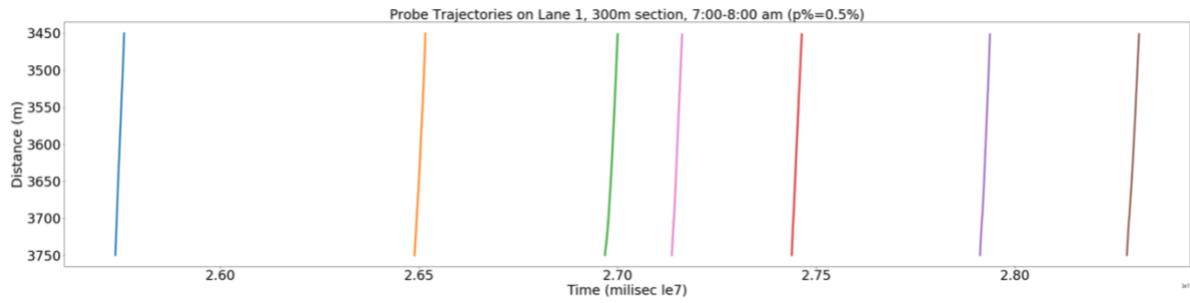
d.)

Figure 5.7 Trajectories of a.) 5%, b.) 3%, c.) 1% and d.) 0.5% of randomly sampled probe vehicles (extracted from 100% ZTD)

driving on the Lane 1 of 300 m section of ZTD: L001_F001
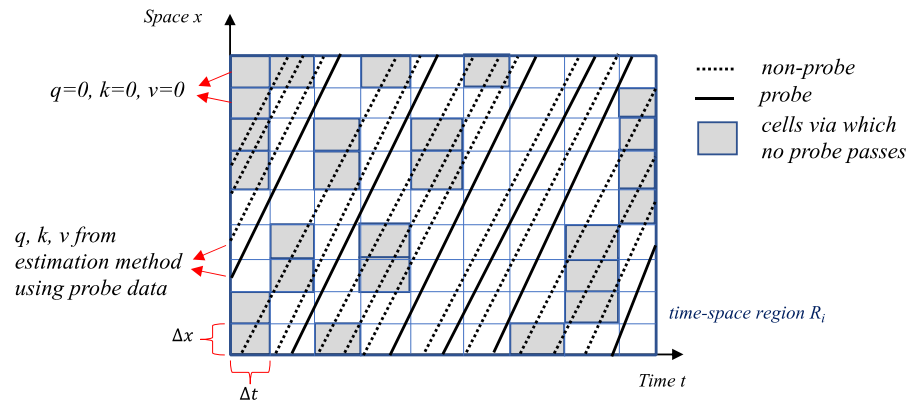
Figure 5.8 Representation of observed cells i.e., cells via which at least one probe vehicle traverse
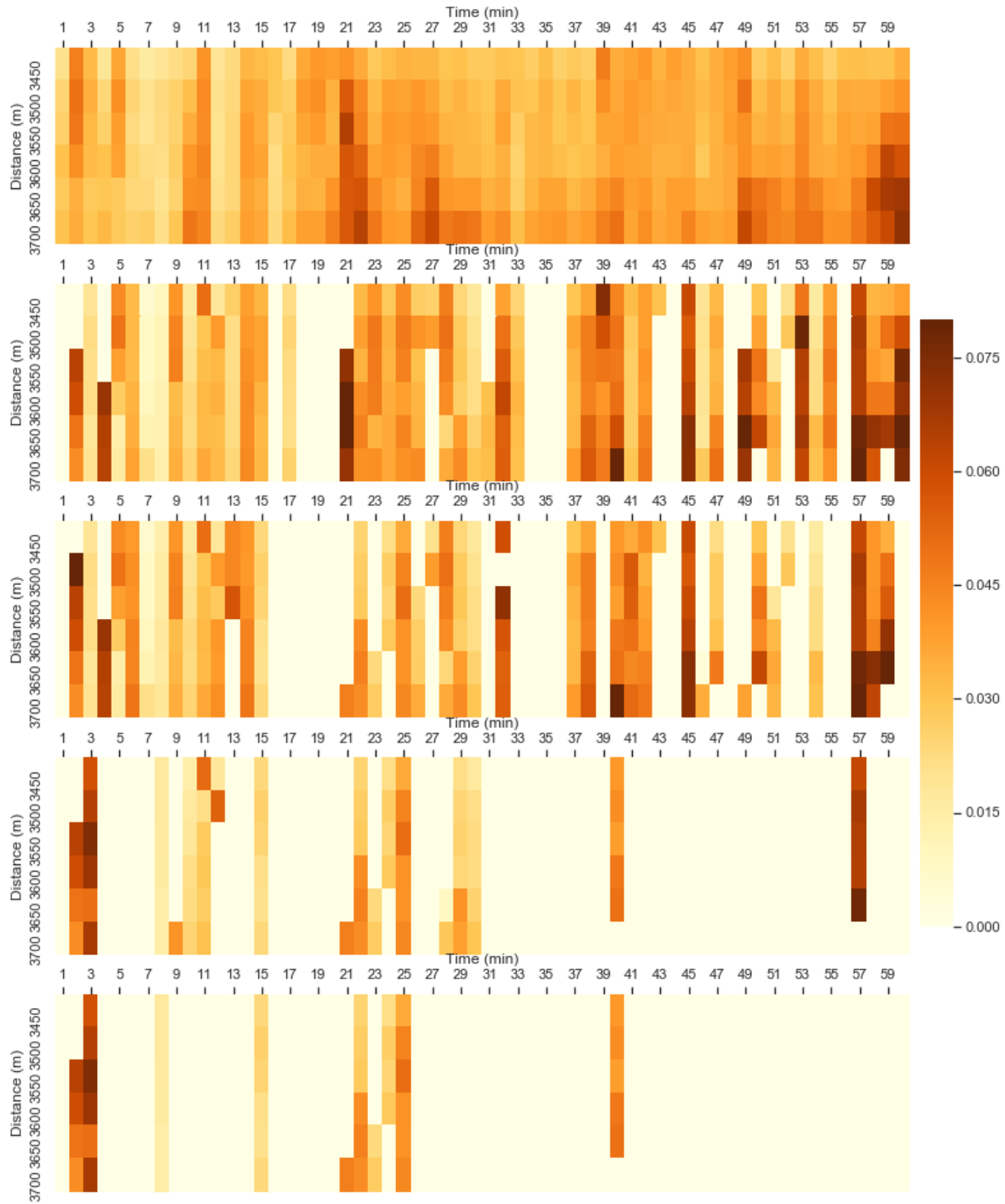
Figure 5.9 Density k (veh/m) estimated from Edie's definitions and 100% ZTD (topmost row) and estimation method for Δx = 50 m, Δt = 60 s, p% varying from 5% to 0.5%) for Lane 1 of 300 m section (bottom four rows from top to bottom order)
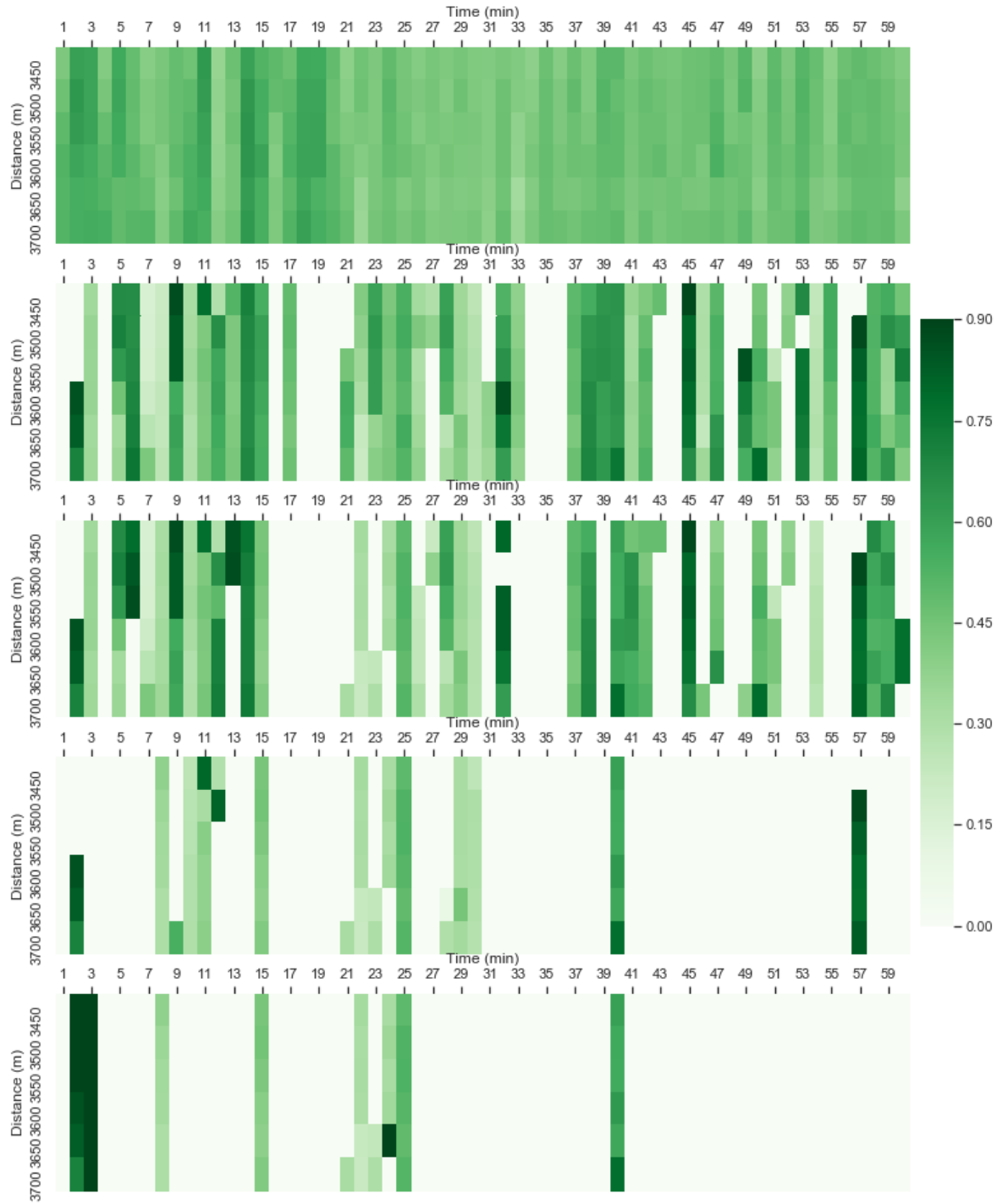
Figure 5.10 Flow q (veh/s) estimated from Edie's definitions and 100% ZTD (topmost row) and estimation method for Δx = 50 m, Δt = 60 s, p% varying from 5% to 0.5%) for Lane 1 of 300 m section (bottom four rows from top to bottom order)
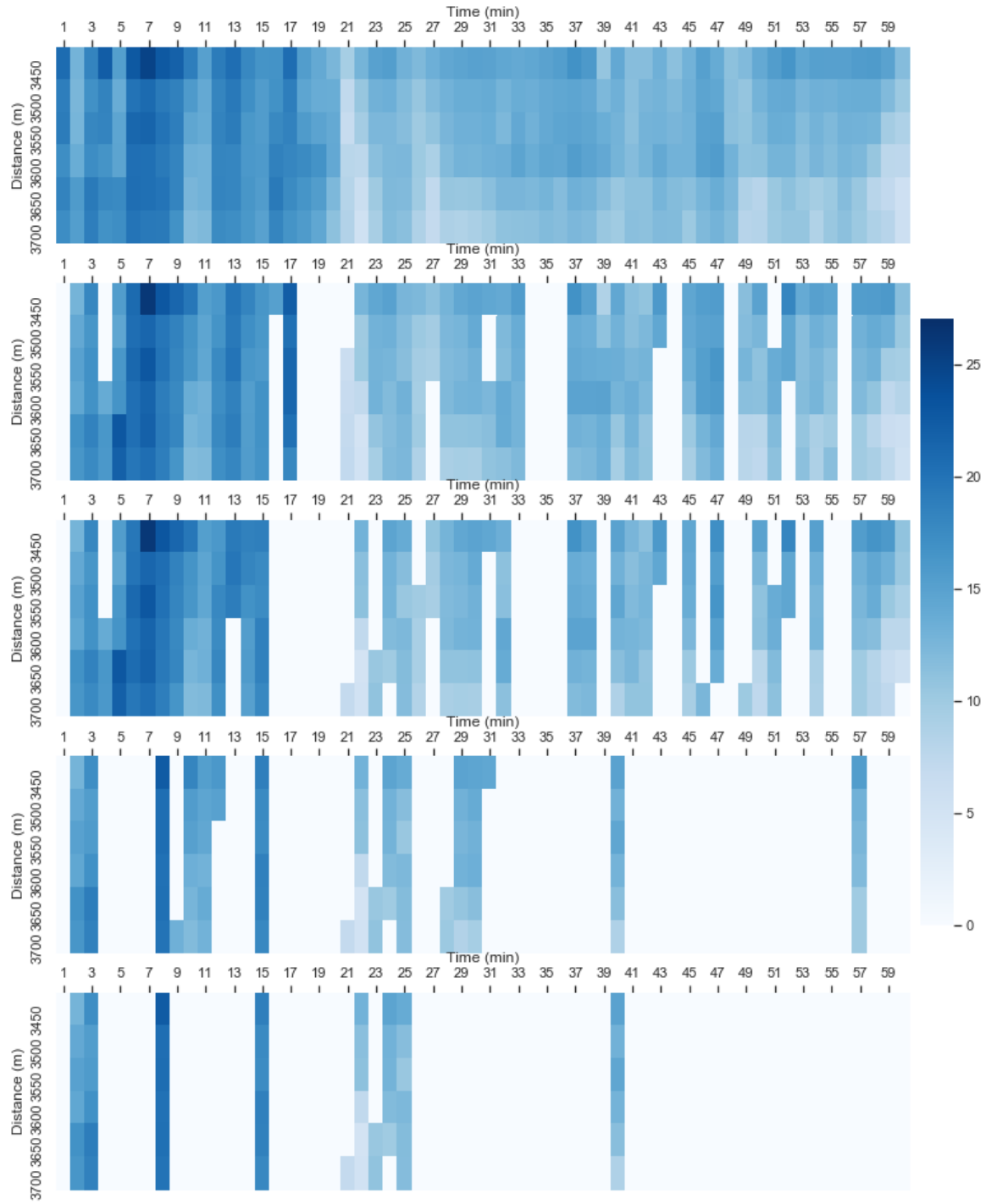
Figure 5.11 Velocity v (m/s) estimated from Edie's definitions and 100% ZTD (topmost row) and estimation method for Δx = 50 m, Δt = 60 s, p% varying from 5% to 0.5%) for Lane 1 of 300 m section (bottom four rows from top to bottom order)

The topmost rows in Figure 5.9, Figure 5.10 and Figure 5.11 correspond to the traffic state, k (veh/m), q (veh/s), and v (m/s), respectively, estimated using Edie's definitions and the ZTD of 100% vehicles for R_1 ($\Delta x = 50\ m, \Delta t = 60\ s$). The following rows in Figure 5.9, Figure 5.10 and Figure 5.11 illustrate the traffic states, k (veh/m), q (veh/s) and v (m/s), respectively, estimated from the estimation method for $p\% = 5\%, 3\%, 1\%\ and\ 0.5\%$, in this order for R_1 ($\Delta x = 50\ m, \Delta t = 60\ s$). For any cell through which no probe vehicle passes, the values of the allocated traffic state equal zero, as illustrated in Figure 5.8. This is a type of missing data that is different from missing data caused by randomness, attrition, or unobserved original data; rather, it is an intentional missing as part of extracting only $p\%$ data for this analysis.

5.5 Empirical analysis

A fixed combination of Δx, Δt and $p\%$ is referred to as a *setting*. The total number of such *settings* equals 100. The traffic states obtained under each *setting*, for each cell A of all spatiotemporal regions R_i, using the estimation method are compared with traffic state obtained using ZTD of all the vehicles driving through cell A on a one-to-one basis. To yield the least biased comparison for cells through which no probe passed, the analysis strategy used is a direct approach: *Deletion Method (Listwise Deletion)*. It is a complete-case analysis, where only the cells with observed probes are considered from both datasets. The $p\%$ probe vehicles are selected randomly; therefore, the cells with no probes do not occur in any systematic order, which could lead to a bias. Its advantages are simplicity and comparability across analyses. The reasons for not considering value-allocating methods for assigning values to the cells through which no probe drives (such as the mean imputation method, using information from related cells, or a hybrid of both methods) are discussed. The objective of this analysis is to study the accuracy of the estimation method for different $p\%$ values. For this method to be applicable in actual scenario, it is important to check the accuracy by not deliberately adding any biases. When $p\%$ is very less then technique-filled cells, for higher spatiotemporal resolutions, will be much larger than the cells with method-estimated data. This would not reflect true errors during comparison. When we fill the empty cells with values from other *settings*, it will give an amalgamation of values and it will not reflect the true variation in error over spatiotemporal resolutions and $p\%$.

To visualize the performance of the estimation method, flow-density $(q - k)$ diagrams were plotted for all combinations of spatiotemporal resolutions and probe vehicle penetration rates combined for all four regions R_i. A few of them are illustrated in Figure 5.13. The $q - k$ plots suggest that the estimation method is able to capture the robust behavior of actual traffic dynamics when the traffic is in the free-flow regime. However, for densities beyond the density around critical density the performance of the estimation method appears degraded. Although there exists a cloud of incorrect estimations beyond the critical density, it coexists with the correct estimations to some extent. This implies that existence of a density greater than the critical density in a spatiotemporal cell A is not the sole reason for the diversion of predictions made by the estimation method from actual traffic states in that cell A. For an extensive evaluation, statistical analysis was conducted as discussed in the following section.
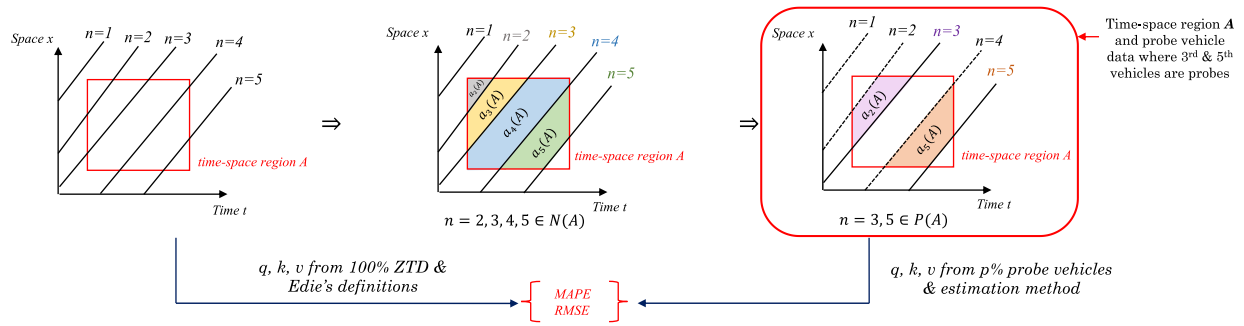
Figure 5.12 Representation of the process of comparison through error analysis

$p\% = 5\%$ $p\% = 1\%$

$\{25\, m \text{ x } 15\, s\}$

$\{25\ m \times 120\ s\}$

$\{100\ m \times 15\ s\}$

$\{100\ m \times 120\ s\}$
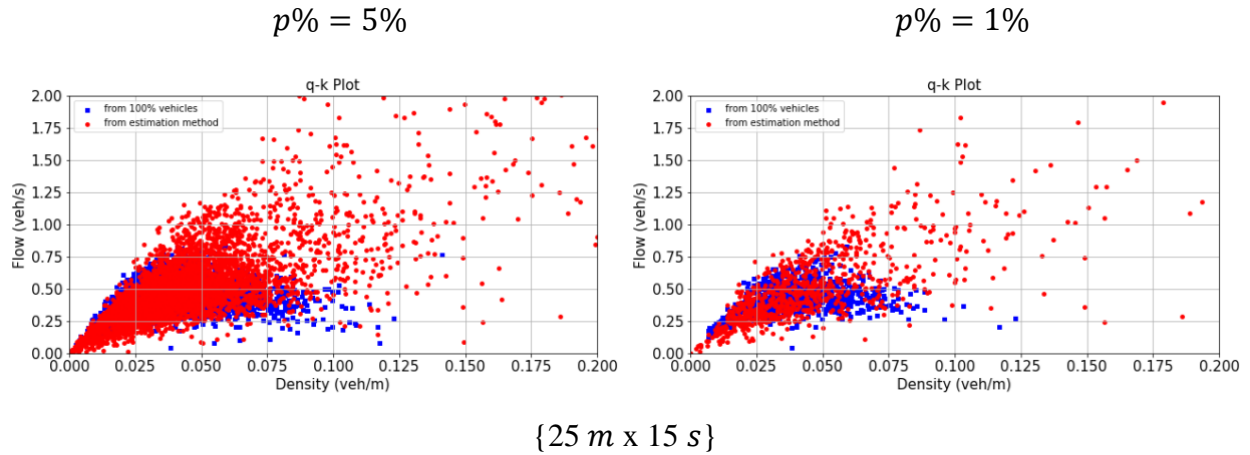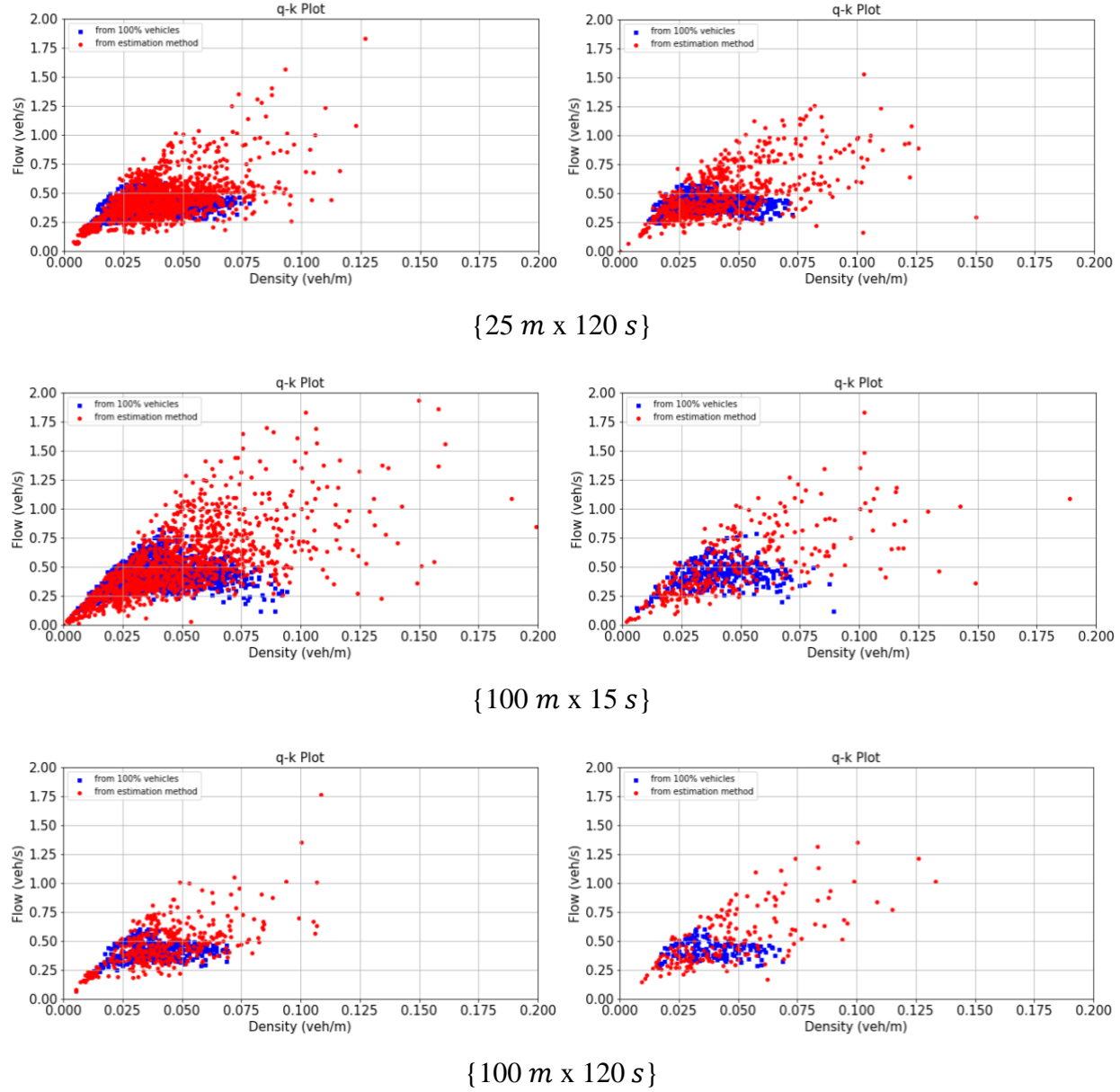
Figure 5.13 $q - k$ plot for traffic state estimated from Edie's definitions using the ZTD of 100% vehicles (Blue) and from the estimation method (Red) for a few different settings

5.5.1   Statistical error analysis

To analyze the numeric differences in the traffic states estimated by the probe vehicle-based estimation method (E_i) and those obtained from the ZTD of 100% vehicles (O_i) driving in a spatiotemporal cell A of region R_i, the percent error is calculated for each considered cell A under all 100 *settings* as per equation (5.11). Furthermore, as illustrated in Figure 5.12, the mean absolute

percentage errors (MAPEs) and root mean square errors (RMSEs) are also calculated (n: number of cells considered) as per equations (5.12) and (5.13).

$$Percent\ error\ (\delta) = \left|\frac{E_i - O_i}{O_i}\right| . 100\%$$ (5.11)

$$Mean\ absolute\ percentage\ error = \frac{100\%}{n}\sum_{i=1}^{n}\left|\frac{E_i - O_i}{O_i}\right|$$ (5.12)

$$Root\ mean\ square\ error = \sqrt{\frac{\sum_{i=1}^{n}(E_i - O_i)^2}{n}}$$ (5.13)

Additionally, the number of probes driving through each spatiotemporal cell was recorded for all combinations of considered spatial resolution, temporal resolution, and probe vehicle penetration rate. Intuitively, as the spatial resolution and/or temporal resolution becomes more coarser, or the probe vehicle penetration rate increases, the average number of probes in each cell is expected to increase. However, to determine the precise numerical value, Table 5.3 details the average number of probes observed in the cells through which at least one probe vehicle passed under a few of the different *settings*, averaged over all four regions (R_i). Under the considered *settings*, the higher values of the average number of probes observed in the cells ranges from 6.22 to 6.75 for $\Delta t = 300s$ and $p\% = 5\%$. The value of Δx is not influencing the averages as such. The second reason that can be considered for the deviation of estimated traffic states from the actual ones is the average number of probe vehicles in the spatiotemporal area under consideration. Figure 5.14 illustrates that with an increase in average number of probe vehicles in a spatiotemporal area result in a drastic decrease in the MAPE in the estimated density and flow. When the average number of probes is 1 in a cell A, the MAPE in the estimated density and flow is as high as around 140%. At the same time number of probes in a cell is not influencing the errors in the estimated speed very much. Similarly, Figures 5.15, 5.16 and 5.17 show the depletion in RMSE in estimated k, q, and v with an increase in the average number of probe vehicles in the spatiotemporal area, respectively. When the average number of probes is as high as around 6 or 7, the MAPE in estimated k, q, and v are as low as around 20% for k and q and less than 10% for v.

Table 5.3 Average number of probe vehicles in each cell A of space-time domain at different settings

Δx	25m					100m					200m					300m				
Δt	15s	30s	60s	120s	300s	15s	30s	60s	120s	300s	15s	30s	60s	120s	300s	15s	30s	60s	120s	300s
p%=5%	1.176	1.345	1.764	2.743	6.217	1.251	1.434	1.878	2.876	6.351	1.318	1.505	1.974	3.018	6.354	1.556	1.753	2.258	3.250	6.917
p%=3%	1.081	1.162	1.397	1.920	3.965	1.115	1.211	1.452	1.991	4.032	1.168	1.265	1.467	2.041	3.978	1.244	1.397	1.667	2.265	4.348
p%=1%	1.037	1.071	1.141	1.261	1.784	1.047	1.080	1.157	1.270	1.805	1.056	1.080	1.119	1.218	1.743	1.092	1.170	1.235	1.400	1.941
p%=0.5%	1.004	1.016	1.031	1.031	1.210	1.012	1.015	1.035	1.037	1.225	1.000	1.000	1.000	1.000	1.148	1.073	1.074	1.105	1.125	1.417

Table 5.2 RMSE obtained by comparing traffic state estimated using the estimation method and from the ZTD of 100% vehicles for a few different settings

Spatiotemporal resolution		RMSE in Density (veh/m)				RMSE in Flow (veh/s)				RMSE in Speed (m/s)			
						Probe penetration rate (p%)							
Δx	Δt	5%	3%	1%	0.50%	5%	3%	1%	0.50%	5%	3%	1%	0.50%
25m	15s	0.114	0.123	0.124	0.152	1.119	1.232	1.323	1.657	1.672	1.720	1.608	1.326
	30s	0.084	0.086	0.085	0.104	0.819	0.816	0.848	0.827	1.351	1.468	1.382	1.498
	60s	0.052	0.049	0.040	0.044	0.459	0.434	0.446	0.387	1.350	1.409	1.437	1.521
	120s	0.029	0.025	0.024	0.031	0.259	0.223	0.277	0.302	1.269	1.478	1.654	1.857
	300s	0.009	0.013	0.022	0.023	0.087	0.153	0.249	0.233	1.224	1.351	1.772	2.272
100m	15s	0.096	0.104	0.104	0.130	1.029	1.020	0.913	1.322	1.555	1.573	1.245	1.262
	30s	0.092	0.087	0.101	0.130	0.985	0.772	0.761	0.817	1.203	1.179	1.163	1.264
	60s	0.037	0.042	0.038	0.035	0.392	0.475	0.513	0.326	1.095	1.079	1.158	1.208
	120s	0.018	0.017	0.028	0.035	0.181	0.207	0.340	0.325	1.008	1.234	1.434	1.615
	300s	0.010	0.013	0.025	0.023	0.098	0.148	0.302	0.234	1.080	1.176	1.589	2.074

Also, the RMSE in k, q and v will be around 0.01 veh/m, 0.09 veh/s (5.4 veh/min) and 0.75 to 1.25 m/s, when the average number of probe vehicles in a spatiotemporal region is around 6 or 7. Primarily, high vehicular density and/or low availability of probes driving through a spatiotemporal region leads to a substandard performance of the estimation method in replicating the actual behavior of traffic flow and estimating traffic state. When the probe penetration rate drops below 3% and the temporal resolution becomes finer than 2 min, the average number of probe vehicles in the considered spatiotemporal regions falls below 2 and the MAPE in the estimated density and flow rises over 40%.
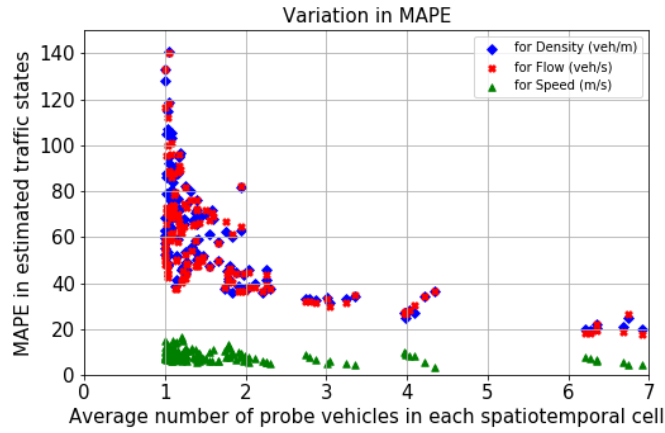
Figure 5.14 Variation in MAPE with respect to the variation in the average number of probes in a cell A of the spatiotemporal mesh
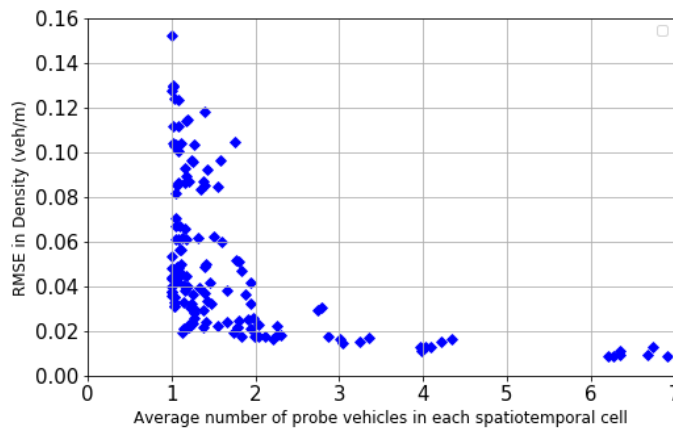
Figure 5.15 Variation in RMSE in Density k (veh/m) with respect to the variation in the average number of probes in a cell A of the spatiotemporal mesh
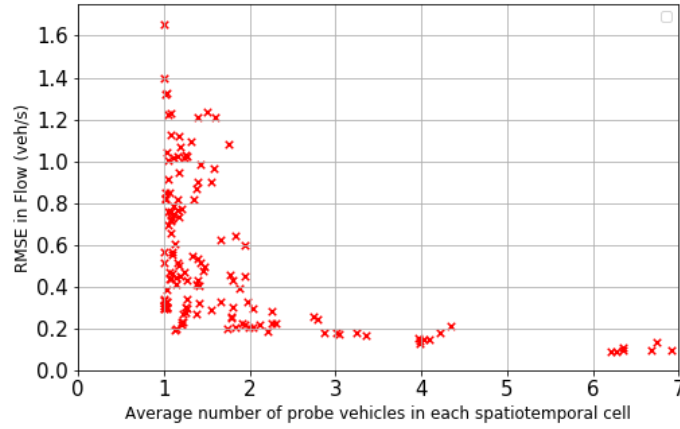
Figure 5.16 Variation in RMSE in Flow q (veh/s) with respect to the variation in the average number of probes in a cell A of the spatiotemporal mesh
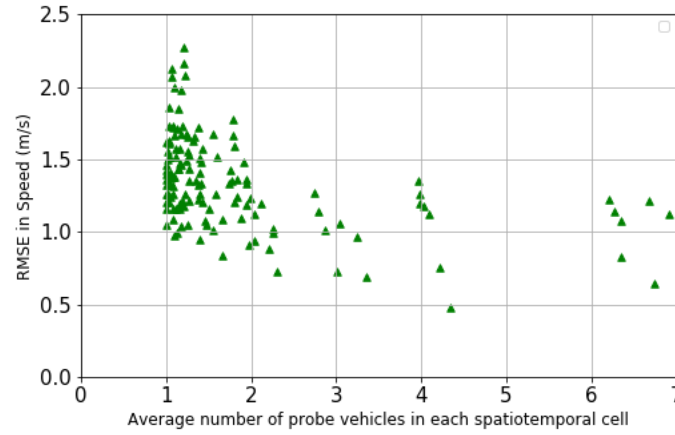
Figure 5.17 Variation in RMSE in Velocity v (m/s) with respect to the variation in the average number of probes in a cell A of the spatiotemporal mesh

The variation in MAPE under all the different *settings* can be more clearly visualized in Figure 5.18. Under all *settings*, the MAPE for k, q, and v went as low as around 20%, 18%, and 4.5%, respectively. The variation in Δx did not significantly affect the average number of probe vehicles that drove through the considered spatiotemporal cells of fixed Δt and $p\%$ and in turn did not affect much the variation in MAPE in k, q, and v. However, for a fixed Δx and $p\%$, Δt exhibits a monotonically increasing nonlinear relationship with the average number of probes observed driving through the cells of the spatiotemporal mesh. This implies that as Δt becomes coarser, the MAPE is expected to decrease. Likewise, to Δt, a drop in $p\%$ leads to a decrease in the average

number of probes; however, this drop is gradual for a Δt and steep when Δt is greater than $120\ s$. This, by its nature, has a direct effect on the propagation of MAPE i.e., for a fixed Δx and Δt, a drop in $p\%$ results in an escalation in MAPE. A similar trend was observed with the variation in RMSE of the estimated traffic state being predominantly affected by Δt and $p\%$ (Table 5.2). The method estimates v with much lower MAPE and RMSE, as compared to the k and q, irrespective of the observation *settings* and the average number of probe vehicles in the spatiotemporal cell. As also described in Figure 5.19, the analysis reveals that when the freeway is in congested regime and when the probe penetration rate is less than 3% and/or the temporal resolution is finer than $120\ s$, the MAPE in estimated density and flow increases which leads to substandard performance of the estimation method.

To analyze the effect of the employed random sampling method on the stability of estimation, the estimation method was evaluated for different series of randomly sampled probe vehicles from the complete ZTD at the same *settings*. It implied that the variation in MAPE in k, q, and v at different *settings* was similar, except for a very fine temporal resolution (say $\Delta t = 15\ s$) and a low probe percentage (such as 1%). Under such *settings*, the estimation performance was unstable but definitively poor. This instability in estimation using the TSE method can be lessened by considering relatively larger $p\%$ or setting the temporal resolution to be coarser than $15\ s$. Overall, this justifies the reliability of the employed *random sampling procedure* for evaluating the estimation capability of the considered estimation method. The selection of the $p\%$ of probes is random; therefore, it is possible that a probe belongs to a logistic fleet, which may lead to a slower than average traveling speed. This will lead to a biased traffic state estimation in the space-time cells via which such a probe vehicle passes. This bias, in general, can be ignored for this analysis when $p\%$ is not very small; however, when $p\%$ is very small such as 1% or 0.5%, the MAPE and RMSE, calculated between traffic states obtained from Edie's generalized definitions and the estimation method, may be affected. In such a case, the differences between the individual sampled probe and others in a particular cell, that could be due to driver's and/or vehicular condition, may lead to a lower accuracy. Additionally, certain vehicle_ids that were changing lanes in the 'lane change prohibited' area was excluded beforehand from the ZTD, which could have led to a false recognition of the leading vehicle to a probe vehicle. The accuracy of the estimation method in estimating traffic states positively correlates with the number of probe vehicles in the space-time region. According to the available $p\%$ or the required accuracy, the practitioners can choose the

desired spatiotemporal resolution *settings*. The accuracy depends on the *settings*: mainly, temporal resolution (Δt), and probe penetration rate ($p\%$), but indirectly. This analysis provides an insight into various combinations of *settings*, expected probe vehicles in spatiotemporal cells, and the corresponding expected accuracy. Another important factor to be considered when employing a set of *settings* in estimating traffic states is the covering percentage ($c\%$), which is discussed in the following section.
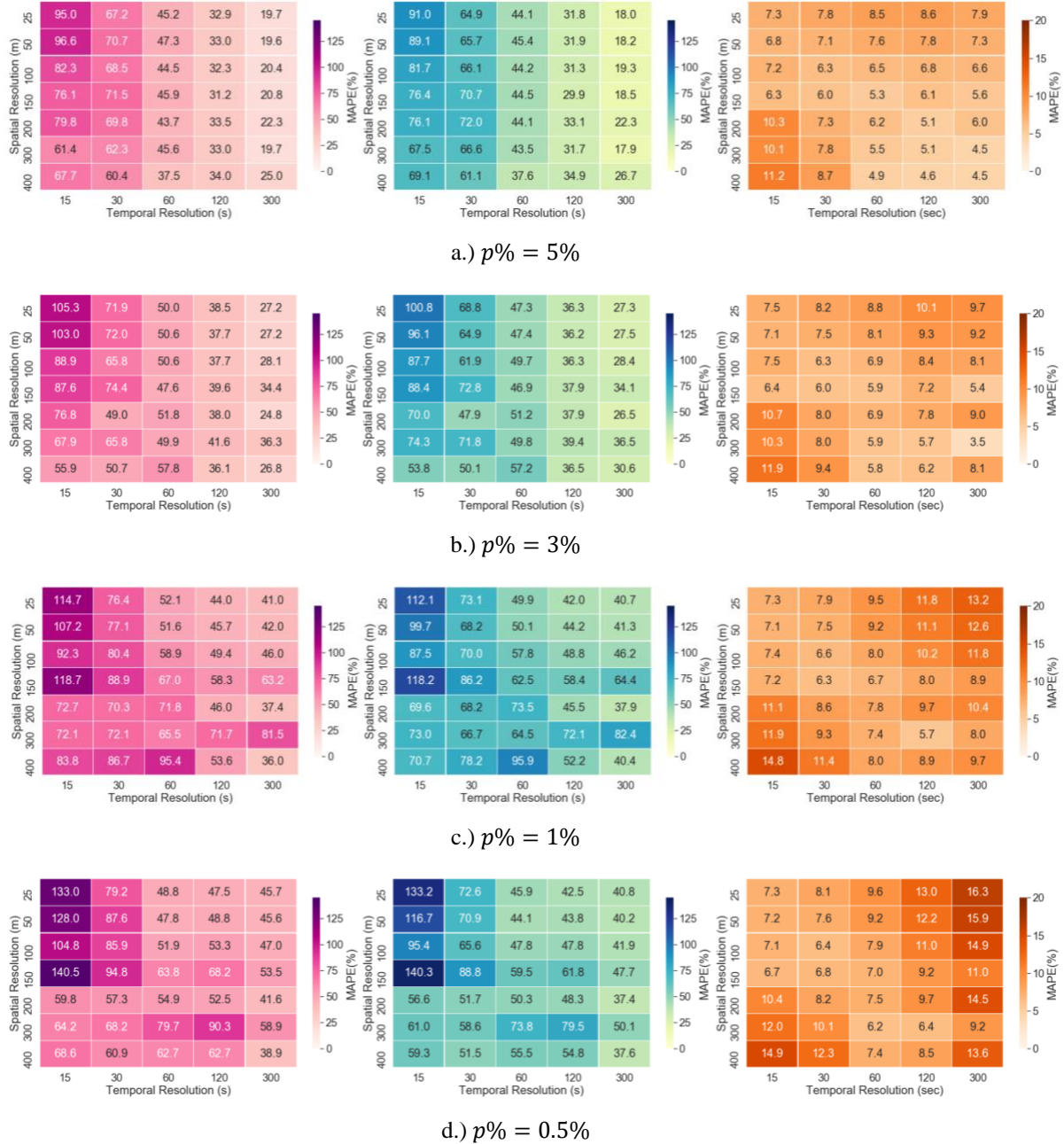
Figure 5.18 Variation in MAPEs in Density (veh/m) (left), Flow (veh/s) (middle) and Velocity (or speed) (m/s) (right) over varying settings for R1, R2, R3 and R4 combined
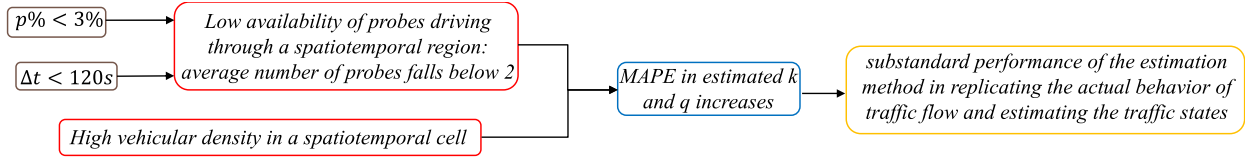
Figure 5.19 Influence of settings on the performance of $xFCD$-based TSE method in estimating traffic states

5.5.2   Covering percentage

The covering percentage ($c\%$) is the percentage of cells through which probe vehicles pass given a fixed *setting* over a region R_i. It is intuitive that the $c\%$ has a positive correlation with the probe vehicle penetration rate i.e., the number of probes and the size of the cell in R_i, which was corroborated by the inferences from the analysis. Unlike the accuracy of the estimation method on which Δx has a low to negligible effect, Δx has a positive correlation with the $c\%$. In fact, in terms of the difference in $c\%$ brought about by unit change in a *setting*, the factors that affect the $c\%$ in order of decreasing dominance are $p\%$, Δt, and Δx. The variation in $c\%$ over different *settings* for R_1 (for instance) is shown in Figure 5.20. However, to be able to retrieve the estimates of traffic states in complete spatiotemporal domain is always desirable i.e., to have a higher $c\%$. The $c\%$ is positively related to the $p\%$, implying that the $c\%$ increases as the average number of probe vehicles driving through the spatiotemporal cells in the mesh of the space-time region R_i increases. However, a higher covering percentage does not imply a high accuracy by an estimation method for obtaining traffic states. For instance, the traffic states of a very large spatiotemporal area estimated using trajectory data from a single probe may lead to a high covering percentage, but with lower accuracy. Hence, for a combination of finer Δt (finer than $2\ min$) and a lower $p\%$ i.e., below 3%, a compromise is made with both accuracy and the $c\%$.
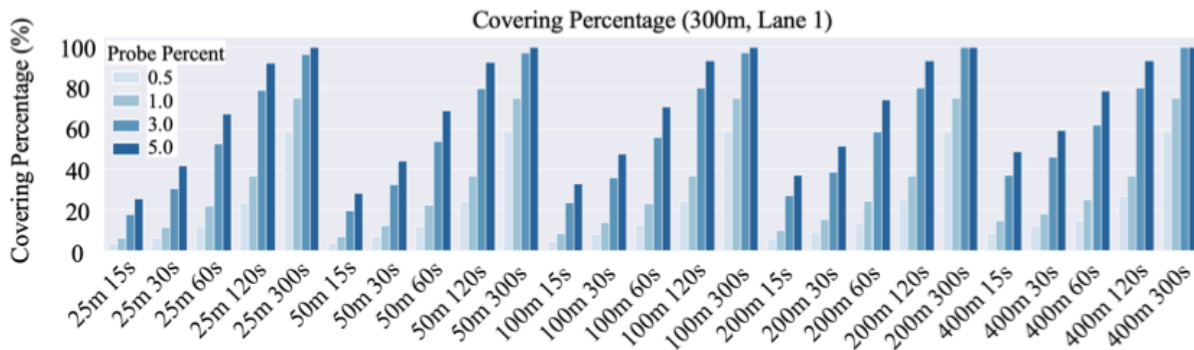
Figure 5.20 Variation in covering percentage in R1 over varying settings

5.6   Conclusions and discussions

Conclusions: The $q - k$ plots for the estimated traffic states along with the actual traffic states suggested that in the free-flow regime, the estimation method was able to reproduce the scatter present in the $q - k$ plots of the actual traffic states, in the estimated states without the assumption of stationarity. As the density increases further, the performance of the estimation method deteriorates. The statistical analysis suggested that the MAPE and RMSE scores for the estimated density and flow are inversely related to the number of probes in a spatiotemporal region, which is predominantly affected by only the temporal resolution and the probe vehicle penetration rate. Specifically, the MAPE for q and k can be as high as 140% for the finest spatiotemporal resolution among the considered *settings* if the average number of probes in the cells of a spatiotemporal mesh is 1. Whereas, when the average number of probes in the cells of a spatiotemporal mesh is around 6 or 7 the MAPE values can be lower than 20% for k and q and around 10% for v. Concurrently, the RMSE in k, q, and v curtails to 0.01 veh/m, 0.09 veh/s (5.4 veh/min), and 0.75 to 1.25 m/s, respectively. When the probe penetration rate falls below 3% and the temporal resolution is finer than 2 min, the MAPE in estimated k and q rises over 40%. Nevertheless, under all the *settings* considered for this analysis, the MAPE for k, q, and v went as low as around 20%, 18%, and 4.5%, respectively. The method estimates v with much lower MAPE and RMSE values, irrespective of the observation *settings*, as compared to k and q. The accuracy of the estimates depends on two *settings*: temporal resolution (Δt), and probe penetration rate ($p\%$), but indirectly.

This analysis provides an insight into the various combinations of *settings*, expected probe vehicles in spatiotemporal cells, the corresponding covering percentage, and the expected accuracy. It is always desirable to be able to retrieve the estimates of traffic states in a complete spatiotemporal domain i.e., to have a higher $c\%$. However, for a combination of a finer Δt i.e., finer than 2 min and a lower $p\%$ i.e., below 3%, a compromise is made with both accuracy and the $c\%$. Additionally, the consideration of appropriate value of Δx may be ignored in terms of accuracy yet Δx has a positive correlation with the $c\%$. Thus, according to the available $p\%$ or the required accuracy and $c\%$, practitioners could select the desired and appropriate spatiotemporal resolution *settings*.

Discussions: The initial challenge in evaluating the performance of an $xFCD$-based traffic state estimation method lies in the identification of the leading vehicle to a probe vehicle. This was meticulously performed with the aid of the ZTD, which enabled the identification of the exact trajectories of the leading and the probe vehicles. The detailed resolution of the ZTD played a critical role in evaluating the actual performance without any approximations based on the spacing measurements calculated using assumptions. The exact spatiotemporal coordinates of vehicles were utilized in reckoning the spatiotemporal area between a probe vehicle and its leading vehicle. The importance of this result lies in the utilization of detailed ZTD in estimating the traffic state using the discussed estimation method, while using other conventional datasets failed to provide the same degree of accuracy evaluation. The ZTD is more reliable than other conventional datasets in deducing inferences from the performance or accuracy evaluation of estimation methods. A unique vehicle ID has been allocated to each vehicle that traveled on the expressway, which is observed and maintained throughout a target section and target time duration. There is a continuity of data at $0.1\ s$ time step with no loss.

However, in actual, few percentages of GPS probes are expected in the actual highways of Japan (where the maximum cell size for traffic control is $\Delta x = 200\ m$ and $\Delta t = 300\ s$), and the *settings* considered in this analysis aided in visualizing expected errors in the estimation results using this method at finer Δx and Δt and a lower $p\%$. The accuracy of the estimation method in estimating traffic states positively correlates with the number of probe vehicles in the space-time region. According to the available $p\%$ or the required accuracy, the practitioners can choose the desired spatiotemporal resolution *settings*. This analysis provides an insight into various combinations of *settings*, expected probe vehicles in spatiotemporal cells, and the corresponding expected accuracy. With few percentages of prove vehicles, the method can estimate traffic states at coarser resolutions with 100% coverage when the expressway is not in the congested state. This low resolution is sometimes useful for planning purposes and for potential area-wide traffic management.

5.7   Gist: input, assumptions, output

This chapter included the evaluation of performance of an $xFCD$-based traffic state estimation method, unconfined by any exogenous assumptions such as FD, proposed by Seo *et al.* (2015b).

This was conducted at several spatiotemporal resolutions (including fine resolutions) and varying probe vehicle penetration rates using high resolution complete trajectory data, the Zen Traffic Data.

The *input* required for estimating the traffic states using this TSE method is the information on the positioning and spacing between a probe vehicle and its leading vehicle. Using that information, the approximate spatiotemporal area between two vehicles in a spatiotemporal cell can be computed which form a part of the state estimation equations.

The *output* will be the estimates of traffic states in the observed spatiotemporal cells of the covered domain. Based on the quality and quantity of probe vehicle data, the *assumptions* will be associated with the calculation of spatiotemporal area between a probe vehicle and its leading vehicle. The limitation and future research directions are discussed in section 7.2.2.

6

TSE USING DATA ASSIMILATION (DA)

This chapter describes the development and implementation of a physical model-based TSE method using DA framework that utilizes spacing and headway measurements from probe vehicles.

6.1 Background and objective

In spite simple probe vehicles or floating cars are impotent to collect data as detailed as ZTD yet, inspecting the traffic state estimation method in chapter 5 using ZTD elucidated the application of the estimation method using $xFCD$ which can record the spacing measurements. At present, 2–3% of probe vehicles are expected in highways in Japan (where maximum cell size for traffic control can be $dx = 200\ m$, $dt = 300\ s$). When working with such percentages of probe vehicles, the method can estimate traffic states at coarser resolutions with 100% coverage when the expressway it is not in the congested state. Also, this low resolution is sometimes useful for planning purposes and analyzing MFD for possible area-wide traffic managements. Under such situations the analysts can estimate traffic states with satisfactory accuracy at coarser spatiotemporal resolution with the approach. However, due to a smaller number of probes the accuracy at even coarser resolutions isn't found out to be the best, which may be improved with the advancement in ICT as more probes are likely to be realized.

The important inferences from the visual and statistical analysis of traffic state estimation method (explored in chapter 5) reveal that the method was able to capture the robust behavior of actual traffic dynamics when the traffic is in free-flow regime. For the free-flow regime, the estimation method was able to reproduce the scatter in the $q - k$ plots of the actual traffic states with the estimated states without the assumption of stationarity. For density beyond critical density, the performance appeared degraded, and the performance of the estimation method deteriorates. For instance, the same has been depicted in Figure 6.1. It can be visualized that beyond critical density, cloud of incorrect estimations coexists with the correct estimations to some extent. Also, working with fewer penetration rates and/or high space-time resolution led to the problem of

unavailable estimates in unobserved cells of the space-time regions. At lower $p\%$ or higher spatiotemporal resolution, the c% is less i.e., TSE was obtained for partially observed cells only. To produce accurate estimates (in non-congested regime) at high resolution, the estimation method may require larger probe penetration rates and the accuracy may not be as high as that of model-driven or data-driven approaches.
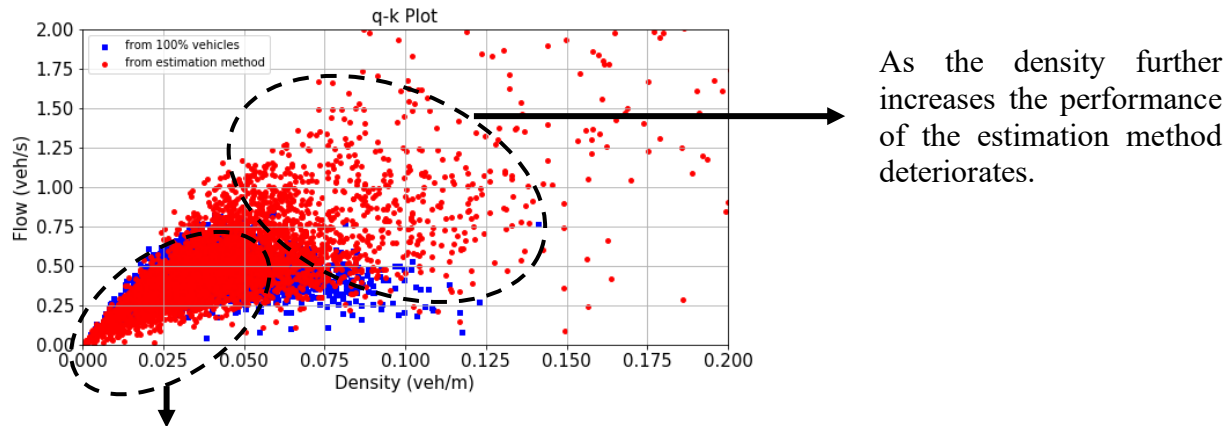
As the density further increases the performance of the estimation method deteriorates.

For the free flow regime, the estimation method was able to reproduce the scatter in the $q - k$ plots of the actual traffic states with the estimated states without the assumption of stationarity.

Figure 6.1 Performance analysis of $xFCD$-based TSE method (Seo et al., 2015b)

However, to be able to retrieve much accurate traffic state estimates in complete spatiotemporal domain (including unobserved cells i.e., cells via which no probe vehicle traversed) at high space-time resolution by utilizing fewer probe vehicles in both the regimes, congested and non-congested, is always desirable. With such requirements, utilizing a model-based approach along with a data assimilation (DA) framework is a vital research direction which needs to be explored in combination with the exploration of smart solutions using ITS. Utilization of DA techniques is expected to provide more accurate estimates under the discussed requirements. In such a pursuit, the TSE method analyzed in chapter 5 is believed to have provided a useful foundation for extending the estimation approach by incorporating a model-based approach along with a data assimilation (DA) framework. Hence, the third objective of this dissertation is to contribute to the development and implementation of a physical model-based method for traffic state estimation and to facilitate an adaptation of the model by utilizing advance probe data to the conditions of highways and roadway links and is described in this chapter. To improve the

estimation capability, it extends the '*weaker*' assumption-based approach to estimate the traffic state more accurately by utilizing a data assimilation (DA) framework using probe vehicle data as depicted in Figure 6.2. The study endeavors to propose a model-based traffic state estimation method that can provide reliable and reasonably acceptable accurate traffic state estimates, 1.) using few probe vehicles i.e., small probe penetration rate ($= 5\%$), 2.) in complete space-time domain, 3.) for both regimes of free-flow and congested, and 4.) at high spatiotemporal resolution. The formulation involves additional assumptions such as consideration of a triangular form on FD of traffic flow and a discretization of a physics-based model namely, Lighthill–Whitham–Richards Model (LWR Model) (Lighthill and Whitham, 1995; Richards, 1956), which are often accepted by traditional traffic flow theory. In it, the state variable, density (k), is estimated by simulating the k obtained from a physical model (Cell Transmission Model: CTM) (Daganzo, 1994) which are then integrated (fused) with the observed traffic states (k and v) using Ensemble Kalman Filtering (EnKF) technique (Evensen, 1994). In addition, the parameters of physical model are obtained by automatic calibration (AC) of a triangular FD.

Figure 6.2 Hypothesis of extending $xFCD$-based TSE method to model-based TSE method

6.2   Modeling and workflow: an adaptive approach

This model-based traffic state estimation approach consists of two major steps: a.) automatic calibration of a triangular FD, which is used to define the parameters of a physics-based model namely, Cell Transmission Model (CTM) and b.) TSE employing the calibrated CTM and EnKF technique, as described in Figure 6.3. Before proceeding with the discussion on the AC of FD, it is important to briefly discuss the data utilized in both the subtasks of formulating the TSE method. Detailed utilization of ZTD in each subtask in further discussed in section 6.4.3 and section 6.5.1 separately.

1. k and v computed using xFCD-based method using 5% probes at {150m x 5s}

2. k is updated from observed k and v, calibrated FD parameters, estimated k in previous step, and a traffic flow model using DA framework

3. TSE from model-based method and xFCD-based approach compared with TSE using Edie's generalized definitions of TS using 100% ZTD (source truth)

TSE from model-based method employing DA (EnKF) using probe data at {150m x 5s}

Automatic calibration of a triangular FD using headway and spacing measurements calculated using probe vehicles (to their leading vehicles): v_f, k_c, k_J at {150m x 5s}

100% ZTD for 2 km and 1 hour (5 datasets)

5% vehicles randomly selected from 100% ZTD and are considered as probes

Figure 6.3 Methodology and workflow

Assumption 6.1: On the Hanshin Expressway (around Tsukamoto Junction), two smaller sections (one of $300\ m$ and one of $150\ m$), each with two lanes (driving lane and passing lane), are particularly considered for this analysis. The 5 datasets of ZTD of Hanshin Expressway (around Tsukamoto Junction) are L001_F001, ..002, ..003, ..004 and ..005. The ZTD corresponding to the considered subsections of expressway is extracted from each larger dataset and are termed as DS1, DS2, DS3, DS4 and DS5 for a clearer understanding. Diving into deeper details of data, DS1 now consists of 4 space-time domains namely, $300\ m$ section: lane 1, $300\ m$ section: lane 2, $150\ m$ section: lane 1 and $150\ m$ section: lane 2, as illustrated in Figure 6.4, and the same is valid for the rest DS2~DS5.

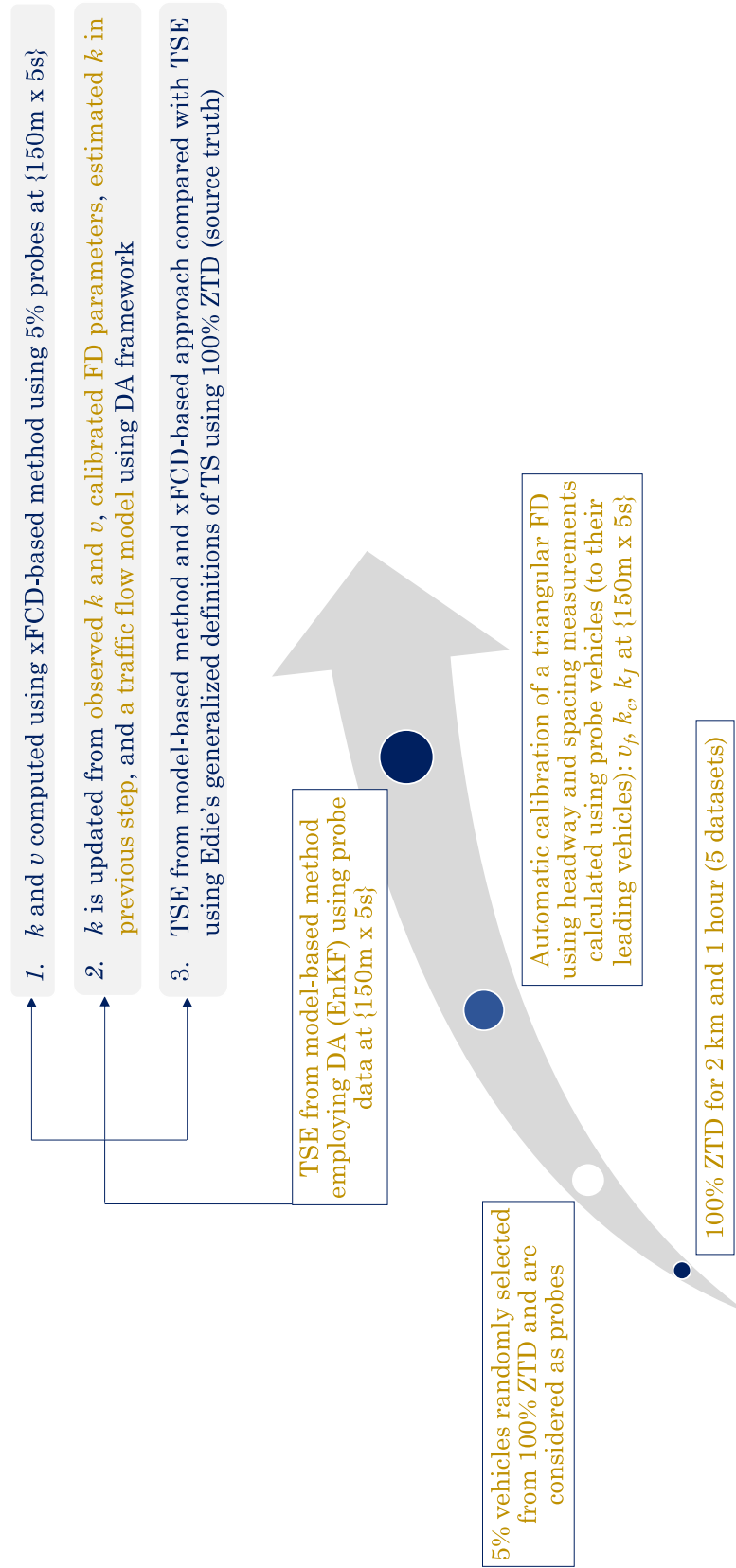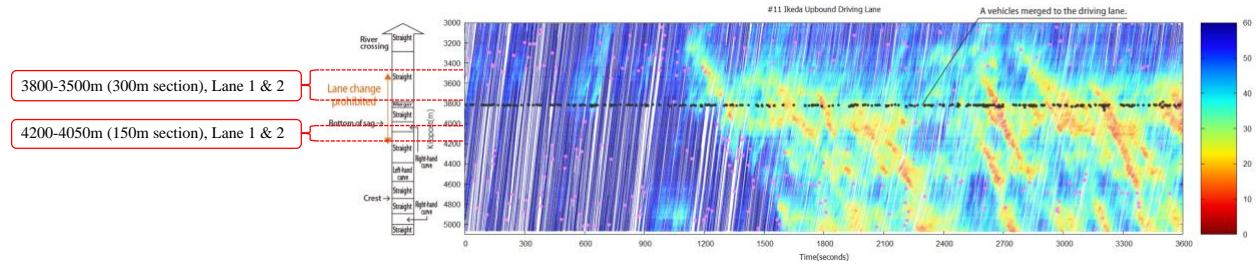*Figure 6.4 Considered sections with minimum lane changing behavior*

(Source: https://zen-traffic-data.net/english/outline/)

1. *Study area:*

The first major part of this chapter involves the automatic calibration (AC) of a triangular FD using data from all 4 space-time domains of each of 5 datasets (DS1~DS5), followed by implementation of proposed TSE method on 1 space-time region of DS1 ($300\ m$: lane 1) and validation using real data (i.e., ZTD itself from $300\ m$: lane 1 space-time domain of DS1), initially. Later, the proposed method has been implemented on the complete space-time domain of $2\ km$ distance and $1\ hour$ (07:00 – 08:00 am) and validated using L001_F001 and in that case the AC of FD is also performed using the data from the same space-time domain i.e., L001_F001.

2. *Setting up the resolution based on CFL condition:*

Now, the maximum speed observed in each lane of the considered space-time domains (total 20) was observed to be $110\ km/hr$ at multiple occasions. Although, the space-time resolutions of

the observation and that of the system model of EnKF implementation can be different, keeping in mind the Courant–Friedrichs–Lewy (CFL) condition, the spatial-temporal resolution for both, automatic calibration of FD (subtask a.)) and TSE using model-based method (subtask b.)), is set as: $\Delta x = 150m$, $\Delta t = 5s$. Hence, for both the subtasks, same space-time resolution is set–$\{150\ m$ x 5 $s\}$, in accordance with the CFL condition. Then, all 20 space-time regions are divided into mesh of spatiotemporal resolutions $\{150\ m$ x 5 $s\}$ i.e., multiple discrete, identical, and rectangular space-time regions.

3. *Probe data extraction from complete ZTD:*

5% of vehicles are randomly sampled from 100% ZTD corresponding to the 4 space-time domains of each dataset DS1~DS5. These randomly sampled vehicles are considered as probe vehicles and from hereon are referred to as *probe vehicles* and ZTD corresponding to these vehicles is referred to as *probe vehicle data*. This is required to formulate, experiment, and validate the proposed methodology by utilizing partially observed traffic data and this extracted data is considered similar to data collected by probe vehicles. It is needless to mention that the 100% ZTD of each dataset (DS1, DS.2, DS3, DS4, and DS5) includes the complete trajectory details of all the vehicles driving on target sections around Tsukamoto Junction on Hanshin Expressway for different 1- $hour$ intervals and is therefore, considered as the source truth for validation the methodology at various steps.

4. *Automatic calibration (AC) of FD:*

AC of the triangular FD (discussed in detail in section 6.4) requires the headway and spacing measurements of each probe vehicle to its leading vehicles. Such data is generally the data obtained from extended floating cars and is termed as $xFCD$ (extended floating car data). In case of probe vehicle data extracted from ZTD, such headway and spacing measurements are mathematically extracted from the trajectory information of each probe vehicle and the vehicle leading to each probe vehicle. Next, since triangular FD and CTM are interdependent, the AC of FD involves calibration of the FD to find the optimized values of its parameters, which in turn defined the parameters of the CTM for TSE. The calibration is done at a space-time resolution of $\{150\ m$ x 5

s}. In other words, the headway and spacing measurements from the probe vehicles are aggregated at a resolution of {$150\ m$ x $5\ s$}. For unobserved cells i.e., cells via which no probe vehicle traversed (thus, the headway and spacing measurements cannot be extracted) the headway and spacing measurements are interpolated from the coarser resolutions such as {$150\ m$ x $60\ s$} and {$150\ m$ x $150\ s$}.

5. *TSE upon combining CTM and EnKF:*

For the next subtask of formulating and implementing the TSE method using DA framework, the estimation of traffic state (density k) using EnKF technique and CTM involves three steps. The CTM is a numerical computational method for solving the LWR model (Lighthill and Whitham, 1995; Richards, 1956) and is utilized as the traffic flow model. For the DA technique, Ensemble Kalman Filter is employed. In the *first step*, the density k and velocity v are computed using the $xFCD$-based TSE approach (Seo *et al.*, (2015b), TSE method discussed in chapter 5) from 5% probe vehicles' data at a space-time resolution of {$150\ m$ x $5\ s$} and are considered as *observations* for the observation equation of the EnKF. In the *second step*, density k is updated from the observed density k and velocity v, calibrated FD parameters (required to simulate density using CTM) and estimated density k in the previous step using DA framework (EnKF). The *third step* involves the validation and comparison analysis of the proposed TSE method. In it, traffic state estimates (density k) from both, the proposed model-based method, and the $xFCD$-based method, are compared with the traffic states computed using Edie's generalized definition (Edie, 1963) and corresponding 100% ZTD (DS1: 300 m section: lane 1), which is considered as the source truth for this analysis.

6.3 The Cell Transmission Model (CTM)

This Lighthill–Whitham–Richards Model (LWR Model) (Lighthill and Whitham, 1995; Richards, 1956), also known as the first-order traffic flow model and kinematic wave theory, is a simplified yet sufficient physics-based traffic flow model that describes the evolution of traffic density k through a partial differential equation (PDE) described as follows:

$$\frac{\partial k(x,t)}{\partial t} + \frac{\partial (k(x,t)v(k(x,t)))}{\partial x} = 0 \qquad (6.1)$$

$$k(x,t) \in [0, k_J] \qquad (6.2)$$

Its two main principles include a FD (equation (6.3)) and the CL (equation (6.1)). Assuming that the traffic dynamics are described by the LWR model then, to close the model, a constructive relation between k and v must be specified. One simplified and common assumption is a triangular FD ($q = k \times v(k)$) (Newell, 1993):

$$v(k(x,t)) = \begin{cases} v_f, & k \leq k_c \\ -w_c(1 - \frac{k_J}{k}), & otherwise \end{cases} \qquad (6.3)$$

Here, $k(x,t)$ is the density at a location x and time t, k_J denotes the jam density, v_f is the maximum velocity i.e., the free-flow velocity, w_c is the maximum backward propagation wave speed and k_c denotes the critical density. These are the parameters involved in the triangular FD.
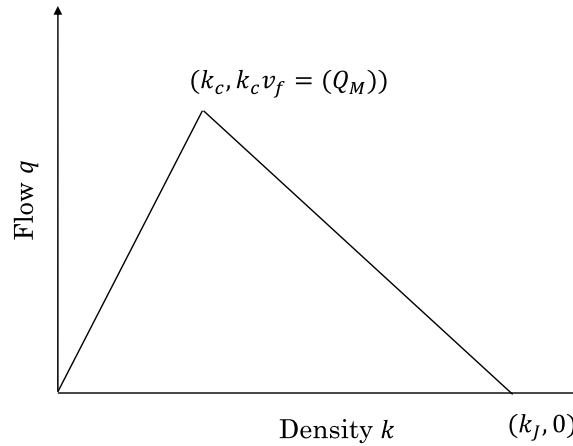
Figure 6.5 Triangular FD

Several numerical computational schemes for solving the LWR model have been proposed to determine the cumulative flow in the space-time area of interest based on given boundary conditions. The CTM (Daganzo, 1994) is a Godunov discretization scheme (Godunov, 1959) of simplified Lighthill–Whitham–Richards (LWR) model (Lighthill and Whitham, 1995; Richards, 1956), which divides a freeway corridor into n cells, each with one on-ramp and one off-ramp and

be characterized by an FD. The FDs can be uniform over all cells or allowed to vary from cell to cell and thus, the parameters of a cell are: v_f (free-flow speed), w_c (backward congestion wave speed), Q_M (the maximum allowable flow), k_J (the jam density) and k_c (critical density). As a consensus in transportation literature, traffic density is a natural measure for traffic surveillance and control purposes as it characterizes level of congestion so, for each cell $i = 1, 2, \dots, n$, at time $t = 1, 2, \dots, h$, the density k of cell i evolves according to the conservation of vehicles as in equation (6.4):

$$k_i(t + 1) = k_i(t) + \frac{\Delta t}{l_i}(q_i(t) - q_{i+1}(t) + r_i(t) - f_i(t)) \qquad (6.4)$$

where $k_i(t)$ is the vehicle density for cell i at time index t, l_i is the length of cell i, $q_i(t)$ is total flow ($veh/unit\ time$) entering cell i during time interval $[t\Delta t, (t + 1)\Delta t)$, $q_i(t + 1)$ is the total flow ($veh/unit\ time$) leaving cell i during time interval $[t\Delta t, (t + 1)\Delta t)$, and r_i and f_i are flow entering cell i from on-ramp and flow leaving cell i to off-ramp, respectively and they can be measured by detectors. One requirement of this model known as Courant–Friedrichs–Lewy condition, as also mentioned earlier, is that the cell length must be longer than the free-flow travel distance, i.e., $v_{f,i}\Delta t \leq l_i$.
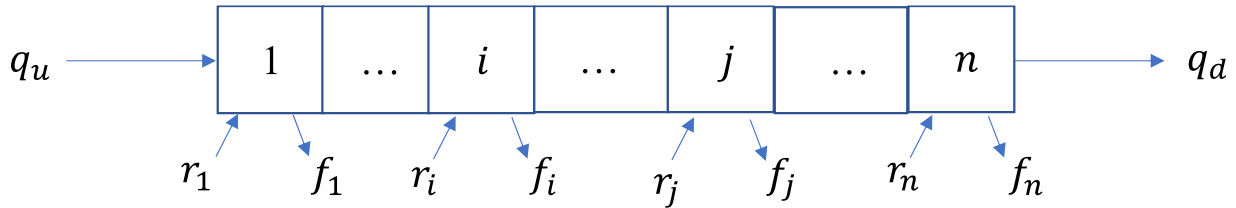
Figure 6.6 Cell discretization for CTM

Assumption 6.2: The FD parameters are considered to be uniform over all cells and it is presumed that detectors are installed at the boundaries of the section such that the aggregated boundary traffic flows ($q_u\ and\ q_d$) and densities ($k_u\ and\ k_d$) are measured.

Assumption 6.3: As depicted in Figure 6.7, it is considered that the section has no cells with on-ramp or off-ramp i.e., r_i and f_i are zero for all cells.

Figure 6.7 Cell discretization with no on-ramp or off-ramp

$q_i(t)$ is determined by taking minimum of the maximum flow supplied by cell $i-1$ over interval $[t, t+1)$ under free-flow condition and the maximum flow that can be received by cell i under congested condition over the same time interval (Zhong *et al.*, 2016).

$$q_i(t) = \min \{v_{f,i-1}k_{i-1}(t), Q_{M,i-1}, Q_{M,i}, w_{c,i}(k_{J,i} - k_i(t))\} \qquad (6.5)$$

In consistency with the explanation of Zhong *et al.* (2016) regarding boundary conditions, CTM assumes that the downstream end of section can always discharge vehicles at either maximum allowed speed (v_f) or maximum allowed flow rate (or capacity), i.e., the downstream end is connected to a sink. However, in actual traffic section, traffic at the downstream end may be either free-flowing or congested so, the model considers the congested condition at downstream boundaries. Hence,

$$q_1(t) = \begin{cases} \min\left\{q_u(t), Q_{M,1}, w_{c,1}\left(k_{J,1} - k_1(t)\right)\right\}, & if\, k_u(t) < k_{c,1}, \\ \min\{Q_{M,1}, w_{c,1}(k_{J,1} - k_1(t))\}, & otherwise \end{cases} \qquad (6.6)$$

$$q_{n+1}(t) = \begin{cases} \min\{v_{f,n}k_n(t), Q_{M,n}\}, & if\, k_d(t) < k_{c,n}, \\ \min\{v_{f,n}k_n(t), Q_{M,n}, k_d(t)\}, & otherwise \end{cases} \qquad (6.7)$$

These calculations of flow in each cell as per equations $(6.5) - (6.7)$ are a key input for the discretized evolution equation of density equation (6.4). The density simulated by equation (6.4) is a key input for the optimization problem of calibrating the triangular FD as described in the following section 6.4.

6.4   Automatic Calibration (AC) of FD

The concept of FD has a significant role in methods based on KFTs and most methods assume exogenous conditions on the FD such as its functional form and parameters. However, FD is a complicated phenomenon which involves various factors that cannot be described completely. Therefore, careful calibration of FD prior to TSE is vital. Regarding calibration of FD, a standard practice is to formulate it as a Least-Square (LS) estimation problem, but such conventional calibration methods do not take traffic flow dynamics into consideration, which renders the simulation to be unrobust and the simulation may not be adaptive to the variability of traffic data caused by uncertainties such as accidents, adverse weather conditions, etc. However, utilizing the local neighborhood information of a particular data point to construct the principal curve in a calibration process can improve the model accuracy and thus, traffic flow models may be better choice for accessing 'local neighborhood information' (Zhong *et al.*, 2016). To tackle such issues, the AC method is adopted to calibrate the triangular FD[4] which considers the spatiotemporal causalities of traffic data and in turn to improve the accuracy of TSE by adapting to the variability of data.

The AC of FD is done through a dynamic approach and in an iterative manner on similar guidelines as Zhong *et al.* (2016). The FD calibrated from last step is incorporated into the CTM to simulate its effect on traffic flow modeling. Simulated density from the CTM is compared against the measured density wherein an optimization merit is conducted. The objective of this optimization is to seek parameters (of the FD) that minimizes the discrepancy between simulated (model-generated) data and real data in terms on mean squared error-based cost function. Through this integration of the advantages of data-driven (i.e., optimization counterpart that corresponds to the adaptiveness) and the model-driven (i.e., the CTM that relates to the robustness), the adaptiveness and the robustness are achieved. After finding the optimized values of the FD parameters, the CTM is defined and is used as the system model of the process equation of EnKF technique, and TSE is then to be done as per the methodology explained in section 6.5.

---

[4] By employing an approximate functional form, FD can be estimated empirically based on sufficiently high‑resolution traffic data (e.g., Chiabaut *et al.*, 2009; Qu *et al.*, 2015).

6.4.1   Methodology

Density k is used to define the merit function, which is a mean square error-based cost function to minimize discrepancy between simulated traffic density ($k_i(t)$) and its measured counterpart ($\hat{k}_i(t)$). The cost function is defined as in equation (6.8):

$$g = \sum_{t=1}^{h}\sum_{i=1}^{n}(\hat{k}_i(t) - k_i(t))^2 \tag{6.8}$$

As all the parameters of assumed triangular shaped FD, free-flow velocity, critical density, jam density and backward wave speed, are not mutually independent, so the independent parameter set is identified i.e., the free-flow speed, critical density, and jam density and are chosen as the decision variables $x_i = [v_f, k_c, k_J]^T$ for all cell i along the roadway section. Letting $\boldsymbol{x}$ be the vector of all decision variables; the objective becomes to find x^* that minimizes g. Since determining the freeway capacities empirically is not a trivial task hence, operational capacity i.e., maximum flow observed across the space-time domain of the considered sections is considered.

Assumption 6.4: As illustrated in Figure 6.8, it is presumed that detectors are installed at the boundaries of the section such that the aggregated boundary traffic flows (q_u and q_d) and densities (k_u and k_d) are measured.

a.) $3.5{-}3.8\ k.p.$ (300 m section Lane 1, Lane 2)   b.) $4.05{-}4.2\ k.p.$ (150 m section Lane 1, Lane 2)
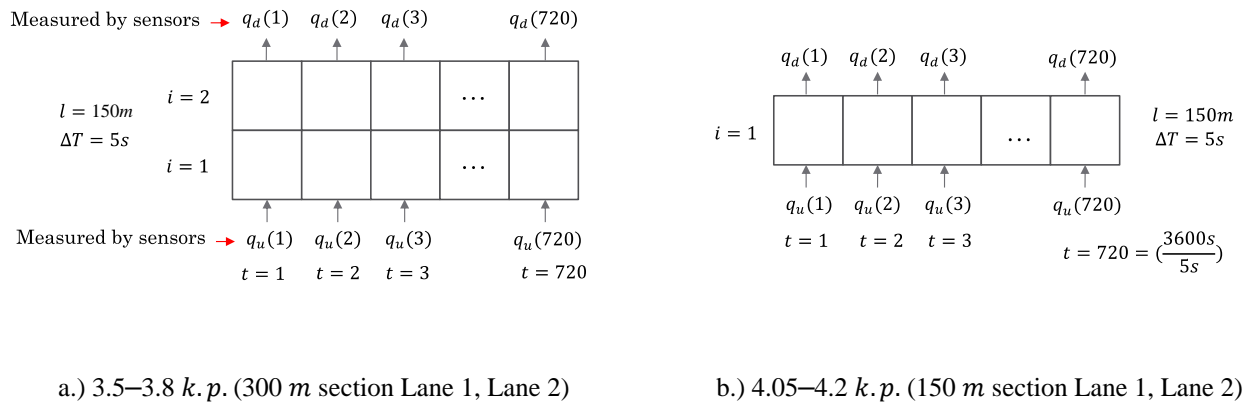
Figure 6.8 Boundary flow measurement in a.) 300 m section and b.) 150 m section

6.4.2   Optimization problem and initialization

The optimization problem of automatically calibrating the triangular FD can be stated as:

$$Problem\ QP1:\ x^* = arg\ {}^{min}_{xg} \tag{6.9}$$

Equality constraints:

$$k_i(t+1) = k_i(t) + \frac{\Delta t}{l_i}(q_i(t) - q_{i+1}(t)) \tag{6.10}$$

$$q_1(t) = \begin{cases} \min\left\{q_u(t), Q_M, w_c\left(k_J - k_1(t)\right)\right\}, & if\ k_u(t) < k_{c,1}, \\ \min\left\{Q_M, w_c(k_J - k_1(t))\right\}, & otherwise \end{cases} \tag{6.11}$$

$$q_i(k) = \min\{v_f k_{i-1}(t), Q_M, w_c(k_J - k_i(t))\} \tag{6.12}$$

$$q_{n+1}(t) = \begin{cases} \min\{v_f k_n(t), Q_M\}, & if\ k_d(t) < k_{c,n}, \\ \min\{v_f k_n(t), Q_M, q_d(t)\}, & otherwise \end{cases} \tag{6.13}$$

Definition constraints:

$$v_f \Delta t \le l,\ \forall i, \tag{6.14}$$

$$Q_M = v_f k_c,\ \forall i, \tag{6.15}$$

$$w_c = \frac{Q_M}{k_J - k_c},\ \forall i, \tag{6.16}$$

$$w_c < v_f,\ \forall i, \tag{6.17}$$

$$v_f,\ w_c,\ Q_M,\ k_c,\ k_J > 0,\ \forall i. \tag{6.18}$$

The constraints should hold for all cell i and time step t. Sequential Quadratic Programming (SQP) algorithm, which is a non-linear programming algorithm, has been used to solve the problem of parameter estimation and the iterative process is as depicted in Figure 6.9.
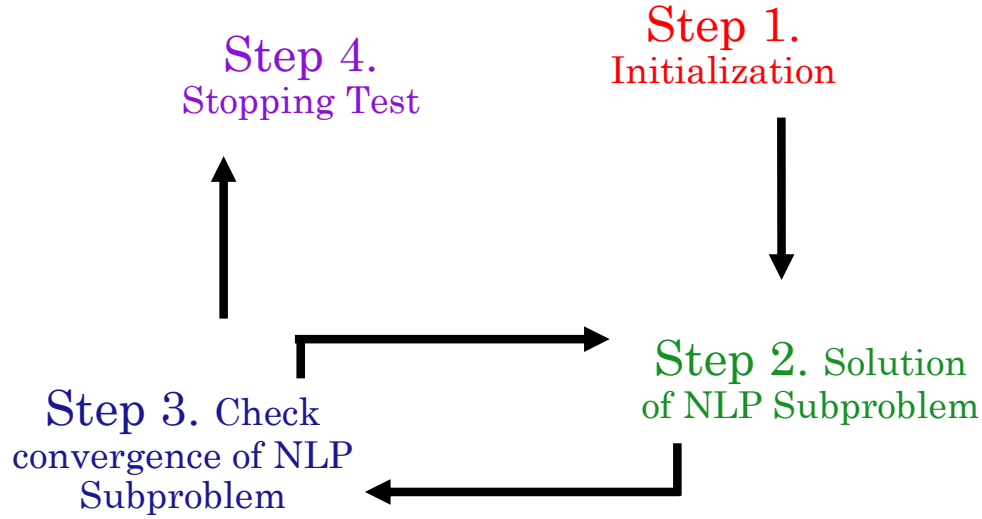
Figure 6.9 Iterative process of solving optimization problem for AC of FD

The steps involved in solving the optimization problem are:

Step 1 – Initialization: The initial FD parameters are derived from regression of headway-spacing relation in the probe vehicle data and the problem posed is same as described in Seo *et al*. (2015a). The values of v_f, k_c and k_J are solution of the following optimization problem:

$$\begin{array}{c} argmin \\ v_f, k_c, k_J \end{array} \sum_{cell \in Region\ R} \sum_{(m,\tau) \in P(cell)} D(h_{m,\tau}, s_{m,\tau}, v_f, k_c, k_J)^2 \qquad (6.19)$$

$$s.t. v_f \geq 0, k_c \geq 0, k_J \geq 0 \qquad (6.20)$$

where $h_{m,\tau}$ is the average stationary headway of vehicle m at time τ in a cell of spatiotemporal mesh, $s_{m,\tau}$ is the average stationary spacing of vehicle m at time τ in a cell of spatiotemporal mesh,

D is the function returning minimum distance from a point $(q, k) = (^1/_{h_{m,\tau}}, ^1/_{s_{m,\tau}})$ to a curve $q = F(k, v_f, k_c, k_J)$ and F is the function representing a triangular FD. This problem finds FD parameter values that minimize the total distance between observed stationary headway-spacing points and the FD curve. The term stationary headway-spacing points implies that the change rates of the variables headway and spacing in a small duration of time $\Delta\tau$ e.g., $(^{h_{m,\tau} - h_{m,\tau-\Delta\tau}}/_{h_{m,\tau}})$ are small enough and the criteria for stationary headway-spacing determination is set as 1% during $\Delta\tau$ i.e., $^{h_{m,\tau} - h_{m,\tau-\Delta\tau}}/_{h_{m,\tau}} \le 0.01$.

The initialization step also includes specification of simulation configurations. The number of cells is set as 2 for $300\,m$ section (3.8–3.5 $k.p.$) and 1 for $150\,m$ section (4.2–4.05 $k.p.$), cell length l is constant for all cells which is $150\,m$. According to the CFL condition, the time step Δt is set to be $5\,s$ (as the maximum observed speed was around $30\,m/s$). The initial feasible FD is identified from the conventional calibration method as described above and is denoted by x^1. Then, the dynamic cell densities are estimated by the CTM with x^1 and the objective function g^1 is calculated.

Step 2 – Solution of NLP subproblem: Sequential Quadratic Programming is applied to solve the nonlinear programming subproblem.

Step 3 – Check convergence of NLP subproblem: If the present tolerance ε_1 or the maximum iteration number $Iter_m$ of the NLP is achieved, declare the solution to be x^{s+1}, and go to Step 4. Otherwise, declare the solution to be initial condition of NLP and go to Step 2 (Zhong *et al.*, 2016).

Step 4 – Stopping test: If $\|x^{s+1} - x^s\| \le \varepsilon$, where $\varepsilon \in R_+$ is a preset tolerance (0.001), stop and declare $x^* \approx x^{s+1}$. Otherwise, set $s = s + 1$ and go to Step 1 with the last feasible solution from NLP as the initial feasible FD.

6.4.3   Utilization of ZTD for AC of FD

On the distance of $2\ km$ ($5\ k.p.$ to $3\ k.p.$ i.e., $5000\ m$ to $3000\ m$) the lane changing is prohibited for the distance between $4200\ m$ to $3400\ m$ and a merging from outside entrance lane happens at $3.8\ kilopost$ (Tsukamoto Junction).

Assumption 6.5: In this lane change prohibited distance, for simplification of analysis two smaller sections (one of $300\ m$ i.e., $3.80\ k.p.$ to $3.50\ k.p.$ and one of $150\ m$ i.e., $4.20\ k.p.$ to $4.05\ k.p.$), each with two lanes, between $4.2\ k.p.$ and $3.4\ k.p.$ are particularly considered for this analysis that have minimum lane-changing behavior and maintain the conservation of vehicles throughout each section. In each lane of these sections there is no vehicle's overtaking nor merging/diverging sections (i.e., a first-in first-out (FIFO) condition and a Conservation Law (CL) is satisfied).

The 5 datasets of ZTD of Hanshin Expressway (around Tsukamoto Junction) are L001_F001, ..002, ..003, ..004 and ..005. The ZTD corresponding to the considered subsections of expressway is extracted from each larger dataset and are termed as DS1, DS2, DS3, DS4 and DS5 for a clearer understanding. Diving into deeper details of data, as depicted in Figure 6.10, DS1 now consists of 4 space-time domains viz., $300\ m$ section: lane 1, $300\ m$ section: lane 2, $150\ m$ section: lane 1 and $150\ m$ section: lane 2, and the same is valid for the rest DS2, DS3, DS4 and DS5. Now even though the lane changing was prohibited in the considered subsections, certain lane changing behavior was still observed as shown in Table 6.1. Such vehicles have been excluded for this part of analysis. The aggregated boundary traffic flows ($q_u\ and\ q_d$) and densities ($k_u\ and\ k_d$) are presumed to be measured by the detectors installed at the boundaries of the section. Therefore, 100% ZTD is used to calculate aggregated boundary traffic flows and densities at the boundaries of the sections.

For AC of FD, 5% of vehicles are randomly sampled from 100% ZTD corresponding to the 4 space-time domains of each dataset DS1~DS5. These randomly sampled vehicles are considered as probe vehicles and from hereon are referred to as probe vehicles and ZTD corresponding to these vehicles is referred to as probe vehicle data. Using ZTD it was possible to identify the sequential order of vehicles driving in each lane of each space-time domain for $1\ hour$, that was maintained throughout the section due to minimum lane changing behavior. Hence, the leading

vehicle to each vehicle was identified with their trajectories in their respective space-time region. This serves as a very essential ingredient in:

a.) finding the spacing and headway between a probe vehicle and its leading vehicles at time t for automatic calibration of FD

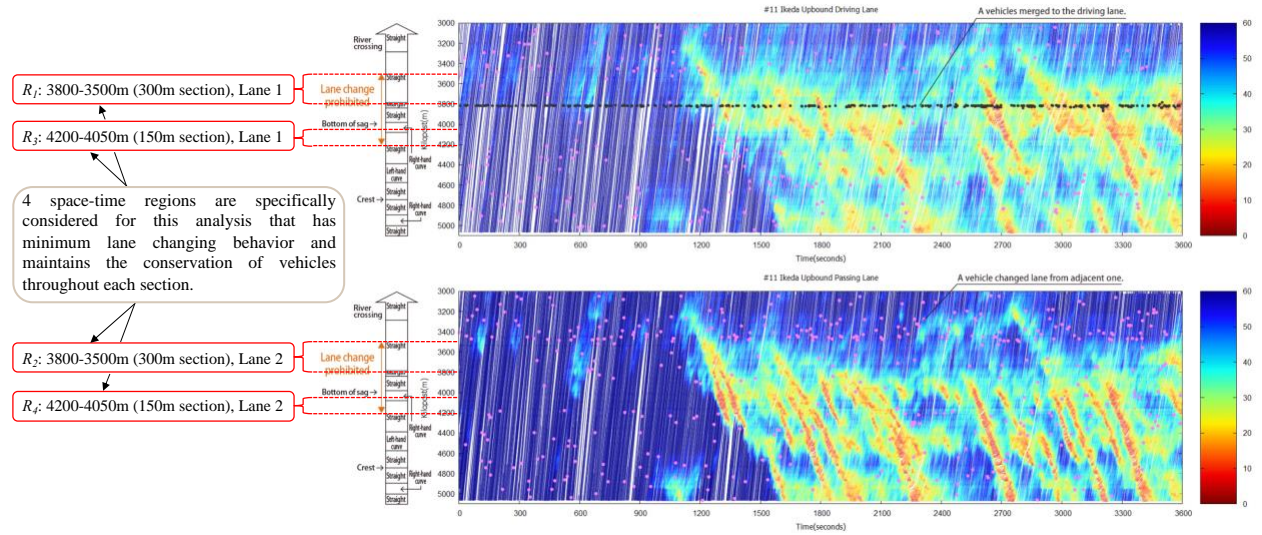b.) observing traffic state using the $xFCD$-based method (step 1. of second subtask)

Figure 6.10 Four spatiotemporal regions considered for the study

(Source: https://zen-traffic-data.net/english/outline/)

Table 6.1 Lane changing behavior observed in the considered section

	4.2–4.05 $k.p.$ (150 m section)	**3.8–3.5 $k.p.$ (300 m section)**
DS1 from L001_F001	19 out of 2976 (0.64%)	38 out of 3261 (1.16%)
(7–8 a.m.)	Lane 1: 1214, Lane 2: 1743	Lane 1: 1467, Lane 2: 1756
DS2 from L001_F002	15 out of 3123 (0.48%)	41 out of 3392 (1.21%)
(7–8 a.m.)	Lane 1: 1298, Lane 2: 1810	Lane 1: 1523, Lane 2: 1828
DS3 from L001_F003	13 out of 2806 (0.46%)	31 out of 3134 (0.99%)
(3–4 p.m.)	Lane 1: 1204, Lane 2: 1589	Lane 1: 1498, Lane 2: 1605
DS4 from L001_F004	23 out of 2876 (0.80%)	37 out of 3200 (1.16%)
(3–4 p.m.)	Lane 1: 1168, Lane 2: 1684	Lane 1: 1482, Lane 2: 1681
DS5 from L001_F005	16 out of 2721 (0.59%)	19 out of 2885 (0.66%)
(10–11 a.m.)	Lane 1: 1158, Lane 2: 1547	Lane 1: 1318, Lane 2: 1548

Following that, each space-time region is divided into mesh of spatiotemporal resolutions $\{150\ m\ \text{x}\ 5\ s\}$ i.e., multiple discrete, identical, and rectangular space-time regions as illustrated in Figure 6.11.

a.) $3.5-3.8\ k.p.$ ($300\ m$ section Lane 1, Lane 2)   b.) $4.05-4.2\ k.p.$ ($150\ m$ section Lane 1, Lane 2)
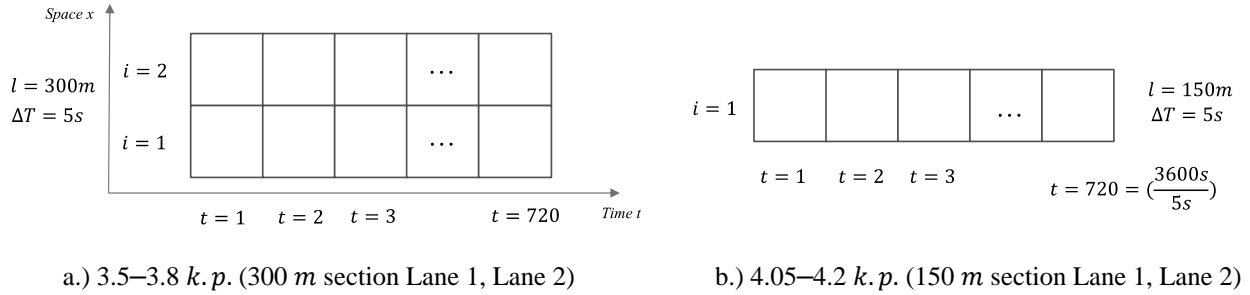
Figure 6.11 Discretization of spatiotemporal region for CTM

The average headway and spacing measurements of probe vehicles in a cell to their leading vehicles, both in a particular cell, are used to compute the flow-density (q, k) points in each cell of a spatiotemporal mesh. They serve as the input data for initializing the optimization problem for automatically calibrating the triangular FD. The average headway and spacing measurements in a cell are calculated by finding the arithmetic average of all stationary headway and spacing measurements of each probe vehicle to its leading vehicle in that cell as given by equations (6.21) – (6.22). The headway and spacing measurements are mathematically extracted from the trajectory information of each probe vehicle and its leading vehicle from the probe data extracted from 100% ZTD as shown in Figure 6.12 and Figure 6.13. The relation between average headway and spacing measurements and (q, k) points are given by equation (6.23).

$$h_m = average(h_{m,\tau1}, h_{m,\tau2}, h_{m,\tau3}) \tag{6.21}$$

$$s_m = average(s_{m,\tau1}, s_{m,\tau2}, s_{m,\tau3}) \tag{6.22}$$

$$\left(q_{i,t}, k_{i,t}\right) = \left(^1/_{h_m}, ^1/_{s_m}\right) \tag{6.23}$$

The (q, k) points are calculated for all four space-time regions ($150\ m$ section Lane 1, $150\ m$ section Lane 2, $300\ m$ section for lane 1, $300\ m$ section lane 2) and for all 5 datasets (DS1~DS5) at a spatiotemporal resolution of $\{150\ m\ \text{x}\ 5\ s\}$ and for cells via which no probe vehicles passed

the (q, k) points computed from coarser resolutions such as $\{150\ m \text{ x } 60\ s\}$ and $\{150\ m \text{ x } 150\ s\}$ are used for those unobserved cells. In other words, the headway and spacing measurements from the probe vehicles are aggregated at a resolution of $\{150\ m \text{ x } 5\ s\}$. For unobserved cells i.e., cells via which no probe vehicle traversed (thus, the headway and spacing measurements cannot be extracted) the headway and spacing measurements are interpolated from the coarser resolutions such as $\{150\ m \text{ x } 60\ s\}$ and $\{150\ m \text{ x } 150\ s\}$ and finally the input for the initialization of the calibration of FD problem at a space-time resolution of $\{150\ m \text{ x } 5\ s\}$ is ready. Note that for AC of FD, to create an optimization density between simulated density and measured density, the density k computed using these headway measurements are also used as the observed density for each cell of spatiotemporal meshes of the considered space-time domains.
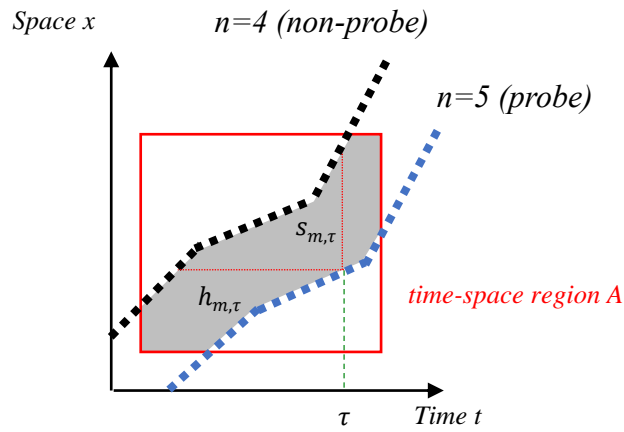

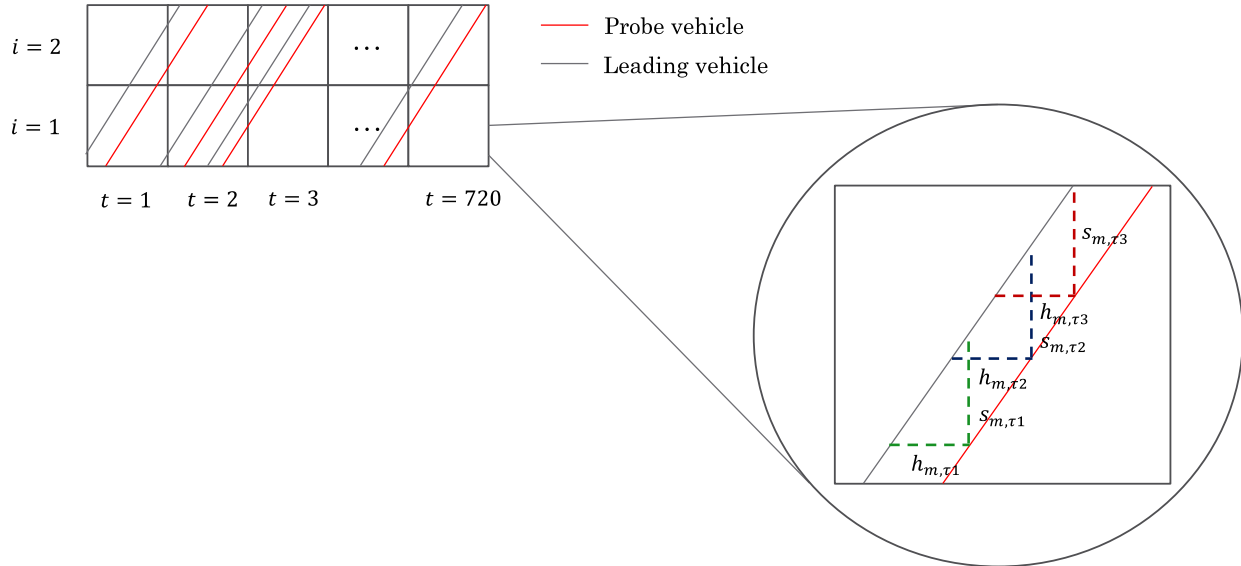*Figure 6.12 Headway and spacing measurement between a probe vehicle and its leading vehicle*

Figure 6.13 Average headway and spacing measurement in a particular cell

6.4.4   Calibration results and their utilization

The calibration of FD for defining parameters of CTM relies upon several factors:

i.   **traffic measurements**: we're assuming the density is calculated from the spacing measurements obtained from the probe data and the probe data is extracted from real traffic data i.e., ZTD (which is reliable)

ii.   **measure of goodness-of-fit used to create objective function**: traffic density is natural measure to characterize traffic congestion and therefore, density is used to define the merit function (mean square error-based cost function) that minimizes the discrepancy between the simulated density $(k_i(t))$, and it's measured counterpart $(\hat{k}_i(t))$.

$$objective\ function:\ g = \sum_{t=1}^{h} \sum_{i=1}^{n} (\hat{k}_i(t) - k_i(t))^2 \qquad (6.24)$$

$$objective:\ \text{find } x^* \text{that minimizes } g \qquad (6.25)$$

iii.   **traffic model**: the CTM model

iv.   **parameters to be calibrated (subject to triangular shape that minimize the cost function)**: as not all parameters of FD of CTM are mutually independent therefore, the independent parameters are identified to reduce effort. $x_i = \left[u_i, k_{c,i}, \kappa_i\right]^T$ represents the decision variable for each cell i along the stretch of the section and **x** be the vector of decision variables.

Because of the non-smoothness of the CTM (induced by the min operator), the algorithm may admit a deficiency that only local optimal solutions can be found. Whereas, it has been proven by Sumalee *et al.* (2011) that CTM is a convex program that admits a unique solution. The objective function of the calibration algorithm is strictly convex function while the feasible region defined by CTM is also convex, the calibration method would admit a unique solution and a local minimizer would be also a global one. However, given the iterative nature of solving the

optimization problem through SQP, there is a possibility that the solution may not converge under certain conditions. Therefore, the solution needs to be carefully acknowledged.

The (q, k) points calculated using headway-spacing measurements of 5% probes in all the space-time regions using all datasets are plotted as shown in Figure 6.14 for various combinations (such as described in Table 6.2). These (q, k) points are used to calibrate an initial FD by conventional LS calibration method. These LS-fitted parameters are then used as initial condition for the optimization problem of automatic calibration of triangular FD. The values of optimized FD parameters for various combination of datasets are described in Table 6.2. The automatically calibrated FD of v_f, k_c, and k_J, calibrated using 5% probe vehicles lie in the range of [15.99, 22.55] m/s, [0.041,0.054] veh/m, and [0.102,0.143] veh/m, respectively. The standard deviation in optimized v_f, k_c, and k_J for various combination of datasets is 2.10 m/s, 0.004 veh/m and 0.014 veh/m, respectively, which are quite low and provides meaning to the reliability of optimized parameters. The average of these parameters over all combinations of datasets is 19.39 m/s for v_f, 0.046 veh/m for k_c and 0.113 veh/m for k_J. In Figure 6.14, the blue curve is the FD obtained from the LS regression fitting. In fact, parameters of this LS fit FD are used as initial conditions for the optimization problem of AC of FD. The pink curve depicts the automatically calibrated FD whose parameters are listed in Table 6.2. Compared with the conventional LS calibration method, the AC results are quite different in terms of capacity, jam density and congestion wave speed. Another interesting finding is even though these 2 FDs are so different, their free-flow parts are close. The conventional LS method generally underestimates the flow, and the automatic calibrated FD outperforms because it searches for the 'best capacity' (as well as other parameters simultaneously). The primary reasons for the differences between the FDs estimated using two approaches are:

o   Usually, the FD is assumed to be valid under the equilibrium state of traffic. Since, a rigorous and accurate steady state analysis is difficult to perform before the calibration of FD, there exist a lot of unstable (q, k) points which results in underperformance of LS fit. However, if such unsteady points can be removed the calibration results using LS fit and AC of FD are likely to become similar.

o   At the same time, AC approach utilizes the CTM for better understanding the dynamics of traffic based on observations to calibrate a better FD where the bias caused by the unstable (q, k) points is subdued to some extent.

o   Finally, the LS fit aims to just minimize the Euclidian distances between the (q, k) points to a triangular FD. Under situations such as when there is high density of unstable points compared to stable points (due to poor or no steady state analysis) or absence of enough (q, k) points (when the freeway doesn't undergo severe congestion), the LS fit will give equal weightage to the unstable points and will estimate an incorrect FD in terms of maximum capacity, jam density or congested wave speed.

To compare the reliability and closeness of the optimized FD parameters, the similar automatic calibration optimization problem is implemented for all the considered 20 space-time regions using 100% ZTD (instead of using only 5% ZTD i.e., probe vehicle data). Figure 6.15 and Figure 6.16 illustrate the plots of LS fit FD and automatically calibrated FD over the (q, k) points. Note that here, (q, k) points are not computed through the headway and spacing measurements, rather Edie's generalized definitions are used which makes the calibration even more reliable. Now, even though the AC of FD, depicted in Figure 6.15 and Figure 6.16, utilize 100% ZTD and employ Edie's generalized definitions for calculating (q, k) points, the interesting finding is that the values of optimized parameters (of FD) lie close to the parameters found using (q, k) points computed using the headway and spacing measurements of 5% ZTD (considered as probes). The same has been shown in Table 6.3 and Table 6.4. The average values of optimized v_f, k_c, and k_J for different lanes of 300 m section is 17.33 m/s, 0.045 veh/m and 0.111 veh/m, respectively. The average values of optimized v_f, k_c, and k_J for different lanes of 150 m section is 21.88 m/s, 0.033 veh/m and 0.097 veh/m, respectively. The values of automatically calibrated FD using 5% probe vehicles' headway-spacing measurements are similar to the ones of automatically calibrated FD using 100% vehicles of ZTD using which the (q, k) points are calculated by Edie's generalized definitions. This implies that the parameters of automatically calibrated FD are calibrated with reasonable accuracy. Therefore, the optimized parameters can be utilized to define the CTM for the next subtask of estimating the traffic state (density) using a physics-based model i.e., CTM (for system equation), observations of density and velocity using $xFCD$-based TSE method (Seo *et al.*,

2015b) (for observation equation) and a DA technique i.e., EnKF (for estimating the most probable state).

Here, the main reason for conducting a long exercise of calibrating FD for various combination of datasets was to analyze the performance of calibration methodology in terms of accuracy and variation of datasets. Since the reliability is now verified therefore, the optimized v_f, k_c, and k_J obtained from (q, k) points from all datasets combined i.e., Figure 6.14 e.) are taken forward which are: $v_f = 18.42\ m/s$, $k_c = 0.054\ veh/m$ and $k_J = 0.113\ veh/m$.
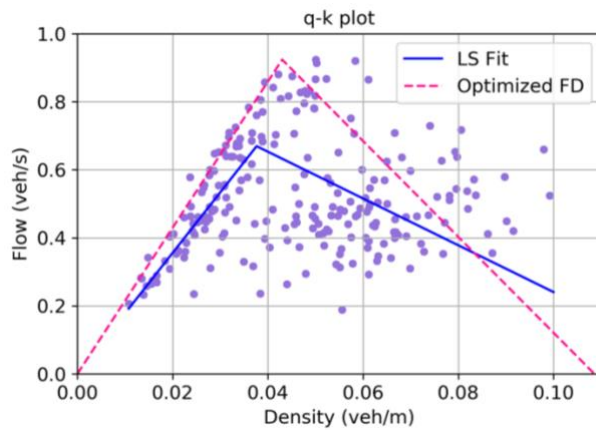
a.) all regions for 150 m section
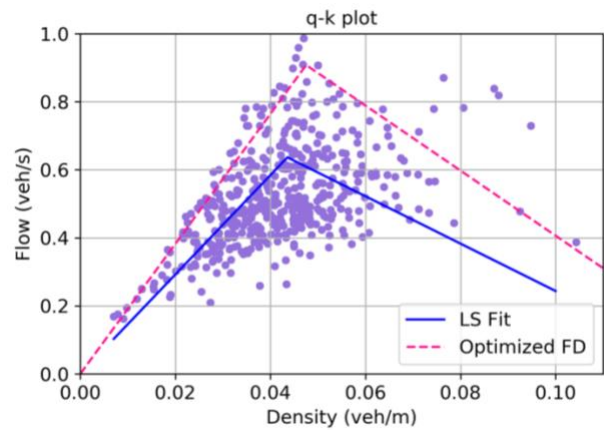
b.) all regions for 300 m section
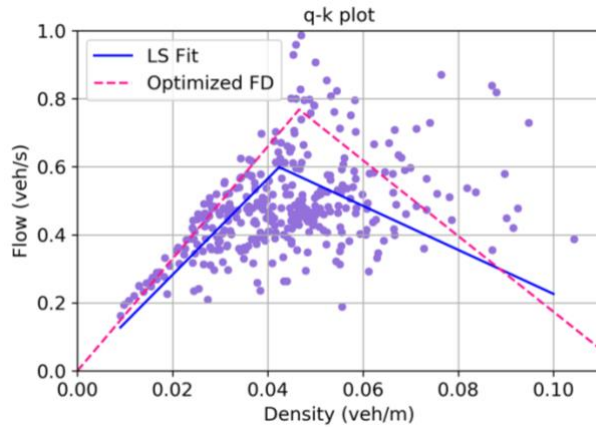
c.) all regions for Lane 1

d.) all regions for Lane 2

e.) all data
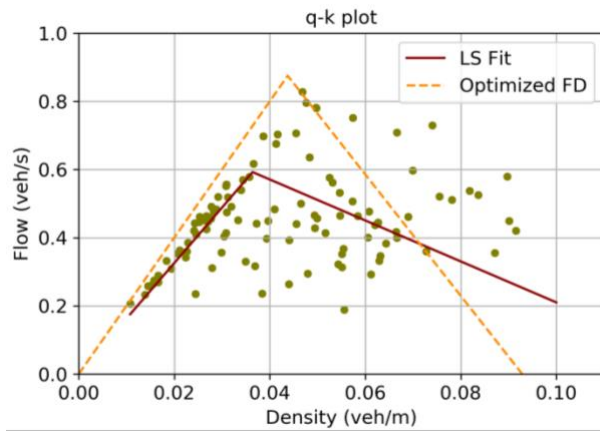
f.) all regions for 150 m section Lane 1
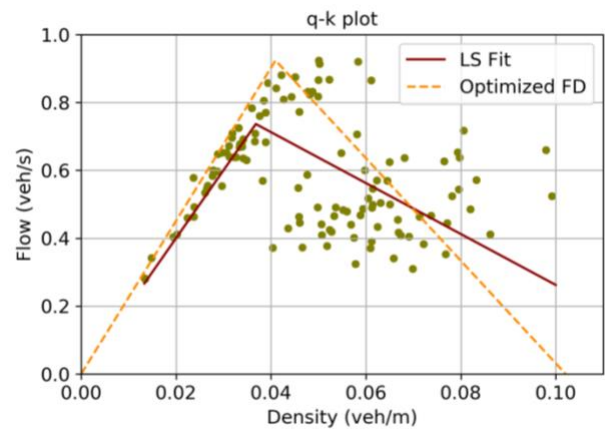
g.) all regions for 150 m section Lane 2
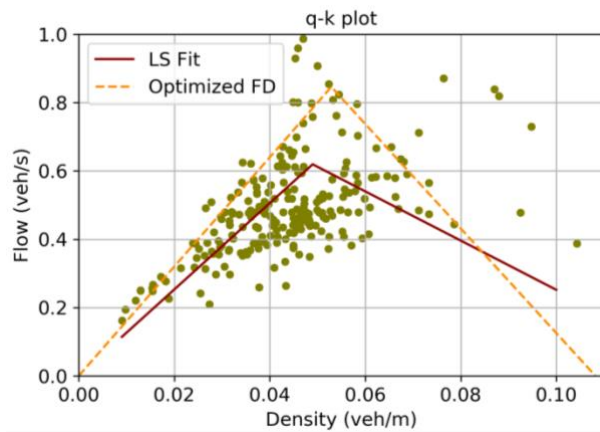
h.) all regions for 300 m section Lane 1
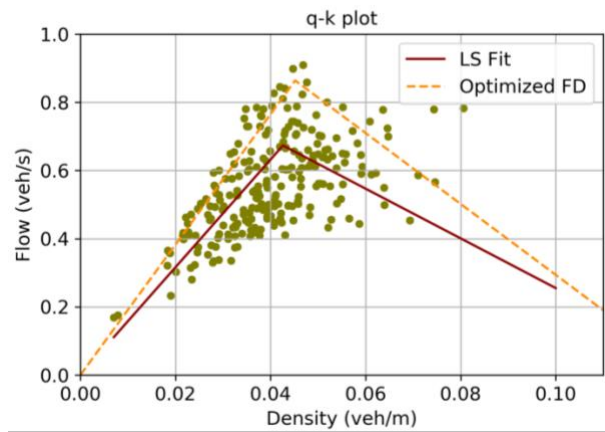
i.) all regions for 300 m section Lane 2
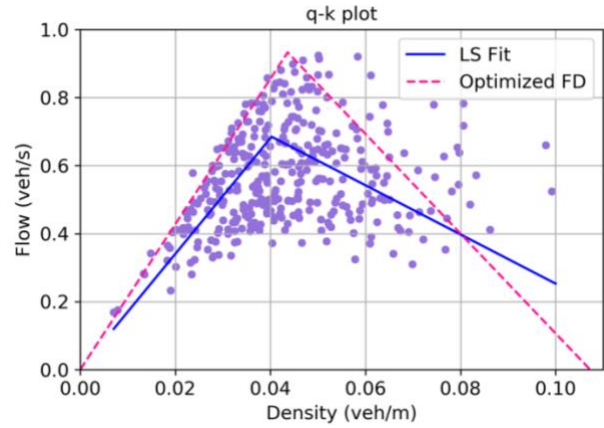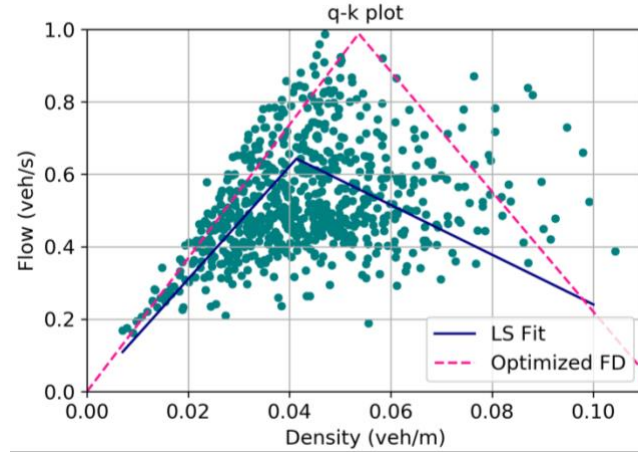
Figure 6.14 Automatic calibration of FD using 5% probe vehicles

Table 6.2 Optimized FD parameters calibrated from 5% probes with headway-spacing measurement

	optimized v_f	optimized k_c	optimized k_J
all data for 150 m	21.48	0.043	0.109
all data for 300 m	19.10	0.048	0.143
all data for lane1	16.49	0.047	0.116
all data for lane 2	21.37	0.044	0.107
all data	18.42	0.054	0.113
all data 150 m lane1	19.99	0.044	0.093
all data 150 m lane2	22.55	0.041	0.102
all data 300 m lane1	15.99	0.053	0.108
all data 300 m lane2	19.12	0.045	0.128
Standard deviation	**2.10**	**0.004**	**0.014**
Average	**19.39**	**0.046**	**0.113**
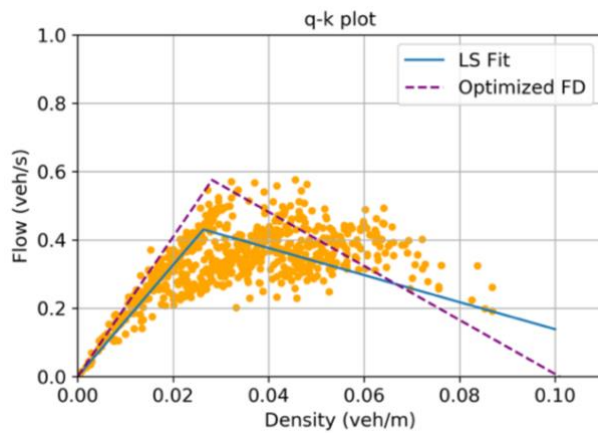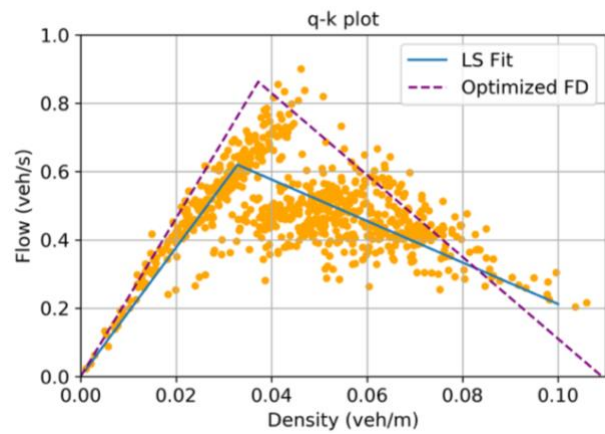
a.) For DS1, 150 m section Lane 1   b.) For DS1, 150 m section Lane 2
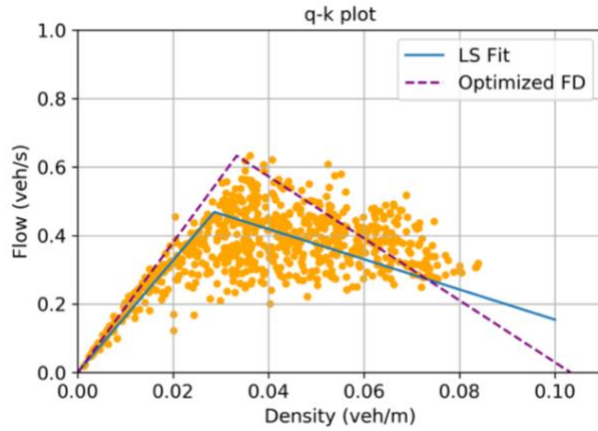
c.) For DS2, m section Lane 1
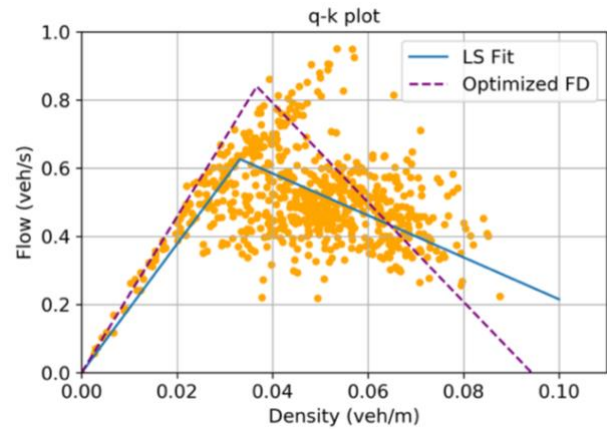
d.) For DS2, 150 m section Lane 2
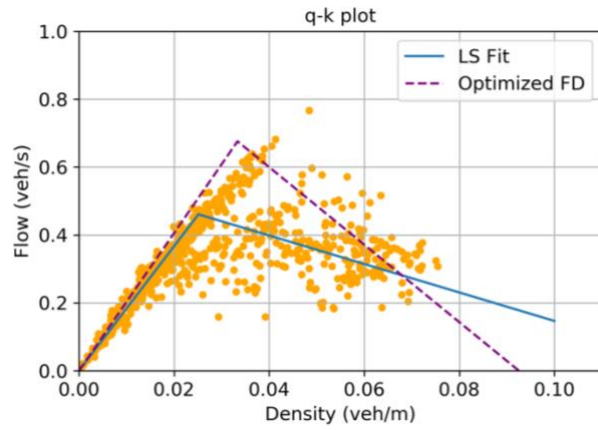
e.) For DS3, 150 m section Lane 1
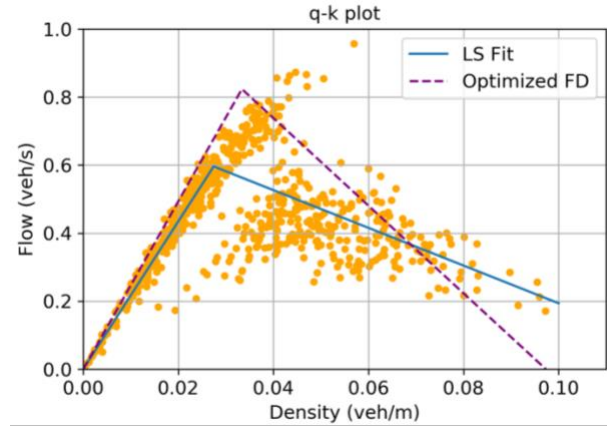
f.) For DS3, 150 m section Lane 2
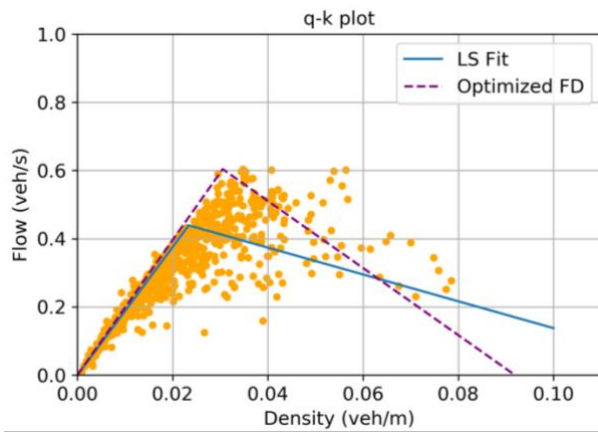
g.) For DS4, 150 m section Lane 1
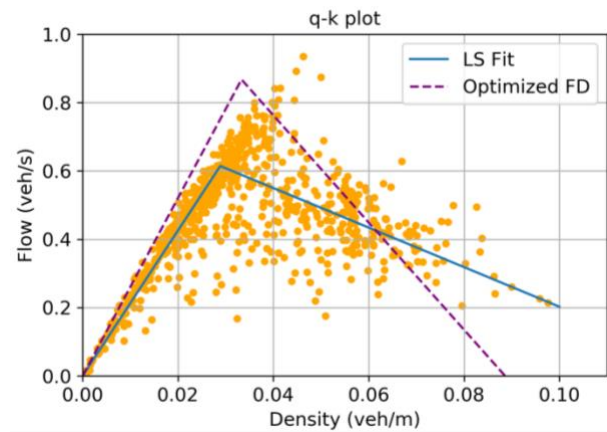
h.) For DS4, 150 m section Lane 2
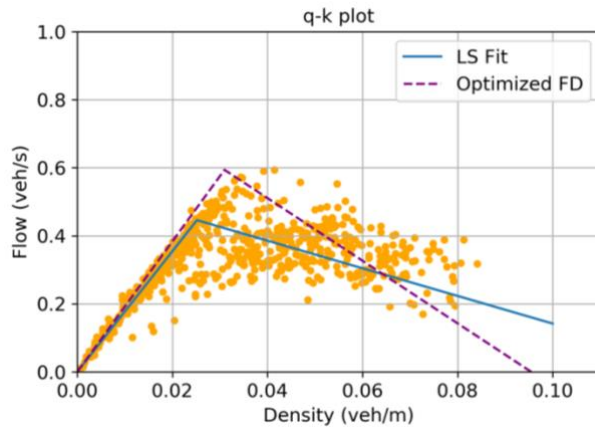
i.) For DS5, 150 m section Lane 1   j.) For DS5, m section Lane 2
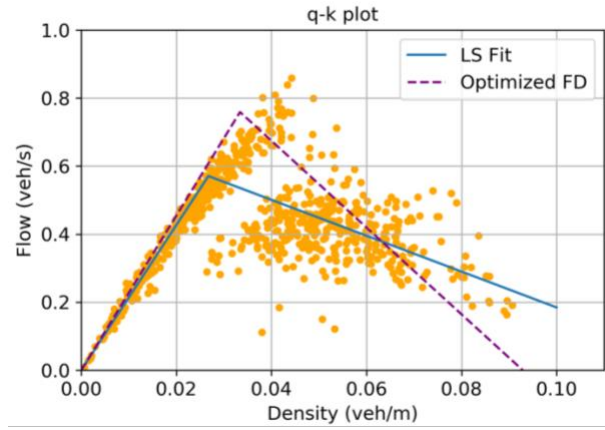
Figure 6.15 AC of FD from 100% ZTD using Edie's generalized definitions (4.2–4.05 k.p.)

Table 6.3 Optimized FD parameters calibrated from 100% ZTD using Edie's generalized definitions (4.2–4.05 k.p.)

		optimized v_f	optimized k_c	optimized k_J
DS 1	**150 m Lane 1**	20.44	0.028	0.101
	150 m Lane 2	23.18	0.037	0.109
DS 2	**150 m Lane 1**	18.99	0.033	0.103
	150 m Lane 2	22.90	0.037	0.094
DS 3	**150 m Lane 1**	20.27	0.033	0.093
	150 m Lane 2	24.67	0.033	0.097
DS 4	**150 m Lane 1**	19.79	0.031	0.092
	150 m Lane 2	26.02	0.033	0.089
DS 5	**150 m Lane 1**	19.17	0.031	0.096
	150 m Lane 2	22.72	0.033	0.093
Standard deviation		**2.30**	**0.003**	**0.006**
Average		**21.81**	**0.033**	**0.097**
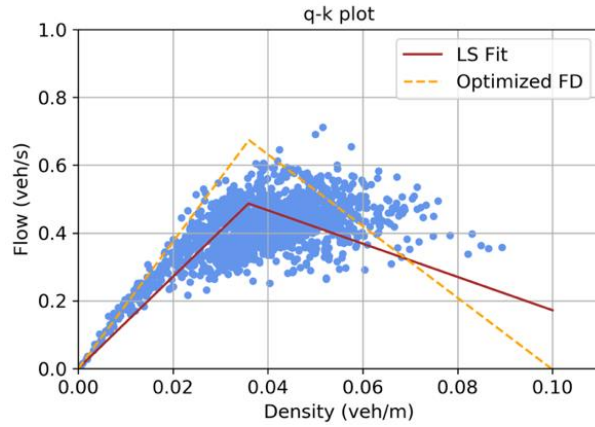
a.) For DS1, 300 m section Lane 1
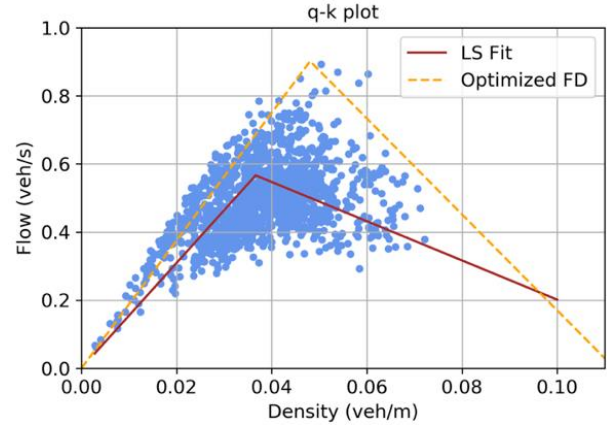
b.) For DS1, 300 m section Lane 2
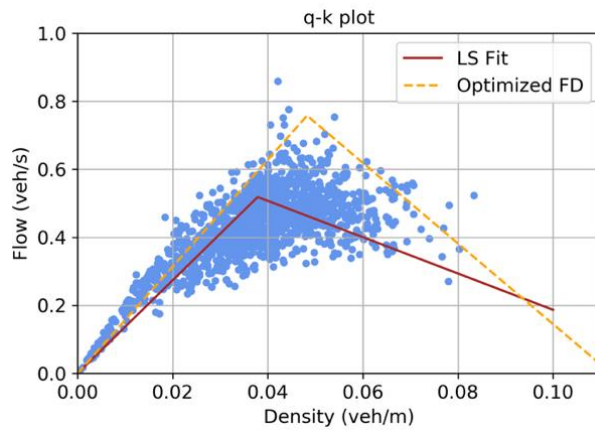
c.) For DS2, 300 m section Lane 1
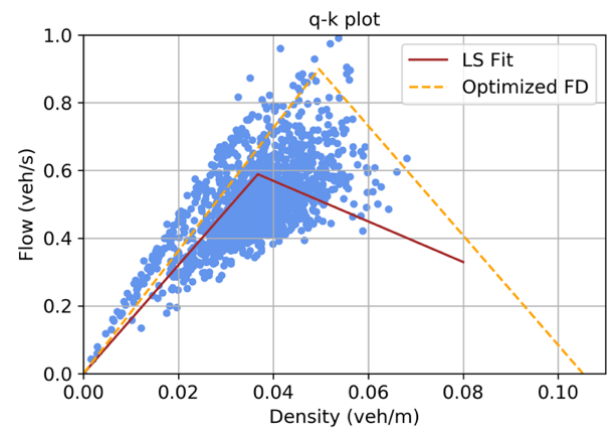
d.) For DS2, 300 m section Lane 2
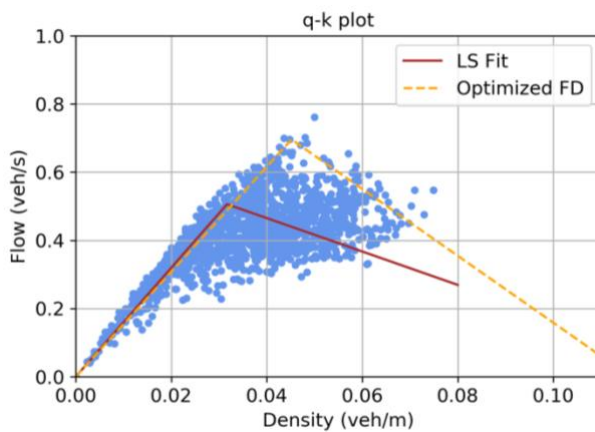
e.) For DS3, 300 m section Lane 1
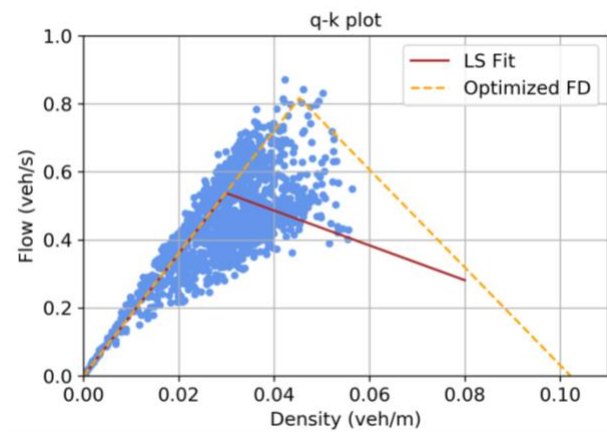
f.) For DS3, 300 m section Lane 2
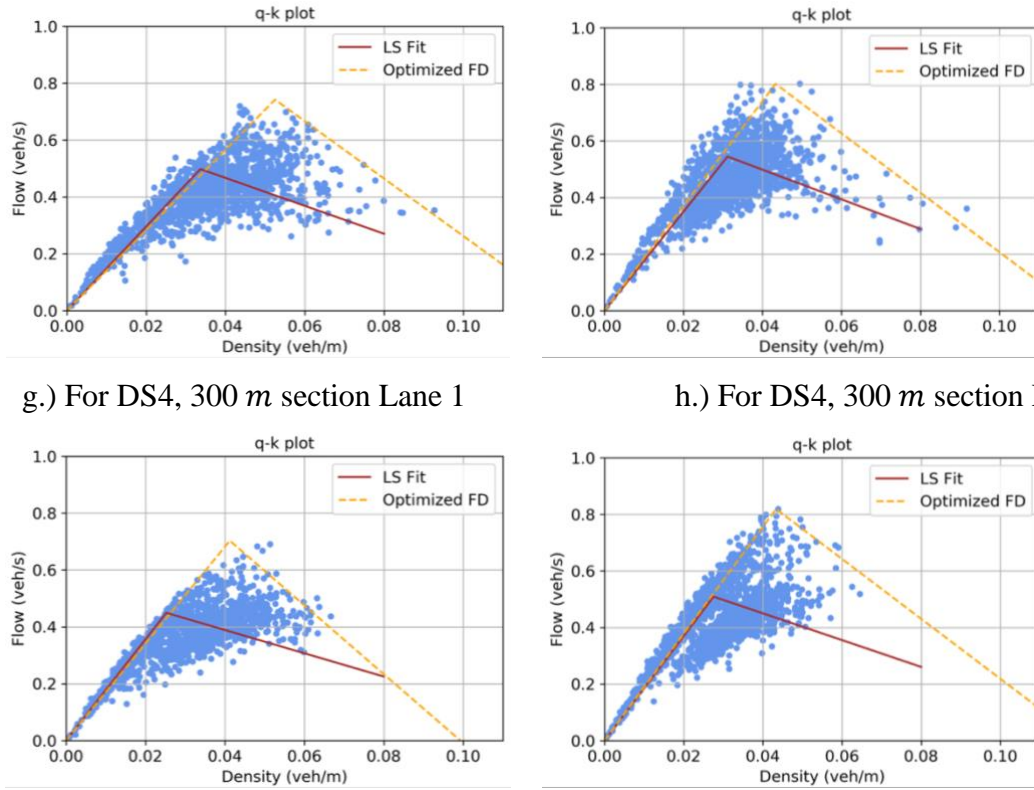
g.) For DS4, 300 m section Lane 1   h.) For DS4, 300 m section Lane 2

i.) For DS5, 300 m section Lane 1   j.) For DS5, 300 m section Lane 2

Figure 6.16 AC of FD from 100% ZTD using Edie's generalized definitions (3.8–3.5 $k.p.$)

Table 6.4 Optimized FD parameters calibrated from 100% ZTD using Edie's generalized definitions (3.8–3.5 $k.p.$)

		optimized v_f	optimized k_c	optimized k_J
DS 1	**300 m lane 1**	18.72	0.036	0.100
	300 m lane 2	18.76	0.048	0.112
DS 2	**300 m lane 1**	15.70	0.048	0.112
	300 m lane 2	18.13	0.050	0.105
DS 3	**300 m lane 1**	15.40	0.045	0.116
	300 m lane 2	18.03	0.045	0.102
DS 4	**300 m lane 1**	14.13	0.052	0.126
	300 m lane 2	18.51	0.043	0.120
DS 5	**300 m lane 1**	17.05	0.041	0.099
	300 m lane 2	18.90	0.043	0.121
Standard deviation		**1.60**	**0.004**	**0.009**
Average		**17.33**	**0.045**	**0.111**

6.5   TSE: combining CTM and Ensemble Kalman Filtering (EnKF) technique

For this study, Ensemble Kalman Filter (EnKF) is employed as a DA technique due to its capability of dealing nonlinear phenomena such as traffic flow for system model.

System model of EnKF (Ensemble Kalman Filter): It is also known as process equation, represents the dynamic of system such as nonlinear system equation such as traffic dynamics.

$$x_t = f(x_{t-1}) + \omega_{t-1}$$
(6.26)

Here, at timestep t, x_t is the state vector, f_t depicts the system model representing numeric scheme used for continuous PDE traffic flow model, and ω_t represents the noise associated with the traffic model. For this study, as described earlier the continuous PDE of the traffic flow model considered is the LWR model (Lighthill and Whitham, 1995; Richards, 1956) and the corresponding numeric scheme used is the Godunov discretization scheme (Godunov, 1959) of LWR, i.e., CTM (Daganzo, 1994). The parameters of CTM comes from the process of AC of FD (section 6.4). Additive noise model is used for both the evolution and observation equations. For this study, it is assumed to follow a normal distribution: $\mathcal{N}(0, 1.0^2)$.

Observation equation:

$$z_t = h_t(x_t) + \eta_t$$
(6.27)

At timestep t, z_t represents the vector of traffic state measurements (corresponding to traffic data). Traffic density measurements from $xFCD$-based method is estimated with 5% probe vehicles at $\{150\,m \text{ x } 5\,s\}$. For the unobserved cells, traffic density measurements from coarser resolutions are used to estimate density using EnKF. h_t depicts the nonlinear observation operator that related the system state with the measurements (observed), and it needs to be defined to link

the system state to the measurements. The system state at time t is defined by the vector $x_t = [k_t^0, \; ..., k_t^{imax}]$. The observation operator h is given by:

$$h_t(x_t) = H_t \begin{bmatrix} x_t \\ v(x_t) \end{bmatrix}$$

(6.28)

Here, Measurement errors are represented by the observation noise η_t, and the matrix H_t is constructed based on locations where the measurements are acquired. The observation noise term:

$$\eta_t = \begin{bmatrix} \eta_t^{density} \\ \eta_t^{velocity} \end{bmatrix}$$

(6.29)

is composed of two parts, $\eta^{density}$ and $\eta^{velocity}$. It explains that different error models are assumed for density and speed measurements and for this study the observation noises related to measured density k and velocity v are also assumed to follow a normal distribution: $\mathcal{N}(0, 1.0^2)$.

6.5.1   Utilization of ZTD for TSE and observed traffic states

In section 6.5, the implementation and validation of proposed model-based TSE method is done on the $300\, m$ (Lane 1) space-time domain of DS1. 5% probe vehicles from this target region are used to estimate the observed traffic state z_t from the $xFCD$-based TSE method (Seo *et al.*, 2015b) at a resolution $\{150\, m \text{ x } 5\, s\}$ as per the equations (6.30) – (6.31) where $A_{T,X}$ is the rectangular spatiotemporal area of a cell in a mesh of space-time domain and $a_n(A_{T,X})$ is the spatiotemporal area between a probe vehicle n and its leading vehicle as depicted in Figure 6.17.

$$\hat{k}(A) = \frac{\sum_{n \in P(A_{T,X})} t_n(A_{T,X})}{\sum_{n \in P(A_{T,X})} |a_n(A_{T,X})|}$$

(6.30)

$$\hat{v}(A) = \frac{\sum_{n \in P(A_{T,X})} d_n(A_{T,X})}{\sum_{n \in P(A_{T,X})} t_n(A_{T,X})}$$

(6.31)

$$A_{T,X} = \{(x,t) \mid X \le x \le X + \Delta x, \; T \le t \le T + \Delta t\} \tag{6.32}$$

$P(A)$ denotes the set of all probe vehicles in the cell A, $d_n(A)$ is the total distance traveled by vehicle n in cell A and $t_n(A)$ is the total distance traveled by vehicle n in cell A.
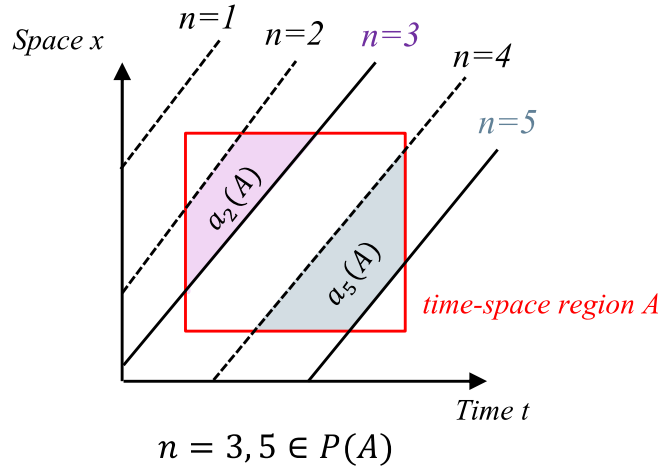
Figure 6.17 Spatiotemporal area between a probe vehicle and its leading vehicle

Equations (6.30) – (6.31) are the observed density and velocity, respectively from the probe vehicle data and $\Delta x = 150m$ and $\Delta t = 5s$ are predetermined space and time resolutions. For cells via which no probe vehicles passed the (q,k,v) points computed from coarser resolution ($\{150\ m$ x $60\ s\}$ and $\{150\ m$ x $300\ s\}$) are used for those unobserved cells as shown in Figure 6.18. The aggregated boundary traffic flows (q_u and q_d) and densities (k_u and k_d) are presumed to be measured by the detectors installed at the boundaries of the section. Therefore, 100% ZTD is used to calculate aggregated boundary traffic flows and densities at the boundaries of the target section: DS1, $300\ m$ (Lane 1).
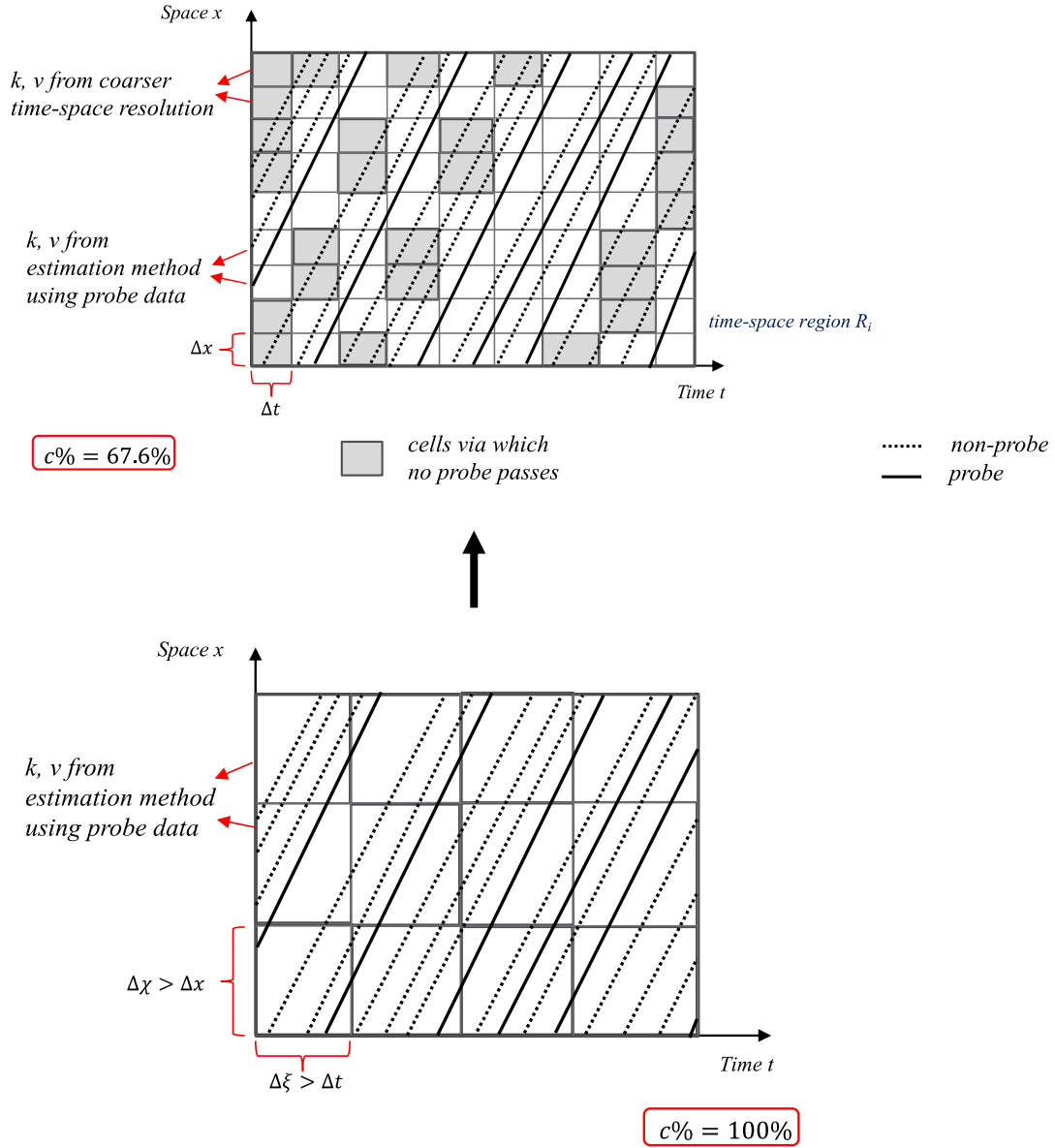
Figure 6.18 Utilizing information from coarser resolution

6.5.2   State estimation process and application conditions

As described in the Figure 6.19, the state estimation process using EnKF comprise of 6 stages namely, 'predicted state', 'predicted covariance', 'Kalman Gain' calculation, 'update state', 'update covariance' and 'state selection'. Firstly, certain number of ensembles are created. Here, M denotes the total number of ensembles considered and l denotes the ensemble index. Using the system model f the state is predicted at each ensemble l. Then the covariance matrix is predicted

using the predicted state and other defined parameters of the EnKF such as observation operator. This step is followed by the computation of Kalman Gain. After the measurements are received, the predicted state and the covariance are updated using the measurements at the current step and the computed Kalman Gain in the update state step and update covariance step, respectively. The subindex $t-1|t$ denote the prior of a variable (before the measurements are obtained), and the subindex $t|t$ denote the posterior of a variable (after the measurements are obtained). Finally, the state selection step is performed that delivers the predicted state at time step t.
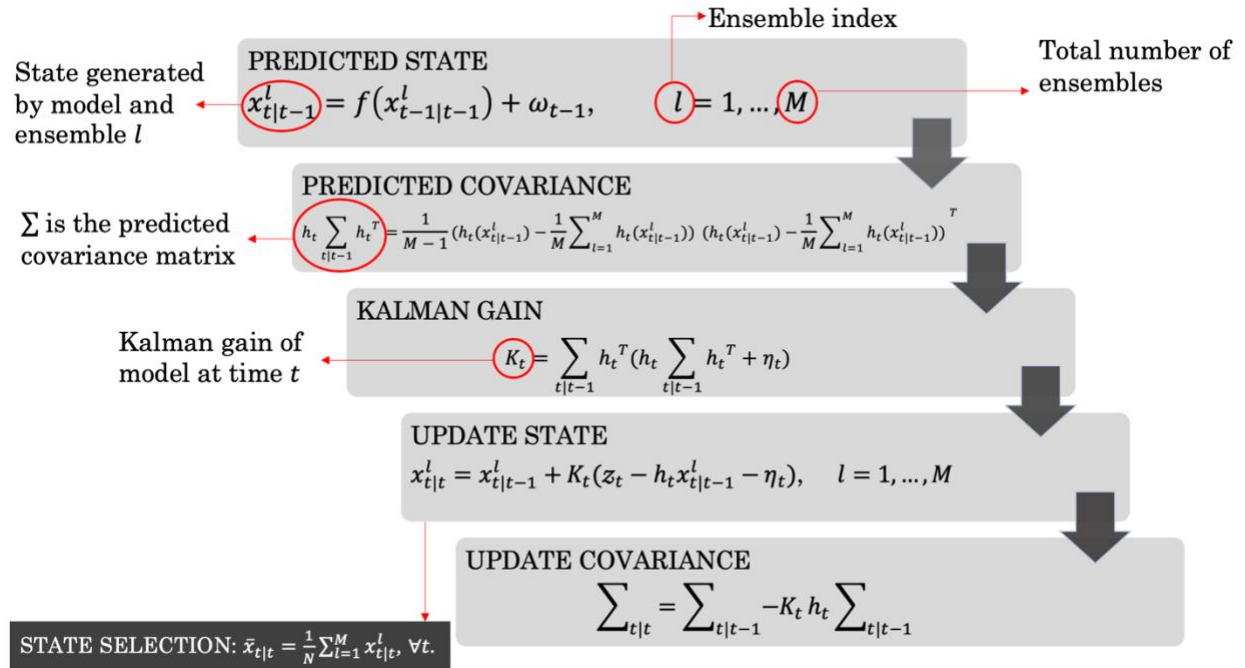
Figure 6.19 Flow of Ensemble Kalman Filtering (EnKF) technique

The application conditions include the choice of traffic flow model as the state model for EnKF, defining the parameters of the calibrated model and the choice of noise distributions. Now since, 1st order models are widely used in ATM systems due to their capability of capturing many important traffic phenomena in an efficient and stable manner, for this study, first order traffic model namely, LWR model (Lighthill and Whitham, 1995; Richards, 1956) has been considered for the state model. CTM is the Godunov discretization (Godunov, 1959) of the LWR model and thus employed to utilize in the EnKF mechanism and its parameters are automatically calibrated to improve the accuracy of the model in simulating the traffic density by adapting to the variability

of the data. As described in section 6.2, the first major part of this chapter involves the AC of FD using data from all 4 space-time domains of each of 5 datasets (DS1~DS5) and implementation and validation of proposed TSE method using data from $300\ m$ (Lane 1) space-time domain of DS1. So, the space-time region of lane 1 on $300\ m$ section of DS1 dataset, results in the number of cells as 2. This is so because as per the CFL conditions the resolution subject to TSE has been fixed as $\{150\ m$ x $5\ s\}$. Since the temporal domain of the subject area is $1\ hour$ hence, a $\Delta t = 5\ s$ results in 720–time steps. In order to analyze the maximum capability of this model-based method in estimating traffic state this study, as its first implementation, is conducted on such small length of section. Although this leads to a smaller number of cells to utilize or simulate the CTM, however, this should not affect the appropriateness of method formulation and accuracy in TSE in small sections rather it may provide a strong foundation for the appropriateness of this model to be applied in a wider section. The initial conditions in all cells are assumed to follow a normal distribution, where the mean is the average of the density measurements from the $xFCD$-based TSE method using 5% probe vehicles and the standard deviation is 5% of the mean. All the noise models are specified by a Gaussian distribution. The number of ensembles for the model is set as $M = 100$. The algorithm for $300\ m$ long section with temporal domain of $1\ hour$ runs in less than a minute, and thus it is suitable for real-time applications. The same application conditions are also tabulated in Table 6.5.

6.6 Estimation results

The objective of this study is to propose a model-based traffic state estimation method that can provide reliable and reasonably acceptable accurate traffic state estimates, 1.) using few probe vehicles i.e., small probe penetration rate ($= 5\%$), 2.) in complete space-time domain, 3.) for both regimes of free-flow and congested, and 4.) at high spatiotemporal resolution.

The settings and configurations of implementation of the proposed model-based method is in alignment to the fact that it is tried to retrieve the traffic state (density) using 5% probe data (small probe penetration rate) and at high spatiotemporal resolution of $\{150\ m$ x $5\ s\}$. Figure 6.22 illustrates that the traffic state, using the proposed method, has been estimated in the complete space-time domain of $300\ m$ section (Lane 1) and $1\ hour$. Unlike in the case of $xFCD$-based TSE method (Figure 6.21) where the traffic estimates are unavailable in the unobserved cells due to

small probe penetration rate and high spatiotemporal resolution, the proposed method estimates the traffic state in the complete space-time domain and at a fine resolution of $\{150\ m$ x $5\ s\}$. Figure 6.20 shows the actual density on the target section for the same space-time domain (obtained using 100% ZTD and Edie's generalized definitions) and it is visible that at multiple positions and situations, several regions have observed density more than the critical density. It implies that the regions subject to TSE in Figure 6.22 include both the regimes of free-flow and congested. The process of analyzing the estimation capability of proposed model-based TSE (utilizing EnKF) boils down to statistically analyzing the accuracy of estimates in each spatiotemporal cell of the mesh of target space-time domain. The following section 6.7 includes a visual and statistical analysis of the proposed method with respect to the ground truth. It also includes a comparison analysis of the estimation accuracy with the $xFCD$-based TSE method.

Table 6.5 Application conditions for TSE in DS1: 300 m (Lane 1) using EnKF

Section	3.8–3.5 $k.p.$ (DS1, Lane 1)
Section length (km)	0.300
Number of cells	2
$\Delta t\ (hour)$	$^{5}/_{3600} = 0.001389$
$\Delta t\ (km)$	0.150
$v_f\ (km/hr)$	66.312
$k_c\ (veh/km)$	540
$k_J\ (veh/km)$	1130
ω	$\mathcal{N}(0, 1.0^2)$
$\eta^{density}$	$\mathcal{N}(0, 1.0^2)$
$\eta^{velocity}$	$\mathcal{N}(0, 1.0^2)$

Density (veh/m) using Edie's generalized definitions in DS_1, 300m section, Lane 1 using 100% ZTD
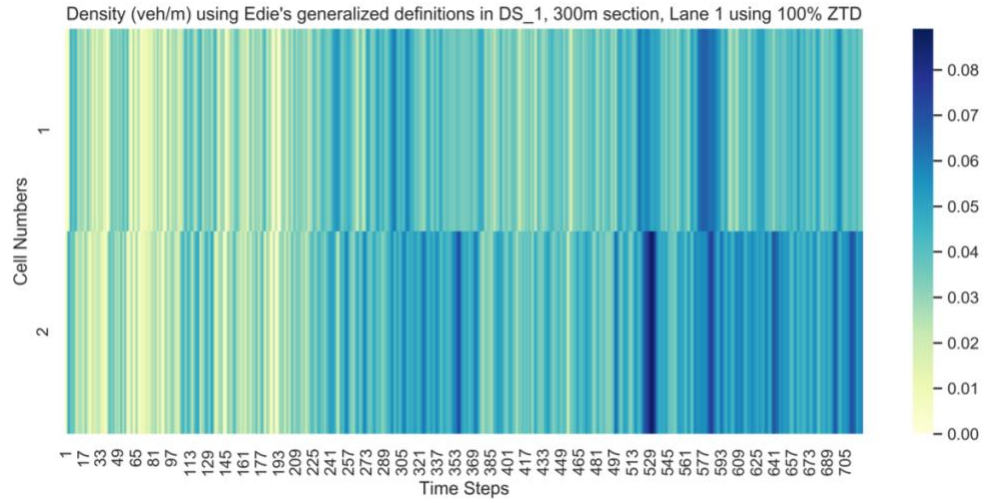
Figure 6.20 Density k (veh/m) obtained using 100% ZTD and Edie's generalized definitions

Density (veh/m) by xFCD in DS_1, 300m section, Lane 1 using 5% probes
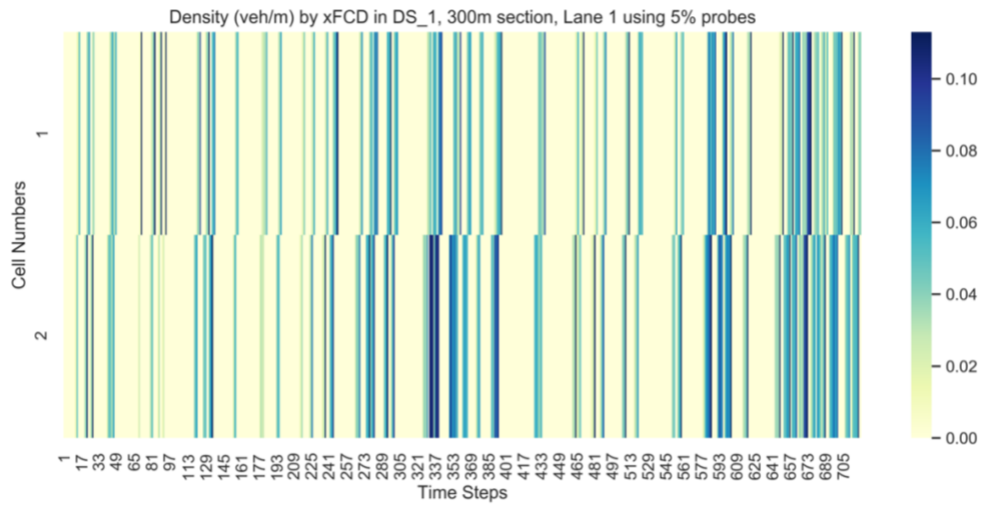
Figure 6.21 Density k (veh/m) obtained using 5% probe data and xFCD-based TSE method (Seo et al., 2015b)

Density (veh/m) using EnKF in DS_1, 300m section, Lane 1 using 5% probes
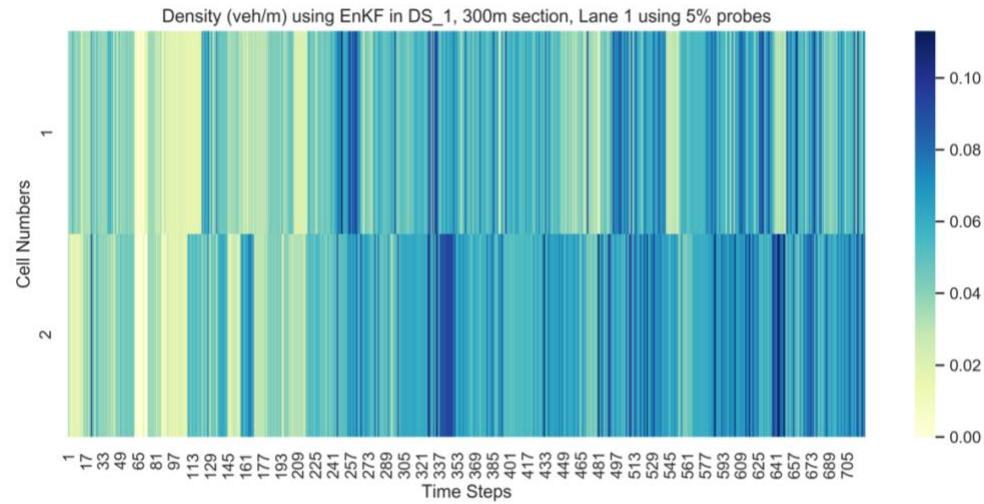
Figure 6.22 Density k (veh/m) obtained using 5% probe data and model-based TSE method (employing EnKF)

6.7   Evaluation of the proposed DA-based TSE method

The traffic state (density k) estimates from a.) $xFCD$-based TSE method and b.) model-driven TSE method employing EnKF, for all cells of the spatiotemporal mesh are compared against the density k obtained using 100% ZTD and Edie's generalized definitions. The flow of comparison is as shown in Figure 6.23.
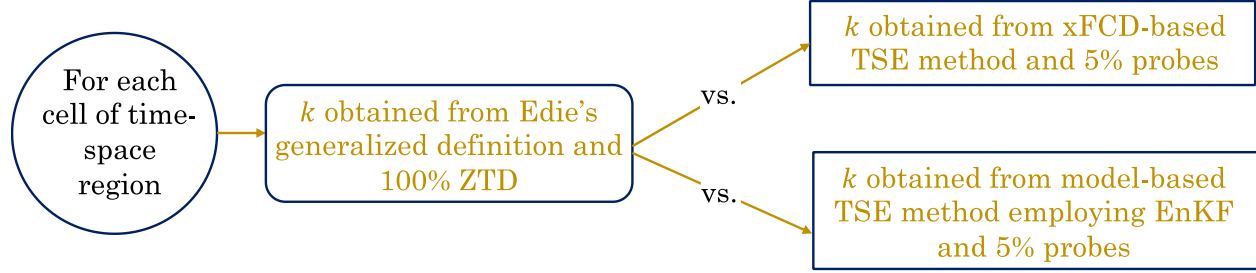
Figure 6.23 Flow of comparison analysis

6.7.1   Ground truth

The density k obtained for each spatiotemporal cell of the target section (DS1, 300 m (Lane 1)) using 100% ZTD and Edie's generalized definitions is considered as the source truth for analyzing the numerical characteristics of the proposed TSE method. Equation (6.33) gives the Edie's generalized definition (Edie, 1963) for obtaining density in a cell A.

$$k(\boldsymbol{A}) = \frac{t(\boldsymbol{A})}{|\boldsymbol{A}|} \tag{6.33}$$

6.7.2   Comparison among two TSE methods: error analysis

The visual analysis reveal that the traffic state values estimated using only 5% probe vehicles and the model-based method employing the DA technique (gray points) lies close to the traffic state values computed from 100% vehicles' data and Edie's generalized definitions (red points) as shown in Figure 6.24 and Figure 6.27 for cell 1 and cell 2 of the target section, respectively. Figure 6.25 and Figure 6.28 illustrates the density estimates obtained from $xFCD$-based TSE method

143

using 5% probe vehicle data in the same target section for cell 1 and cell 2, respectively. It is clearly visible that no visual correlation can be developed between these estimates and the ones obtained from 100% vehicles' data and Edie's generalized definitions (red points). The reason could be the presence of multiple unobserved areas. Hence, for a clearer understanding and inferences, it is vital to perform statistical comparison analysis by calculating metric scores such as root mean square error (RMSE), mean absolute error (MAE) and Bias. The statistical error analysis reveals that the metric scores of RMSE, ARE and Bias are smaller when density computed using 100% vehicles and Edie's definitions is compared with ones estimated from model-based method than the ones estimated using $xFCD$-based method. The same can be visualized in Figure 6.26 and Figure 6.29 for cell 1 and cell 2, respectively. Figure 6.26 a.) and Figure 6.29 a.) correspond to the metric scores when only the observed cells (with respect to $xFCD$-based TSE method) are considered, and the rest are excluded for a fairer comparison.
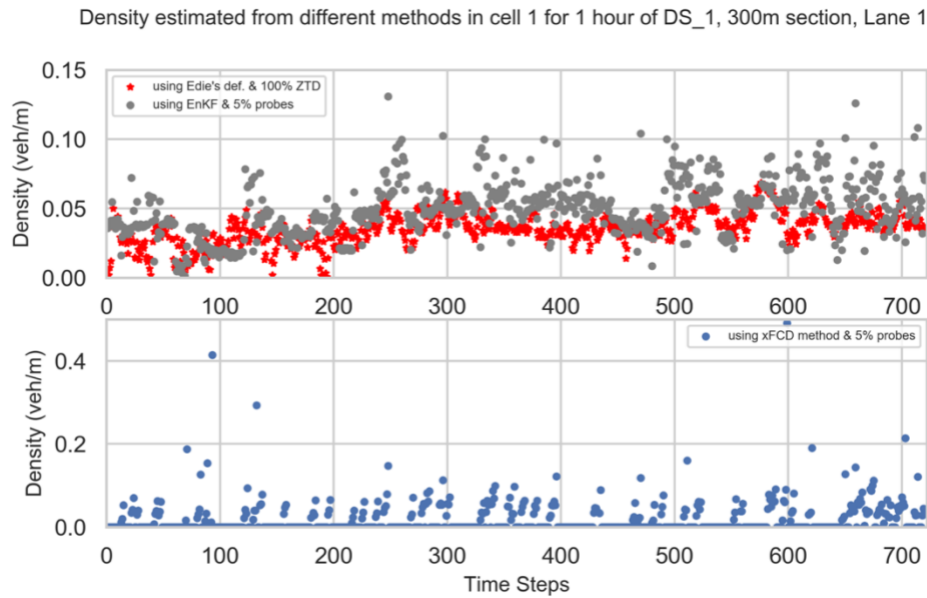
Figure 6.24 Density k (veh/m) estimated from different methods in cell 1 of DS1: 300 m (Lane 1)
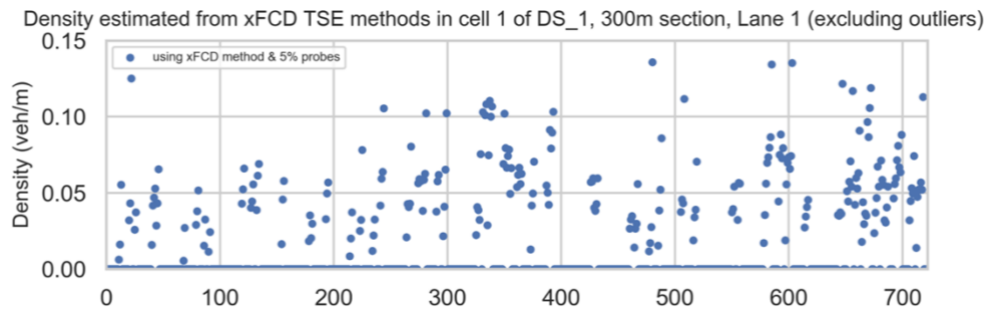
Figure 6.25 Density k (veh/m) estimated from xFCD-based TSE method in cell 1 of DS1: 300 m (Lane 1) (excluding outliers)

a.) only for observed cell   b.) including all cells

($k = 0$ for unobserved cells in case of $xFCD$-based method)
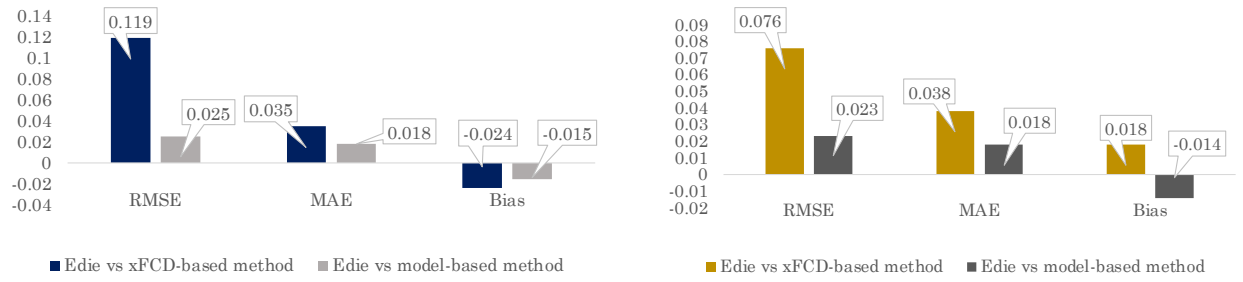
Figure 6.26 Statistical comparison analysis of cell 1 of DS1: 300 m (Lane 1)

Density estimated from different methods in cell 2 for 1 hour of DS_1, 300m section, Lane 1
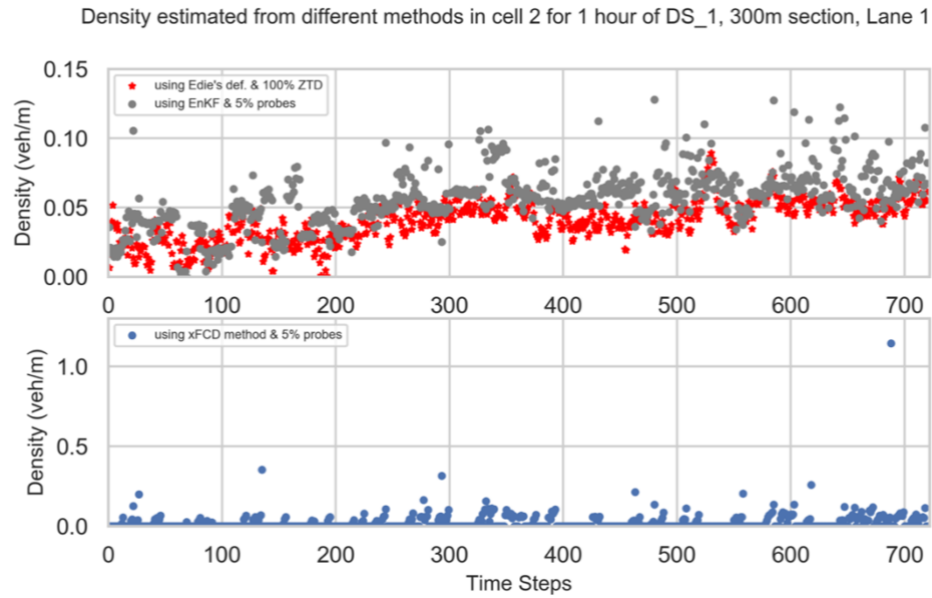
Figure 6.27 Density k (veh/m) estimated from different methods in cell 2 of DS1: 300 m (Lane 1)

Density estimated from xFCD TSE methods in cell 2 of DS_1, 300m section, Lane 1 (excluding outliers)
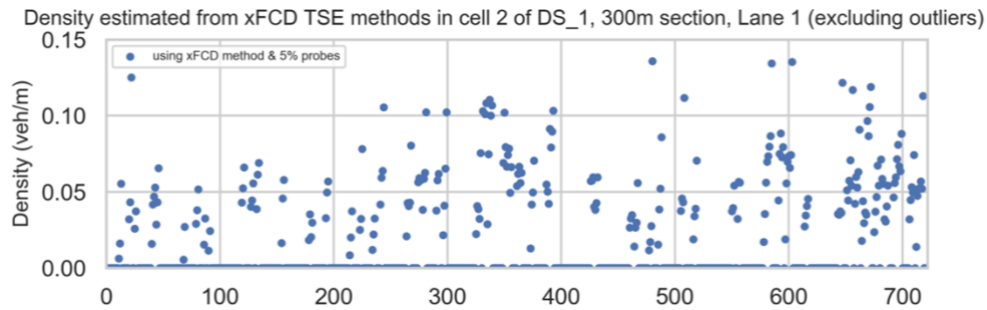
Figure 6.28 Density k (veh/m) estimated from xFCD-based TSE method in cell 2 of DS1: 300 m (Lane 1) (excluding outliers)
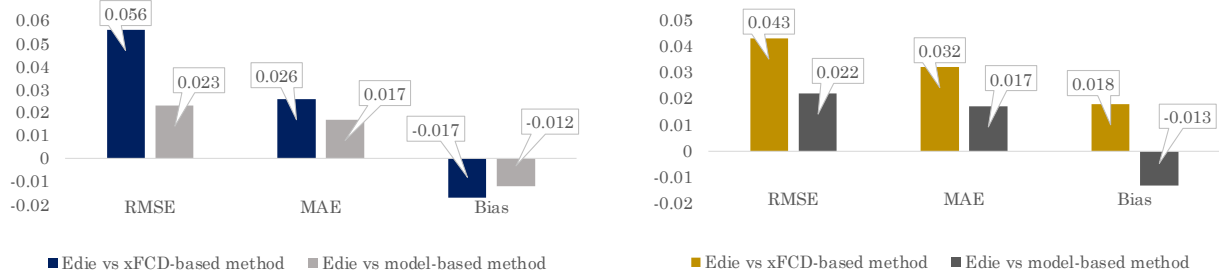
a.) only for observed cell

b.) including all cells

($k = 0$ for unobserved cells in case of $xFCD$-based method)

Figure 6.29 Statistical comparison analysis of cell 2 of DS1: 300 m (Lane 1)

6.7.3   Conclusions and recommendations

From the visual and statistical analysis, it can be concluded that the proposed model-based traffic state estimation method can provide reliable and reasonably acceptable accurate traffic state estimates, 1.) using few probe vehicles i.e., small probe penetration rate ($= 5\%$), 2.) in complete space-time domain, 3.) for both regimes of free-flow and congested, and 4.) at high spatiotemporal resolution ($\{150\ m$ x $5\ s\}$). Utilization of DA techniques proved to be useful in providing more accurate estimates under the discussed requirements. The TSE method analyzed in chapter 5 provided a useful foundation for extending the estimation approach by incorporating a model-based approach along with a data assimilation (DA) framework. This study contributed to the development and implementation of an improved (in terms of estimation accuracy) physical model-based method for traffic state estimation and to facilitate an adaptation of the model by utilizing advance probe data to the conditions of highways and roadway links. The '*weaker*' assumption-based approach is successfully extended to estimate the traffic state more accurately by utilizing a data assimilation (DA) framework. In addition, the parameters of physical model are obtained by automatic calibration (AC) of a triangular FD which made the estimation more robust by adapting to the variability of data. The results from the calibration and estimation show that the accuracy of estimating the traffic state using this approach increases and the estimated k corresponds well with the k computed using Edie's generalized definitions (Edie, 1963) and 100% trajectory data (ground truth).

Even though the traffic state estimation is desirable in wider section, the implementation in a 300 m wide section (resulting in only 2 cells for simulating density using CTM) provides a base for applicability of this model-based method in much wider sections based on its capability to estimate in smaller sections. The further section 6.8 includes the application of this model-based method in TSE on wider roadway section where the CTM model involves larger number of cells.

6.8 Application of DA-based TSE method on a wider section

This section includes the implementation of the proposed model-based TSE method, which employs a DA framework to provide accurate traffic state estimates, in a wider section of 2 km. The motivation comes from the successful implementation and retrieval of reliable traffic state estimates from the proposed methodology for a smaller section i.e., a single lane (Lane 1) of 300 m long section of Hanshin Expressway Ikeda Route 11 (around Tsukamoto Junction). The ZTD corresponding this section is part of a larger dataset namely, L001_F001. L001_F001 includes the complete and continuous vehicle trajectory information of 3,475 vehicles on Hanshin Expressway Ikeda Route 11 (around Tsukamoto Junction). The objective is to explore the estimation capability of the proposed method now on this wider section. L001_F001 includes the ZTD of a wider section that spans for 2 km and a time duration of 1 $hour$ (07:00 – 08:00 a.m.). In such a case, the number of cells will be much larger than 2 while utilizing CTM for simulating density, either for the purpose of automatic calibration of FD or utilizing it for estimating density using a DA framework.

6.8.1 Utilization of ZTD and application conditions

The methodology of implementing the proposed method to obtain traffic state estimates on a wider section are very similar to its application on the 300 m short length section except for a few changes. As discussed earlier, the model-based TSE approach consists of two major steps: a.) automatic calibration of a triangular FD, which is used to define the parameters of a physics-based model (CTM) and b.) TSE employing the calibrated CTM and EnKF technique. The objective is to implement and validate the method on the complete space-time domain of 2 km distance and 1 $hour$ and in that case, the AC of FD is also performed using the data from the same space-time

domain i.e., L001_F001. As per the Courant–Friedrichs–Lewy (CFL) condition, the spatiotemporal resolution for AC of FD and TSE using DA is set the same as: $\Delta t = 150m$, $\Delta t = 5\ s$. Then, the complete space-time region is divided into mesh of spatiotemporal resolutions $\{150\ m \times 5\ s\}$ i.e., multiple discrete, identical, and rectangular space-time regions. 5% of vehicles are randomly sampled from 100% ZTD corresponding to L001_F001 and are referred to as *probe vehicles* and ZTD corresponding to partial traffic data referred to as *probe vehicle data*. To treat the 5% randomly sampled vehicles from 100% vehicles (whose information is included in ZTD), it is essential to extract data from ZTD that has similar nature to the data collected by extended floating cars i.e., headway measurements, spacing measurements, velocity, positioning etc. Therefore, this time no special considerations have been given to the vehicles showing the lane changing behavior. The task of identifying the leading vehicle to any probe vehicle can be done at every available instance of time. It means that since the temporal sampling rate of ZTD is $0.1\ s$, so to identify the leading vehicle to any probe vehicle the trajectories can be analyzed at every $0.1\ s$. However, spacing and headway measurements (required for AC of FD) at such precise time steps are not essential so the identification of the leading vehicle is done at an interval of $1\ s$. The FDs are considered to be uniform over all cells and the aggregated boundary traffic flows and traffic densities are presumed to be measured by detectors and therefore such aggregated flows and densities are computed using 100% ZTD at a fixed length interval of $300\ m$. In addition, the assumption on on-ramp and off-ramp stays put. The average headway and spacing measurements of probe vehicles in a cell to their leading vehicles, both in a particular cell, are used to compute the flow–density (q, k) points in each cell of a spatiotemporal mesh.

The calibration is done at a space-time resolution of $\{150\ m \times 5\ s\}$. In other words, the headway and spacing measurements from the probe vehicles are aggregated at a resolution of $\{150\ m \times 5\ s\}$. For unobserved cells i.e., cells via which no probe vehicle traversed (thus, the headway and spacing measurements cannot be extracted) the headway and spacing measurements are interpolated from the coarser resolutions such as $\{150\ m \times 60\ s\}$ and $\{150\ m \times 150\ s\}$.

In the next subtask of formulating and implementing the TSE method using DA framework, first, the density k and velocity v are computed using the $xFCD$-based TSE approach from 5% probe vehicles' data at a space-time resolution of $\{150\ m \times 5\ s\}$ and are considered as *observations* for the observation equation of the EnKF. In the second step, density k is updated from the observed density k and velocity v, calibrated FD parameters (required to simulate density using

CTM) and estimated density k in the previous step using DA framework (EnKF). The third step involves the validation and comparison analysis of the proposed TSE method. In it, traffic state estimates (density k) from both, the proposed model-based method, and the $xFCD$-based method, are compared with the traffic states computed using Edie's generalized definition and corresponding 100% ZTD (L001_F001, which is considered as the source truth for this analysis). For each cell of the mesh of space-time domain, the observed traffic state z_t is obtained from the $xFCD$-based TSE method using probe vehicle data at a resolution {$150\ m$ x $5\ s$}. For cells via which no probe vehicles passed the (q, k, v) points computed from coarser resolution ({$150\ m$ x $60\ s$} and {$150\ m$ x $300\ s$}) are used for those unobserved cells.

The number of cells to be 14 for simulating density using CTM. This is so because as per the CFL conditions the resolution subject to TSE has been fixed as {$150\ m$ x $5\ s$}. Since the temporal domain of the subject area is 1 $hour$ hence, a $\Delta t = 5\ s$ results in 720–time steps. The initial conditions in all cells are assumed to follow a normal distribution, where the mean is the average of the density measurements from the $xFCD$-based TSE method using 5% probe vehicles and the standard deviation is 5% of the mean. All of the noise models are specified by a Gaussian distribution. The number of ensembles for the model is set as $M = 100$. The same application conditions are also tabulated in Table 6.6.

Table 6.6 Application conditions for TSE in L001_F001 using EnKF

Section	L001_F001
Section length (km)	2
Number of cells	14
Δt ($hour$)	$5/3600 = 0.001389$
Δx (km)	0.150
v_f (km/hr)	70.128
k_c (veh/km)	700
k_J (veh/km)	2100
ω	$\mathcal{N}(0, 1.0^2)$
$\eta^{density}$	$\mathcal{N}(0, 1.0^2)$
$\eta^{velocity}$	$\mathcal{N}(0, 1.0^2)$

6.8.2   Estimation results

The (q, k) points calculated using headway-spacing measurements of 5% probes in all the space-time regions using all datasets are plotted as shown in Figure 6.30. These points are used to calibrate an initial FD by conventional LS calibration method. These parameters are then used as initial condition for the optimization problem of automatic calibration of triangular FD. The values of optimized FD parameters for various combination of datasets are:

$$v_f = 19.48 \, m/s$$
$$k_c = 0.07 \, veh/m$$
$$k_J = 0.21 \, veh/m$$

In Figure 6.30, the blue curve is the FD obtained from the LS regression fitting. In fact, parameters of this LS fit FD are used as initial conditions for the optimization problem of AC of FD. The pink curve depicts the automatically calibrated FD. As discussed in the case of short length section, the conventional LS method underestimates the flow, and the automatic calibrated FD outperforms because it searches for the 'best capacity' (as well as other parameters simultaneously). Figure 6.32 illustrates that the traffic state, using the proposed method, has been estimated in the complete space-time domain of $2 \, km$ and $1 \, hour$. Figure 6.31 shows the actual density on the target section for the same space-time domain (obtained using 100% ZTD and Edie's generalized definitions) and it is easy to make a visual correlation between the two figures.
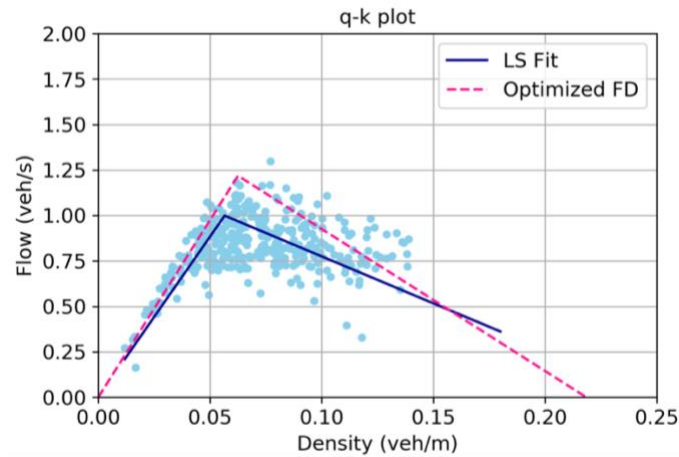
Figure 6.30 AC of FD using 5% probe data from wider section (L001_F001)
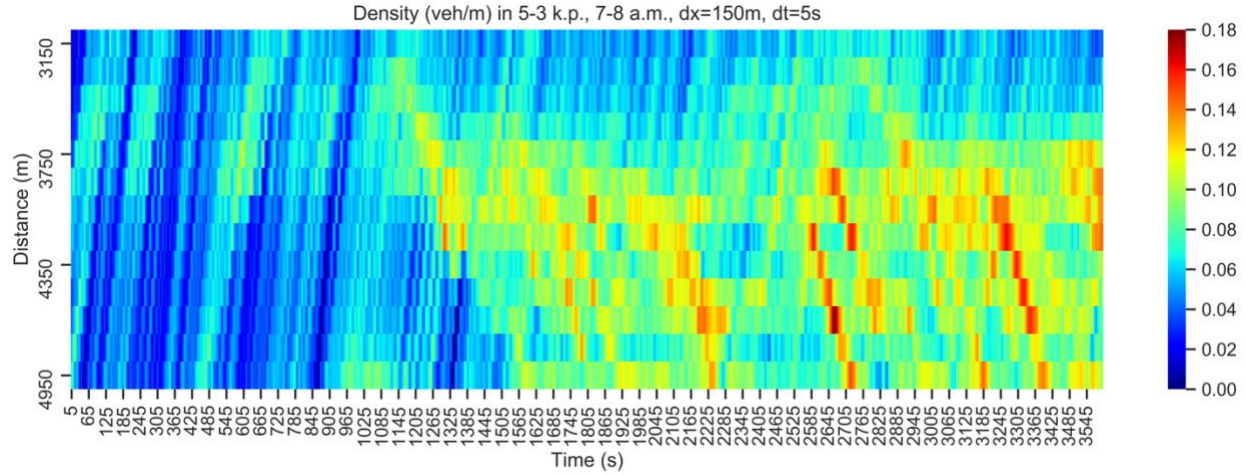
Figure 6.31 Density k (veh/m) from 100% ZTD and Edie's generalized definitions on wider section
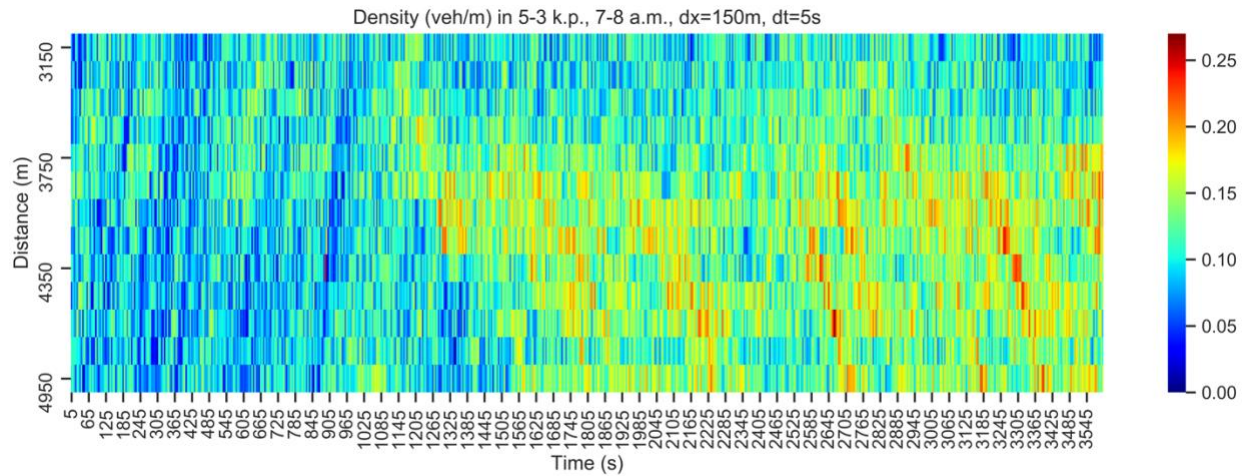
Figure 6.32 Density k (veh/m) using 5% probe vehicles and model-based TSE method (using EnKF) on wider section

6.8.3   Error analysis

Unlike in the case of $xFCD$-based TSE method (Figure 6.33 c.)) where the traffic estimates are unavailable in the unobserved cells due to small probe penetration rate and high spatiotemporal resolution, the proposed method estimates the traffic state in the complete space-time domain and at a fine resolution of $\{150\ m$ x $5\ s\}$ as shown in Figure 6.33 b.). Figure 6.33 a.) shows the actual density on the target section for the same space-time domain (obtained using 100% ZTD and

151

Edie's generalized definitions) and it is visible that at multiple positions and situations, several regions have observed density more than the critical density. The visual analysis reveal that the traffic state values estimated using only 5 % probe vehicles and the model-based method employing the DA technique (Figure 6.33 b.)) are highly correlated to the traffic state values computed from 100% vehicles' data and Edie's generalized definitions (Figure 6.33 a.)).

The traffic state (density k) estimates from a.) $xFCD$-based TSE method and b.) model-driven TSE method employing EnKF, for all cells of the spatiotemporal mesh are compared against the density k obtained using 100% ZTD and Edie's generalized definitions. The density k obtained for each spatiotemporal cell of the target section using 100 % ZTD and Edie's generalized definitions is considered as the source truth for analyzing the numerical characteristics of the proposed TSE method. The statistical comparison analysis is done by calculating metric scores such as root mean square error (RMSE), mean absolute error (MAE) and Bias. The analysis reveals that the metric scores of RMSE, ARE and Bias are smaller when density computed using 100% vehicles and Edie's definitions is compared with ones estimated from model-based method than the ones estimated using $xFCD$-based method. Figure 6.34 a.) correspond to the metric scores when only the observed cells (with respect to $xFCD$-based TSE method) are considered, and the rest are excluded for a fairer comparison. Figure 6.34 b.) correspond to the metric scores when comparing all the cells of the target spatiotemporal mesh.

a.)

b.)

c.)
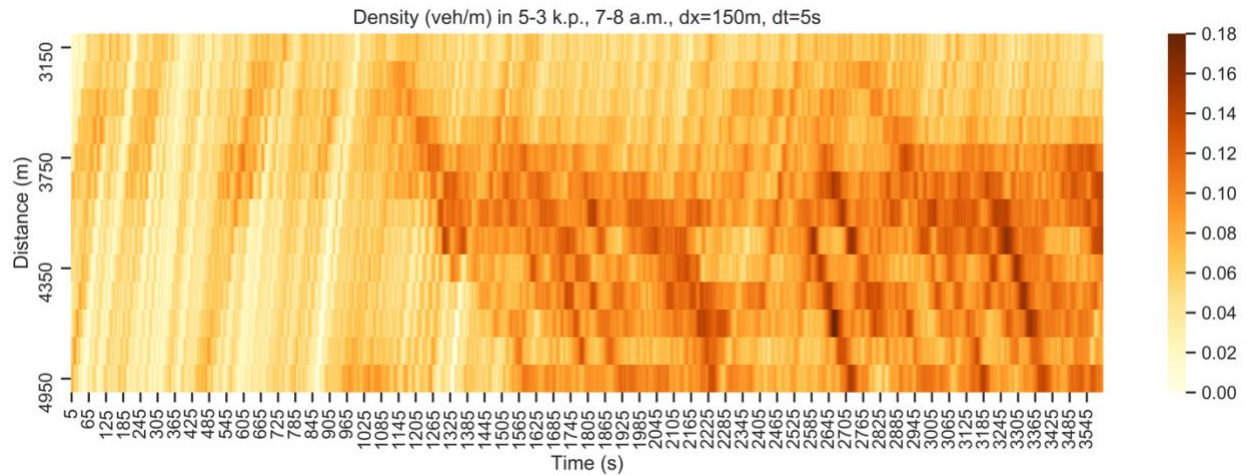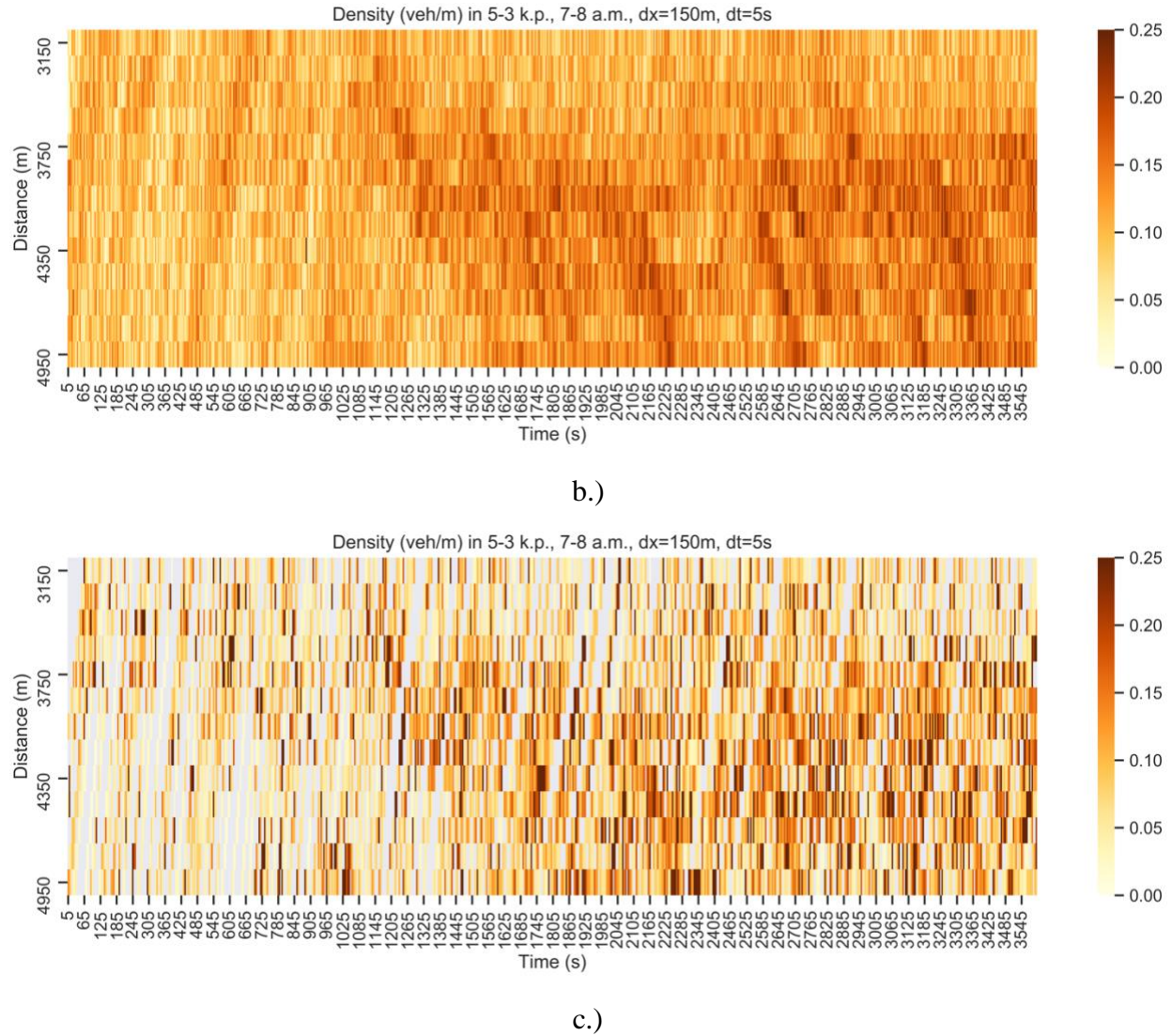
Figure 6.33 Density k (veh/m) from a.) 100% ZTD & Edie's definitions, b.) 5% probes and model-based TSE method (EnKF), and c.) 5% probes and xFCD-based TSE method

a.) only for observed cell   b.) including all cells

($k = 0$ for unobserved cells in case of $xFCD$-based method)
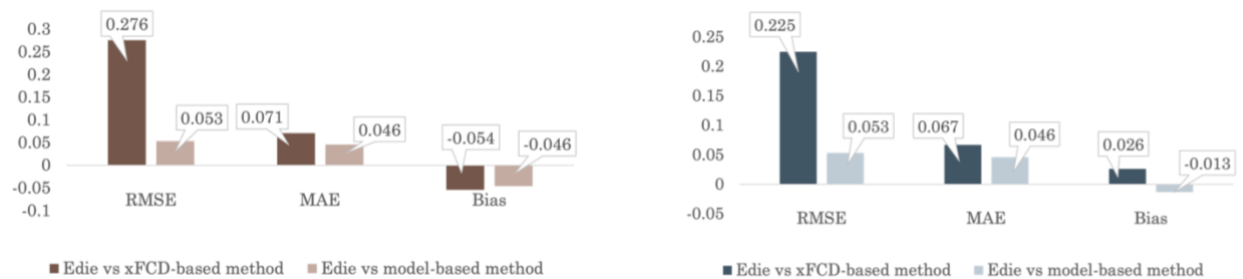
Figure 6.34 Statistical comparison analysis in wider section

6.9   Conclusions and discussions

Conclusions: The results from the implementation and verification of the improved estimation capability of proposed model-based TSE on a wider section reveal that it is possible to implement the proposed methodology in a wider section for estimating more accurate traffic state estimates as compared to the $xFCD$-based TSE method. Moreover, using this methodology it is possible to estimate traffic state in complete space-time domain at high spatiotemporal resolutions and by utilizing the data from few probe vehicles and roadside detectors. The results from the calibration and estimation show that the accuracy of estimating the traffic state using this approach increases and the estimated k corresponds well with the k computed using Edie's generalized definitions and 100% trajectory data (ground truth). The error metric scores of RMSE, MAE and MB have reduced significantly when estimating density using model-based approach. On the wider section, RMSE dropped by around 75–80%, the MAE dropped by around 30–35%, and there is a decrease in MB by 15–50%. However, when the method was implemented on a smaller section where special consideration was given to the lane changing behavior, RMSE dropped by around 50–80%, the MAE dropped by around 35–52%, and there is a decrease in MB by 30–40%.

Discussions: There are several factors that are believed to support the outperformance of the proposed method than the *'weaker'* assumption-based TSE method which are as follows:

1)   Data assimilation technique is utilized to find the most probable state of the traffic where neither the physics-based model nor the observation from probe data is considered perfect.

2)   The method is based on model-based approach and assumes a priori knowledge on traffic dynamics through physics-based model (CTM) and triangular FD.

3)   This CTM is defined through automatically calibrating the FD which takes the variability of data into consideration and renders the TSE method to be robust and adaptive.

4)   Regarding EnKF specification, the observation equation embodies additional information from probes i.e., observed velocity along with the observed density.

   In fact, the AC of FD and the utilization of additional observed information i.e., observed velocity from the probe vehicles can be considered as the *two major key factors* for the outperformance of the proposed method. Due to the above reasons, at similar traffic conditions

and available traffic data, the proposed method is anticipated to perform better than the *'weaker'* assumption-based method irrespective of cell size (provided that the CFL condition is satisfied) or probe penetration rate. However, it can factually be stated upon detailed analysis with respect to variation in resolution and probe penetration rate (which is out of scope of this research).

At the same time, it is indisputable that the performance of the proposed method depends on the quality and quantity of traffic data available. Data from probe vehicles should include spacing and headway measurements and the total boundary flows and densities at the boundaries of the target section or total flows and densities at fixed (couple of hundreds) interval of distance such as $300\ m$ can be collected by fixed sensors. It is indeed true that the model-based TSE method (employing DA framework) depends not just on the data from the probe vehicles but also the boundary flows and densities from the detectors whereas the $xFCD$-based TSE method requires only the spacing and headway measurements. In fact, the detector data is very easy to obtain at present situation due to advancements in ITS infrastructures. However, it is worth exploring the TSE approach by relaxing certain assumptions such as boundary flows and densities from detectors. Moreover, exploring smart solutions to obtain boundary conditions from probe vehicles itself are worth the challenge.

The TSE demonstrated in chapter 6 is under traffic flow conditions with is relatively higher than very low traffic flow situations such as after midnight. The proposed method utilizes spacing and headway measurements of probe vehicles to its leading vehicle. Although there are no restricts or assumptions considered for the minimum or maximum observable spacing and headway distances, it will not be possible to utilize the probe vehicle to their full potential for obtaining the observations if the distance between the probe vehicles and their leading vehicles is too high such that the leading vehicle is not identifiable by the probe vehicle. This kind of situation is highly likely to happen during very low traffic flow and low traffic density situations. Therefore, the proposed TSE method will not be able to estimate the traffic state under low flow, low density situation.

6.10   Gist: input, assumptions, output

This chapter contributed to the development and implementation of a physical model-based method for TSE and to facilitate an adaptation of the model by utilizing advance probe data to the

conditions of highways and roadway links. To improve the estimation capability, it extended the '*weaker*' assumption-based approach to estimate the traffic state more accurately by utilizing a data assimilation (DA) framework using probe vehicle data. The study endeavors to propose a model-based traffic state estimation method that can provide reliable and reasonably acceptable accurate traffic state estimates, 1.) using few probe vehicles i.e., small probe penetration rate ($=$ 5%), 2.) in complete space-time domain, 3.) for both regimes of free-flow and congested, and 4.) at high spatiotemporal resolution.

The formulation involves additional *assumptions* such as consideration of a triangular form on FD of traffic flow and a discretization of a physics-based model namely, Lighthill–Whitham–Richards Model (LWR Model) (Lighthill and Whitham, 1995; Richards, 1956), which are often accepted by traditional traffic flow theory. In it, the state variable, density (k), is estimated (*output*) by simulating the k obtained from a physical model (Cell Transmission Model: CTM) (Daganzo, 1994) which are then integrated (fused) with the observed traffic states (k and v) (*input*) using Ensemble Kalman Filtering (EnKF) technique (Evensen, 1994). In addition, the parameters of physical model are obtained by automatic calibration (AC) of a triangular FD.

The ***major difference*** between the $xFCD$-based TSE method explored in chapter 5 and the method proposed in chapter 6 is the estimation approach of the TSE. $xFCD$-based method is a streaming-data-driven TSE method which only relies on '*weaker*' assumptions. The proposed method utilizes a model-driven TSE approach and involves assumptions which are generally acceptable in traffic flow theory such as a traffic flow model, functional form of the FD as triangular, values of total flows and densities from detectors etc. Even though it is desirable to have estimates from methods based on '*weaker*' assumptions, however, model-driven TSE methods have high explanatory powers and tend to provide more accurate estimates because the model is representative of the physics of traffic and add values to the observations. It is easier to integrate this method to traffic control operations. The only key task is to calibrate the model-driven TSE method carefully. This study showcases careful selection and calibration of FD utilized to define the CTM and the validity of the model is conducted using large and complete real world traffic data i.e., ZTD. The assumptions, limitation, and future research directions are discusses in section 7.2.3 and section 7.2.4.

7   SUMMARY AND FUTURE DIRECTIONS

7.1   Achievements, overall conclusions, and practical implications

Due to increased demand in mobility because of an overwhelming increase in population, congestion is causing poor traffic performance that has negative impacts on economy, environment, and safety. Instead of building new infrastructures for reducing congestion, this study explored smart solutions by focusing on recent advancements in ICT and contributes to the sustainable solutions for optimally using the existing transportation. For managing congestion efficiently and sustainably, one of the several challenges is to provide accurate information about current traffic state (flow q, density k, speed v), which are essential inputs for operations, traffic management and control and information provision for route choice guidance, using partially observed traffic data (collected by probe vehicles and roadside detectors). By using the methodologies and analysis described in this research it becomes possible to understand the current traffic flow characteristics with reasonable accuracy. Through this research, various existing FDs were systematically analyzed, followed by the performance evaluation of a '*weaker*' assumption-based TSE method which was then successfully extended to develop a physical model-based TSE method by utilizing data assimilation (DA) framework.

ZTD, an excellent data product collected through advanced methodologies and image processing technology obtained from Hanshin Expressway Co. Ltd., played a vital role in successfully conducting this research. A major part of the motivation for this doctoral research also came from the fact that ZTD has extreme potential for the evaluation of classical concepts in the fundamental theory of traffic flow, traffic flow models, functional forms of FDs, traffic state estimation methods, several of which have been developed and proposed by researchers over past decades, some based on theoretical assumptions and others driven by data and have not been evaluated or validated with complete trajectory data (ground truth) to verify their capabilities. In fact, in this study, ZTD has been successfully utilized in formulation and evaluation of a new traffic state estimation method for estimating reasonably accurate traffic states at high spatiotemporal

resolutions and complete space-time domain. The summary corresponding to each achieved objective is as follows:

I.   First objective (in chapter 4)

Achievements: Through the fulfilment of the first objective of this doctoral research, in Chapter 4 various existing speed-density $(v - k)$ FDs were empirically and theoretically analyzed, in terms of their accuracy, correlation to the real traffic data, whether the considered relations are theoretical valid with respect to the static and dynamic properties of FDs, at varying spatiotemporal resolutions by utilizing the complete trajectory data. Eventually, a model a.) with less complex form; b.) based on '*weaker*' assumptions; c.) reasonably achieves mathematical elegance and empirical accuracy, was identified namely, May and Keller's model. The empirical accuracy of the model is very close to the outperforming complex forms of modified Lee *et al.* (rational model) and Wang *et al.* (logistic model) models. Moreover, the reliability of the analysis was provided weight by conducting the empirical validation over several space-time resolutions which also provides theoretical and practical support to practitioners in decisively choosing most workable FD at a particular resolution.

Overall conclusions: Overall, the May and Keller's functional linear relation proved to be a sound mathematical models that represent the FD due to its empirical accuracy and mathematical elegance. Due to its simple and fast computational cost it has been supported to have a lot of potential for real world applications and it can assist in understanding the traffic characteristics with very low costs, especially when the traffic engineers are working with extensive traffic data. This analysis was vital and unique from the past research as none of the previous studies have analyzed the model performance and application conditions of different $v - k$ relations with respect to the space-time resolution, in addition with a focus to identify an overall simple (less complex and compact natured), less parameterized, '*weaker*' assumption-based $v - k$ model.

Practical implications and possible applicability in real-world scenario: Based on prevailing traffic conditions, the inferred FD (May and Keller's model) can assist active traffic management (ATM) in alleviating congestion by accessing network dynamics accurately (such as when and

where congestion builds and how it dispatches) under fast and low computation cost. It can play a crucial role for traffic control and assignment, predicting the capability of road system, or predict its behavior when applying inflow regulations and speed limits. For application that do not require precise and detailed estimated of traffic state in complete space-time domain, May and Keller's FD can help in estimating the traffic state by locating where the system is on the FD at a desired moment.

For understanding the fundamentals such as maximum flow rate, critical density, free-flow speed *on expressway and highways*, which are very important to evaluate the quality of the road and road networks, the results of analysis can be directly utilized by traffic engineers. Due it its high empirical accuracy, dependency on simple assumptions, and ease of handling with its noncomplex and compact nature (which makes it a model with low computation cost), May and Keller's model can be as it is utilized with its parameters estimated as in the study. Similarly, based on the resolution of interest, practitioners can utilize the result of analysis and decide the most workable FD (with parameters as estimated in the study) for understanding the traffic dynamics through FD. Practitioners working with extensive traffic data can estimate the parameters of the May and Keller's functional form ($v_f, k_j, m, and\ n$) using the available extensive data for understanding the fundamentals of *any kind traffic link* (other than expressways and highways as well). The available data such as headway and spacing measurements from extended floating car data can be used to obtain the (q, k) points to estimate the parameters of the chosen FD that can in turn, aid in predicting the congestion, its propagation, and mutual relationship between change in level of services and traffic volume.

II.   *Second objective (in chapter 5)*

Achievements: The fulfillment of second objective of this dissertation successfully contributed to the performance evaluation of an $xFCD$-based TSE method, unconfined by any exogenous assumptions such as FD, proposed by Seo *et al.*, (2015b) in chapter 5. The analysis was conducted at finer spatiotemporal resolutions and varying probe vehicle penetration rates using high resolution complete trajectory data (ZTD). It revealed that the accuracy of the estimates depends on two *settings*: temporal resolution (Δt), and probe penetration rate ($p\%$), but indirectly. It is always desirable to be able to retrieve the estimates of traffic states in a complete

spatiotemporal domain i.e., with a higher $c\%$. However, for a combination of a finer Δt i.e., finer than 2 min and a lower $p\%$ i.e., below 3%, a compromise is made with both accuracy and the $c\%$. Thus, according to the available $p\%$ or the required accuracy and $c\%$, practitioners could select the desired and appropriate spatiotemporal resolution *settings*. The achievement, here, is that the analysis provides an insight into the various combinations of *settings*, expected probe vehicles in spatiotemporal cells, the corresponding covering percentage, and the expected accuracy. Thus, according to the available $p\%$ or the required accuracy and $c\%$, practitioners could select the desired and appropriate spatiotemporal resolution *settings*.

Overall conclusions: Like several other TSE methods developed over past decade which utilize probe vehicle data for estimating traffic state, the estimation capabilities of this estimation method had not been validated using vehicles' high-resolution, complete, and detailed trajectory data with high space-time coverage. The analysis of the estimation capability of the method using real world complete trajectory data was vital and essential because the method does not rely on '*strong*' assumptions, rather is based on '*weaker*' assumptions, which are preferable for practical applications. In actual, few percentage of GPS probes are expected in the actual highways of Japan (where the maximum cell size for traffic control is $\Delta x = 200\ m$ and $\Delta t = 300\ s$), and the *settings* considered in this analysis aided in visualizing expected errors in the estimation results using this method at finer Δx and Δt and a lower $p\%$ (current low penetration environment).

Practical implications and possible applicability in real-world scenario: With few percentages of prove vehicles, the method can estimate traffic states at coarser resolutions with 100% coverage with reasonable accuracy when the expressway is not in the congested state. This low resolution is sometimes useful for planning purposes and for potential area-wide traffic management. Inspecting the $xFCD$-based TSE method using the ZTD elucidated the application of the estimation method in estimating traffic states at freeways at desired *settings* using probe vehicles that are proficient at providing information regarding the spacing between it and its leading vehicle. However, due to a smaller number of probes the accuracy at even coarser resolutions isn't the best, which may be improved with the advancement in ICT as more probes are likely to be realized. Furthermore, at an age of near ubiquitous sensor (e.g., cell phone) penetration, and with the massive emergence of connected vehicles, the validation result suggests

that the approach might become prevalent in the near future for transportation planning purposes with a probe vehicle penetration rate of several percentages. So, with the information on total flow, traffic engineers can understand the expected average number of probe vehicles in a spatiotemporal cell of a particular spatiotemporal resolution combination and probe penetration rate. This will ultimately help in deducing the expected accuracy in estimating TS using this method. In another situation, with total traffic flow information, traffic engineers can understand the number of probe vehicles required to attain a certain level of accuracy. Thus, according to the available $p\%$ (dependent on total flow) or the required accuracy and $c\%$, practitioners could select the desired and appropriate spatiotemporal resolution *settings* for TSE.

III.   Third objective (in chapter 6)

Achievements: To be able to retrieve much accurate traffic state estimates in complete spatiotemporal domain (including unobserved cells i.e., cells via which no probe vehicle traversed) at high space-time resolution by utilizing fewer probe vehicles in both the regimes, congested and non-congested, is always desirable. Hence, with a focus on such requirements, the third achievement of this thesis successfully contributed to the development and implementation of a physical model-based method for traffic state estimation of highways and roadway links in chapter 6. In such a pursuit, the TSE method analyzed in chapter 5 provided a useful foundation for extending the estimation approach by incorporating a model-based approach along with a data assimilation (DA) framework. To improve the estimation capability 1.) by using few probe vehicles i.e., small probe penetration rate (= 5%), 2.) in complete space-time domain, 3.) for both regimes of free-flow and congested, and 4.) at high spatiotemporal resolution, it extended the '*weaker*' assumption-based approach to estimate the traffic state more accurately by utilizing a data assimilation (DA) framework and vehicles' complete trajectory data.

Overall conclusions: In alignment to the hypothesis, utilization of DA techniques provided more accurate estimates under the discussed requirements. The results from the adaptive approach of AC of FD and TSE (employing DA framework) show that the accuracy of estimating the traffic state increases and the estimated k corresponds well with the k computed using Edie's generalized definitions (Edie, 1963) and 100% trajectory data (ground truth).

Practical implications and possible applicability in real-world scenario:* The proposed model-based TSE method can be utilized to estimate reasonably accurate traffic states on a freeway by utilizing few percentages of probe penetration ($= 5\%$) and detector data including only the total flows and densities at fixed lengths of $300\ m$. In this study, the significance of interval length between observations from detectors is not explored. Therefore, a couple of 100 meters of intervals can be considered. In fact, such information can be easily obtained from roadside fixed sensors. Additional data required for the application of this method in real world scenario includes spacing and headway measurements of probe vehicles to their leading vehicles. For estimating TS on a freeway's space-time domain of interest, the probe data from the target section with probe penetration rate of around 5%, will be utilized to first calibrate the triangular FD by finding optimized its parameters namely, free-flow speed, critical density, and jam density. These parameters will be used to define the CTM which plays a vital role in TSE using DA framework. Based on probe data information, the spatiotemporal resolution for AC of FD and TSE can be set in accordance with the CFL condition. The resolution will aid in configuring the EnKF correctly. The measurements from the probe data will be fed as an input to the $xFCD$-based TSE method (explored in chapter 5) for obtaining the observed traffic states (density and velocity). The final output will include much accurate TS estimates over complete domain at desired spatiotemporal resolutions. Since it is essential to retrieve much accurate traffic state estimates in complete spatiotemporal domain, at high space-time resolution by utilizing fewer probe vehicles in both the regimes, congested and non-congested, the proposition of this methodology earns a great scope of application.

In fact, these were the principal postulates that motivated the studies carried out as per the research plan of this thesis. It is within the context that information technology (IT) and traffic blend together to create Intelligent Transport Systems (ITS). One of the practical outcomes of utilizing ZTD is the retrieval of information for making better informed decisions. In summary, this thesis studied analysis and modeling of FDs and TSE methods using complete trajectory data: ZTD. The analyses and the devised TSE method are expected to be utilized and implemented in real-world traffic design, planning, management, and control to mitigate traffic issues, congestion being the major one.

Since highly detailed and technical data like ZTD is not possible to be obtained and utilized for real application over all transportation networks, objective 2 and objective 3 of this doctoral

research utilized the ZTD by creating probe vehicles-like situation (datasets). For real-world application, highly precise temporal sampling rate of the probe vehicle data is not a compulsory requirement for implementing the results and methodologies described in the thesis, however it is beneficial for the temporal sampling rate of collected data to be smaller than the desired temporal resolution of the target space-time region under analysis.

Interconnection between chapter 4, chapter 5, and chapter 6: The explanations, analysis and discussions in chapter 4 revolves around the Fundamental Diagram (FD) and chapter 5 and chapter 6 encompass the concepts and methodologies associated with Traffic State Estimation (TSE). Both are crucial for understanding the traffic phenomena and dynamics of road traffic. Chapter 4 and chapter 5 included independent studies on several speed-density FDs and a *weaker'* assumption-based TSE method, respectively.

In chapter 4, parameters of several existing speed-density were estimated by utilizing complete vehicles' trajectory data to identify a simple, *'weaker'* assumption-based FD that reasonably achieves empirical accuracy and theoretical elegance, and to identify the most workable form of a FD at various spatiotemporal resolutions. The key ingredients required were the stationary $k \ and \ v$ points from stationary cells (an assumption) of mesh of a spatiotemporal domain which were computed using 100% ZTD and Edie's definitions. The direct output included the parameters of considered speed-density relations using which the statistical analysis was performed.

In chapter 5, *'weaker'* assumption-based TSE method was analyzed using probe vehicle-like data obtained using ZTD. The key ingredient required was the spatiotemporal area between a probe and its leading vehicle which can be computed using the headway and spacing measurements from probes and positioning of probes. The direct output included the TS estimates at different spatiotemporal resolutions using which the performance of TSE was evaluated.

However, chapter 6 proposes an adaptive approach of calibrating a FD which is directly utilized in estimating TS using a DA framework. If the sections considered in chapter 5 and chapter 6 were exactly same, the output of the chapter 5 could have been directly utilized in chapter 6 as the observation from probe vehicles (for observation equation of EnKF). The same headway and spacing measurements from probes are used for AC of FD. It is also important to highlight the fact that the approach of calibrating the FD in chapter 6 is theoretically stronger with more explanatory

power as compared to the calibration approach in chapter 4. In chapter 6, a dynamic approach is adopted that takes the variability of data into account by using simulated density from CTM for providing optimized parameters of FD. The direct comparison of final output from TSE method discussed in chapter 5 (TS estimates using *'weaker'* assumption-based TSE method) and chapter 6 (TS estimates using model-based TSE method) are compared in section 6.7 and section 6.8.3 of chapter 6 itself.

7.2   Dependency of expected average number of probe vehicles in a space-time cell on the total flow

In chapter 5 and chapter 6, certain percentage of vehicles ($p\%$) have been randomly sampled from the 100% vehicles (whose trajectory information is included in ZTD) and are considered as probe vehicles.

In chapter 6, 5% (~172 vehicles) of vehicles are utilized to estimate the traffic state at a resolution of {150 m x 5 s} where the total flow of this ZTD (L001_F001) was 3,415 vehicles driving for a distance of 2 km and for 1 hour. Under such conditions the average number of probe vehicles passing through observed cells is 1.14 vehicles with a covering percentage of ~68%. Moreover, the traffic before 1200 s (i.e., before 7:20 a.m.) appears to be in the free-flow regime and no congestion can be seen as per the velocity profile of L001_F001. With same set of probes the average number of probe vehicles passing through observed cells is 1.07 vehicles. After 1200 s (i.e., between 7:20 a.m. and 8:00 a.m.), the congested traffic conditions seem to appear (as per the velocity profile of L001_F001) and the average number of probe vehicles passing through observed cells is 1.16 vehicles.

Before 7:20 a.m. the total flow observed was 1204 veh/20 mins (i.e., 3612 veh/hour). Extracting 5% of this total flow will result in ~60 vehicles. Under such flow conditions the average number of probe vehicles passing through observed cells is 1.32 vehicles with a covering percentage of ~43%. Between 7:20 a.m. and 8:00 a.m., the total flow observed was 2324 veh/40 mins (i.e., 3486 veh/hour). Extracting 5% of this total flow will result in ~116 vehicles. Under such flow conditions the average number of probe vehicles passing through observed cells is 1.48 vehicles with a covering percentage of ~58%.

As that number of vehicles considered as 5% probes depend on the total flow, hence, it proves that it is better to highlight that the expected accuracy of TSE method is also influenced by the traffic flow conditions (total flow). Accuracy of a TSE method depends on the expected average number of probe vehicles in a cell at a particular setting i.e., spatial resolution, temporal resolution, and probe penetration rate. And, at the same time the expected average number of probes depend on, obviously, 1.) the settings and 2.) the total flow in the target space-time region which tells about the minimum number of probes required to make a particular probe penetration rate.

In chapter 5 as well, the performance analysis of weaker assumption-based TSE method at varying spatiotemporal resolution and probe penetration rate has an indirect but significant dependency on the total flow of the considered space-time regions. In simpler words, the total flow determines the minimum number of vehicles required to make a certain probe penetration rate and in turn, the expected average number of probes in a cell. The average number of probe vehicles passing through observed cells at different spatiotemporal resolutions and probe penetration rate with the total flow of each section as ~ 3400 vehicles per hour is then shown by Table 5.3 of chapter 5. The table is important because the average number of probes in a spatiotemporal area is a key factor in accurately estimating the traffic states. So, Table 5.2 and Table 5.3 collectively assist in determining the expected accuracy in the estimates by the estimation method at various combinations of settings.

For practical applications, in order to determine the expected accuracy at any combination of setting the total flow is required to find what penetration rate it is with available probes. Alternatively, when analysts have a desired accuracy level then total flow will help in deciding the minimum number of probes required to attain that accuracy at a specific combination of settings.

When the total flow on a freeway is around $3400 - 3600$ veh/hour, the expected average number of probe vehicles in observed cells at these settings: $\Delta x = 150m, \Delta t = 5s, p\% = 5\%$, is in the range of $1.14 - 1.48$ vehicles. Then, this kind of relation between total flow and expected average number of probes in a spatiotemporal cell at a particular setting is very meaningful and also, very important for traffic flow analysis. This is so because 5% of probe vehicles at a different flow rate, such as when the flow is very less, can result in different expected number of probe vehicles in a cell of such spatiotemporal resolutions. The thesis, however, doesn't include the research on the mathematical or analytical relationship between the two. Rather the above discussion highlights the presence of influence of total flow in determining minimum number of

probes required to make certain percentage of probes and in turn inferencing the expected average number of probe vehicles in a cell at a particular setting (which ultimately affect the accuracy of the TSE method).

7.3   Limitations and future directions

7.3.1   Single-regime speed-density ($v - k$) functional relations

While analyzing various existing speed-density ($v - k$) relations in chapter 4, the improved data quality and data quantity led to some theoretical challenges for single-regime fundamental relations, which are unable to explain the reasons behind the scatter and unstableness in the traffic states. The reasons could be the theoretical assumptions made when devising these functional forms in regard to the multi-lane multi-class traffic treated as single-lane single-class and the stationarity of traffic, which have been widely used is past studies and current study as well. Another reason for the difficulty in explaining the scatter can be the inherent nature of traffic flow, specifically the uncertainty in human behaviors, their respective desired speeds and critical headway distances, highway geometries, and vehicle characteristics. A big assumption for most of the $v - k$ relations is that a specific value of velocity corresponds to each value of density, which in the actual scenario can be a form of a distribution function. In this context, this study analyzed only single-regime $v - k$ relations, which serves as a limitation of the study. By contrast, with the recent developments in technology, the actual disaggregated data (such as ZTD) can be collected from a multi-lane multi-class environment and be used to evaluate more complex and multi-class FDs such as for different vehicle types. Moving forward in the same direction, development of a potentially better speed-density ($v - k$) relation can be attempted through further studies by incorporating other parameters of the ZTD with physical significance, such as the number of lanes, type of facility, and composition of vehicles etc.

7.3.2 $xFCD$-based TSE utilizing large ubiquitous sensor penetration

In context with the analysis of '*weaker*' assumption-based TSE method in chapter 5, at an age of near ubiquitous sensor (e.g., cell phone) penetration, and with the massive emergence of connected

vehicles, the validation result suggests that the approach might become prevalent in the near future for planning purposes with a probe vehicle penetration rate of several percentages. Namely, for traffic management and control purposes, the proposed method may require a higher penetration rate but considering the possible widespread implementation of ADAS in the future, such a high penetration rate might be realized. Since the analysis in chapter 5 limits the scope of space-time domain to smaller section and special considerations are given to the lane changing behavior, to test the applicability of the method in real world situation with the assumption of large ubiquitous sensor penetration, it becomes a vital research problem to evaluate the estimation method 1.) in a wider section, 2.) with larger penetration rate, and 3.) inclusive of all kinds of user road behavior.

7.3.3   Aggregated boundary flows and densities using probe data

The model-based TSE devised in chapter 6 employs EnKF for estimating the most probable traffic state using the model simulated density obtained from CTM. However, the application of CTM involved a few assumptions. First, it is assumed that the section has no cell with on-ramp or off-ramp, second, the FD parameters are assumed to be constant over all the discretized cells for CTM and third, it is presumed that detectors are installed at the boundaries of the section such that the aggregated boundary traffic flows (q_u and q_d) and densities (k_u and k_d) are measured. For this study the aggregated flows and densities are computed using 100% ZTD at a fixed length interval of $300\ m$ and are assumed to be obtained from detectors. These assumptions can be considered as a limitation of the study. To further enhance the formulation methodology, the third assumption can be relaxed making the estimation method independent of the boundary flows and densities collected by the detectors. In fact, such boundary flows can be mathematically computed using the available probe data at the boundaries of the section and this can be considered a future direction worth exploring.

7.3.4   Short-term traffic state prediction using DA

The model-based TSE method employing DA framework can be further extended to contribute to the development and implementation of a model for making short-range prediction of the future traffic state. The good news is that there is a growing amount of data available and the

corresponding increase in computing power due to advancement in Information and Communication Technology (ICT). Therefore, there is a possibility of developing prediction methodology at the intersection of machine learning (ML) and data assimilation by focusing on the opportunities offered by advance data-driven techniques to improve and/or correct out knowledge-based models. The prime predominant purpose of this research will be twofold, 1.) implementation the model-based TSE method (proposed in chapter 6) running on DA framework that includes automatic calibration (AC) of FD, and 2.) formulating and implementing the prediction model where the final accurate predictions are obtained from assimilating parametric and non-parametric short-term predictions. The current state estimates obtained from the model-based approach can be used to make future predictions of traffic state by implementing a hybrid prediction approach that assimilates parametric and non-parametric short-term prediction based on data assimilation framework. To obtain non-parametric prediction ML algorithm (such as neural network) can be utilized, while the parametric predictions can be obtained by running forward in time the CTM model to predict future traffic state. Although few studies have been conducted to predict the traffic states using DA methods however, none of the studies have utilized such detailed estimates of traffic state values which can be available in complete space-time domain at a resolution as fine as $\{150\ m\ \text{x}\ 5\ s\}$ and probe penetration rate of probe vehicles as low as 5%. In other words, the motive here is to assimilate the parametric predictions of traffic state with non-parametric predictions to obtain the best possible short-range forecast of the traffic state as per the flow illustrated in Figure 7.1. Data assimilation will be at the center of our predictive system and will be used to minimize the error for predictive systems where there is uncertainty in both the predictive models. These precise traffic state predictions will aid in mitigating congestion effectively.
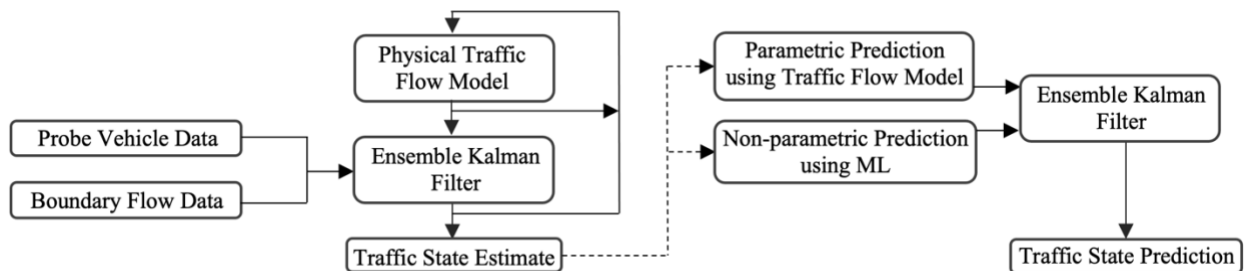

Figure 7.1 Short-term traffic state prediction using model-based TSE method, DA framework and machine learning (ML)

BIBLIOGRAPHY

Barmpounakis, E., & Geroliminis, N. (2020). On the new era of urban traffic monitoring with massive drone data: The pNEUMA large–scale field experiment. *Transportation Research Part C: Emerging Technologies, 111*, 50–71.

Bekiaris-Liberis, N., Roncoli, C., & Papageorgiou, M. (2016). Highway traffic state estimation with mixed connected and conventional vehicles. *IEEE Transactions on Intelligent Transport Systems. 17*(12), pp. 3484–3497.

Bladin, S., Argote, J., Bayen, A. M., & Work, D. B. (2013). Phase transition model of non-stationary traffic flow: definition, properties and solution methods. *Transportation Research Part B: Methodological, 52*, 31–55.

Braden, B. (1986). The surveyor's area formula. *The College Mathematics Journal, 17(4)*, 326–337.

Cassidy, M. J. (1998). Bivariate relations in nearly stationary highway traffic. *Transportation Research Part B: Methodological, 32*(1), 49–59.

Cauchy, A. (1846). Sur les intégrales qui s'étendent à tous les points d'une courbe fermée. *(On integrals that extend over all of the points of a closed curve), Comptes rendus, 23*, 251–255.

Chiabaut, N., Buisson, C., & Leclercq, L. (2009). Fundamental diagram estimation through passing rate measurements in congestion. *IEEE Transactions on Intelligent Transport Systems, 10*(2), 355–359.

Coifman, B. (2002). Estimating travel times and vehicle trajectories on freeway using dual loop detectors. *Transportation Research Part A: Policy and Practice, 36 (4)*, 351–364.

Coifman, B. (2014). Revisiting the empirical fundamental relationship. *Transportation Research Part B: Methodological, 68*, 173–184.

Coifman, B., & Li, L. (2017). A critical evaluation of the Next Generation Simulation (NGSIM) vehicle trajectory dataset. *Transportation Research Part B: Methodological, 105 (C)*, 362–377.

Daganzo, C. F. (1994). The Cell Transmission Model: A dynamic representation of highway traffic consistent with the hydrodynamic theory. *Transportation Research Part B: Methodological, 28*(4), 269–287.

Dahiya, G., Asakura, Y., & Nakanishi, W. (2020). A study of speed-density functional relations for varying spatiotemporal resolution using Zen Traffic Data. *2020 IEEE 23rd International Conference on Intelligent Transportation Systems (ITSC)*. (pp. 1–8). Rhodes, Greece.

Dahiya, G., & Asakura, Y. (2021). Exploring the performance of streaming-data-driven traffic state estimation method using complete trajectory data. *International Journal of Intelligent Transportation Systems Research, 19*, 572–586.

Dahiya, G., Asakura, Y., & Nakanishi, W. (2022). Analysis of the single-regime speed-density fundamental relationships for varying spatiotemporal resolution using Zen Traffic Data. *Asian Transport Studies, 8*, 2185–5560.

Del Castillo, J. M., & Benítez, F. G. (1995). On the functional form of the speed-density relationship-I: General theory. *Transportation Research Part B: Methodological, 29*(5), 373–389.

Drake, J. S., Schofer, J. L., & May, A. D. Jr. (1966). A statistical analysis of speed-density hypotheses. *Highway Research Record 154*, 53–87.

Drew, D. R. (1968). *Traffic flow theory and control.* New York: McGraw–Hill.

Duckstein, L., Unwin, E. A., & Boyd, E. T. (1970). Variable perception time in car following and Its effect on model stability. *IEEE Transactions on Man Machine Systems, 11*, 149–156.

Edie, L. C. (1961). Car–following and steady-state theory for noncongested traffic. *Operations Research, 9*(1), 66–76.

Edie, L. C. (1963). Discussion of traffic stream measurements and definitions. *2nd International Symposium on the Theory of Traffic Flow*, (pp. 139–154). London, The U. K.

El Faouzi, N.-E., Leung, H., & Kurina, A. (2011). Data fusion in intelligent transportation systems: Progress and challenges-a survey. *Information Fusion, 12*(1), 4–10.

Evensen, G. (1994). Sequential data assimilation with a non-linear quasi-geostrophic model using Monte Carlo methods for forecast error statistics. *Journal of Reophysical Research: Oceans*, *99*,(C5), 10143–10162.

Fan, S., Herty, M., & Seibold, B. (2014). Comparative model accuracy of a data-fitted generalized Aw-Rascle-Zhang model. *Networks and Heterogenous Media*, *9*, 239–268.

Gaddam, H. K., & Rao, K. R. (2019). Speed-density functional relationship for heterogeneous traffic data: a statistical and theoretical investigation. *Journal of Modern Transportation, 27*, 61–74.

Gazis, D. C., Herman, R., & Potts, R. (1959). Car–following theory of steady-state traffic flow. *Operations Research, 7*(4), 499–505.

Godunov, S. K. (1959). A difference method for numerical calculations of discontinuous solutions of the equations of hydrodynamics. *Matematicheskii Sbornik, 89*(3), 271–306. (In Russian).

Goodwin, P. (1996). Empirical evidence on induced traffic. *Transportation*, *23*(1), 35–54.

Göttlich, S., Ziegler, U., & Herty, M. (2013). Numeric discretization of Hamiltion-Jacobi equations on networks. *Network and Heterogenous Media, 8*(3).

Greenberg, H. (1959). An analysis of traffic flow. *Operations Research, 7*(1), 79–85.

Greenshields, B. D., Bibbins, J., Channing, W. S., & Miller, H. H. (1935). A study of traffic capacity. *Highway Research Board Annual meeting*, (pp. 448–477). Washington D. C., U. S. A.

Grumert, E. F., & Tapani, A. (2018). Traffic state estimation using connected vehicles and stationary detectors. *J. Adv. Transp., 2017*.

Hall, F. L., Allen, B. L., & Gunter, M. A. (1986). Empirical analysis of freeway flow-density relationships. *Transportation Research Part A: General, 20*, 197–210.

Hanshin Expressway Co. Ltd. (2018). Retrieved from ZTD: https://zen-traffic-data.net

Herrera, J. C., & Bayen, A. M. (2010). Incorporation of Lagrangian measurements in freeway traffic state estimation. *Transportation Research Part B: Methodological, 44*(4), 460–481.

Herrera, J. C., Work, D. B., Herring, R., Ban, X. J., Jacobson, Q., & Bayen, A. M. (2010). Evaluation of traffic data obtained via GPS-enabled mobile phones: the Mobile Century field experiment. *Transportation Research Part C: Emerging Technologies, 18*(4), 568–583.

Hills, P. (1996). What is induced traffic? *Transportation*, *23*(1), 5–16.

Huber, W., Lädke, M., & Ogger, R. (1999). Extended floating car data for the acquisition of traffic information. *6th World Congress on Intelligent Transport Systems (ITS)*, (pp. 1–9). Toronto, Canada.

Kalman, R. E., & Bucy, R. S. (1961). New results in linear filtering and prediction theory. *Journal of Basic Engineering, 83*(3), 95–108.

Koshi, M., Iwasaki, M., & Okura, I. (1983). Some findings and an overview on vehicular flow characteristics. *8th International Symposium on Transportation and Traffic Flow Theory* (pp. 403–426). Toronto, Ontario, Canada: University of Toronto Press.

Krajewski, R., Bock, J., Kloeker, L., & Eckstein, L. (2018). The highD dataset: a drone dataset of naturalistic vehicle trajectories on German highways for validation of highly automated driving systems. *21st International Conference on Intelligent Transportation Systems (ITSC)*, (pp. 2118–2125). Maui, Hawaii, U. S. A.

Lam, T., & Rothery, R. (1970). The spectral analysis of speed fluctuations on a freeway. *Transportation Science, 4*, 293–310.

Laval, A. (2011). Hysteresis in traffic flow revisited: An improved measurement methodology. *Transportation Research Part B: Methodological, 45*(2), 385–391.

Lee, H. Y., Lee, H. W., & Kim, D. (1998). Origin of synchronized traffic flow on highways and its dynamic phase transitions. *Phys. Rev. Lett., 81*(5), 1130–1133.

Lighthill, M., & Whitham, G. (1955). On kinematic waves. I: flood movement in long rivers, II: a theory of traffic flow on long crowded roads. *Quality and Theory of Traffic Flow. A Symposium Proceedings of the Royal Society (London) A229.* (pp. 281–345).

Litman, T. (2004). Generated traffic and induced travel. *Implications for Transportation Planning.* Victoria: Victoria Transport Policy Institute.

Lu, X. Y., Varaiya, P., & Horowitz, R. (2019). Fundamental diagram modelling and analysis based NGSIM data. *IFAC Proceedings Volumes*, *42(15)*, (pp. 367–374).

May, A. D., & Keller, H. E. M. Jr. (1967). Non-integer car-following models. *Highway Research Record, 199*, 19–32.

May, A. (1990). *Traffic flow fundamentals.* Englewood Cliffs: Prentice-Hall, Inc.

Meister, A. L. F. (1769). Generalia de genesi figurarum planarum et inde pendentibus earum affectionibus. *Nov. Com. Gött. (in Latin), 1*, 144.

Mihaylova, L., Boel, R. (2004). A particle filter for freeway traffic estimation. *IEEE 43rd Conference on Decision and Control, 2*, (pp. 2106–2111).

Mihaylova, L., Boel, R., & Hegyi, A. (2006). An unscented Kalman filter for freeway traffic estimation. *The 11th IFAC Symposium on Control in Transportation Systems.*

Montanino, M., & Punzo, V. (2015). Trajectory data reconstruction and simulation-based validation against macroscopic traffic patterns. *Transportation Research Part B: Methodological, 80*, 82–106.

Nanthawichit, C., Nakatsuji, T., & Suzuki, H. (2003). Application of probe vehicle data for real-time traffic-state estimation and short-term travel-time prediction on a freeway. *Transportation Research Record: Journal of the Transportation Research Board, 1855*(1), 49–59.

Newell, G. F. (1961). Nonlinear effects in the dynamics of car following. *Operations Research, 9*(2), 209–229.

Newell, G. F. (1962). Theories of instability in dense highway traffic. *Journal of the Operations Research Society of Japan, 5*(5), 9–54.

Newell, G. F. (1993). A simplified theory of kinematic waves in highway traffic part I: General theory. *Transportation Research Part B: Methodological, 27*(4), 281–287.

Ni, D., & Leonard, J. II (2005). Markov chain monte carlo multiple imputation using bayesian networks for incomplete intelligent transportation systems data. *Transportation Research Record: Journal of the Transportation Research Board, 1935*, 57–67.

NPTEL (2012). Traffic Engineering and Management (Civil Engineering course by Dr. Tom V. Mathew, IIT Bombay): https://archive.nptel.ac.in/courses/105/101/105101008/

Ouessai, A., & Keche, M. (2019). Real-time freeway traffic state estimation based on the second–order divided difference Kalman Filter. *Transport and Telecommunication Journal. 20*(2), 114–122.

Ozaki, H. (1993). Reaction and anticipation in the car–following behavior. *12th International Symposium on the Theory of Traffic Flow and Transportation*, (pp. 349–366). Berkeley, U. S. A.

Papageorgiou, M., Blosseville, J. M., & Hadj–Salem, H. (1989). Macroscopic modelling of traffic flow on the Boulevard Périphérique in Paris. *Transportation Research Part B: Methodological, 23*(1), 29–47.

Payne, H. J. (1984). Discontinuity in equilibrium freeway traffic flow. *Transportation Research Record, 971*, 140–146.

Pipes, L. A. (1967). Car following models and the fundamental diagram of road traffic. *Transportation Research, 1*(1), 21–29.

Qu, S., Wang, S., & Zhang, J. (2015). On the fundamental diagram for the freeway traffic: Anovel calibration approach for single-regime models. *Transportation Research Part B: Methodological, 73*, 91–102.

Richards, P. (1956). Shockwave on the highway. *Operations Research, 4*(1), 42–51.

Seo, T., Kusakabe, T., & Asakura, Y. (2015a). Traffic state estimation with the advanced probe vehicles using data assimilation. *2015 IEEE 18th International Conference on Intelligent Transportation Systems*, (pp. 824–830). Gran Canaria, Spain.

Seo, T., Kusakabe, T., & Asakura, Y. (2015b). Estimation of flow and density using probe vehicles with spacing measurement equipment. *Transportation Research Part C: Emerging Technologies, 53*, 134–150.

Seo, T., Bayen, A. M., Kusakabe, T., & Asakura, Y. (2017). Traffic state estimation on highway: A comprehensive survey. *Annual Reviews in Control, 43*, 128–151.

Seo, T., Tago, Y., Shinkai, N., Nakanishi, M., Tanabe, J., Ushirogochi, D., Kanamori, S., Abe, A., Kodama, T., Yoshimura, S., Ishihara, M., Nakanishi, W. (2021). Evaluation of large–scale complete vehicle trajectories dataset on two kilometers highway segment for one hour duration: Zen Traffic Data. *2020 International Symposium on Transportation Data and Modelling.* Ann Arbor, Michigan, U. S. A.

Sunderrajan, A., Vishwanath, V., Cai, W., & Knoll, A. (2016). Traffic state estimation using floating car data. *The International Conference on Computational Science*, *80*, (pp. 2008–2018).

Sumalee, A., Zhong, R. X., Pan, T. L., & Szeto, W. Y. (2011). Stochastic cell transmission model (SCTM): A stochastic dynamic traffic model for traffic state surveillance and assignment. *Transportation Research Part B: Methodological, 45*(3), 507–533.

Sun, D., Zhao, H., Yue, H., Zhao, M., Cheng, S., & Han, W. (2017). ST TD outlier detection. *IET Intell. Transp. Syst., 11*(4), 203–211.

Sun, X., Muñoz, L., & Horowitz, R. (2003). Highway traffic state estimation using improved mixture Kalman filters for effective ramp metering control. *2003 IEEE 42nd Conference on Decision and Control*, *6*, (pp. 6333–6338).

Sutandi, C. (2007). Advanced traffic control system impacts on environmental quality in a large city in a developing country. *The 7th International conference of Eastern Asia Society for Transportation Studies, 6.*

Tampere, C. M. J., & Immers, L. H. (2007). An Extended Kalman Filter application for traffic state estimation using CTM with implicit mode switching and dynamic parameters. *2007 IEEE 10th International Conference on Intelligent Transportation Systems (ITSC)*. (pp. 209–216). Seattle, W. A., U. S. A.

Tan, H., Wu, Y., Cheng, B., Wang, W., & Ran, B. (2014). Robust missing traffic flow imputation considering nonnegativity and road capacity. *Mathematical Problems in Engineering 2014*.

Thai, J., & Bayen, A. M. (2015). State estimation for polyhedral hybrid systems and applications to the Godunov scheme for highway traffic estimation. *IEEE Transactions on Automatic control. 60*(2), pp. 311–326.

Treiterer, J., & Myers, J. (1974). The hysteresis phenomena in traffic flow. In Buckley, D. J. ed. *Transportation and Traffic Theory,* Springer.

Underwood, R. T. (1961). Speed, volume and density relationships. *Quality and Theory of Traffic Flow. A Symposium* (pp. 141–187). Yale University Bureau of Highway Traffic.

US Department of Transportation. (2006). NGSIM-Next Generation Simulation. Retrieved from Next Generation Simulation: http://ngsim.fhwa.dot.gov/

van Erp, P. B. C., Knoop, V. L., & Hoogendoorn, S. P. (2017). Macroscopic traffic state estimation: understanding traffic sensing data-based estimation errors. *J. Adv. Transp., 2017*.

van Lint, J. W. C., Hoogendoorn, S. P., & Hegyi, A. (2008). An Ensemble Kalman filtering approach to highway traffic estimation using GPS enabled mobile devices. *17th IFAC World Congress*, (pp. 14078–14083).

van Lint, J. W. C., & Hoogendoorn, S. P. (2010). Arobust and efficient method for fusing heterogenous data from traffic sensors on freeway. *Computer-Aided Civil and Infrastructure Engineering, 25*(8), 596–612.

Wang, Y., & Papageorgiou, M. (2005). Real-time freeway traffic state estimation based on extended Kalman filter: a general approach. *Transportation Research Part B: Methodological, 39*(2), 141–167.

Wang, Y., Papageorgiou, M., Messmer, A., Coopola, P., Tzimitsu, A., & Nuzzolo, A. (2009). An adaptive freeway traffic state estimator. *Automatica, 45*(1), 10–24.

Wang, H., Li, J., Chen, Q., & Ni, D. (2010). Representing the fundamental diagram: the pursuit of mathematical elegance and empirical accuracy. *Transportation Research Board (TRB) 89th Annual Meeting.* Washington D. C., U. S. A.

Wang, H., Ni, D., Chen, Q. Y., & Li, J. (2013). Stochastic modeling of the equilibrium speed-density relationship. *J. Adv. Transp., 47*, 126–150.

Wong, G. C. K., & Wong, S. C. (2002). A multi-class traffic flow model-an extension of LWR model with heterogenous drivers. *Transportation Research Part A: Policy and Practice, 36*(9), 827–841.

Work, D. B., Tossavainen, O. -P., Bladin, S., Bayen, A. M., Iwuchukwu, T., & Tracton, K. (2008). An Ensemble Kalman filtering approach to highway traffic estimation using GPS enabled mobile devices. *2008 IEEE 47th Conference on Decision and Control*, (pp. 5062–5068).

Wright, M., & Horowitz, R. (2016). Fusing loop and GPS probe measurements to estimate freeway density. *IEEE Transactions on Intelligent Transport Systems*. *17*(12), pp. 3577–3590.

Xu, C., Qu, Z., & Chen, X. (2014). Analysis of traffic flow speed-density relation model characteristics. *Journal of Highway and Transportation Research and Development (English Edition), 8*(4), 104–110.

Yang, H., Jin, P. J., Ran, B., Yang, D., Duan, Z., & He, L. (2018). Freeway traffic state estimation: a Lagrangian-space Kalman Filter approach. *Journal of Intelligent Transportation Systems, 23*(6), 525–540.

Yuan, Y., van Lint, J. W. C., Wilson, R. E., van Wageningen-Kessels, F., & Hoogendoorn, S. P. (2012). Real-time lagrangian traffic state estimator for freeways. *IEEE Transactions on Intelligent Transportation Systems, 13*(1), 59–70.

Zheng, F., Jabari, S. E., Liu, H. X., & Lin, D. (2018). Traffic state estimation using stochastic Lagrangian dynamics. *Transportation Research Part B: Methodological, 115*, 143–165.

Zhong, R., Chen, C., Chow, A. H., Pan, T., Yuan, F., & He, Z. (2016). Automatic calibration of fundamental diagram for first–order macroscopic freeway traffic models. *J. Adv. Transp., 50*, 363–385.

Zito, R., D'Este, G., & Taylor, M. A. P. (1995). Global positioning systems in the time domain: How useful a tool for intelligent vehicle-highway systems? *Transportation Research Part C: Emerging Technologies, 3*(4), 193–209.